THE UNIVERSITY
of EDINBURGH

Improved predictive models for pre-clinical drug toxicity studies

MARIA DOLORES NAVARRO-ZORNOZA

Doctor of Philosophy
The University of Edinburgh
2015

Doctor of Philosophy – The University of Edinburgh – 2015

Declaration

This thesis is submitted for the degree of Doctor of Philosophy at the University of Edinburgh and this work has not been submitted for any other degree or professional qualification. My supervisors corrected the first draft of all chapters to offer advice on the English language grammar and spelling and provide critical feedback. Otherwise, except where clearly stated in the text, the thesis has been composed by my own work carried out in the Hepatology Laboratory at the University of Edinburgh, located at Royal Infirmary of Edinburgh and under the supervision of Professor John Plevris, Dr Leonard Nelson, Dr Olga Tura-Ceide and Kay Samuel except for the following:

Kay Samuel provided training for flow cytometry analysis.

Dr Forbes Howie contributed in developing a protocol to measure total glutathione content using the Cobas Fara Centrifugal Analyser (Roche) at The Queen's Medical Research Institute, The University of Edinburgh.

Dr Mai Abd El-Aziz developed protocols for real time PCR and design primers. She was very kind to measure and analyse my samples.

Dr Scott Inglis developed Cell Imaging and Analysis Package programme in order to do the migration imaging.

Maria Dolores Navarro Zornoza

Abstract

Increasingly, drug-induced liver injury is one of the main reason for drugs to be withdrawn from the market even after passing toxicity studies in pre-clinical and clinical trials because of risks of toxicity and ineffective treatments. Human immortalised hepatocyte cell lines used in drug testing are widely available, inexpensive and easy to culture. However, these cell lines are commonly known to have poor predictive capabilities and improved *in vitro* hepatic models are required for predicting hepatotoxicity of large numbers of compounds in drug discovery.

In this study, the primary goal was to develop an improved *in vitro* human hepatic model using a combination of the C3A human hepatic cell line and human umbilical vein endothelial cells (HUVECs), for prediction of acetaminophen (APAP) hepatotoxicity. Initial experiments showed that co-culture of HUVEC:C3A in EGM-2, an endothelial medium, was essential to support both cell types, and that co-cultures maintained the initial cell seeding ratio of 1:1 (HUVEC:C3A) after 3 days. Phenotyping of co-cultured cells using platelet endothelial cell adhesion molecule (PECAM-1/CD31) for HUVECs, and hepatic epithelial (EpCAM) markers for C3As demonstrated that at ratio 1:1 (HUVEC:C3A), there is cross-talk between HUVECs and C3As and cells in co-culture showed properties of self-organisation. This interaction resulted in improved hepatic metabolic activity *in vitro* in respect of albumin synthesis and cytochrome P450 activity.

Treatment with low (5 mM), intermediate (10 mM) and high doses (20 mM) of APAP, showed that prediction of hepatotoxicity using specific kits for cell viability and mitochondria function, was significantly improved in C3As in the presence of HUVECs, thus demonstrating an *in vitro* human hepatic co-culture could be an invaluable model for drug toxicity studies. We observed that the intermediate APAP dose had no effect on cell viability and mitochondrial function in co-cultures, whilst by comparison both lactate levels

and oxidative stress were perturbed in mono-cultures. Co-cultures also up-regulated expression of vascular endothelial growth factor receptor-2 (VEGFR-2) in HUVECs following APAP exposure, which may be important in modulating the toxic effect of APAP on C3As.

To further improve the *in vitro* liver-like model, Matrigel™ was incorporated to promote vascular formation by HUVECs and support hepatic organization, migration and function of C3As.

In HUVEC mono-cultures, Matrigel™-promoted vascularization, haptotaxis and self-organization and in HUVEC:C3A co-cultures formation of structures reminiscent of liver sinusoids and maintenance of hepatic albumin synthesis and CYP3A4 activity. Time-lapse imaging showed haptotactic migration of hepatocytes towards endothelial cells, with Matrigel™ likely having a chemotactic effect on HUVECs and C3As, resulting in interconnected vascular network. APAP inhibited angiogenesis in HUVEC mono-cultures whereas APAP had no effect in HUVEC:C3A co-cultures.

In conclusion, the development of an *in vitro* human organotypic co-culture model of HUVECs and C3As significantly enhanced hepatic function, demonstrated by significant improvement in hepatic metabolism, evidence of greater resistance to APAP toxicity, and improved cell-cell communication. Co-cultures markedly modulated APAP hepatotoxicity compared with C3A mono-cultures. Furthermore, co-culture of HUVECs and C3As using a complex basement membrane biomatrix (Matrigel™) produced a self-assembling interconnected vascular network, improved hepatocyte function as well as reproducibility of responses to APAP toxicity. The application of the described co-culture models may improve the accuracy, efficacy and predictive power of drug toxicity testing strategies in drug development.

Acknowledgements

I would like to thank Dr Olga Tura-Ceide and Kay Samuel for giving me the opportunity to take part in a project as part of a collaboration between Cell Therapy Research Group, SNBTS and the Hepatology Laboratory at the University of Edinburgh and their daily teaching in cell culture techniques, data analysis and valuable advice with English Grammar.

My thanks go also to Professor Peter Hayes, Professor John Plevris and Dr Leonard Nelson for encouraging me to apply for a PhD programme at the Hepatology Laboratory and for their supervision through the PhD programme. Finally, my thanks go to Dr Steve Morley for proof-reading and advising with English Grammar of the thesis manuscript.

I am also very grateful to the members of the Hepatology Laboratory, in particular to Anne Pryde, Patricia Lee and Pauline Cowan for their kindness in teaching me good laboratory practice and also to Dr Philipp Treskes for reviewing my first manuscript for publication. Indeed, I am also very grateful to the members of Orthopaedic Surgery, Natalia Harasymowicz, Deborah MacDonald, Dr Robert Wallace and especially to Antonello Spadaccini for making very grateful the office for working during this time.

Elisabeth Skinner was very kind to introduce and teach me time-lapse imaging and she also very kind to supply HUVECs.

Dr Gareth Sullivan for giving me the opportunity to spend two months, July and August in 2013 to learn about stem cells methodology and work with Sebastian Greenhough and Richard Siller who helped me with training and protocols in stem cell differentiation at the Norwegian Center for Stem Cell Research at the University of Oslo in Norway.

Finally, I would like to thank my family, my dad, mum and brother who believed in me from the initial day to today and encouraged me every day to keep fighting. To my friends, in

particular to Dr Navnit Makaram and Celia de la Cruz, for their patience and long skype conversations during these years. To my flatmates Alison McGarvey and Alisdair Macleod who played live music every night at the flat and to Dr James Andrade, Claire Lebled and Andrew Koulovasilopoulos for visiting the Hepatology laboratory.

Funding

The research reported here was supported by a University of Edinburgh Principal's Career Development PhD Scholarship (2011-2014) and Chief Scientist Office (ETM/182)

Travelling Fellowship was sponsored by The Company of Biologists' journals – to make a collaborative visit to The Norwegian Center for Stem Cell Research at the University of Oslo with Dr. Gareth Sullivan (01/07-01/09/2013).

Contents

List of Figures

List of Tables

Abbreviations

ALB	**Albumin**
ATP	**Adenine Triphosphate**
APAP	**Acetaminophen**
BALSS	**Bio-artificial Liver Support Systems**
BSA	**Bovine Serum Albumin**
bFGF	**Basic Fibroblast Growth Factor**
C3As	**Human Hepatoblastoma Cell Line**
CYP450	**Cytochrome P450 enzymes**
CPR	**Cell Proliferation Rate**
DAPI	**4', 6-Diamidino-2-PhenylindoleDILI**
DILI	**Drug Induced Liver Injury**
ECM	**Extracellular Matrix**
EDTA	**Ethylenediaminetetraacetic Acid**
EGM-2	**Endothelial Growth Media-2**
ETC	**Electron Transport Chain**
FBS	**Fetal Bovine Serum**
FGF	**Fibroblast Growth Factor**
GSH	**Glutathione**
GSSG	**Glutathione Disulphide**
HBSS	**Hank's Balanced Salt Solution**
HGF	**Hepatic Growth Factor**
HUVECs	**Human Umbilical Vein Endothelial Cells**
LDH	**Lactate Dehydrogenase**
LSECs	**Liver Sinusoidal Endothelial Cells**
MEME	**Minimum Essential Medium Eagle**

MFI	**Mean Fluorescence Intensity**
MG	**Matrigel™**
MG-GFR	**Matrigel™ Growth Factor Reduced**
mtDNA	**Mitochondrial DNA**
NAC	**N-Acetylcysteine**
NAD+	**Nicotinamide Adenine Dinucleotide**
NADH	**Reduced Nicotinamide Adenine Dinucleotide**
NAPQI	**N-Acetyl-p-Benzoquinone Imine**
NO	**Total Nitric Oxide**
NPC	**Non-Parenchymal Cells**
PBS	**Phosphate-Buffered Saline**
PHH	**Primary Human Hepatocytes**
PP	**Periportal**
PV	**Perivenous**
ROS	**Reactive Oxygen Species**
RNS	**Reactive Nitrogen Species**
RT	**Room Temperature**
RLU	**Relative luminescence Units**
RU	**Relative Units**
tGSH	**Total intracellular glutathione levels**
SEM	**Standard Error of the Mean**
VEGF	**Vascular Endothelial Growth Factor**
VEGFR-2	**Vascular Endothelial Growth Factor Receptor 2**

1 Chapter 1: Introduction

Replace, Reduce and Refine

In 1959 W.M.S. Russell and R.L. Burch published "*The Principles of Humane Experimental Technique"*, describing the principle of the three Rs: Replace, Reduce and Refine. This concept promotes the replacement, reduction and refinement of animal testing, encouraging scientists to find alternatives to using animals in experimentation and drug testing to demonstrate the same hypothesis (Flecknell, 2002).

Prediction of drug toxicity *in vitro* is a major challenge for pharmaceutical companies. In spite of drug toxicology studies using *in vitro* animal or human-derived hepatic models, data from these models does not correspond accurately to the same effects or mimic side effects that would be expected to be observed in the equivalent human trials. This is especially the case when drugs are tested in animals, as responses of non-human species are often not representative or predictive of human drug responses (O'Brien et al., 2006, Gomez-Lechon et al., 2010).

As the liver is one of the principal organs involved in drug metabolism, the development of a more representative *in vitro* human hepatic model of *in vivo* would be an ideal alternative to predict drug toxicity and provide information regarding dosing while ensuring efficacy (Jetten et al., 2013, Gomez-Lechon et al., 2010). For example, hepatotoxicity is a significant common side effect for drugs to be withdrawn from the market following successful trials, which is not anticipated using the *in vitro* models or human trials (Arrowsmith and Miller, 2013, Kaplowitz, 2005).

In vitro hepatic models aim to meet three key elements for marketing a new chemical entity: efficacy, safety and rigorous testing of toxicity (Temple and Himmel, 2002, Yoon et al.,

2014). New cell lines and novel technologies have been developed in recent years to improve the prediction of different aspects of hepatotoxicity using *in vitro* hepatic models, particularly in replicating human dose-responses, gene expression and morphological change in response to drug treatment (Donato et al., 2013), but they still do not fully mimic human physiological responsiveness (Soldatow et al., 2013). Animal cell lines and *in vivo* animal testing are costly and are not always representative of human metabolism (Shuey and Kim, 2011). Using primary human hepatocytes (PHH) for an *in vitro* human hepatic model would show inter individual variation which may increase the difficulty to understand drug toxicity studies. One alternative is to use human hepatoblastoma cell lines to investigate how culturing in a more modulated and improved physiological environment could reveal important elements required for improvement of *in vitro* hepatic models.

Indeed, human hepatocytes cultured with other non-parenchymal cells in two (2D) and three dimensions (3D) culture have been widely considered to be a reasonable approach to predicting drug toxicity *in vitro* (Ukairo et al., 2013, McGill et al., 2011).

1.1 Liver structure and composition

The liver is the largest organ in the human body, weighing approximately 2% to 3% of the total weight, located in the upper right quadrant of the abdominal cavity and covered by the capsule of Glisson (Abdel-Misih and Bloomston, 2010).

The liver is connected to the human body via the vascular system. The hepatic blood flow is divided in to two blood flows: the hepatic artery and the portal vein. The hepatic artery supplies oxygenated blood to the liver and the portal vein is responsible for the transfer of nutrients and drugs absorbed in the intestine to be metabolised in the hepatocytes. The portal vein also facilitates clearance of toxics and waste in the liver (Godoy et al., 2013).

Most of the liver consists of parenchymal cells (hepatocytes) and the rest of the liver comprises non-parenchymal cells: liver sinusoidal endothelial cells (LSECs), hepatic stellate cells (HSC), also called 'Ito cells or fat-storing cells', Kupffer cells. The liver synthesises essential proteins to maintain vital functions including synthesis of albumin, blood coagulation factors II, V, VII, VIII, protein S and antithrombin as well as immune factors, bile, cholesterol and storage of glycogen, vitamins and nutrients as well as removing toxins (Biron-Andreani et al., 2010, Godoy et al., 2013, Elvevold et al., 2008, Fomin et al., 2013). The main functions of each hepatic cell type are summarised in Table 1-1.

Table 1-1 Composition and function of liver cells.

Several different liver cell types contribute to overall hepatic function and their strategic location allows them to perform metabolic activities key to the maintenance of homeostasis in the liver. Information adapted from (Godoy et al., 2012, Blouin et al., 1977, Wisse et al., 1996, Elvevold et al., 2008, Fomin et al., 2013).

Liver cells	**% liver cells**	**Main Functions**	**Mitochondria volume**
Parenchymal cell Hepatocytes	70-80%	Detoxification Protein synthesis Biliary secretion	28.3%
Non-parenchymal cells			
Liver sinusoidal endothelial cells (LSECs)	20%	Endocytosis Vascularization Migration signalling Blood Clearance Factor VIII	4.3%
Kupffer cells ‘Sternzellen’	>5%	Phagocytosis Endocytosis Immune response	4.5%
Hepatic stellate cells (HSC) ‘Ito cells or fat-storing cells’	>5%	Immune response Storage Vitamin A and retinol ECM synthesis	4.4%

Abbreviations: ECM: Extracellular Matrix

1.1.1 Liver cells

Hepatocytes are 10–20 μM in size and are characterised by having apical (canalicular) and basolateral poles (sinusoidal) which are directly related to their hepatic functionality (LeCluyse et al., 2012). This is the result of their strategic location in sheets which allows them to perform liver metabolic functions, drug metabolism and communication between parenchymal and non-parenchymal cells (NPC) (Figure 1-2). 30% of the liver comprises NPC; including 20% of LSECs and 10% Kupffer and hepatic stellate cells (HSC) (Table 1-1) (Godoy et al., 2012, Blouin et al., 1977).

Hepatocytes and LSECs are separated by the space of Disse (10–15μM). The space of Disse contains the extracellular matrix (ECM), which mainly contains fibronectin and collagen-I, but also some laminin and collagen-III (Godoy et al., 2013). Its composition maintains hepatocyte phenotype and supports HSC which usually exist in a quiescent state. HSC store vitamin A and the interaction between endothelial cells and the extracellular matrix collagen receptors (α1b1, α2b1), laminin (α3b1, α6b1) and fibronectin receptors (α4, α5) has been associated with the promotion of vasculogenesis and cell migration (Hynes, 2007).

Another important characteristic of hepatocytes is their capacity to regenerate in healthy adults and after hepatectomy (Diehl and Rai, 1996). The mechanism of hepatocyte regeneration and differentiation is influenced by LSECs. Hepatic growth factor and vascular endothelial growth factor (VEGFR-2) expressed in bone marrow progenitors cells of LSECs, which are associated to VEGFR1 pathways *in vivo,* play an important role in hepatocytes regeneration (DeLeve, 2013).

LSECs are smaller in size than hepatocytes (6.5 μM) and they are characterised by an open, porous fenestrated endothelium (~100-150 nm) with no basement membrane or diaphragm (DeLeve, 2014). The fenestrae filter and distribute proteins, carbohydrates or fats from the

space of Disse to hepatocytes for their metabolism. LSECs main function is the clearance of waste of macromolecules, including low-density lipoproteins (DeLeve, 2013, Simon-Santamaria et al., 2010, Li et al., 2011) and they also participate in lipid metabolic functions (Salerno et al., 2011). The three main receptors for endocytosis in LSECs are; mannose, scavenger receptor and Fcγ receptor IIb2 (DeLeve, 2013, Simon-Santamaria et al., 2010, Li et al., 2011).

As mentioned previously in Section 1.1, the hepatic sinusoid microcirculation is responsible for the exchange of nutrients and drugs from the blood flow to the hepatocytes through the perisinusoidal space of Disse (McCuskey, 2008). In the absence of a membrane in the hepatic sinusoid, any disruption in the fenestrae can affect the permeability, the filtration of nutrients, the concentration of oxygen and hepatic function (LeCouter et al., 2003). Damage in the hepatic vascular system can also precede the activation of quiescent cells (DeLeve, 2014) and lead to liver diseases such as non-alcoholic fatty liver disease (NAFLD), alcoholic liver diseases, fibrosis (Zhang et al., 2014). In hepatotoxicity, disturbances in the vascular system and in the fenestrae can interfere with blood vessel formation, potentially leading to the infiltration of erythrocytes into the space of Disse in liver drug toxicity, swelling of LSECs and cause necrosis in the hepatic sinusoid (Ito et al., 2003, DeLeve et al., 1997, McCuskey, 2008).

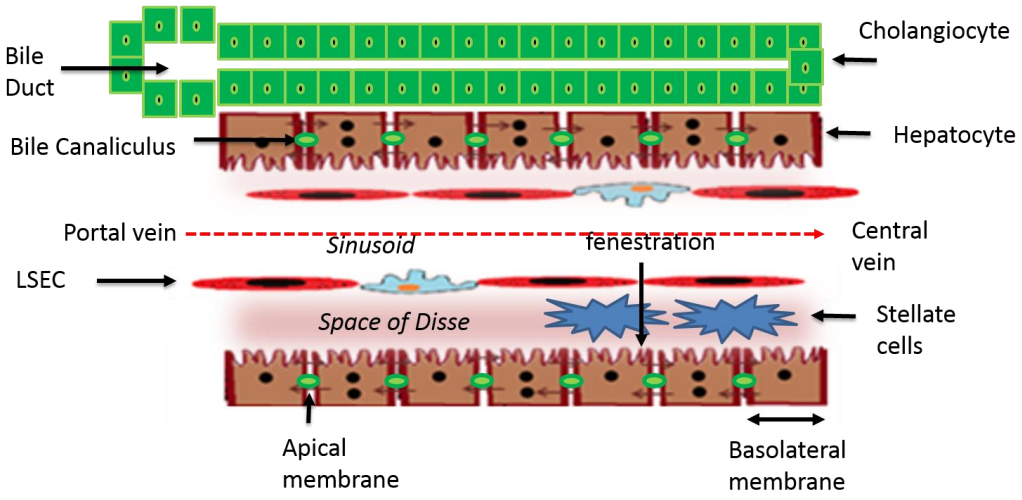

Figure 1-1 Architecture of the liver and liver cells location in the liver

The liver is composed of 80% of hepatocytes (parenchymal cells) and 20% of non-parenchymal cells (LSECs, HSC and Kupffer cells). In the parenchymal area, hepatocytes and LSECs are separated by the space of Disse, which contains the ECM. Although in indirect contact, LSECs filter through the fenestrations nutrients and drugs to be metabolised by hepatocytes.

1.2 Hepatic lobule: acinus

The liver is organised by parenchymal (hepatocytes) and non-parenchymal cells dividing the liver into hexagonal lobules of 1mm in diameter and 2mm in thickness. Their functional subunit is the acinus, a mass of hepatocytes surrounding the sinusoids formed by blood vessels (Figure 1-2). The expanse of the acinus ranges from the terminal portal venule and a terminal hepatic arteriole, delivering blood into the hepatic sinusoid, to the central vein, which ultimately delivers blood to the hepatic vein (Jungermann and Kietzmann, 1996). Oxygen delivery to hepatocytes therefore depends on their proximity to the sinusoid and the size of the fenestrae (DeLeve, 2014), dividing the acinus into three major zones (Figure 1-3): Zone 1 or the periportal area (PP) receives approximately 75% of the oxygen supply and it is where regulation and synthesis of bile, metabolism of urea from ammonia, oxidative metabolism and gluconeogenesis occurs. Zone 2 or pericentral (PC) and Zone 3 or perivenous (PV) areas each receive approximately 25% of oxygen and it is where processes such as detoxification of ammonia into glutamine, metabolism of xenobiotics and glycolysis occur (Jungermann and Kietzmann, 1996).

Cholangiocytes and hepatocytes have their origin in the intrahepatic bile ductules from oval cells (Yovchev et al., 2013) and both are characterised by a polarized structure. The bile canaliculus collects bile secreted by hepatocytes to the gut and the bile is an important way of drug excretion via canalicular transporters such as multidrug resistant-associated protein (Raynaud et al., 2011, Mottino and Catania, 2008).

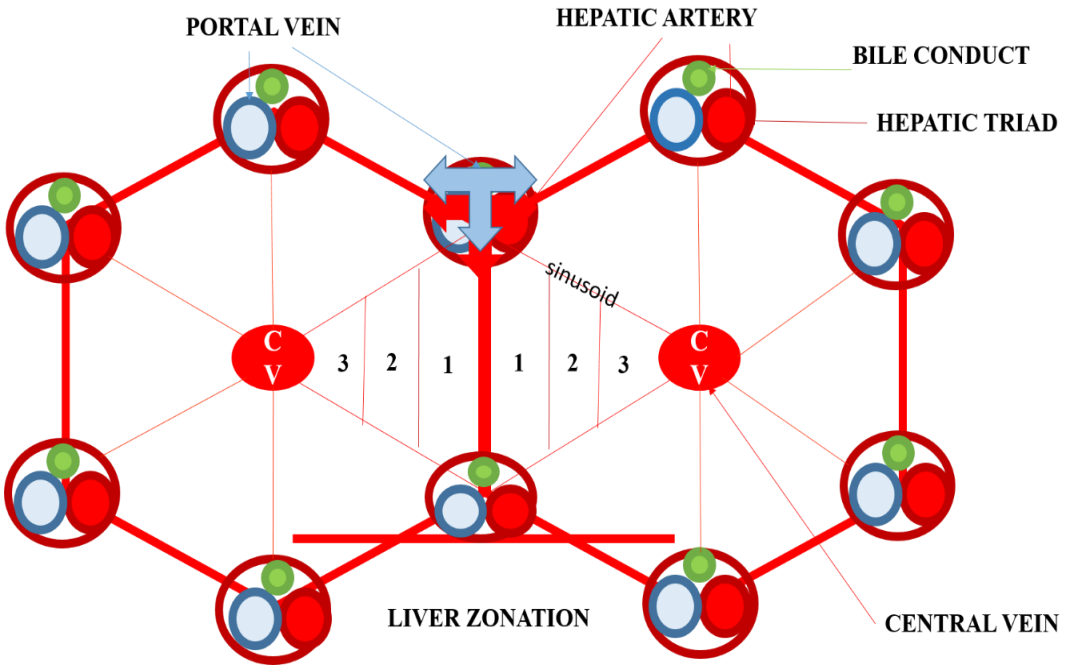

Figure 1-2 Liver lobule; acinus

The liver hexagonal lobules contain the acinus, a microcirculatory functional unit. The acinus is exposed to hepatic blood flow through sinusoids from the portal vein to the central vein and, depending on the quantity of oxygen, the acinus can be divided into three zones with each performing specified functions:

Zone 1 or the periportal area (PP) receives approximately 75% of the oxygen and it is the closest to the portal triad where bile synthesis, β-oxidation, cholesterol synthesis, and glycogen synthesis from lactate and ureogenesis occurs. Zone 2 or pericentral (PC) and Zone 3 or perivenous (PV) areas receive approximately ~25% of oxygen. Glycogen synthesis from glucose, glycolysis, lipogenesis, glutamine and heme synthesis, as well as metabolism of xenobiotics all occur here. Adapted from Godoy et al.(Godoy et al., 2013).

1.3 Intracellular organelles

The intracellular organelle targets involved in drug metabolism are mainly mitochondria, endoplasmic reticulum and lysosomes. However, the mitochondrion is the main organelle in regulating cell death via apoptosis and necrosis. Mitochondrial dysfunction is significantly associated with drug toxicity or non-alcoholic fatty liver disease (Sassi et al., 2014, Lockman et al., 2012).

1.3.1 Mitochondrial structure and function

Mitochondria are approximately between 0.5µm and 10µm in size per cell. Mitochondria are essential in cellular respiration and their main function is to generate most of the adenosine triphosphate (ATP) as the main source of energy (Yehuda-Shnaidman et al., 2013, Ribeiro et al., 2014).

Mitochondria are characterised by a double membrane separated by the intermembrane space: the external membrane and the inner membrane. The inner membrane is characterised by cristae, which provide a larger surface area for the mitochondrial function. In terms of their content, mitochondria have DNA, RNA and ribosomes, which encode 13 polypeptides. Mitochondrial DNA (mtDNA) has a very high genomic density which makes it more susceptible to mutation and reduces the capacity to repair mechanism in the mitochondria (Ribeiro et al., 2014).

1.3.2 Mitochondrial respiration and membrane integrity

Mitochondria oxidise fatty acids via the β-oxidation pathway, synthesise heme, steroids and regulate calcium concentration, which is crucial in several cellular mechanisms such as cell death and the regulation of the mitochondrial permeability transition (MPT) (Pivovarova and Andrews, 2010, Ribeiro et al., 2014).

Glycolysis and oxidative phosphorylation (OXPHOS) are the main mechanisms in ATP production and the amount produced is determined by the type of metabolism: aerobic (high ATP levels) or anaerobic (low ATP levels).

1.3.2.1 Glycolysis metabolism

Glycolysis transforms glucose, taken up by the glucose transporters (GLUTs) in the cytosol. In the liver, the glucose transporter is GLUT2 which transports glucose into the hepatic cytosol to start a chain of reactions and transforms glucose into glucose-6-phosphate by the hexokinase enzyme followed by a series of reactions, to produce pyruvate and lactate as end products (Marin-Juez et al., 2014, Adeva et al., 2013). The balance between pyruvate and lactate is a reversible mechanism that depends on the oxidative state of the cell. This glycolytic pathway can be disrupted, (e.g. in drug toxicity) increasing the conversion from pyruvate to lactate. Pyruvate is transported into the mitochondria and the pyruvate dehydrogenase complex catalyses conversion of pyruvate to acetyl-CoA (Adeva et al., 2013). Then, acetyl-CoA is oxidised by enzymes in the Krebs or tricarboxylic acid. During the Krebs cycle, reduced nicotinamide adenine dinucleotide/flavin adenine dinucleotide ($NADH/FADH_2$) are produced and transported to the electron transport chain (ETC) in oxidative phosphorylation mechanism to finally produce ATP (Sekine et al., 2013).

High levels of lactate can lead to lactate acidosis, which is observed in acetaminophen (APAP) toxicity (Schneider et al., 2014). DILI can lead to reduction in the quantity of ATP formation in the mitochondria and stress in hepatocytes, and thus can cause a reduction in energy and lead to mitochondrial necrosis or apoptosis (Han et al., 2013). This is because ATP levels contribute in a direct way to mitochondrial function. Mitochondria need energy to maintain essential activities including in drug metabolism.

1.3.3 Oxidative phosphorylation (OXPHOS)

Oxidative phosphorylation (OXPHOS) is the series of enzymatic Red-Ox reactions used to produce ATP as a source of energy in the mitochondria. The electron transport chain (ETC) is located in the inner mitochondrial membrane and is composed of five enzyme complexes, complex I (NADH dehydrogenase), complex II (succinate dehydrogenase), complex III (cytochrome bc_1 complex), complex IV (cytochrome oxidase) and complex V (ATP synthase) where ATP is generated. Cytochrome C and coenzyme Q are transporters (Feichtinger et al., 2014, Ribeiro et al., 2014). In this mechanism, the proton pump (complex I, III and IV) generates an electrochemical gradient across the mitochondrial membrane (pH gradient and membrane potential $\Delta\Psi$) (Ribeiro et al., 2014) from the Red-Ox reactions, in which the enzyme complexes act successively as donors (reduction) and acceptors of electrons (oxidation) from bio-products of Krebs cycle and β-oxidation.

In the mitochondria, during the metabolic process of the Krebs cycle, NADH and $FADH_2$ co-factors are generated. NADH is transferred into complex I, and FADH into complex II, to be oxidised. The electrons generated are transferred into complex III by the electron carrier ubiquinone or coenzyme Q and electron carrier cytochrome c makes the transfer to complex IV where the electrochemical gradient is used to generate ATP (Ribeiro et al., 2014) (Figure 1-3).

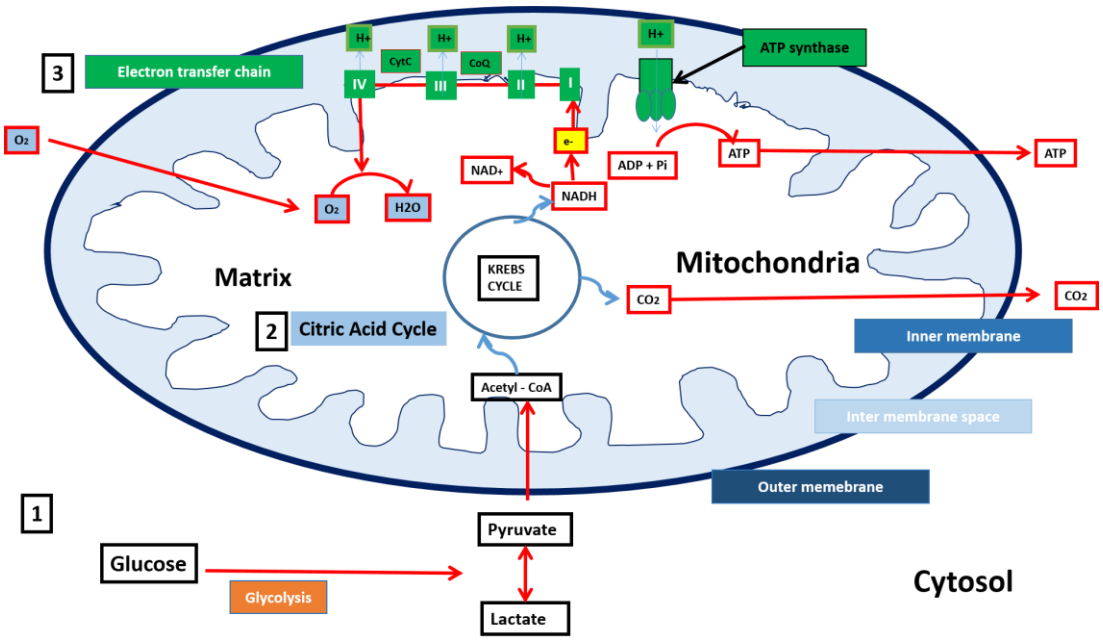

Figure 1-3 Mitochondrial structure and metabolism.

- During the glycolysis, the glucose is broken down to pyruvate, itself potentially reduced into lactate, depending on the cytosolic redox potential (or NAD/NADH ratio). The glycolysis produces 2 molecules of ATP per molecule of glucose oxidised, as well as NADH.

- The pyruvate is transferred into the mitochondria and serves as substrate of the pyruvate dehydrogenase to produce acetyl-coA before it enters the Krebs cycle - also known as tricarboxilic acid cycle or citric acid cycle - generating NADH.

- The NADH, but also FADH2 generated from the oxidation of fatty acids, are reoxidised by the ETC, which transfers protons into the intermembrane space, generating the proton-motive force, while channeling electrons, finally accepted by O2 at complex IV to form H_2O.

- The proton motive force, created by the accumulation of protons in the intermembrane space, is necessary for the production of ATP by the complex V, or ATP synthase.

1.4 Drug metabolism: Phase I and Phase II

Hepatocytes metabolise drugs by transforming them from lipophilic to hydrophilic molecules to facilitate subsequent metabolism and excretion. These drug biotransformations are carried out in two main phases, namely Phase 1 in which changes in drug polarity are achieved through oxidation, reduction and hydrolysis reactions catalysed principally by Cytochrome P450 enzymes (CYP450) and Phase 2 in which drug molecules and biomolecules from phase I are conjugated to increase solubility and facilitate excretion (Deenen et al., 2011).

1.4.1 Cytochrome P450 enzymes (CYP450)

Approximately 90% of drugs are oxidised and reduced by the cytochrome P450 enzymes (CYP450) (Zhu, 2010). CYP450 are heme proteins and the majority of them are located in the human liver but some varieties can be also found in the human small intestine and other organs. There are a number of different CYP450 divided into families and subfamilies (Paine et al., 2006). In the liver, most functional CYP450 enzyme families are CYP1, 2 and 3 and their subfamilies CYP3A4, 2C9, 2C8, 2E1 and 1A2. Most of these are expressed on the endoplasmic reticulum in hepatocytes (Zanger and Schwab, 2013). The most important are CYP3A and subfamily 3A4/5 (Zanger and Schwab, 2013). In drug toxicity, CYP450 activity can be compromised by the volume of drug administered which can reduce efficacy and induce toxicity. Indeed, Phase I metabolism can lead to the formation of highly toxic molecules, the lack of detoxification of which can result in alteration in Ca^{2+} homeostasis, mitochondrial function and oxidative stress in hepatocytes (Gomez-Lechon et al., 2010). These reactive bio molecules can be detoxified by phase II metabolism. For example, in acetaminophen (APAP) mechanism, CYP2E1/CYP3A4/CYP2A1 enzymes transform APAP

into a reactive N-Acetyl-p-Benzoquinone Imine **(**NAPQI) which is detoxified by glutathione (GSH).

Furthermore, co-administration of different drugs at the same time can cause unfavourable drug-drug interactions, leading to further drug toxicity and compromising CYP450 activity (Kamel and Harriman, 2013).

Phase II reactions include glucuronidation, acetylation, s-methylation, glutathione conjugation and sulfo and amino acid conjugation (Deenen et al., 2011). In this phase, drug intermediate compounds such as NAPQI in APAP metabolism, are mainly detoxified by the glutathione S-transferase enzyme family and impairment in their function is associated with hepatotoxicity. The main transferases are UDP-glucuronosyltransferases (UGTs), Glutathione S-transferases (GSTs), and sulfotransferases (SULTs) (Jancova et al., 2010).

In drug toxicity, hepatic membrane transport proteins plays an important role in the absorption of drugs, drug-drug interactions, and excretion of drugs into the biliary and sinusoidal system (Le Vee et al., 2006, Kunze et al., 2012, Shukla et al., 2014). Hepatic membrane transport proteins can regulate the accumulation of drugs in the system, influencing the development of liver failure, and can alter the prediction of the plasma concentration-time curve (Yoshida et al., 2012). Receptors present in the sinusoids and canaliculi such as multidrug-resistance-associated proteins are associated with drug toxicity resistance. Multidrug-resistance-associated proteins receptors can adapt to APAP or carbon tetrachloride toxicity and can up-regulate their expression and increase waste removal in response to such toxicity (Aleksunes et al., 2008).

1.5 Drug induced liver injury (DILI)

Drug-induced liver injury (DILI) is a major issue in drug discovery. Approved drugs can cause DILI even after successfully passing pre-clinical drug toxicity studies in animals and humans trials (Kaplowitz, 2005). For example, in 2011 approximately 86% of drugs did not achieve efficacy and safety standards (Arrowsmith and Miller, 2013).

As the liver is the principal organ in detoxifying the vast majority of external agents, there is a need to develop a more physiologically-relevant human hepatic *in vitro* model to predict drug toxicity and produce more relevant pre-clinical data. And in particular to evaluate the pathways involved in the activation of the cellular mechanisms in apoptosis and necrosis in drug toxicity (McGill et al., 2011, Xie et al., 2014b). This is greatly important for pharmaceutical companies who invest in developing highly effective *in vitro* human models and *in vitro* assays for drug testing (Tourovskaia et al., 2014). These studies are principally based on the importance of improving *in vitro* human models to represent *in vivo* liver-like function, and additionally in an attempt to reduce the use of animal models (Xie et al., 2014b).

Drug toxicity in the liver mainly occurs as a sequential chain of events and is linked to the regulation of nuclear receptors, including pregnane X receptor, constitutive androstone receptor or hepatocyte nuclear factor-4. Those mechanisms regulate the CYP450 enzyme activity which is crucial in the metabolism of most of drugs and a reduction in their activity can determine the accumulation of toxins inside cells (Hoekstra et al., 2013, Zanger and Schwab, 2013, Wang et al., 2004, Sahi et al., 2009, Ulvestad et al., 2013). Accumulated toxins can then perturb mitochondrial function and enhance reactive nitrogen species (RNS) and reactive oxygen species (ROS) formation (Nel et al., 2006).

When a drug is associated with organ failure, a warning is displayed on the label requiring the notification of patients by a health professional; alternatively the drug can be directly withdrawn from the prescribing list (Shah et al., 2013). The list of hepatotoxic drugs is getting longer with the constant addition of drugs associated with liver injury.

Alcohol or APAP are examples of external agents causing major induced liver injury (Jaeschke et al., 2013). Therefore, APAP is a typical example of a hepatotoxic drug used in *in vivo* and *in vitro* hepatic models. APAP can be obtained over the counter and it is safe at therapeutic doses for treatment of pain and fever. However, adults should not exceed 1g of APAP per dose and 4g per day because APAP can be highly hepatotoxic when taken at doses > 4 g/day (Schafer et al., 2013).

Primary human hepatocytes (PHH) became necrotic at 24hr in acetaminophen (APAP) overdose (Xie et al., 2014b). This mechanism is the result of the activation of C-Jun N-terminal kinase following mitochondrial dysfunction, and causes a rise in ROS formation in the mitochondria (Xie et al., 2014b). However, there are additional mechanisms which can also be activated through mitochondrial dysfunction, leading to cell death. For example, cysteine proteases (caspases 3, 8, 10) are additionally activated by the mitochondria-apoptosis mechanism (Xiong et al., 2014).

APAP has been widely investigated in rodents (Agarwal et al., 2012, Kato et al., 2011) and conventional *in vitro* hepatic models (McGill et al., 2011, Aritomi et al., 2014). However, its mechanism of action in the liver not only affects hepatocyte function, but may also have deleterious effects on the endothelium, especially in the early stages of hepatotoxicity (DeLeve et al., 1997, Ito et al., 2003). Prediction of APAP toxicity using an *in vitro* hepatic model using a combination of parenchymal and non-parenchymal cells might therefore be valuable in determining unknown APAP toxicity mechanisms and also cell-cell interaction in the activation of drugs in the liver, not revealed in mono-culture (Ito et al., 2003, Toyoda et

al., 2012). APAP is often used as a model to understand cytotoxicity *in vitro*, but a model of DILI to fully predict human drug toxicity is still lacking (Jaeschke et al., 2013). In humans, APAP can be toxic at high doses and only rarely at normal doses does toxicity arise due to an idiosyncratic reaction (immune response) depending on race, age and sex (Han et al., 2013).

1.6 Drug induced mitochondrial dysfunction

As described previously, mitochondria are a critical target in the activation of intracellular mechanisms of hepatotoxicity.

Drug toxicity can specifically affect mitochondrial permeability transition (MPT), integrity of the mtDNA, and function of glutamate dehydrogenase, reducing the probability of cell survival (McGill et al., 2014). When drug toxicity affects mitochondria, the MPT pore opening increases its permeability, increasing exposure to reactive nitrogen species (RNS) and reactive oxygen species (ROS) (Pessayre et al., 2010).

Mitochondria are one of the main organelles responsible for the formation of ROS as by products during ATP production. However, the formation of reactive oxygen molecules from drug activation can increase the ROS formation and often leads to mitochondrial dysfunction and susceptibility to lipid peroxidation in hepatocytes, resulting in widespread necrosis (Agarwal et al., 2012, Jaeschke et al., 2013).

Under normal conditions, the principal antioxidant superoxide dismutase, glutathione peroxidase and catalases neutralise ROS formed during ATP generation or drug metabolism via CYP450 activity (Knight et al., 2002, Jaeschke et al., 2003). Oxidants such as hydrogen peroxide, formed from the superoxide anion radical, are produced in low concentrations and can be detoxified by antioxidants in the mitochondria. However, when oxidants are at high

concentrations, the electron transport chain can be disrupted and the mtDNA can become fragmented (Maharjan et al., 2014).

ROS and RNS are not only generated in the mitochondria, they can also be generated in the endoplasmic reticulum or by peroxisomes (Fransen et al., 2012). The disruption of the mechanism of β-oxidation of fatty acids can cause accumulation of lipid peroxides in the mitochondria (steatosis). Liver disease such as steatosis can also cause liver failure (Germano et al., 2014).

Drugs such as APAP or tamoxifen (TAM) can compromise mitochondrial function (Ribeiro et al., 2014, Jaeschke et al., 2012b). APAP at high doses, can compromise mitochondrial respiratory function and form superoxide anion radicals (O2·-) which are associated with the excess of NAPQI formation (McGill and Jaeschke, 2013, Pessayre et al., 2010, Martin et al., 2003). The O2·- in contact with nitric oxide can form ROS and RNS, including the peroxynitrite anion (ONOO-). The formation of ROS and cytokines such as tumour necrosis factor-α (TNF-α), is not restricted to hepatocytes and also occurs in NPC liver cells such as Kupffer cells (Kojima et al., 2014) or hepatic stellate cells (Hsieh et al., 2014) leading to enhanced mtDNA fragmentation. In the absence of ROS, an increase in nitric oxide (NO) output by LSECs can play a protective role, inducing vasodilation, whilst its reduction is associated with endothelial dysfunction (Zhang et al., 2014).

Under standard conditions, levels of oxidative stress are low compared to the relatively high levels of antioxidants such as GSH. In cytotoxicity, GSH levels are low and oxidants high (ROS and RNS formation).

In hepatotoxicity, there are many mitochondrial apoptosis mechanisms induced by cell signalling which remain unknown. However, one of the most important activation mechanisms in apoptosis is the caspases pathway (Xiong et al., 2014) which, in contact with TNF-α, can cause cell death (Feldstein et al., Ray and Jena, 2000).

During drug induced oxidative stress, mitochondria respond with the activation of antioxidant pathways, including transcription factor erythroid 2-related factor 2 or hypoxia-inducible factor 1-α antioxidant defence (Pullikotil et al., 2012, Aleksunes et al., 2008). However when these cellular mechanisms and antioxidants are not sufficient to cope with the oxidants produced in drug metabolism, cells can activate apoptosis pathways. One of the early mechanisms leading to this is mitochondrial dysfunction (Nel et al., 2006, McGill et al., 2014). For example, this could be triggered when NAPQI depletes mitochondrial GSH content, which would normally inhibit formation of ROS and peroxynitrite in the mitochondria (Jaeschke et al., 2003).

The activation of caspases, which contribute to the apoptosis mechanism, can be inhibited by the addition of small molecule inhibitors such as small molecules or inhibitor such as 2-aminoethoxy-diphenyl-borate or Bcl-2 (anti-apoptotic protein) (Du et al., 2013, Xie et al., 2014b).

The administration of APAP can disrupt the respiratory chain with ATP depletion and increase ROS formation, overwhelming antioxidants systems and thus causing mitochondrial dysfunction and cell death (Panatto et al., 2011). To reduce APAP-induced liver injury, antioxidants can be administered, including glutathione (GSH) or n-acetylcysteine (NAC) (Saito et al., 2010). However, NAC seems to be most effective, when is administrated within 48hr after APAP exposure (Martin et al., 2003). Otherwise, in later stages ROS will already have activated apoptosis mechanisms resulting in liver cell damage (Badmann et al., 2012, Du et al., 2013). Between GSH and NAC, it seems that GSH is more effective in increasing ATP levels than NAC (Saito et al., 2010).

Tamoxifen (TAM) also can cause idiosyncratic DILI. Although TAM is not a dose-dependent drug, long-term therapy can cause an increase in lipid production and reduction in

superoxide dismutase activity (antioxidant) within the mitochondria, resulting in steatohepatitis (Ribeiro et al., 2014).

Both APAP and TAM can raise the hepatic enzyme release, which become measurable in the patients' blood, such as aspartate aminotransferase (AST) or alkaline phosphatase (ALP) (Agarwal et al., 2012, Ribeiro et al., 2014, Aleksunes et al., 2008).

The study of those two drugs demonstrate the importance of mitochondrial dysfunction in the development of hepatotoxicity and the need to focus on mitochondrial function in studies with new drugs to minimise and avoid drug toxicity.

1.7 *In vitro* hepatic models for drug metabolism studies

As mentioned previously, the liver metabolises most of the drugs and the majority of *in vitro* hepatic models are based on mono-culture of animal or human hepatocyte cell lines. However, despite several significant advances, drug-induced liver injury is still a major difficulty to predict in those models. Using a more physiological *in vitro* human hepatic model could help in predicting drug toxicity before drugs are tested in human trials and may also reduce animal testing (Jetten et al., 2013). Development of a high throughput screening compatible *in vitro* hepatic model, combining hepatocytes and endothelial cells, would improve the study of drug metabolism by the liver.

Significant hepatic functions such as drug metabolism or albumin synthesis, are difficult to maintain in hepatocytes when they are cultured *in vitro*, and this makes the available hepatic models, (which include liver slices, microsomes and liver S9 fractions) not ideal for hepatotoxicity studies (Gomez-Lechon et al., 2014, Soldatow et al., 2013). The main reason for thus is the short-viability of these models and the lack of the major phase I or phase II enzymes (Gomez-Lechon et al., 2004). Since the use of *in vitro* animal hepatic models lead to unreliability in extrapolating data to humans, the selection and combination of different

cells lines to achieve a more physiological model is the principal difficulty (Jetten et al., 2013).

PHH are considered the gold standard because they contain the main enzymes and hepatic membrane transport proteins for drug metabolism analysis and can be used as a potential model to evaluate new drugs (Rotroff et al., 2010). However, their isolation from liver tissue is complex and with a low percentage of success (Bhogal et al., 2011) and their stability is limited with considerable reductions in drug metabolising enzyme activity occurring during isolation and short term culture (Jetten et al., 2013). The other main disadvantage of PHH is the inter-individual differences in the expression of drug metabolizing enzymes between donors (Zhou et al., 2009, Jetten et al., 2013). A number of alternatives have been developed during the last decade to address these problems. One of these uses immortalized hepatocytes cell lines.

Immortalized hepatocytes cell lines are a valuable alternative for *in vitro* hepatotoxicity studies as they provide an unlimited supply, are reproducible, easily maintained and inexpensive models (Tsiaoussis et al., 2001).

One of the cell lines most used by the pharmaceutical industry is the C3A clonal derivative of the HepG2 cell line selected for strong contact inhibition of growth, high albumin production, high production of alpha fetoprotein (AFP) and ability to grow in glucose deficient medium (Seeland et al., 2013, Ramaiahgari et al., 2014, Choucha Snouber et al., 2013). C3As are metabolically active and mostly used for drug toxicology studies (Gomez-Lechon et al., 2014), bio artificial liver supports systems (Filippi et al., 2004, Yang et al., 2013b) or for the development of *in vitro* non-alcoholic fatty liver disease models (Lockman et al., 2012). Other immortalized cell lines, which include Huh 7 for example, lack expression of important Phase I or Phase II metabolising enzymes, when compared with PHH (Guo et al., 2011, Sjogren et al., 2014).

Recent approaches have emerged to improve current *in vitro* hepatic models. Novel hepatic cell lines are being exploited to predict drug toxicity *in vitro.* Gripon *et al* have described the novel HepaRG hepatic cell line (Gripon et al., 2002), which shows promise for pharmaceutical applications, and may be comparable to PHH for drug metabolism and hepatotoxicity studies (Parent et al., 2004, McGill et al., 2011, Lübberstedt et al., 2011, Aninat et al., 2006). HepaRG cell cultures are bipotential comprising a combination of hepatocyte-like and biliary-like epithelial cells and possess a variable percentage of each cell line between passages, thus representing the natural variability observed in a hepatic co-culture system (Gripon et al., 2002, Jetten et al., 2013).

Human hepatocyte surrogates such as HepaRG or primary hepatocytes have been used to determine drug metabolism and drug-drug interactions as they are more representative of predicting drug toxicity *in vivo* than microsomes or liver slides (Ferreira et al., 2014, Gomez-Lechon et al., 2004).

These cells are therefore used for High Throughput Screening (HTS) become of their high reproducibility for investigation of hepatotoxicity (Kostadinova et al., 2013, Gomez-Lechon et al., 2014, Aritomi et al., 2014). HTS is a technique that allows the screening of thousands of compounds candidates to identify those with therapeutically efficacy and lack of drug toxicity. The use of HTS allows investigation drug-drug interactions and multi doses. A human model for HTS may represent an alternative for animal drug testing (Ramaiahgari et al., 2014). However, despite their advantages in drug discovery, cell lines such as HepG2 have shown lower CYP450 expression than PHH or HepaRG (Jetten et al., 2013) and improvements in cell culture are needed to characterise drug toxicity *in vitro.*

However, as mentioned in Section 1-2, drug toxicity can also affect hepatic non-parenchymal cells such as endothelial cells (Badmann et al., 2012, Toyoda et al., 2012). These limitations may be overcome with the addition of different cell lines using co-cultures

to promote hepatic function and vascularization *in vitro.* The reproduction of liver cell-cell interactions in *in vitro* hepatic models will be essential in the understanding of intercellular protective mechanisms in drug metabolism.

In vitro co-cultures models combining primary hepatocytes (rat, mouse or human) with a type of endothelial cells have shown important advantages in supporting hepatocyte function, including albumin synthesis in the long term and hepatic vascularization *in vitro* (Ohno et al., 2009, Nahmias et al., 2006, Soto-Gutierrez et al., 2010). Most of the *in vitro* co-culture studies concluded that secretion of different cytokines and soluble factors from non-parenchymal cells enhance hepatocyte differentiation and hepatic function (Bale et al., 2014a, Leong et al., 2013, Soto-Gutierrez et al., 2010, Kim et al., 2012, Ohno et al., 2009, Salerno et al., 2011).

Endothelial cells activate significant cytoprotective signals which lead to important functions including angiogenesis, migration, vasodilation, ROS formation in repair liver injury and result in reduced cell death (Donahower et al., 2010). In these mechanisms, endothelial cells secrete and express cytokines and adhesion molecules, which are essential to regulate the aforementioned pathways. For example, platelet endothelial cell adhesion molecule (PECAM-1), also known as cluster of differentiation CD31, expressed on different endothelial cells can regulate vascularization, superoxide dismutase formation and caspase activation (Liu et al., 2006, Saragih et al., 2014, Tsuneki and Madri, 2014).

Vascular endothelial growth factor expressed in hepatocytes can regulate endothelial receptors such as vascular endothelial growth factor receptor-1 and receptor-2 (VEGFR-1 and VEGFR-2 (Hwa et al., 2007). VEGFR-2 regulates the generation of anti-oxidants such as NO which is highly important in the regulation of vasodilation, migration, angiogenesis and has a cytoprotective effect in mitochondria, inhibiting the PI3K apoptosis mechanism

(Aharoni-Simon et al., 2012, Cox et al., 2014, Jaeschke et al., 2012b, Alva et al., 2013, Saraswati et al., 2013, Zachary and Gliki, 2001). Hepatic VEGF signalling is essential in restoring the hepatic vascular system in injury (Wang et al., 2012a, Stolz et al., 2007) and also in liver organogenesis in the embryo (Matsumoto et al., 2001).

The appropriate selection of endothelial cells to reconstruct an accurate *in vitro* hepatic model is complex, as LSECs are difficult to obtain and to conserve their phenotype *in vitro* (Elvevold et al., 2008, DeLeve et al., 2004, March et al., 2009). However, published studies have addressed this disadvantage using cell lines such as HUVECs (Inamori et al., 2009, Salerno et al., 2011). HUVECs share properties to LSECs such as the expression of CD31 (Elvevold et al., 2008, Kjaergaard et al., 2013) or von Willebrand factor (Shahidi et al., 2014). Furthermore, HUVECs have been used in combination with hepatocytes to reproduce better the hepatic sinusoid and investigate paracrine signalling (Nahmias et al., 2006, Ho et al., 2013) and modulate drug response and toxicity *in vitro* (Toyoda et al., 2012).

1.8 *In vitro* hepatic model in two-dimensional and three-dimensional culture

Hepatocytes cultured in two-dimensional (2D) static culture rapidly lose polarity and differentiated function, and have poor levels of viability and gene expression for drug metabolism and toxicity assays (Nelson et al., 2010, Donato et al., 2013). Meanwhile, hepatic and endothelial cultures in more physiological extracellular matrix have been shown to maintain proliferation and promote hepatic and endothelial differentiation, allowing the establishment of a better hepatic drug metabolising model for drug toxicity studies (Godoy et al., 2013, Tourovskaia et al., 2014, Toyoda et al., 2012).

A further advantage of this approach is to be able to culture hepatocytes in three dimensions (3D). Hepatic activity of albumin synthesis, urea synthesis and expression of drug metabolising enzymes (CYP3A4 activity) improve when hepatocytes are cultured in a more liver-like environment using novel technologies like 3D culture using scaffolds or extracellular matrices (Kostadinova et al., 2013, Leong et al., 2013).

Spinner flasks, perfusion systems, rotating wall vessels and microfluidic chips are widely used in tissue engineering and these systems could provide 'proof-of-feasibility' and more physiologically representation of the *in vivo* situation (Allen et al., 2005, Bhatia and Ingber, 2014). Spheroids have demonstrated that collagen as an ECM results in a covered hepatic vascularised tissue *in vitro* (Inamori et al., 2009). Similar observations have been shown using endothelial and hepatocytes in hydrogel fibres (Leong et al., 2013), cell sheets (Harimoto et al., 2002) or using an open porous scaffold (Chou et al., 2013).

Culturing cells in appropriate 3D micro environments allows for the development of more complex (and physiological) cell-cell and cell-matrix interactions and establishes gradients of growth factors to cultured cells better than using 2D systems (Tourovskaia et al., 2014). Moreover, recapitulation of the proper micro environment, is also important for encouraging

in vivo–like cell migration and characteristic paracrine signalling (Leong et al., 2013, Nahmias et al., 2006, Swartz and Fleury, 2007).

Extracellular matrix (ECM) containing collagen, fibronectin, laminin and cell adhesion molecules plays an important role promoting cell differentiation and migration in liver organogenesis (Moir et al., 2012). For example, hyaluronic acid is an essential component of the ECM synthesized by hepatic stellate cells (HSC) and endothelial cells in rats during liver regeneration (Vrochides et al., 1996). Puramatrix maintains rat primary hepatocytes in a fully functional state for up to 90 days (Giri et al., 2013). However, compared to these available matrices, Matrigel™ provides a better 3D culture environment for stem cells differentiation (Rowland et al., 2013).

The development of an *in vitro* vascularised model would allow understanding of the principles of vascularization and cell migration. To regenerate an accurate *in vitro* human hepatic model it is thus essential to be able to control mechanisms of vasculogenesis in two or three dimensional culture.

Vasculogenesis and angiogenesis are two different processes both leading to vascularisation. Vasculogenesis refers to the formation of new vessels, whereas angiogenesis is the formation of vessels from existing vessels (Carmeliet, 2000). These two mechanisms can be initiated with or without stimulation of paracrine signalling (e.g. VEGF) during liver organogenesis in the embryo or in response to disease (Lee and Niklason, 2010, Matsumoto et al., 2001). Angiogenesis taking place in wound healing is regulated mainly by endothelial signalling, including VEGF, (Knudsen and Kleinstreuer, 2011). Endothelial cells can up-regulate VEGFR-1 and VEGFR-2, CD31 or VE-Cadherin receptors which act as regulators in differentiation, permeability, migration, wound healing, angiogenesis and maintenance of fenestrae (LeCouter et al., 2003, Matsumoto et al., 2001, DeLeve, 2014, Schmidt et al., 2007). VEGFR-2 stimulates endothelial mobilization in hypoxic conditions by activation of

hypoxia-inducible factors, resulting in an increase in permeability and vasodilation with participation of nitric oxide (NO), regulation of endothelial receptor such as CD31 (Carmeliet, 2000) and maintenance of the phenotype in LSECs (DeLeve, 2014). The presence of NO also contributes in maintaining HSC in a quiescent state (DeLeve, 2014) and HSC can be activated in response to liver damage, becoming myofibroblast-like cells with induction of extracellular matrix synthesis, laminin or collagen synthesis, causing fibrosis (Godoy et al., 2012, Reichen, 1999, Schuppan et al., 2001, Vinken, 2013).

The representation of an *in vitro* vascular system is fast becoming an important prerequisite in accurate representation of drug metabolism and maintenance of hepatic function. In liver injury, a phenomenon of "hepatocyte-sinusoid alignment" occurs, in which hepatocytes proliferate along the sinusoids when endothelial cells are still viable (Hoehme et al., 2010). The phenomenon emphasises the importance of keeping the vascular system healthy and in contact with hepatocytes, as when the distance between hepatocytes and the sinusoid increases hepatocytes lose function (Hoehme et al., 2010). There are several studies which focus on the importance of this aspect of cell-cell contact. For example Inamori *et al*. demonstrated in 2009 that HUVECs can attach to rat hepatocytes when they are covered by collagen-I to form spheroids, suggesting the importance of cell-extracellular matrix interaction. In *in vitro* hepatic co-culture models, LSECs contribute to hepatocyte viability in microfluidic systems (Maher et al., 2014) and co-cultures in bioreactors provides better understanding about paracrine signalling and the source of hepatic growth factors for further liver regeneration mechanisms (Schmelzer et al., 2009). The simulation of the blood flow can contribute to the regulation of the oxygen and the exposure to a shear stress to cells can improve function and improve interpretation of cell migration in drug studies (Bhatia and Ingber, 2014). Microfluidic systems simulates shear stress and induce paracrine signalling between hepatic cells. The dynamic flow distributes these chemokines, resulting in better metabolic and functional activities (Marrone et al., 2014).

1.9 Conclusions

In this introduction, evidence has been presented on the current weaknesses in predicting drug toxicity using only hepatocytes alone as an *in vitro* hepatic model. Current *in vitro* hepatocyte models do not fully predict drug toxicity as they do not fully represent *in vivo* liver functions. Although hepatocytes have high plasticity, their metabolic capacity and morphology are compromised when cultured in conventional 2D mono-cultures. The reasons for their dysfunction and phenotype lose may be due to the lack of interactions between hepatocytes and non-parenchymal cells in an appropriate extracellular matrix (Godoy et al., 2013).

The improvement of *in vitro* hepatic models, combining hepatocytes and endothelial cells to more accurately represent *in vivo*, could thus reduce the unnecessary exposure of humans to unknown drug toxicities and ineffective drugs as well as reduce animal testing.

To summarise, *in vivo*, hepatocytes can suffer a potential damage but also endothelial cells can be affected by drug toxicity (Ito et al., 2003). These are reasons to consider in an *in vitro* hepatic model, the use of endothelial cells in combination with hepatocytes to predict drug toxicity (Godoy et al., 2013, Ito et al., 2003).

For example, in APAP toxicity, endothelial cells and hepatocytes act synergistically to activate cellular mechanism, including VEGF signalling to induce hepatic regeneration after APAP toxicity (Kato et al., 2011, Ito et al., 2003) and the lack of endothelial cells in an *in vitro* hepatic model probably makes more difficult to represent paracrine signalling happening in hepatotoxicity.

This type of evidence reflects the significant contribution of endothelial cells to a hepatic model and the importance of maintaining an intact and functional vascular system in 2D or 3D culture to accurately represent cell-cell interactions using endothelial and hepatocytes for

drug studies. As discussed previously, this is because when a drug is administered, other liver cells in addition to hepatocytes have an important effect on the metabolism of the drug including drug activation and metabolism (LeCluyse et al., 2012, Toyoda et al., 2012, Badmann et al., 2012). Development of a system which efficiently provides nutrients and distributes oxygen, simulating the acinus zonation and interstitial flow seen *in vivo*, may enhance current pharmaceutical drug evaluation strategies (Bhushan et al., 2013, Nelson et al., 2010, Bhatia and Ingber, 2014).

Moreover, an *in vitro* human hepatic model should offer an improvement over animal-based cultures in predicting a large number of drug toxics compounds and the data should be able to be extrapolated to humans and used to establish the maximum tolerated dose. Finally, approaches to increase efficacy and to maximise the safety of human drugs can provide a positive impact in the reduction of side effects and emergency treatments for adverse drug related injury.

1.10 Thesis aims

The major aim was to develop an improved *in vitro* human hepatic model for prediction of hepatic toxicity by exploring co-culture of hepatocytes with endothelial cells. Most of the available *in vitro* hepatic models use animal or human hepatocytes or cells lines in mono-culture. The reproduction of hepatocyte and endothelial cell interactions may provide more reliable prediction of metabolic indicators of drug toxicity.

To develop this *in vitro* human co-culture model, several key points needed to be investigated:

1. **Development of an *in vitro* human co-culture model using Human Umbilical Vein Endothelial Cells (HUVECs) and hepatocytes (C3As) (HUVEC:C3A) in conventional culture:** Investigation of the biocompatibility, proliferation and culture conditions of an *in vitro* hepatic model using HUVECs and C3As.
2. **Morphological, phenotypic and functional characterization of an *in vitro* hepatic co-culture model:** Comparison of morphology, phenotype and hepatic function including albumin synthesis and drug metabolism enzymes (CYP450) of hepatic and endothelial mono- and co-cultures for the pre-clinical assessment of new candidates for drug development.
3. **Drug toxicity studies: Investigation of the effect of the hepatotoxic model acetaminophen (APAP) on parameters of mitochondrial function and oxidative stress:** Investigation of cellular mechanisms involved in hepatotoxicity using HUVEC and C3A in mono- and co-cultures.
4. **Cell migration studies:** Investigation of cell migration and cross-talk between endothelial and hepatocytes using a rich extracellular matrix, to build an *in vitro* vascularised hepatic tissue.

2 Chapter 2: Heterotypic co-culture of HUVECs with the human hepatic cell line C3A: Morphological, phenotypic and functional characterization

2.1 Introduction

Drug-induced liver injury (DILI) is a major ongoing challenge for the pharmaceutical industry. Pre-clinical investigation of new candidate drugs, using *in vitro* hepatic models which closely resemble human liver function, is highly desirable to mimic *in vivo* metabolism and reduce animal testing. Also, animal studies may be insufficient to predict human drug toxicity due to inter-species differences in drug metabolic pathways (O'Brien et al., 2006). Furthermore, current *in vitro* human hepatocyte mono-cultures models are limited by tissue availability and do not always accurately represent drug metabolic pathways that occur *in vivo* (Gomez-Lechon et al., 2014).

Over the period 1991-2000, approximately 30% of licensed drugs were withdrawn from the market despite passing both *in vitro* and *in vivo* toxicity testing (Kola and Landis, 2004). With recent estimates for development of each new drug of between $868m to $1,241m USD, this represents a huge financial cost to the pharmaceutical industry and a disincentive to future drug development (Ciociola et al., 2014).

Hepatic models using primary human hepatocytes (PHH) are currently preferred for *in vitro* drug testing; however, they have major limitations for prediction of drug toxicity. PHH are scarce and expensive, while they present batch variation in hepatic function, with CYP450 activity declining rapidly in culture (Gomez-Lechon et al., 2014). Practical alternatives for PHH in drug testing include immortalized cell lines, such as C3A cells. Although C3As have somewhat limited CYP450 activity, they are inexpensive and easy to culture while maintaining stable metabolic activity and provide a reproducible and sustainable supply of

cells to model hepatic function. Indeed, C3As have been successfully applied previously in our laboratory, investigating non-alcoholic fatty liver disease (Lockman et al., 2012) and bio artificial liver systems (Filippi et al., 2004).

For improved prediction of *in vivo* drug metabolism mechanisms using *in vitro* hepatic models, hepatocytes require an environment which reproduces *in vivo* interaction and cross-talk with endothelial cells (Ohno et al., 2009, Soto-Gutierrez et al., 2010, Toyoda et al., 2012).

Endothelial cells have a significant role in clearance from the portal venous circulation (Smedsrod et al., 1990, DeLeve, 2013); and while hepatocytes are mainly responsible for hepatic drug metabolism and are the principal targets of hepatotoxic drugs, endothelial cells can be also affected by drug toxicity (Badmann et al., 2012, Ito et al., 2003, Deleve, 1994). To emphasise the contribution of endothelial cells in maintaining the hepatocyte phenotype, important interactions between hepatocytes and endothelial cells have also been observed during hepatocyte differentiation and hepatic organization for liver tissue development *in vitro* (Xin et al., 2001, Matsumoto et al., 2001, Bale et al., 2014a, Inamori et al., 2009, Soto-Gutierrez et al., 2010, Nahmias et al., 2006).

In vivo, the secretion of cytokines such as vascular endothelial growth factor (VEGF) and hepatic growth factor (HGF) from endothelial cells implicates vascular function in hepatocyte differentiation (Matsumoto et al., 2001, Soto-Gutierrez et al., 2010), regeneration and the maintenance of liver sinusoidal endothelial cell (LSECs) markers, including: CD31 (March et al., 2009, Hwa et al., 2007). Expression of the endothelial cell marker, CD31, has been used to monitor the endothelial phenotype (Elvevold et al., 2008); whilst epithelial cell adhesion molecule (EpCAM) has been used as a marker for adult hepatocytes (Mitra et al., 2012).

However, CD31 is not expressed by all types of endothelial cells, and its expression on rat liver sinusoidal endothelial cells can be suppressed in the presence of hepatocytes or stellate cells via paracrine and autocrine pathways (DeLeve et al., 2004, March et al., 2009). To date, this inhibition in CD31 expression has not been investigated in HUVECs co-cultured with other human hepatic cell types.

Human LSECs differ from other vascular endothelial cells in the human body (Elvevold et al., 2008). They have also been shown to have different phenotype compared to mouse LSECs (e.g. immune-factors)(Fomin et al., 2013). LSECs have open fenestrations in their cytoplasm to allow nutrients transfer to hepatocytes and another characteristic is the lack of basal lamina underneath the endothelium. Amongst its function, LSECs have a strong endocytotic capacity not observed in other cell lines (Elvevold et al., 2008) and synthesis of Factor VIII (Fomin et al., 2013). LSECs are, however, difficult to isolate and present an unstable phenotype (DeLeve et al., 2004, Salerno et al., 2011, Elvevold et al., 2008, Fomin et al., 2013). Published studies have therefore used macro-vascular endothelial cells, principally HUVECs, as hepatic sinusoid endothelial cell surrogates to demonstrate the importance of the interaction between endothelial and hepatocytes in drug metabolism (Toyoda et al., 2012, Salerno et al., 2011) and in liver tissue formation *in vitro* (Nahmias et al., 2006).

One of the most relevant function of endothelial cells is the capacity to interact with other liver cells which implicates activation of endothelial receptors and mechanisms to maintain normal phenotype and functionality *in vitro* (DeLeve et al., 2004, March et al., 2009, Khodarev et al., 2003).

My hypothesis was that the combination of HUVECs and C3As as ‘organotypic’ co-cultures in an *in vitro* hepatic model would promote cell-cell interactions as well as cell-matrix

interactions and improve hepatic function and endothelial phenotype to provide a better human liver function representation *in vitro*, particularly in the context of drug testing.

Here, the aim was to develop an improved human hepatic *in vitro* organotypic co-culture model for use in drug toxicity studies *in vitro.* To achieve this, HUVECs and C3As were co-cultured to test the hypothesis that endothelial cells could both improve functionality of C3As in co-cultures, and provide a more physiologically-relevant model for drug testing. The first step in developing the model was to define a suitable cell culture medium, which would provide trophic support for both cell types whilst maintaining their individual phenotypically differentiated functions. Next, we sought to identify the optimal ratio of HUVECs and C3As required to maintain growth and function in co-cultures; and to design protocols to optimise cell seeding and assay of hepatic function. To determine the effect of culture conditions on each cell type and the contribution of paracrine regulation, in each experiment co-cultures were phenotyped using cell type-specific markers.

Experiments were designed to assess the following research questions:

(i) Characterization of hepatic and endothelial cell type-specific (HUVECs or C3As) phenotypic markers for identification of each cell line in co-cultures.

(ii) The selection of an optimal cell culture medium, either hepatic medium (MEME) or endothelial medium (EGM-2), suitable for maintenance of HUVECs and C3As in co-cultures, without altering their phenotype from that seen in standard mono-cultures. Monitoring the maintenance of specific-endothelial (CD31) and hepatic adhesion molecule (EpCAM) expression, and cell morphology, which are vital in construction of an *in vitro* co-culture system because a reduction in their expression and morphology might reflect a reduction in function and viability.

(iii) The period and relative ratio of HUVECs and C3A required in co-cultures was also tested. A titration was used to test alternative ratios (1:3; HUVEC:C3A),

1:1 (HUVEC:C3A), 3:1 (HUVEC:C3A) which were assessed on day 3 and day 7 after plating, with proliferation rate and viability being used to determine the optimum ratio and culture period.

(iv) Evaluation of the effect of HUVECs on C3As functionality included measurement of albumin synthesis, urea production and basal CYP3A4 activity in co-cultures as compared with mono-cultures.

(v) The extent of paracrine signalling between endothelial and hepatocytes cells was also evaluated.

2.2 Materials and Methods

2.2.1 Cell culture general maintenance

Human hepatocellular carcinoma, C3A cells were obtained from the American Type Culture Collection (CRL-10741, USA) and cultured in Minimum Essential Medium Eagle (MEME Sigma). HUVECs were obtained from Lonza (C2519A) and cultured in endothelial basal medium-2 (Lonza, EGM-2) supplemented with SingleQuots (Lonza, CC-3162): containing proprietary concentrations of: hEGF, hydrocortisone, gentamicin, amphotericin-B, VEGF, hFGF, IGF-1, ascorbic acid, heparin and fetal bovine serum (FBS) (2% v/v).

HUVECs and C3As were initially grown separately as mono-cultures, on tissue culture plastic flasks of 25 cm^2 or 75 cm^2 with 5 ml or 10 ml of each cell culture media, respectively. When cell were >80% confluent, culture medium was discarded, and flasks were rinsed with phosphate-buffered saline (PBS) to remove serum. Cells were detached using trypsin solution (0.05% (W/V) Trypsin + 0.53 mM EDTA) in 37ºC and 5% (v/v) CO_2 for at least 5 min. Then, trypsin solution was neutralised with the addition of an equal volume of cell culture medium containing 10% (v/v) FBS and the cell suspension centrifuged for 5 min at 350g. The cell pellet was suspended in cell culture media and cell numbers counted using Neubauer haemocytometer and trypan blue was used to assess cell viability. Cell suspensions with cell viability of at least 85-90% were used for experiments or cell culture maintenance.

For *in vitro* co-culture experiments, HUVECs were seeded into cell culture plates 4 hours before addition of C3A cells to allow HUVECs to adhere to the cell culture plastic in EGM-2 for 3 days before the assessment of biocompatibility and hepatic function. Starting cell density was based on surface area at 21,000 cells/cm^2 and modified for ratio 3:1 (HUVEC:C3A) and 1:3 (HUVEC:C3A). Otherwise, except where clearly stated in the text. Media was changed every 48-72hr.

2.2.2 Cell culture maintenance: HUVECs cryopreservation

HUVECs (between passages 3 to 7) were cryopreserved when they achieved 90% confluence. At least 0.5 x 10^6 HUVECs were suspended in 0.5 ml of EGM-2 containing 10% (v/v) of DMSO in cryogenic tubes (Thermo Scientific-Nunc, UK). Cryogenic tubes were maintained at -80ºC overnight before transferring to liquid nitrogen.

2.2.3 Light and immunofluorescence Microscopy

Cell morphology was assessed under phase contrast microscopy using an inverted microscope (Zeiss Axio-Observer A1, Germany) and images were captured with a mounted camera (Zeiss AxioCam MRm). Images were processed and merged using ImageJ 1.46r (National Institute of Health, USA).

2.2.4 Immunocytochemistry

2.2.4.1 Platelet endothelial cell adhesion molecule (PECAM-1/CD31) and epithelial cell adhesion molecule (EpCAM)

Cells were fixed *in situ* with 4% (w/v) paraformaldehyde (Sigma-Aldrich, UK) for 30 min at room temperature (RT), washed with PBS, and treated with 0.1% (v/v) Triton X-100 in PBS for 1 hour at RT, then blocked with PBS containing 5% (w/v) BSA for 30 min.

Cells were incubated with rabbit-anti-human CD31 (eBioScience) endothelial cell marker diluted at 1:50 and/or directly conjugated mouse anti-human APC-EpCAM (Biolegend) diluted 1:50 at 4ºC overnight. Cells were then treated with secondary anti rabbit-IgG Alexa Fluor 488 (Life Technologies, A11034) antibody (1:400) and goat anti-mouse IgG Alexa 555 (Life Technologies, A21424) for 2hr at RT. Finally, cells were washed and stained with DAPI (Sigma) at 1/5000 for 5 min.

2.2.4.2 CYP3A4 and filamentous actin (F-actin) staining

Fixed cells were treated with 0.1% (v/v) Triton X-100 in PBS for 1hr at RT and blocked with PBS containing 5% (w/v) BSA for 30 min. Subsequently, they were incubated with primary rabbit-anti-human Cytochrome P450 Enzyme CYP3A4 Antibody (AB1254, Chemicon, Millipore) (1:800) and F-actin was labelled using Tetramethylrhodamine Isothiocyanate Rhodamine phalloidin (Molecular Probes, R415) (1:100) at RT. After 90 min, cells were washed with PBS before addition of a secondary anti rabbit-IgG Alexa Fluor 488 (Life Technologies A11034) (1:400) for 45 min, then labelled with DAPI (Sigma) at 1/5000 dilution for 5 min. This method was modified from a published method (Pernelle et al., 2011).

2.2.5 Flow cytometry sample preparation

To assess hepatic- and endothelial-specific expression markers, cells were stained with combinations of directly conjugated fluorescent mouse anti-human antibodies: PerCP-CD31, (BD eBioscience, 46-0319-41), APC-EpCAM (BioLegend), PE-VEGFR-2 (R&D Systems) at 4ºC for 20 min: Cells were washed using 2 spin-wash cycles (centrifugation for 7 min at 350g), before final re-suspension in 200µl of PBS supplemented with 0.1% (w/v) BSA and 0.1% (w/v) sodium azide, for data acquisition.

At least 10,000 live events per sample were collected using a FACS-Calibur flow cytometer and data analysed using both CellQuest (Becton Dickinson, UK) and FCS express 4 Software (free version online - DeNovo Software). Dead cells and debris were excluded from the analysis based on scatter characteristics, so that expression of markers was assessed exclusively on live cells. Unstained HUVECs, C3As and co-cultured cells were used as controls for expression of VEGFR-2. In stained cells, endothelial markers and hepatic

markers were analysed using electronic gating for each cell population using $CD31^+$ for HUVEC and $EpCAM^+$ for C3As to assess Mean Fluorescence Intensity (MFI).

MFI was used to quantify the relative level of fluoresence in samples (brightness) which indicate the relative expression of HUVECs and C3As for each antibody in mono-culture and co-cultures. The peak values were obtained from flow cytometry histograms, and calculated as follows:

MFI= stained sample peak channel - negative control peak channel

2.2.5.1 HGF receptor/C-met staining

For intracellular staining to ensure c-met stability, cells were fixed using flow cytometry fixation buffer (R&D Systems, FC004) (100µl/sample), permeabilized with flow cytometry Permeabilization/Wash Buffer (R&D Systems, FC005) for 15 min at RT and stained with Human/Mouse Phospho-HRF R/C-met (Y1234/Y1235) antibody (R&D Systems, AF2480) at 2.5 µg/10^6 cells for intracellular staining by flow cytometry. Cells were washed and resuspended with permeabilization/wash buffer then stained with a secondary antibody anti rabbit-IgG Alexa Fluor 488 (Life Technologies A11034) at 1:50 dilution, at 4ºC for 20 min. Finally, cells were washed twice by centrifugation for 7 min at 350g, before re-suspension in 200µl of PBS supplemented with 0.1% (w/v) BSA and 0.1% (w/v) sodium azide, for acquisition of data by flow cytometry.

2.2.6 Relative Growth Kinetics: Titration, cell growth and proliferation rate

2.2.6.1 Growth rate, population doubling (PD) and population doubling time (PDT)

Growth rate, population doubling (PD), and population doubling time (PDT) were calculated in HUVECs and C3As as a different ways for comparing cell proliferation from number of cells on day 0 (D_0) to the number of cells harvested on the final day (Df) of culture, using the following formulas (Hastings et al., 2004):

Growth rate (%) = Number of cells harvested on final day (D_f)*100%/ Number of cells seeded on initial day (D_0)

Population doubling (PD) = log [D_f/ D_0] / log2

Population doubling time (PDT) = culture time /PD (time was expressed in hours)

2.2.7 Hepatic functional assays

For evaluation of hepatocyte function, C3As were seeded at the same density (12.500 cells per well in a 96 well plate) in mono- and co-cultures.

2.2.7.1 Albumin synthesis

Albumin synthesis was measured in cell culture supernatants taken on day 3 using Albumin Blue 580 Fluorescence Assay after 24hr in serum-free EGM-2 medium.

On the second day of culture, HUVECs and C3A mono- and co-cultures at ratios 1:3 (HUVEC:C3A), 1:1 (HUVEC:C3A) and 3:1 (HUVEC:C3A) were washed twice with PBS to eliminate bovine serum albumin from the EGM-2 media and replaced with endothelial serum-free media. It was important to measure albumin synthesis by cells in bovine serum albumin-free medium to avoid the possibility of overestimating albumin concentration. After

24hr, supernatants were collected and 80 µL per well of samples were added in duplicate into separate wells and mixed with 160 µL of working solution (Working solution: Albumin blue 580 (AB580) diluted in isopropanol at a final concentration of 30mg/l (stock solution). Then, stock solution was diluted in MOPS buffer (see Table 7.3).

The solution and reagents were kept for a month in the dark at 4ºC. The plate was shaken for 30 seconds before reading the fluorescence (excitation at 590nm and emission 645nm). Data were normalised to the number of viable C3A cells seeded on day 0. Samples were read in a 96-well plate on a CytoFluor® series 4000 Fluorescence Multi-Well Plate Reader (Applied Biosystems). Albumin concentration was derived using an appropriate standard curve.

2.2.7.2 Urea synthesis rate

Urea synthesis was determined in cell culture supernatants of HUVECs and C3As in mono- and co-cultures at ratios 1:1 (HUVEC:C3A) and 3:1 (HUVEC:C3A) on day 3 of cell culture, using the Quantitative Colorimetric Urean Determination QuantiChrom^{TM} Urea Assay Kit (DIUR-500, BioAssay Systems). The principle of this method was to measure urea concentration in the cell culture supernatant using a chromogenic reagent that in contact with urea forms a coloured complex at 520nm. In brief, on day 3, cells were washed twice with PBS and incubated with 2 mM ammonium chloride (NH_4Cl) (Sigma, UK) for 2hr at 37ºC in 5% (v/v) CO_2. Supernatants were collected at two different time points, immediately after addition of the NH_4Cl as a control (time 0) and after 2hr of incubation (time 2). Samples were stored at -80ºC for later analysis.

For the urea measurement, samples were incubated for 50 min with working reagent in a 96-well plate at RT, as recommended by the manufactures, and optical density read at 430nm using a GloMax®-Multi-Microplate Multimode Reader (Promega). The urea concentration of each sample was derived using an appropriate standard curve. Then, urea synthesis rate (USR) was calculated per hour by subtracting the urea concentration (C_0) and the volume of

media (V_1) taken at time 0 hours (t=0) values from the urea concentration (C_1) and the volume of media (V_2) taken at time 2 (t=2) and normalised by the number of hepatocytes (NH) and the time of exposure (T) where the equation is:

$$USR = (C_0*V_1)-(C_1*V_2)/T*NH$$

2.2.7.3 Cytochrome P450 3A4 assay (CYP3A4)

CYP3A4 enzyme activity was measured directly in the cells on day 3 of co-culture at both ratio 1:1 (HUVEC:C3A) and ratio 1:3 (HUVEC:C3A) using a luminescence assay P450-Glo™ CYP3A4 Assay with Luciferin-IPA (V9001, Promega). P450-Glo™ CYP3A4 Assay is a luminescent method designed to measured P450 activity. Cells take luciferin-based substrates and converted to luciferin by P450.

On day 3, HUVECs and C3As in mono and co-cultures were washed and incubated for one hour with Luciferin-IPA diluted 1/1000 in EGM-2, and luciferin reagent added to the cells. Samples were transferred to a white-walled 96 well plate to be read by a luminometer GloMax Multi+ plate reader (Promega). Wells with medium alone were also incubated with Luciferin-IPA as background controls.

2.3 Statistical Analysis

Experiments were performed in triplicate culture wells (3 technical replicates were considered as n=1), in at least three independent biological experiments (n=3). GraphPad Prism®5 software was used for statistical analysis. Results were reported as mean ± standard error (SEM). Student's unpaired t-test was used to compare all co-cultures to their appropriate HUVECs and C3As mono-culture controls (statistical significance was defined as: *$p<0.05$).

2.4 Results

2.4.1 Morphology and expression of endothelial and hepatic specific markers: Defining a biocompatible co-culture medium

Standard mono-cultures of HUVECs and C3As are cultured in specialized hepatic growth medium (MEME) or endothelial medium (EGM-2), respectively. To develop an *in vitro* co-culture model using HUVECs and C3As, biocompatibility of both cell types were tested in either endothelial or hepatic medium.

Maintenance of surface marker expression

Morphology and phenotype of cells through expression of cell type-specific endothelial (CD31 for HUVECs) and hepatic markers (EpCAM for C3As), were evaluated for each cell type, cultured in each medium, using phase contrast microscopy, flow cytometry and immunofluorescence techniques.

Morphology

In mono-cultures of HUVECs and C3As on polystyrene using MEME or EGM-2 for 3 days, HUVECs displayed significant abnormal changes in morphology dependent on culture medium (Figure 2-1A,B); whereas C3As maintained characteristic morphology regardless of culture medium. When HUVECs were cultured in MEME+ lost both morphology and viability (Figure 2-1A). However, when HUVECs were cultured in EGM-2, they formed characteristic cobblestone morphology (Figure 2-1B). C3As in MEME+ formed aggregates and maintained their epithelial morphology (Figure 2-1C), which was also maintained in EGM-2 following 3 days in culture (Figure 2-1D).

HUVECs and C3As expression surface markers

Flow cytometry analysis revealed that EpCAM was expressed by C3As equally in culture with MEME or EGM-2 after 3 days. Endothelial adhesion molecule expression, CD31, was not detected on C3As. Due to the low cell viability observed for HUVECs in MEME+ it was only possible to stain those grown in EGM-2. Data showed that CD31 was highly expressed by HUVECs, while expression EpCAM was not detected (Figure 2-2).

Immunohistochemistry photomicrographs show both morphology and phenotype of HUVECs and C3As grown in EGM-2 for 3 days. Cells were stained *in situ* and images revealed HUVECs and C3As expressed CD31 and EPCAM respectively (Figure 2-3).

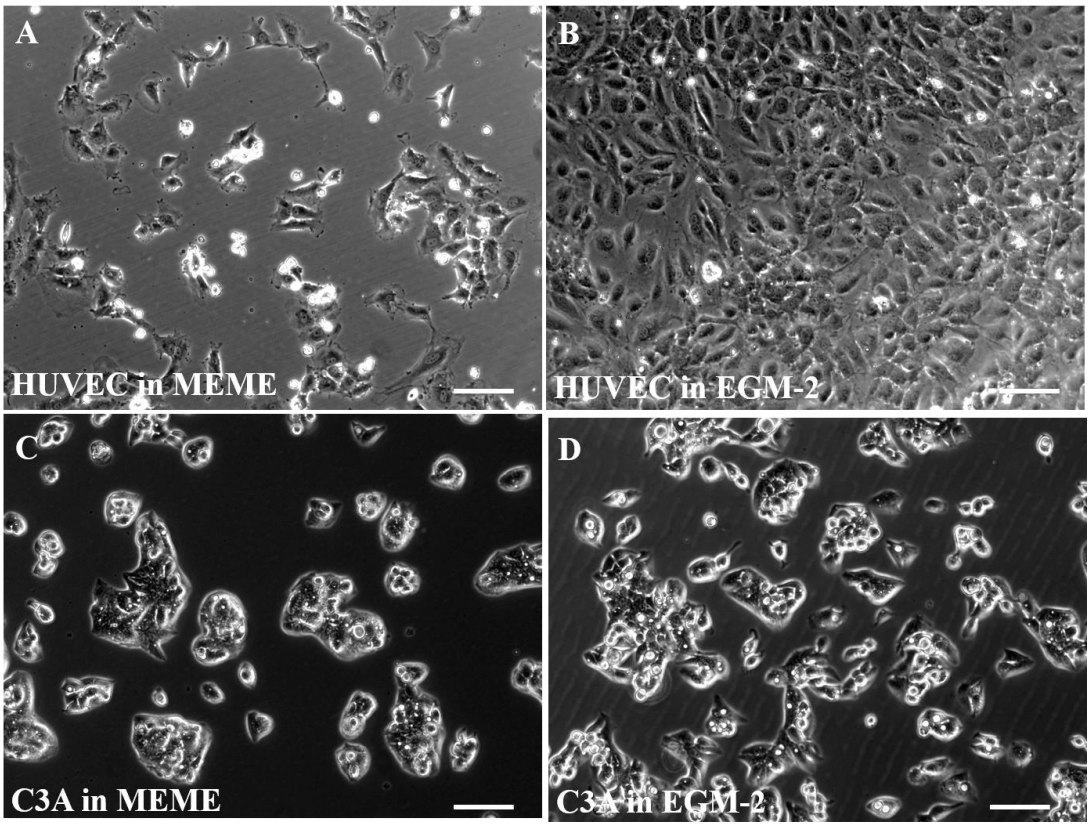

Figure 2-1 Morphology of HUVECs and C3As in two different media; MEME and EGM-2.

Morphology of HUVECs and C3As as mono-cultures on polystyrene in either hepatic medium (MEME) or endothelial medium (EGM-2) on day 3. Phase contrast image of HUVECs mono-cultured in MEME (A) and EGM-2 (B) and C3As mono-cultured in MEME (C) and EGM-2 (D). These images were taken using an inverted microscope (Zeiss Axio-Observer A1, Germany) and acquired at magnification x10 and scale bar of 100µm.

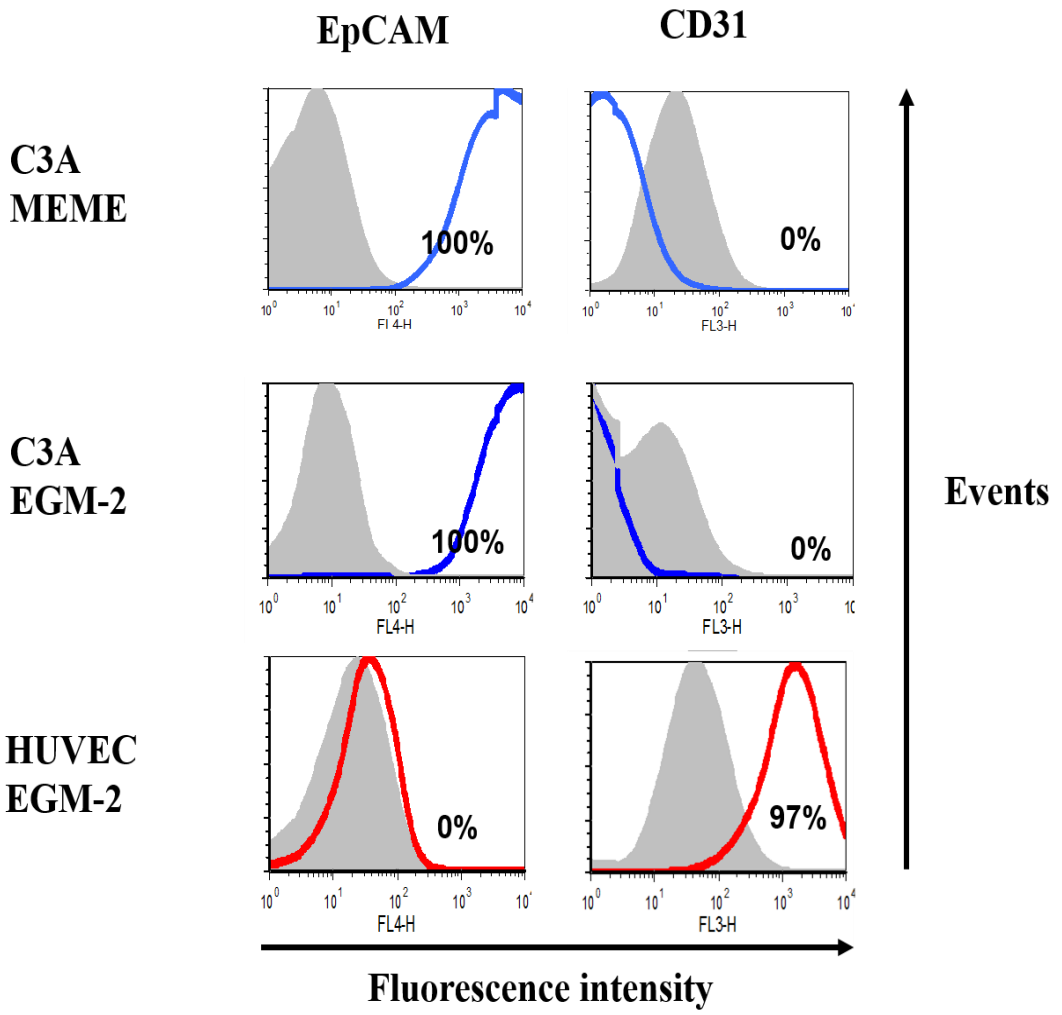

Figure 2-2 Expression of platelet endothelial cell adhesion molecule (CD31), and hepatic epithelial (EpCAM) in two different media; MEME and EGM-2.

Phenotype of HUVECs and C3As as mono-cultures on polystyrene in either hepatic medium (MEME) or endothelial medium (EGM-2). Cells were stained with cell type-specific hepatic (EpCAM) or endothelial (CD31) antibodies for flow cytometry analysis and processed as described in Material and Methods in Section 2.2.6. CD31 and EpCAM cell surface expression was analysed in HUVECs and C3As using flow cytometry histograms: Grey is unstained, red is stained for HUVECs and blue for C3As.

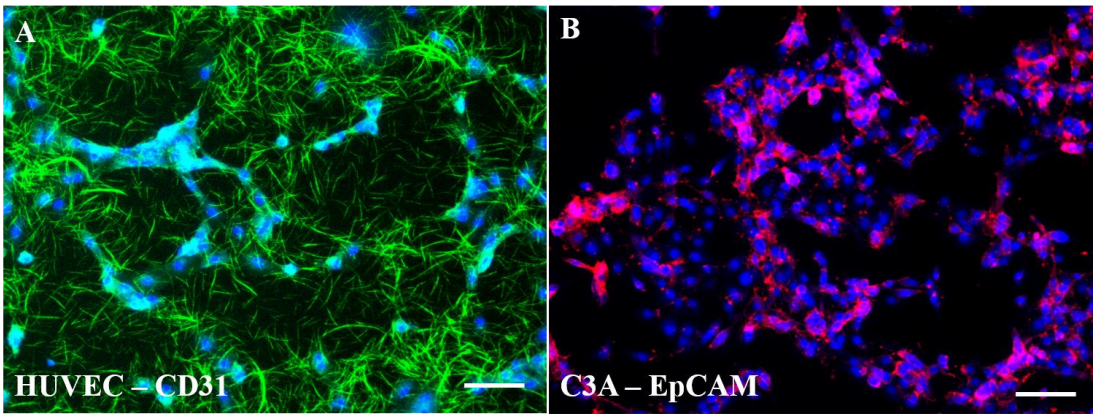

Figure 2-3 Immunofluorescence staining using cell type-specific hepatic and endothelial surface expression markers in HUVECs/CD31^{+} and C3As/EpCAM+ in EGM-2

Morphological phenotype of HUVECs and C3As as mono-cultures on polystyrene in either hepatic medium (MEME) or endothelial medium (EGM-2). On day 3 of culture, HUVECs (A) and C3As (B) were labelled with DAPI (nuclei), EpCAM (red) and CD31 (green) antibodies. Fluorescence images were taken at magnification of 20x and respectively images of DAPI and CD31/EpCAM were taken using an inverted microscope (Zeiss Axio-Observer A1, Germany) and merged using imageJ 1.46r. Scale bar 50µm.

2.4.2 Liver Extracellular Matrix: (ECM): Influence of collagen-I on cell culture phenotype

In the liver, endothelial cells and hepatocytes are separated by the space of Disse, mainly composed of collagen, laminin or fibronectin. *In vitro,* ECM components influence phenotype and behaviour of liver cells. For examples, collagen-I is one of the most abundant ECM components in the liver and can maintain longer hepatocyte viability (De Kock et al., 2011, LeCluyse et al., 2012).

CD31 and EpCAM expression were evaluated in mono-cultures of EGM-2 medium on either collagen-I coated or polystyrene culture plates. Flow cytometry histograms (Figure 2-4) demonstrated no change in the levels of expression markers for HUVECs or C3A mono-cultures on either collagen-1 or polystyrene.

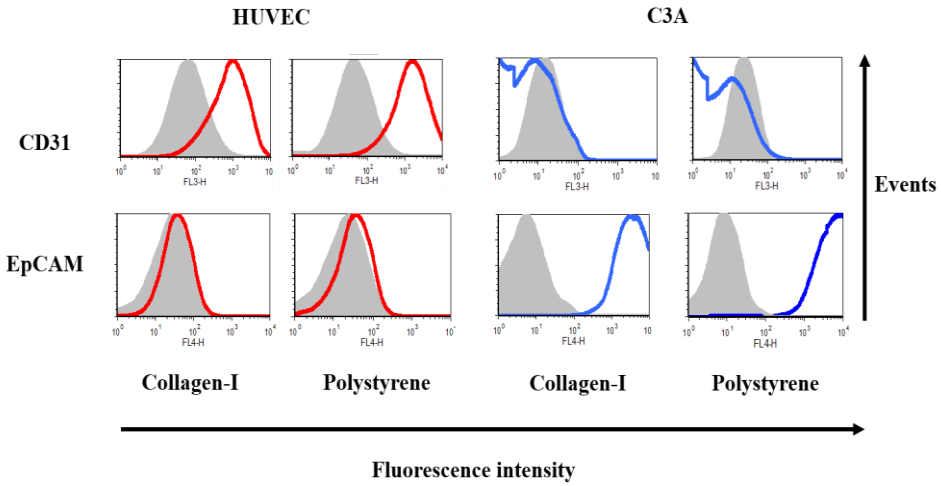

Figure 2-4 Expression of platelet endothelial cell adhesion molecule (CD31), and epithelial cell adhesion molecule (EpCAM) cultured on either collagen-I or polystyrene in EGM-2 media.

Morphological phenotype of HUVECs and C3As as mono-cultures on either collagen-I or polystyrene in EGM-2. CD31 and EpCAM expression were analysed by flow cytometry in HUVECs and C3As as described in Material and Methods Section 2.2.6. The flow cytometry histograms show CD31 and EpCAM expression in HUVECs cultured in collagen-I, polystyrene; and C3As cultured in collagen-I and polystyrene (Grey is unstained and red CD31^{+} stained for HUVECs and EpCAM+ blue stained for C3As).

2.4.3 Optimization of HUVEC:C3A ratios in co-cultures based on cell proliferation

Relative Growth Kinetics in Co-culture: Titration, proliferation rate and viability to determine the optimal ratio and culture period

Following initial titration of HUVEC:C3A ratios used in co-culture experiments, derivation of the optimal ratio was also based upon assessment of growth rate, population doubling and population doubling time of HUVECs and C3As in mono and co-cultures, from day 0 to day 3 (d3), and from day 0 to day 7 (d7).

Growth rate

At day 3 (d3) and day 7 (d7), there were significant differences in cell growth rate between HUVECs and C3As (Figure 2-5A), resulting in significant population doubling between d3 and d7 in HUVECs (p=0.03) and C3As (p=0.01). HUVECs had proliferated significantly more slowly than C3As by d3 (188.9 ± 9.19 % in HUVECs vs 260 ± 11.55 % in C3As, (p=0.0002) and by d7, 257.3 ± 27.60 % in HUVECs vs 417.6 ± 53.04 % in C3As, (p= 0.016) (Figure 2-5A and Table 2-1).

Table 2-1 Percentage of cell growth rate from initial day (D0) to final day (D3 or D7)

*Table shows the percentage of cell growth rate on day d3 and d7, obtained following the evacuation: Growth rate (100%) = Number of cells harvested on final day (D_f)/ Number of cells seeded on initial day (D_0). Data is expressed as the mean ± SEM of three different experiments in triplicate (n=3). *P<0.05, ***P<0.0005, HUVEC d3 vs C3A d3, HUVEC d7 vs C3A d7.*

Cell growth rate %	HUVEC d3	HUVEC d7	C3A d3	C3A d7
Mean	188.9	257.3	260.0***	417.6*
SEM	9.19	27.60	11.55	53.04

Population doubling and population doubling time

Population doubling of C3As showed 1.51 fold increase compared to HUVECs by d3 (from 0.90 ± 0.07 in HUVECs to 1.37 ± 0.06 in C3As; (p=0.0002) and by d7, from 1.28 ± 0.18 in HUVECs to 1.94 ± 0.23 in C3As; (p=0.039) (Figure 2-5B and Table 2-2). This suggests that the population time by d3 was 47.93 ± 6.13 hr in C3As and 76.59 ± 11.53hr in HUVECs and by d7 92.38 ± 17.38hr in C3As and 166.4 ± 49.08hr in HUVECs (Figure 2-5C and Table 2-2).

Table 2-2 Population doubling and population doubling time from initial day (d0) to final day (d3 or d7) expressed in hours

*Table shows the Population doubling and Population double time on day d3 and d7, obtained following the evacuation: Population doubling (PD) = log [D_f/ D_0] / log2. Population doubling time (PDT) = culture time /PD (time was expressed in hours). Data is expressed as the mean ± SEM of three different experiments in triplicate (n=3). *P<0.05, ***P<0.0001, HUVEC d3 vs C3A d3, HUVEC d7 vs C3A d7.*

Population doubling	**HUVEC d3**	**HUVEC d7**	**C3A d3**	**C3A d7**
Mean	0.90	1.28	1.37***	1.94*
SEM	0.07	0.18	0.07	0.23
Population doubling time (hours)				
Mean	76.59	166.4	47.93*	92.38
SEM	11.53	49.08	6.13	17.68

Co-culture phenotype: Flow cytometry

The proportions of each cell line present in co-cultures after 3 and 7 days of culture were compared for three different starting ratios of 3:1 (HUVEC:C3A), 1:1 (HUVEC:C3A) and 1:3 (HUVEC:C3A). Initially, when setting up co-culture experiments, HUVECs and C3As were seeded into wells at the same time. However, this resulted in poor attachment of HUVECs because C3As seems to overtake faster the cell culture surface. This was overcome by seeding HUVECs four hours before the addition of C3As. This allowed adhesion of

HUVECs to the culture surface and resulted in successful co-culture between HUVECs and C3As.

To distinguish the sub-populations of HUVECs from C3As, the proportions of HUVECs and C3As following 3 and 7 days of culture were assessed by flow cytometry of samples stained using endothelial ($CD31^+$) and hepatic ($EpCAM^+$) antibodies. In each case, the initial ratio seeded was more or less maintained at day 3 (Figure 2-5A), whereas by day 7 in all ratios tested, C3As were in the majority (Figure 2-6B). At a HUVEC:C3A starting ratio of 1:1, by day 3, co-cultures showed 37.34 ± 5.36 % of $CD31^+$ and 56.59 ± 4.46 % of $EpCAM^+$ whereas by day 7, co-cultures showed 13.63 ± 6.71 % of $CD31^+$ and 80.77 ± 8.72 % of $EpCAM^+$. At a HUVEC:C3A starting ratio of 1:3, by day 3, co-cultures showed 13.61 ± 2.81 % of $CD31^+$ and 82.98 ± 3.58 % of $EpCAM^+$, whereas at day 7, co-cultures showed 4.84 ± 1.47 % of $CD31^+$ and 92.86 ± 2.90 % of $EpCAM^+$. Finally at a HUVEC:C3A starting ratio of 3:1 (HUVEC:C3A), by day 3, co-cultures showed 55.22 ± 11.24 % of $CD31^+$ and 38.16 ± 10.91 % of $EpCAM^+$ whereas at day 7, co-cultures showed 30.90 ± 9.15 % of $CD31^+$ and 58.47 ± 14.84 % of $EpCAM^+$ (Figure 2-6A-C).

These observations revealed that 7 days of co-cultures, at any of the ratios tested, did not maintain the initially seeded ratio. However, when the assessment was performed on d3, ratio 1:1 and ratio 1:3 (HUVEC:C3A) were able to maintain closer to the starting ratio. This data were subsequently confirmed morphologically with fluorescent staining and phase contrast imaging of HUVECs and C3As in co-cultures. Morphological analyses showed that HUVECs and C3As maintained characteristic epithelial and cobblestone appearance, respectively, when cultured together in EGM-2 culture media for 3 days, at ratio 1:1 (Figure 2-7). These conditions resulted in the least change in relative proportions of cells in co-culture over time. Importantly, this allowed results from functional analyses, to be normalised to initial C3A cell numbers.

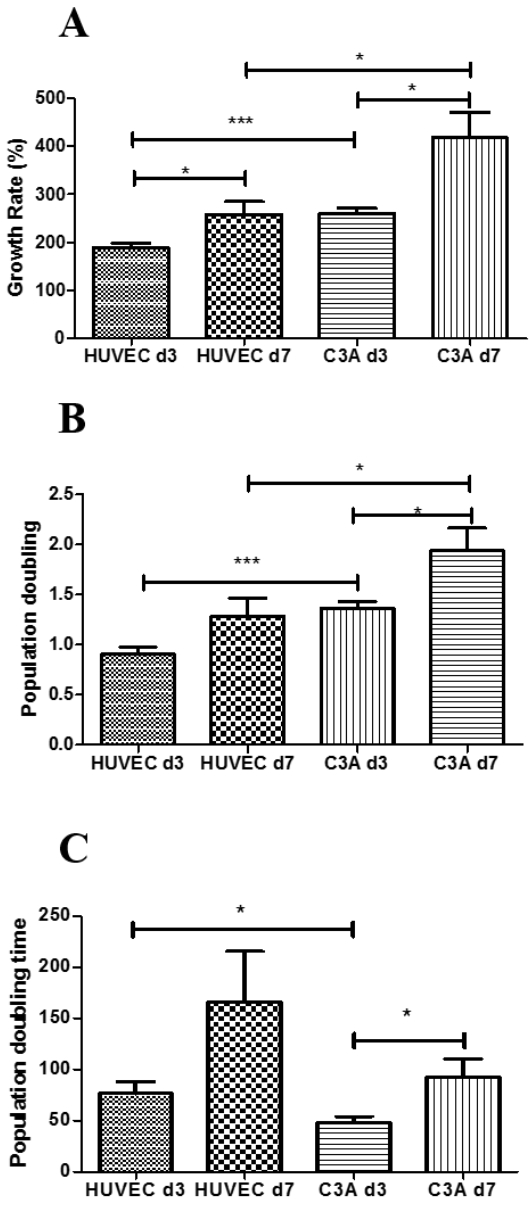

Figure 2-5 HUVECs and C3As proliferation day 3 and by day 7

*Day 3 and day 7 growth kinetics of HUVEC and C3A mono-cultures on polystyrene in endothelial media (EGM-2 media). Numbers of HUVECs and C3As at the end of each period (d3 and d7) was compared to the initial number of cells on day (d0) calculated as indicated in Materials and Methods in Section 2.2.7. A) Growth rate, B) doubling population, and C) doubling population times. Data is expressed as the mean ± SEM of three different experiments in triplicate (n=3). Statistical significant was considered * $p < 0.05$, ** $p < 0.001$.*

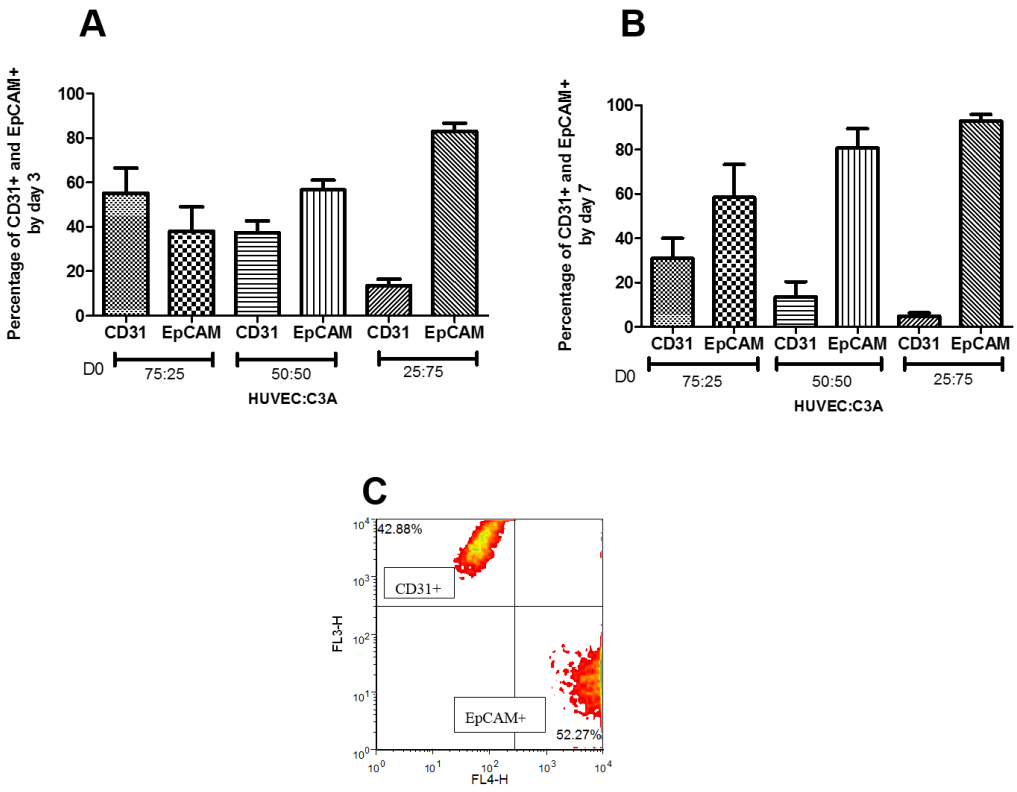

Figure 2-6 HUVEC:C3A co-culture proliferation by day 3 and by day 7

HUVECs and C3As were co-cultured for 3 and 7 days in EGM-2 at three different ratios 3:1 (HUVEC:C3A), 1:1 (HUVEC:C3A) and 1:3 (HUVEC:C3A) and stained with CD31 and EpCAM to be analysed by flow cytometry analyses as described in Material and Methods in Section 2.2.6. The percentage of $CD31^+$ and $EpCAM^+$ cells was compared to the initial number of cells on day 0. A) Percentages of $EpCAM^+$ (C3As) and $CD31^+$ (HUVECs) by day 3 (A) and by day 7 (B). C) Flow cytometry analysis of $CD31^+$ and $EpCAM^+$ in co-culture at ratio 1:1 (HUVEC:C3A) on day 3. Data is expressed as the mean ± SEM of at least three different experiments (n=3).

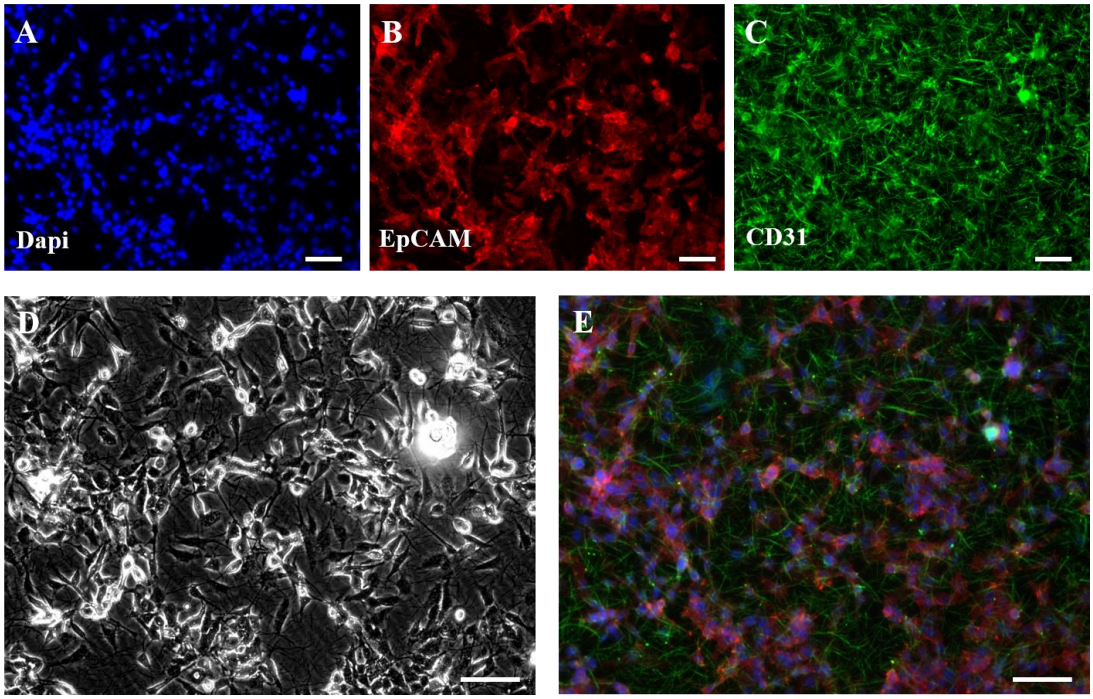

Figure 2-7 Morphology and specific-endothelial and hepatic surface expression in HUVECs and C3As co-cultured at ratio 1:1 in EGM-2 on day 3

HUVECs and C3As were co-cultured in EGM-2 medium for 3 days. On day 3 of culture, HUVECs and C3As were fixed and labelled with EpCAM and CD31 antibodies and DAPI (nuclei). Immunofluorescence images of DAPI (nuclei) (A), EpCAM (red) (B) and CD31 (green) (C) and phase contrast (D) were taken using an inverted microscope (Zeiss Axio-Observer A1, Germany) at magnification of 20x and respectively images of DAPI and CD31/EpCAM were merged using imageJ 1.46r (E). Scale bar 50µm.

2.4.4 Hepatic Functionality in HUVEC:C3A heterotypic co-cultures

Synthetic, detoxification and biotransformation capacity of C3A cells in HUVEC:C3A heterotypic co-cultures were assessed by measuring, respectively, albumin production, urea synthesis and CYP3A4 activity.

2.4.4.1 Albumin synthesis of C3As in mono-culture and HUVEC:C3A heterotypic

Albumin, the most abundant serum protein found in blood, is synthesised by hepatocytes. Hepatic-specific functionality of C3A mono-cultures and HUVEC:C3A co-cultures at three different ratios (3:1 HUVEC:C3A, 1:1 HUVEC:C3A and 1:3 HUVEC:C3A) was therefore assessed by measuring albumin concentration in serum-free endothelial cell growth medium 2 (EGM-2) over 24hr. EGM-2 medium is normally supplemented with 2% FBS, containing albumin, but to assess C3A albumin synthesis, it was necessary to use serum-free EGM-2 cell culture medium. However, while C3As are normally cultured in serum free medium for albumin measurement, the effect of removing serum on endothelial cells is unknown. It was therefore necessary to assess the effect of 24hr in serum-free culture conditions on HUVECs to ensure that differences in albumin secretion between experimental groups would not simply be a result of serum withdrawal.

HUVECs were cultured in 3 different endothelial cell medium: i) endothelial growth medium-2 (EGM-2) (containing growth factors and 2% (V/V) serum), ii) endothelial cell basal medium (EBM-2) (without growth factors or serum) and iii) endothelial cell growth medium (EGM-2-GF) (supplemented with growth factors but no serum). After 24hr, CD31 expression was analysed by flow cytometry to evaluate the effect of EGM-2-GF and EBM-2 on HUVECs.

Flow cytometry dot plot representation data confirmed that CD31 expression was maintained in EGM-2-GF better than in EBM-2 compared with control (EGM-2) (Figure 2-8).

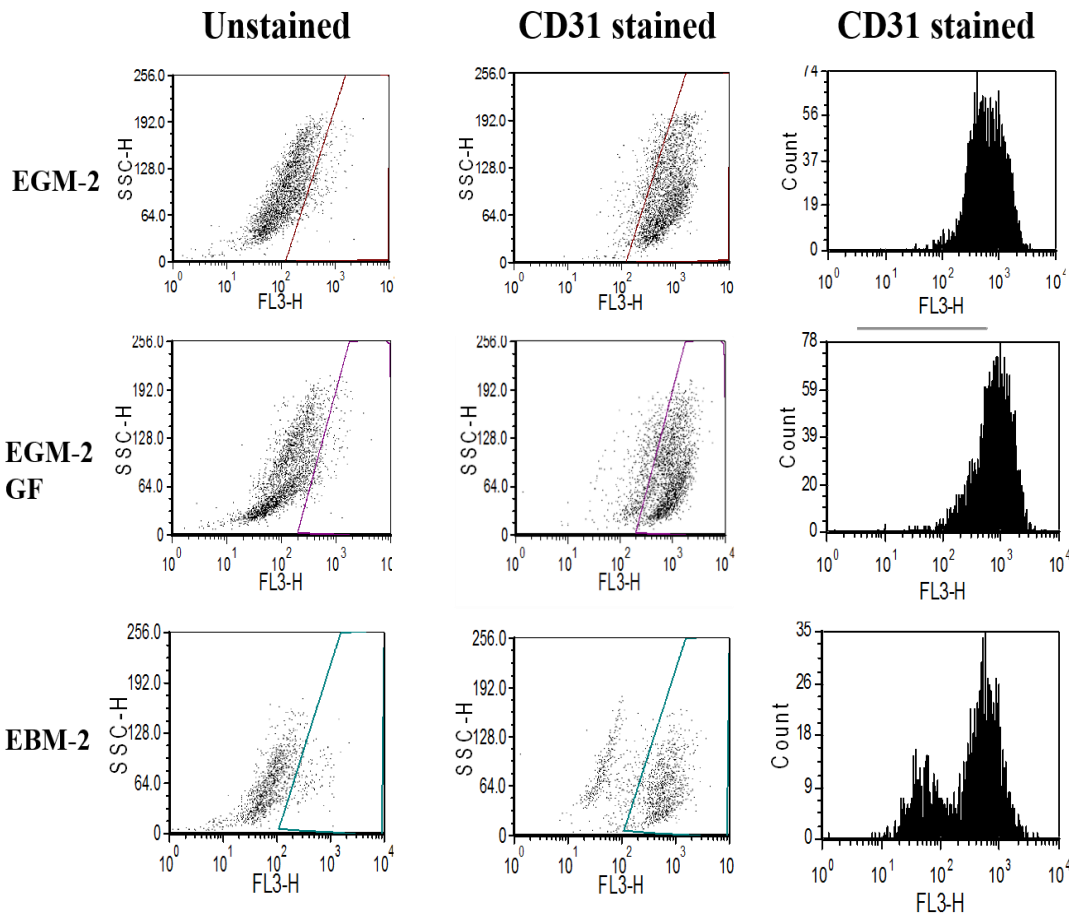

Figure 2-8 Phenotypic characterization of HUVECs cultured in modified endothelial cell growth medium

HUVECs were cultured in three different conditions of endothelial cell growth medium EGM-2; EGM-2 (control, containing growth factors and serum), EBM-2 (without growth factors or serum) and EGM-2-GF (supplemented with growth factors but no serum). After 24hr, CD31 expression was analysed by flow cytometry to evaluate the effect of EGM-2-GF and EBM-2 on HUVECs as described in Material and Methods in Section 2.2.6. The flow cytometry dot plots representation and histogram shows unstained HUVECs, CD31 stained HUVECs in three different media conditions: EGM-2, EGM-2-GF and EBM-2.

Therefore, medium EGM-2-GF (serum-free EGM-2 with growth factors) was selected to measure albumin concentration in mono and co-cultures at ratios 1:3 (HUVEC:C3A), 1:1 (HUVEC:C3A) and 3:1 (HUVEC:C3A) from day 2 to day 3 (i.e. the final 24hr of cell culture). To quantitate albumin concentration in the cell culture supernatants a standard curve was prepared using known concentrations (0-200 µg/ml) of human serum albumin in phosphate buffer (Figure 2-9).

Then, albumin concentration was obtained from the slope and applying the following equation:

$y = mx + c$

$x = y - c / m$

where **x** is unknown albumin concentration, **y** is the relative emission value (arbitrary units), **c** is the x-intercept and m corresponds to the slope of the curve (Figure 2-9) and albumin concentration obtained was normalised by the number of hepatocytes seeded on the initial day.

We found significant differences in albumin concentration in mono-cultures *vs* co-cultures. Not surprisingly, HUVECs mono-cultures did not synthesize albumin, whereas C3A mono-cultures did, while C3As showed elevated albumin synthesis when co-cultured with HUVECs, compared to C3A mono-cultures. Although, levels of albumin synthesis increased in all HUVEC:C3A ratios tested, the increase only reached statistical significance between C3A mono-cultures and HUVEC:C3A co-cultured at ratio 1:1 (20.50 ± 3.46 µg/ml/10^6 in C3As *vs* 34.17 ± 3.59 µg/ml/10^6 in ratio 1:1 (HUVEC:C3A); 1.7-fold; ($p = 0.011$). Conversely, the 3:1 (HUVEC:C3A) ratio showed lowest albumin levels with 25.04 ± 5.00 µg/ml/10^6 in comparison with HUVEC:C3A ratio 1:1 (34.17 ± 3.59 µg/ml/10^6) or ratio 1:3 (31.51 ± 5.25 µg/ml/10^6). Since HUVEC:C3A ratio 3:1 gave the lowest increase in albumin

secretion, and this ratio probably lacks physiological relevance to that seen *in vivo*, it was decided there was no benefit in testing it further *in vitro* (Figure 2-10).

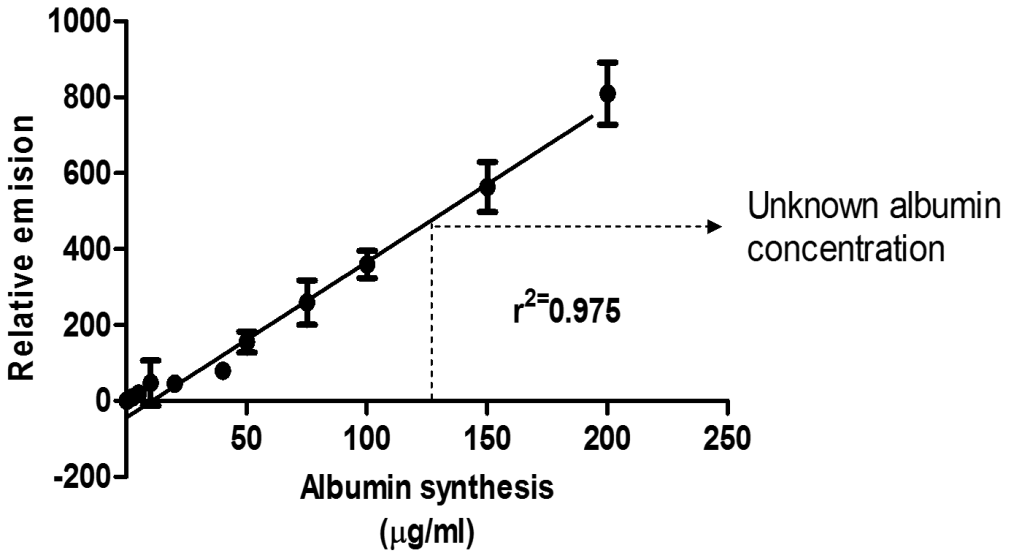

Figure 2-9 Representative standard curve of albumin concentration from 0-200µg/ml.

Human albumin was diluted in phosphate buffer to obtain a serial of albumin concentrations from 0-200 µg/ml. The relative emission and the different points of human albumin provide a linear regression curve which is used to determine the albumin concentration from unknown samples using the equation x = y – c /m; where ***x*** *is unknown albumin concentration (ug/ml),* ***y*** *is the relative emission value (arbitrary units),* ***c*** *is the x-intercept and m corresponds to the slope of the curve. Data is expressed as the mean ± SEM of three different standard curves each prepared in duplicate.*

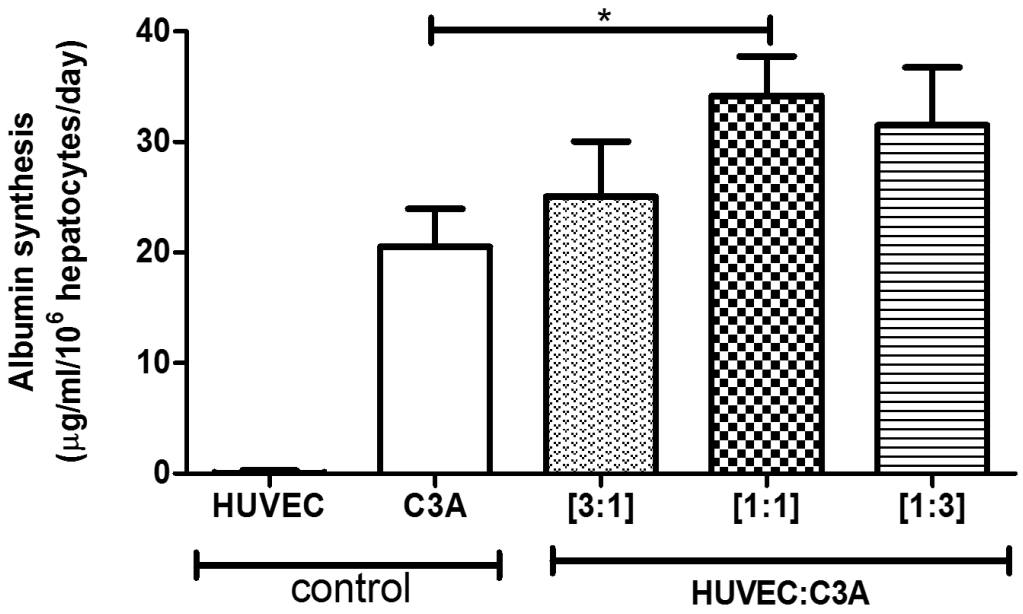

Figure 2-10 Hepatic albumin synthesis of C3As in mono-culture and co-cultures with HUVECs at three different ratios at 3:1, 1:1, 1:3 (HUVEC:C3A)

*Using the same number of C3As in each condition, C3As (white bar), HUVECs (black bar) and co-cultures (patterned bars) were cultured in EGM-2 and albumin synthesis was measured from day 2 to day 3 of culture (24hr) when cells were cultured in EGM-2 serum free using Albumin Blue 580 Fluorescence Assay, as described in Materials and Methods in Section 2.2.7.1. Results are expressed as µg/ml/10^6 of initial viable C3A cells seeded. Data is expressed as the mean ± SEM of three independent experiments in triplicate (n=3). C3As were compared with co-cultures. Statistical significant was considered * $p < 0.05$.*

2.4.4.2 Urea synthesis rate (USR) of C3As in mono-culture and HUVEC:C3A heterotypic co-culture

Urea synthesis rate (USR) was determined for both HUVECs and C3As in mono- and co-culture at ratios of 1:1 (HUVEC:C3A) and 1:3 (HUVEC:C3A) on 3 day of culture in EGM-2. Figure 2-11 shows that HUVECs in mono-cultures synthesised extremely low levels of urea, 1.36 ± 0.93 nmol/hr/10^6. Comparison of urea synthesis in C3As in mono- and co-cultures, demonstrated no significant increase in the presence of HUVECs, compared with C3As alone: 26.21 ± 2.00 nmol/hr/10^6 mono-culture *vs* 1:1 (HUVEC:C3A) 25.16 ± 4.40 nmol/hr/10^6 at co-culture ratio 1:1 (HUVEC:C3A); and 18.11 ± 4.42 nmol/hr/10^6 at co-culture ratio 1:3 (HUVEC:C3A) (Figure 2-11).

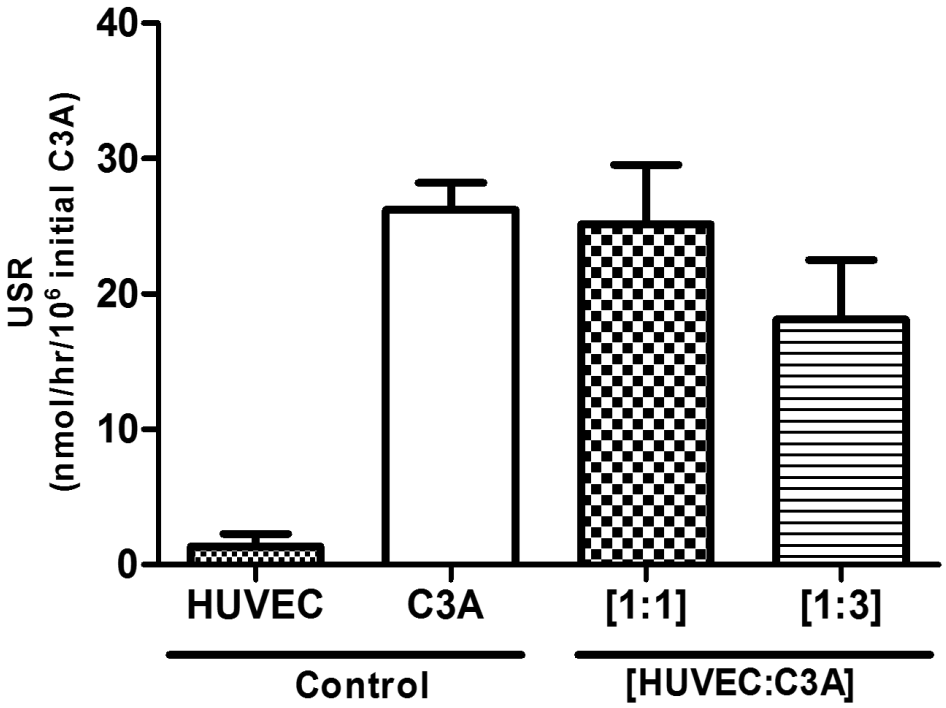

Figure 2-11 Comparison of hepatic urea synthesis in C3As mono- and co-cultures with HUVECs at HUVEC:C3A ratios at 1:1, 1:3 on day 3 in EGM-2 media

Using the same number of C3As in each condition, HUVECs and C3As in mono- (white bars) and co-cultures (patterned bars) at HUVEC:C3A ratios 1:1 and 1:3, were incubated with 2 mM NH_4Cl for 2 hr on day 3 of culture. Urea synthesis rate was determined from time 0 to time 2 hours using a quantitative colorimetric Urea Assay Kit, as described in Materials and Methods in Section 2.2.7.2. Results are expressed as nmol/hr/10^6 of initial C3As. Values are expressed as means ± SEM (n=3).

2.4.5 Cytochrome P450 3A4 (CYP3A4) enzyme activity in C3As in mono-culture and HUVEC:C3A heterotypic co-cultures

Basal levels of CYP3A4 enzyme activity in C3As mono-cultures were measured and compared to the levels seen in C3As in HUVEC:C3A co-cultures, at ratios of 1:1 and 1:3 (HUVEC:C3A) using luminescent biochemical assay, as well as immunofluorescence staining.

In C3A mono-cultures, basal levels of CYP450 activity are known to be very low. Notably therefore, the effect of HUVECs on C3A cellular CYP450 activity, would be an extremely important factor in determining the usefulness of *in vitro* co-culture models for improving drug testing - using human hepatic C3A cells.

CYP3A4 enzyme activity: A) Luminescence raw data values show that HUVECs did not show any CYP3A4 activity; however, comparing C3As with HUVEC:C3A co-cultures, data showed highly significant increases at both ratio 1:1 (HUVEC:C3A) ($p = 0.009$), and ratio 1:3 (HUVEC:C3A) ($p = 0.005$) (Figure 2-12-A); B) Fold change: Raw luminescence data were used to calculate the fold increase between C3As as a control to HUVEC:C3A co-cultures at ratio 1:1 and 1:3. Results showed that C3As in co-cultures had 2.27 ± 0.56 fold increase in CYP3A4 expression at ratio 1:1 and 2.14 ± 0.50 at ratio 1:3 (HUVEC:C3A) (Figure 2-12-B).

Phenotypic staining for CYP3A4 in mono- and co-cultures:

Immunostaining of C3As, HUVECs in mono- and co-cultures for CYP3A4 expression *in situ,* revealed higher fluorescence intensity in co-cultures compared to that seen in C3A mono-cultures (Figure 2-13). Furthermore, F-actin staining demonstrated characteristic cell structure and phenotypic differentiation in mono-cultures. (Figure 2-13).

The functional assays showed a trend for enhanced hepatic functional activity (CYP3A4 biotransformation) in C3A cells, in the presence of HUVECs.

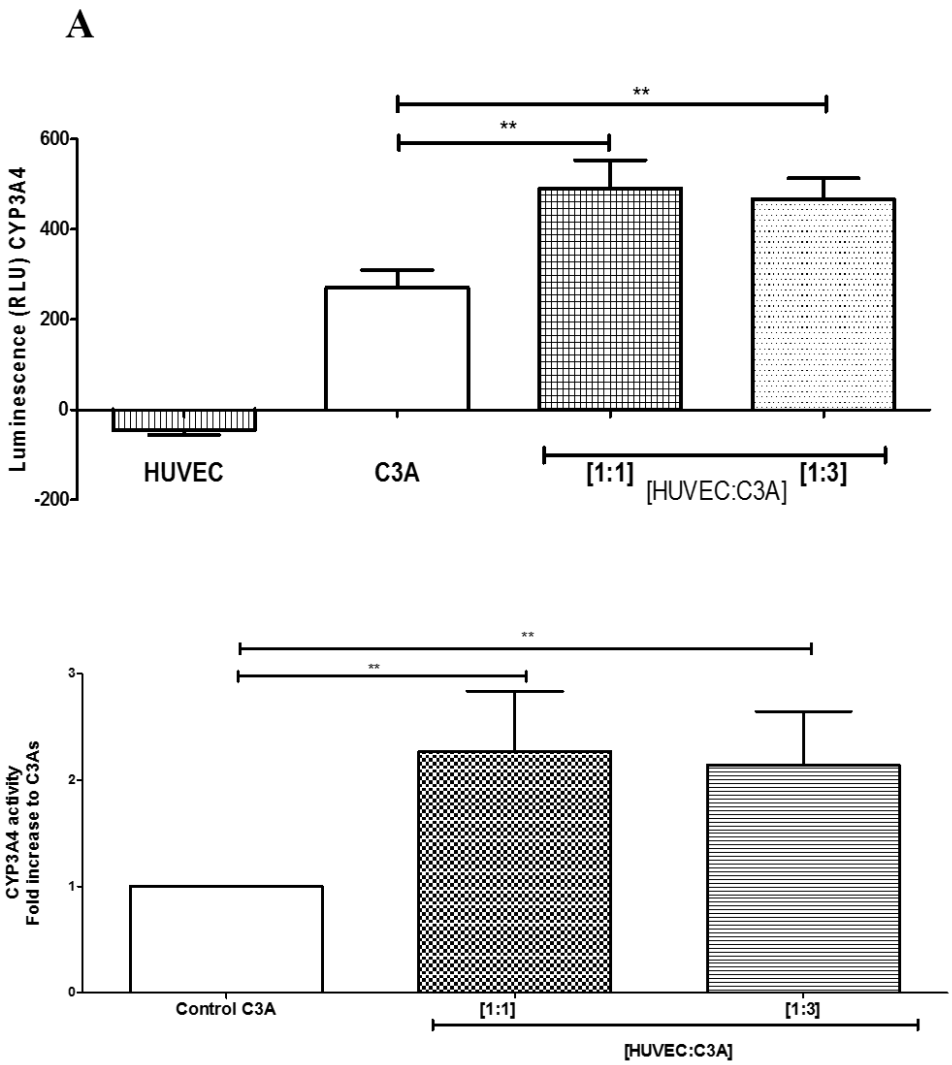

Figure 2-12 CYP3A4 activity in C3As mono- and co-cultures at two different ratios at 1:1, 1:3 (HUVEC:C3A)

HUVECs and C3As in mono and co-culture were cultured for 3 days and basal CYP3A4 activity measurement was performed directly on the cells using P450-Glo CYP3A4 activity assays with Luciferin-IPA (Promega). A) Luminescence raw data values of CYP3A4 activity detected by day 3 of culture in C3As (white bars) or HUVECs (striped pattern) mono-cultures and HUVEC:C3A co-cultures, at ratio 1:1 and 1:3 (HUVEC:C3A) activity and the CYP3A4 activity is expressed in relative luminescence units (RLU). B) Fold increase obtained from the luminescence raw data were used to calculate the fold increase between C3As as a control to co-cultures at ratio 1:1 and 1:3 (HUVEC:C3A). Values represent the mean ± SEM of three different experiments each containing technical triplicates, (n=3).

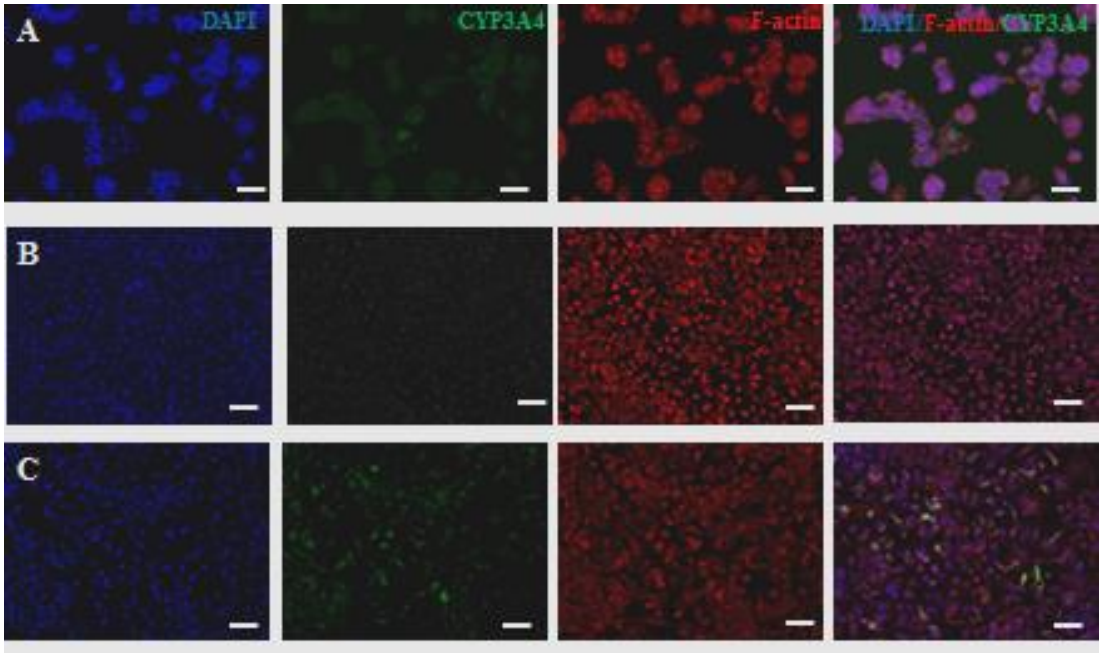

Figure 2-13 CYP3A4 immunofluorescent staining in C3A cells in mono-culture and in co-culture with HUVECs

Representative immunofluorescence photomicrographs showing morphological phenotype of mono- and co-cultures: (A) C3As, (B) HUVECs and mono- and (C) co-cultures at day 3, fluorescently-labelled with F-actin (red), CYP3A4 (green) or DAPI (blue). Photomicrographs of DAPI, F-actin and CYP3A4 were merged using imageJ 1.46r. These images were taken using an inverted microscope (Zeiss Axio-Observer A1, Germany) at magnification x100 and scale bar 100µm.

2.4.6 Regulation of cellular surface marker expression in HUVECs and C3As

Endothelial and hepatic phenotype was evaluated in HUVECs and C3As mono- and co-cultures on day 3 of culture. Adhesion molecules such as CD31 and EpCAM were selected respectively as specific endothelial and hepatic specific markers. Furthermore, modulation of expression of vascular endothelial growth factor receptor 2 (VEGFR-2) and C-met were also evaluated (Figure 2-14). In mono-culture, both cell types showed high expression of the respective phenotypic marker $CD31^+$ (HUVECs) and $EpCAM^+$ (C3As). When HUVECs and C3As were cultured together, HUVECs showed a 1.98 ± 0.16 fold increase in CD31 expression compared to HUVECs mono-cultures, when in contact with C3As. The interaction between HUVECs and C3As also modulated expression of both VEGFR-2 and C-met receptors, involved in paracrine signalling. Analysis revealed that VEGFR-2 was significantly down-regulated in HUVECs when in co-culture with C3As, the fold change being 0.60 ± 0.06 in co-culture ($p=0.0334$) as compared to HUVECs in mono-cultures. C-met receptor expression by HUVEC was not modulated in co-cultures. However, C3A showed a 0.70 ± 1.84 fold change in co-culture compared to C3A mono-cultures (Figure 2-15).

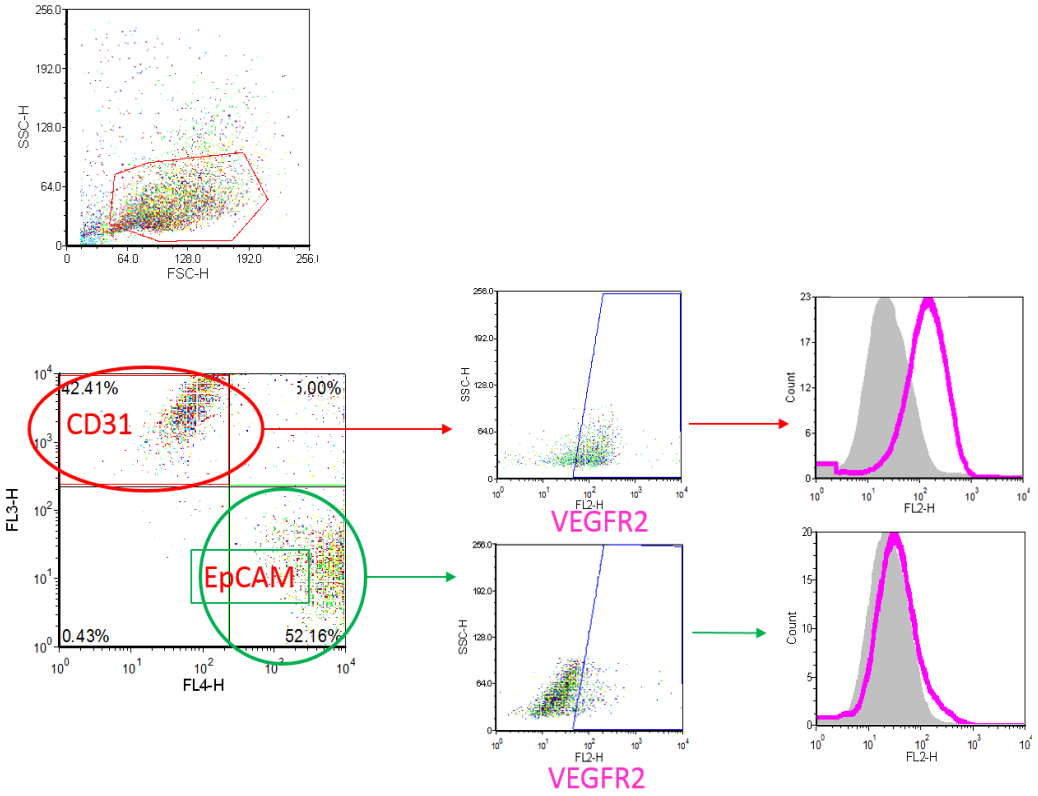

Figure 2-14 CD31^{+} for HUVECs and EpCAM^{+} for C3As gating prior to VEGFR-2 analysis by flow cytometry

HUVECs and C3As in co-cultures, following a staining with: VEGFR-2, EpCAM, CD31 and C-met for analysis by flow cytometry as described in Material and Methods in Section 2.2.6. Flow cytometry analysis show CD31^{+} for HUVECs and EpCAM^{+} for C3As gating prior VEGFR-2 analysis to show an example of the assessment of Mean Fluorescense Intensity (MFI). Unstained cells as control (grey) and stained cells (coloured).

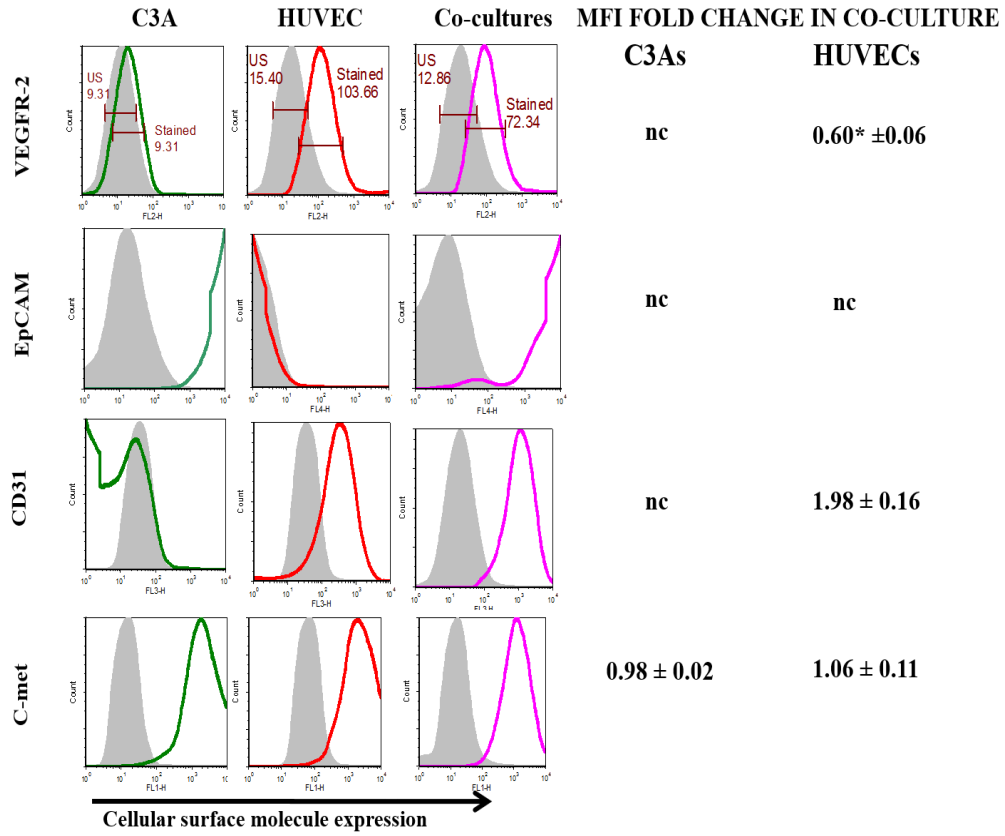

Figure 2-15 Comparison of HUVECs and C3A phenotypes in mono- and co-cultures

*HUVECs and C3As as either mono or co-cultures were cultured for 3 days in EGM-2, following a staining with: VEGFR-2, EpCAM, CD31 and C-met for analysis by flow cytometry as described in Material and Methods in Section 2.2.6. Flow cytometry histograms show VEGFR-2, C-met, CD31 and EpCAM expression in HUVECs and C3As in mono- and co-culture and percentage obtained from the Mean Fluorescence Intensity in co-culture compared with positive HUVECs and C3As controls. Unstained cells as control (grey) and stained cells (coloured). HUVECs and C3As mono-cultures were considered 100% expression and compared to co-cultures. Data is expressed as Mean ± SEM of three different experiments with significant difference at *p < 0.05, against controls (n=3). Abbreviations: nc = no change compared to controls.*

2.5 Conclusions

The data here presents *proof-of-principle* development of an *in vitro* hepatic environment in which hepatocytes (C3As) and endothelial cells (HUVECs) can be co-cultured, and in which they maintain morphology, phenotype, viability and functional properties. In the presence of HUVECs at a ratio 1:1, the function of C3A cells was significantly improved in terms of albumin synthesis and CYP3A4 activity whereas ureagenesis did not show improvements.

Endothelial cells and hepatocytes can interact *in vitro*. CYP3A4 activity (the most important Phase I drug metabolizing enzyme) was increased in C3A cells in co-cultures, this being especially important as the aim is to develop an improved *in vitro* human hepatic model for drug testing which is representative of liver function *in vivo*.

The results from the evaluation of morphology, phenotype, hepatic-specific function and cell- signalling presented in this chapter lead to the following conclusions:

1. **Cell phenotypic profile**: CD31 is expressed only in HUVECs, while EpCAM is expressed only in C3As.
2. **Biocompatibility**: Endothelial cell culture growth medium (EGM-2); EGM-2 maintained for at least 3 days, in culture the characteristic epithelial morphology of C3As cobblestone morphology in HUVECs and optimal expression of EpCAM in C3As and CD31 HUVECs. Hepatic medium, MEME, was not able to maintain HUVECs morphology or viability after only 3 days in culture.
3. **Cell co-culture growth kinetics** C3As proliferate faster than HUVECs and co-cultures at ratio 1:1, and 1:3 (HUVEC:C3A) better maintained the initial seeding ratio at day 3 as compared to day 7. Co-culture seems not to affect cell growth.

4. **Co-culture Functionality**: Co-culture with endothelial cells significantly enhanced C3A albumin synthesis and CYP3A4 activity in the organotypic hepatic model at ratio 1:1 on day 3.
5. **Co-culture phenotype**: HUVEC:C3A co-culture up-regulated CD31 and down-regulated VEGFR-2 expression in HUVECs, while the C3A phenotype was unaffected.

2.6 Discussion

In vitro human hepatic models represent a promising technology for predicting hepatotoxicity in pre-clinical drug discovery. During this complex process, compounds are tested *in vitro and in vivo.* However, as mentioned in the introduction, animal models used for drug testing often do not predict human drug toxicity due to interspecies-differences, and *in vitro* human hepatic models using only hepatocytes, for prediction of human toxicity (Gomez-Lechon et al., 2014).

PHH cultured alone have previously been shown to rapidly lose functionality, polarity and drug enzyme activity (Gomez-Lechon et al., 2010, Nelson et al., 2010). Recently, a new hepatic cell line, HepaRG, derived from a female with hepatocellular carcinoma has been compared to PHH. HepaRG cells have been shown to express the major drug metabolizing CYP450 enzymes including phase II enzymes and hepatic membrane transport proteins (MTP). It comprises cells of two different phenotypes in a bipotential culture: hepatocyte-like and cholangiocytes-like. However, the supply of HepaRG is limited, and they are expensive to purchase and expand *in vitro* (Gerets et al., 2012, Hart et al., 2010) and, on cost grounds alone, should probably only be used when these additional phenotypic characteristics are essential for the investigation being undertaken.

Despite some progress in the pharmaceutical sector, many *in vitro* hepatic models still use either primary hepatocytes or animal-derived cell lines, which limit the interpretation of testing outcomes in respect of human metabolism. In developing an *in vitro* hepatic co-culture model for drug metabolism studies, it is important to consider incorporation of non-parenchymal cells, since cytokines and growth factors secreted by stromal cells, are almost certainly involved in detoxification and when hepatic cell are damage in hepatotoxicity (DeLeve et al., 2004, DeLeve, 2013). To recreate liver-like tissue *in vitro* it is important to allow cell-cell interaction of hepatocytes with non-parenchymal cells for preserving hepatic

function (Bhatia et al., 1999, Kim et al., 2012). Indeed, given the importance of cell-cell interactions this is not surprising, as in the embryo hepatocytes interact with endothelial cells to fully differentiate and form a vascularised liver parenchyma (Matsumoto et al., 2001). Developing an *in vitro* human vascularised hepatic model, that more closely mimics that seen in the liver *in vivo*, could help clarify direct/indirect cell-cell interaction and paracrine signalling involved in drug metabolism. Such models could in fact, improve prediction, screening and detection of hepatic drug activity.

This investigation aimed to develop an *in vitro* hepatic model using HUVECs and human hepatic C3A cells, to examine the hypothesis that co-culture of HUVECs and C3As could provide an improved *in vitro* hepatic model for drug metabolism studies by enhancing cellular interactions. Further, understanding the role of endothelial cells in such a hepatic model may be highly beneficial, to understanding *in vivo* hepatotoxicity.

The use of C3As as an alternative to PHH have a number of advantages: C3A cells is an affordable cell line, easy to proliferate, unlimited cell source and provide reproducible experiments for an *in vitro* hepatic model for metabolic and drug metabolism studies (Lockman et al., 2012, Filippi et al., 2004, Tsiaoussis et al., 2001, Choucha Snouber et al., 2013).

In this study, chemically-defined endothelial growth medium (EGM-2) resulted in a biocompatible medium culture for combining HUVEC and C3A in co-cultures, achieving a human heterotypic *in vitro* hepatic model. EGM-2 was selected to culture mono- and co-cultures as it maintained the morphology and hepatic phenotype of C3As, whereas HUVECs only supported characteristic endothelial *in vitro* 'cobblestone' morphology in EGM-2 endothelial medium (Figure 2-1). HUVECs can be significantly damaged by using a cell culture medium which does not contain essential specific growth factors (Bala et al., 2011). Finally, optimization of this *in vitro* co-culture model required identification of specific

phenotypic markers of hepatic (EpCAM) and endothelial (CD31) cells to distinguish these two cell population in co-culture by flow cytometry. Crucially, this allowed for optimization and assessment of the required proportion of each cell type at the start and end of co-culture (Figure 2-5). Although measurement of lactate dehydrogenase has previously been considered to decide between ratios (Soto-Gutierrez et al., 2010), flow cytometry analysis is likely a more robust methodology to select the optimal ratio for HUVEC:C3A. Flow cytometry permits precise electronic gating, allowing analysis of the relative percentage of $CD31^+$ and $EpCAM^+$, important given different cell types often both proliferate and die at different rates.

In this study, HUVECs and C3As in mono- and co-cultures were evaluated on two different days of culture (d3 and d7). Using these two time points demonstrated that the initial ratio can be lost in the short-term. It was very important to maintain the initial ratio as closely as possible, in order to allow consistency of cell-cell interaction to interpret functional assays and to confirm the maintained presence of HUVECs. Amongst ratios and days, only co-cultures seeded at ratio 1:1 for 3 days were able to maintain the initial ratio. Day 7 cultures showed that the higher proliferation rate of C3As would result in HUVECs being 'overgrown', resulting in C3As being the predominant cell line, at the end of the culture period, which would skew interpretation of results (Figure 2-5). We have shown that endothelial cells can improve C3As function using the optimal *in vitro* ratio of 1:1 of HUVEC:C3A for 3 days. Despite not being physiological, ratio 1:1 (HUVEC:C3A) provides significant benefits in controlling cell growth and maintaining the ratio. Published studies have also shown better approaches with similar but not identical physiological ratios. For examples, co-culture of rat or human primary hepatocytes with endothelial cells improves hepatic function when they are co-cultured at proportion of 60% and 40% respectively (Kim et al., 2012, Kostadinova et al., 2013).

The presence of HUVECs significantly enhanced hepatic functionality including albumin synthesis and CYP3A4 activity (Figures 2-10 and 2-12), supporting the idea that C3As are in a more physiological environment in the presence of endothelial cells, increasing cell-cell interaction and cell-extracellular matrix interaction (Soto-Gutierrez et al., 2010, Nahmias et al., 2006). The maintenance of the 1:1 ratio (HUVEC:C3A) correlated with a significant increase in albumin production. In this study, hepatic function was normalised by the number of C3As on day 0, as C3As were seeded at the same density at each ratio to compare the albumin synthesis using the same number of C3As hepatocytes in combination with HUVECs. An alternate strategy may have been to quantify the extent of albumin synthesis by analysing the percentage of C3As hepatocytes in the co-cultures via FACS, and compare the albumin synthesis in each ratio using this technique. However, measuring albumin synthesis in a 96 well plate using flow cytometry was not the best approach in this study, especially for high throughput screening when you require a large number of samples to be assessed rapidly in different conditions.

Only low levels of urea synthesis were detected as a detoxification activity, and this was not improved in co-cultures (Figure 2-11). Although the ammonia detoxification pathway can be induced in HepG2 (Tang et al., 2008), in C3As it is not clear whether this pathway is functional, or if C3As use alternative pathways (Mavri-Damelin et al., 2008). In this study, CYP3A4 activity, involved in the metabolism of the majority of drugs in the market, was improved approximately two fold in C3As in the presence of HUVECs (Figure 2-12). Additionally, morphological and phenotype assessment using immunofluorescent staining in co-cultures, demonstrated enhanced CYP3A4 expression in C3As when in co-culture (Figure 2-13). Improved CYP3A4 activity has also been seen in primary rat hepatocytes in the presence of HUVECs where the presence of HUVECs maintain CYP3A4 activity in hepatocytes (Leong et al., 2013). The evidence of improvement in C3As hepatic function observed in this *in vitro* model was therefore possible without using specific, liver-derived

endothelial cells. There are studies using mouse LSECs co-cultured with hepatocytes to investigate acetaminophen (APAP) hepatotoxicity (DeLeve et al., 1997) but to date there are few published studies using human LSECs for characterization of phenotype (Fomin et al., 2013), because of difficulty of obtaining sufficient cells for experimentation, meaning that it will be difficult to use human LSECs in drug metabolism.

Previous studies have also demonstrated enhanced albumin synthesis and some CYP450 activity (CYP1A2) in rat hepatocytes, when in contact with HUVECs or human micro vessel endothelial cells (Nahmias et al., 2006) or HepG2 co-cultured with bovine endothelial cells (Ohno et al., 2009). However, whereas many of these *in vitro* hepatic models combine animal and human cell lines to demonstrate a potential advantage, such improvements have not previously been shown using both human hepatic (C3As) and endothelial (HUVECs) heterotypic cells in combination. This study demonstrates the importance of interactions between HUVECs and C3As, and suggests that such interaction may be required for improvement of *in vitro* drug metabolism studies.

In the liver, cells regulate molecular mechanisms through the activation of specific receptors. Paracrine signalling from endothelial cells and hepatocytes are stimulated in regeneration and liver injury, but the precise mechanisms remain unknown. Transcription factors such as DNA binding 1 targets proteins like VEGF and HGF have been shown to stimulate liver regeneration (DeLeve, 2013, Ding et al., 2010). VEGF and HGF can be activated in liver injury and activate mechanism of liver regeneration (Kato et al., 2011, Li et al., 2014). It was important to assess whether cross-talk between co-cultured cells resulted in modulation of phenotypic markers. Here, when HUVECs and C3As were co-cultured at ratio 1:1, flow cytometry analysis revealed that there is a modulation of expression of specific markers. Endothelial cells up-regulated expression of CD31, when in direct contact with C3As (Figure 2-14). CD31 expression has been shown to be down-regulated in rat LSECs when co-culture with hepatocytes (DeLeve et al., 2004) and HGF promotes rat hepatocyte migration to

HUVECs (Nahmias et al., 2006). HUVECs express and can regulate C-met expression in stress conditions (Tomizawa et al., 2014). In this study, C-met which is HGF receptor was identified in both HUVECs and C3As, maintaining strong expression in co-cultures, whereas VEGFR-2 expression was down-regulated, with CD31 maintained (Figure 2-12). These findings show that HUVECs do not show any degradation of phenotype in the presence of C3As.

In this study, the *in vitro* human hepatic model, incorporating hepatocytes and endothelial cells to improve pharmaceutical drug testing, should in future also offer the opportunity to investigate the role of endothelial cells in hepatotoxicity. This is of interest as drugs cause liver injury not only by damaging hepatocytes, but though also LSECs affects (Badmann et al., 2012, DeLeve et al., 1997). Thus, co-cultures of a hepatic cell line and endothelial cells in an *in vitro* model could provide a more physiologically-relevant platform for evaluating drug detoxification. The next stage to more fully characterize the *in vitro* human hepatic co-culture model would be to assess endothelial cell and hepatocyte functional response to detoxification, using a hepatotoxicity drug such as acetaminophen (APAP), including activation of receptors and signals in co-cultures, not normally seen in mono-cultures.

3 Chapter 3: Human organotypic co-culture enhances hepatic drug metabolic activity in acetaminophen (APAP) toxicity

3.1 Introduction

As discussed in the main introduction to this thesis (Section 1.5), drugs are screened extensively in *in vitro* models, animal and human clinical trials during drug development, but hepatotoxicity is not always predicted accurately. As a consequence, drugs can be classified with a warning label or be withdrawn from the market (Kaplowitz, 2005, Arrowsmith and Miller, 2013, Shah et al., 2013). Indeed, drug dose-dependent hepatotoxicity is often not detected in these pre-clinical studies because *in vitro* hepatic model do not accurately represent *in vivo* and drug doses tested *in vivo* do not always achieve toxic levels.

One example of such a drug is APAP which displays dose-dependent hepatotoxicity and is the foremost cause of acute liver failure (ALF) in the UK and the US (Blachier et al., 2013). In a small number of people, even at therapeutic doses, medicines can cause drug hepatotoxicity as an idiosyncratic event which is unpredictable in nature and can lead to severe ALF, with the only life-saving treatment being liver transplantation (Gulmez et al., 2013, Chalasani and Bjornsson, 2010). The available effective antidote for APAP overdose is n-acetylcysteine (NAC). NAC needs to be administered in the first few hours following overdose, before hepatic necrosis occurs. Similar efficacy is also observed using *in vitro* PHH models where NAC is significantly more effective after 6hr of APAP exposure compared to 24hr (Xie et al., 2014b).

The ability to model toxic effects of APAP *in vitro* could enhance drug safety for individuals. In the classic detox pathway APAP metabolized by liver cells (hepatocytes) via the CYP450 system, mainly through the isoform CYP2E1, produces a highly toxic by-

product NAPQI and can also disrupt metabolic processes, resulting in the production of more lactate than pyruvate in early stages of liver failure (Shah et al., 2011). At therapeutic doses, NAPQI is detoxified by GSH conjugation. However, at toxic levels, GSH stores become depleted and cannot neutralise excess of NAPQI; cells then get damaged because NAPQI binds macromolecules (proteins and DNA) causing an increase in the levels of ROS and a toxic reaction, affecting also the glycolysis mechanism (Rashid et al., 2013, Moyer et al., 2011, Shah et al., 2011). This disruption in glycolysis metabolism can reduce ATP formation, the major source of energy produced in the mitochondria, accompanied by activation of oxidants and enhanced drug toxicity (Han et al., 2013, Kon et al., 2004). Further investigation is still required about the APAP mechanism of toxicity. However, APAP may also damage endothelial cells by additional mechanisms. High levels of lactate have been associated with mitochondrial dysfunction in human aortic endothelial cells. APAP can also damage the endothelial fenestrae affecting drug clearance, mitochondria function and accumulation of toxins in the liver (Ito et al., 2003, Badmann et al., 2012, Shah et al., 2011, Deavall et al., 2012).

Necrosis in hepatocytes is associated to the accumulation of the toxic NAPQI. NAPQI reacts with GSH to be neutralised but at high doses APAP toxicity can cause changes in endothelial permeability which can result in haemorrhage and accumulation of erythrocytes in the sinusoidal space (Ito et al., 2003). These findings suggest that APAP at toxic levels, can alter the permeability of LSECs and damage the fenestrae (Kim et al., 2001, Jaeschke et al., 2002, Badmann et al., 2012). Identifying endothelial cells as an early target of drug toxicity would have an important impact in evaluating response to injury caused by drug activation and may lead to improved understanding of the contribution of endothelial cell metabolism in DILI. Therefore, use of an *in vitro* vascularized hepatic model in drug testing, could make clearer the role of endothelial and hepatic intercellular signalling in drug-induced hepatotoxicity. In Chapter 2, the feasibility of developing a physiologically-relevant *in vitro* human hepatic co-

culture model using HUVECs and C3As, which performed better than an *in vitro* mono-culture model using C3As alone was demonstrated. Improved hepatic function (albumin synthesis and CYP3A4 activity) by day 3 of co-cultured is potentially the result of enhanced cell-cell interaction. Indeed, liver tissue modelling using co-cultures combining hepatocytes and fibroblasts, have had improvements in maintaining hepatic functionality *in vitro* for hepatotoxicity studies (Ukairo et al., 2013). However, an *in vitro* human vascularised hepatic co-culture model using HUVECs as a source of endothelial cells may reveal heterotypic interactions which regulate drug toxicity and improve drug discovery. To investigate this possibility, the *in vitro* co-culture model was utilised to evaluate the cellular responses of HUVECs and C3As to the dose-dependent hepatotoxic drug, acetaminophen (APAP).

We therefore hypothesize that an *in vitro* human liver 'co-culture' model comprising different types of cells, may allow closer representation of *in-vivo* liver-like function, especially closer representation of drug metabolism for predicting toxicity at an earlier stage of drug development. To test the hypothesis that the use of HUVECs with C3As is more relevant for prediction of drug toxicity than using C3As alone, the *in vitro* co-culture model described in Chapter 2 was exposed to a dose-dependent hepatotoxic drug, APAP. APAP hepatotoxicity was chosen as a model of drug-induced liver injury, with the aim of evaluating both cellular and metabolic mechanisms involved in hepatotoxicity.

The following experiments were undertaken:

I. Evaluation of the effect of APAP toxicity on intracellular ATP levels and mitochondrial activity as markers of cell viability and metabolic competence: HUVECs and C3As in mono- and co-cultures were exposed to low (5mM), intermediate (10mM) and high (20mM) APAP doses for 6hr and 24hr.
II. Investigation of a known toxic APAP dose on the morphology and viability in mono and co-cultures.

III. Measurement of lactate and pyruvate levels as an indicators of disturbances on the glycolytic metabolic pathway in APAP toxicity.

3.2 Materials and methods

3.2.1 Experimental design

APAP toxicity experiments

HUVECs and C3As were first seeded at density of 21,000 cells/cm^2 in monolayers, or co-cultured together, unless otherwise indicated, at a ratio of 1:1 (HUVEC:C3A) in EGM-2 medium. Subsequently, cells in mono- and co-culture were incubated with: 0 mM, 5 mM, 10 mM and 20 mM APAP for 6hr and 24hr (0 mM APAP represents untreated control). When cells were incubated with n-acetylcysteine (NAC), cells were washed twice in PBS to remove APAP, and then exposed for a further 24hr of 5 mM NAC. Doses have already been used previously with HepG2 cells (Manov et al., 2004) to assess the recovery of cells from APAP exposure.

3.2.2 Cell viability assay: Live/Dead fluorescent staining

The viability of HUVECs and C3A in mono and co-cultures was determined using a LIVE/DEAD® Viability/Cytotoxicity Kit (Life Technologies). Live and dead cells are distinguished enzymatically and by nucleic acid binding using two-colour calcein and ethidium homodimer fluorescent dyes. In brief, Calcein AM detects intracellular esterase activity in cells with intact membranes, producing green fluorescence and ethidium homodimer binds to nucleic acids in damaged cells producing bright red fluorescence.

Calcein and ethidium homodimer dyes were added to control and APAP-treated cells following the manufacturer's instructions. After 45 min incubation at room temperature, in the dark, phase contrast and fluorescence images of controls and treated cells were acquired

using filters for green fluorescence (Calcein = 494/517 nm) and red fluorescence (Ethidium homodimer-1 in the presence of DNA = 528/617 nm) using an inverted microscope (Zeiss Axio-Observer A1, Germany). Images were captured with a mounted camera (Zeiss AxioCam MRm) and processed and merged using ImageJ 1.46r (National Institute of Health, USA, http://imagej.nih.gov/ij/docs/guide/146-2.html).

3.2.3 Total intracellular ATP levels

Total intracellular ATP levels were measured in HUVEC and C3A mono- and co-cultures as an invasive endpoint for hepatotoxicity using the CellTiter-Glo Luminescent Cell Viability assay (Promega). In brief, HUVECs and C3As in mono- and co-cultures were seeded at a density 0.12 x 10^4 cells per well in EGM-2 medium and cultured for 2 days. Subsequently, cells were washed twice with PBS and incubated at 37ºC and 5% (v/v) CO_2 with a serial concentration of 0 mM, 5 mM, 10 mM and 20 mM APAP in EGM-2 medium (0 mM APAP represents untreated control) for 6hr or 24hr. After APAP incubation, cells were lysed using CellTiter-Glo reagent and supernatants transferred to a white-walled 96 well plate to be read on the GloMax plate-reader (Promega). Total intracellular ATP levels in untreated controls were considered as reference control values with nominal 100% ATP content for C3As, HUVECs or co-cultures. ATP levels in treated cells were normalised to appropriate controls values to determine cell viability.

3.2.4 Mitochondrial function and membrane integrity assay

Mitochondrial function can be measured using viability biomarkers of cell membrane integrity and by quantification of the ATP generated during brief incubation with galactose during 90 min at 37ºC and 5% (v/v) CO_2. In this study, mitochondria function was measured using Mitochondria ToxGlo Assay (Promega) following the manufacturer's instructions. This assay measures protease activity associated to necrosis using a fluorogenic peptide

substrate and the capacity of the mitochondria to generate ATP after incubation with D-(+)-galactose.

The capacity of mitochondria to generate ATP was evaluated in HUVEC and C3A mono- and co-cultures following 24hr exposure to 0 mM, 5 mM, 10 mM or 20 mM APAP (0 mM APAP represents untreated control). Following APAP exposure, cells were washed twice with PBS and incubated at 37ºC and 5% (v/v) CO_2 with 5 mM D-(+)-galactose in EGM-2 medium for 90 min to measure membrane integrity using Mitochondria ToxGlo Assay (Promega).

Untreated control cells (0 mM) were considered 100% viable (with no alteration in the integrity of the membrane) for C3As, HUVECs and co-cultures. Values for treated cells were normalised to untreated controls.

The reason D-(+)-galactose was chosen as substrate, instead of glucose, is that metabolism of galactose generates only limited amounts of ATP from glycolysis, forcing the cells to use oxidative phosphorylation to produce additional ATP, a process depending on intact mitochondrial function. For that reason, the use of galactose allows the detection of mitochondrial perturbations in the membrane with greater sensitivity than when using glucose (Dott et al., 2014, Aguer et al., 2011, Marroquin et al., 2007).

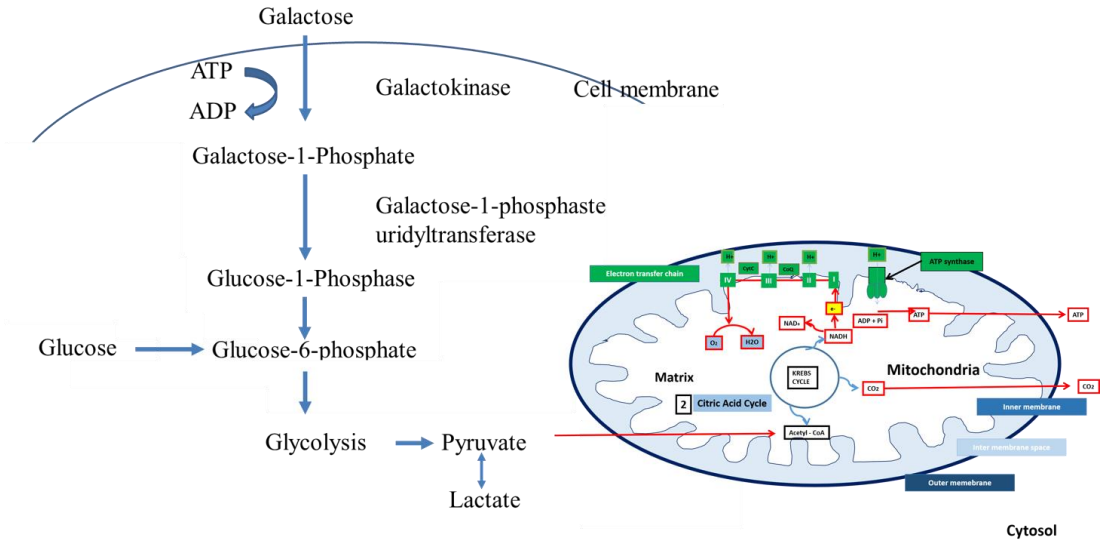

Figure 3-1 Galactose metabolism in glycolysis

The addition of galactose is taken into the cells to produce glucose for ATP production. The use of galactose is more responsive to reflect mitochondria function as cells use mitochondrial oxidative phosphorylation to generate ATP. Image modified from Ostergaard et al. (Ostergaard et al., 2000)

3.2.5 Pyruvate and lactate measurement

The production of lactate and pyruvate from HUVECs and C3As in mono and co-culture are catalysed in a reversible reaction by lactic dehydrogenase (LDH), in the presence of the co-factors adenine dinucleotide reduced (NADH) and dinucleotide oxidized (NAD+) respectively. The measurement of these co-factors in culture supernatants using two different buffers by spectrophotometry can be used to determine lactate/pyruvate concentrations independently. Lactate/NADH can be determined by absorption measurement at 340nm and pyruvate/NAD values can be determined measuring the reduction in absorbance due to the conversion of NADH to NAD with specific buffers pushing the reaction one way or the other.

$$\text{Pyruvate} + \text{NADH} \xleftrightarrow{\text{LDH}} \text{Lactate} + \text{NAD+}$$

For the experiment, cells were exposed to 10 mM APAP on the second day of HUVECs and C3As in mono and co-cultures for 24hr. Then, cells were washed with PBS to remove APAP; 5 mM n-acetylcysteine (NAC) was additional added for another 24hr. After APAP, NAC or EGM-2 (controls) incubations, cell supernatants were removed for measurement and cells were collected and sonicated for total protein measurements (BCA assay, Pierce).

Samples were read in cuvettes (Cuvettes Semi micro ps 100/pk, Fisherbrand) using Unicam UV1 Spectrophotometer (Equionet) and values were normalised by total protein (BCA assay, Pierce).

3.2.5.1.1 Lactate measurement

For lactate measurement, 10µl of each cell supernatant sample or water control was added to cuvettes (Cuvettes Semi micro ps 100/pk, Fisherbrand, UK) containing 1 ml lactate buffer

(freshly prepared by mixing with 50mg NAD+, 3g of glycine, 2ml hydrate hydrazine, 100ml of water and 100µl of LDH). Samples were mixed gently by inverting cuvette and incubated for 1.5hr at RT Following incubation, the NADH concentration was determined by absorbance at 340nm.

The lactate concentration was calculated as following:

$$\text{Lactate (mM)} = \frac{\Delta A\ 340\text{mM} \times \text{RV (ml)}}{6.22 \times \text{VS (ml)} \times \text{lightpath (cm)}}$$

ΔA_{340}: Final absorbance at 340nm

6.22: mM^{-1} .cm^{-1} extinction coefficient of NADH at 340mM

RV: Reaction volume = 1 mL

VS: Volume of sample in cuvette = 10µl (0.01 ml)

Lightpath = 1 cm

3.2.5.1.2 Pyruvate measurement

For pyruvate measurement, 50µl of each cell supernatant sample or water control was were added to cuvettes (Cuvettes Semi micro ps 100/pk, Fisherbrand, UK) containing 1 ml pyruvate buffer, prepared fresh every time by mixing 12mg NADH for 100ml PBS. Then samples were mixed and NADH was detected by absorbance at 340nm. Subsequently, 10 µl of a solution of LDH diluted at 1/11 in water was added into each cuvette, alongside a water sample as control and incubated 15 min at room temperature. After incubation, second reading was recorded, thus:

ΔA_{340} = Initial A_{340} – final A_{340}

$$\text{Pyruvate (mM)} = \frac{\Delta A\ 340\text{mM} \times \text{RV (ml)}}{6.22 \times \text{VS (ml)} \times \text{lightpath (cm)}}$$

ΔA_{340}: Final absorbance at 340nm

6.22: mM^{-1} .cm^{-1} extinction coefficient of NADH at 340mM

RV: Reaction volume = 1 mL

VS: Volume of sample in cuvette = 10µl (0.01 ml)

Lightpath = 1 cm

3.3 Determination of total protein

Cells were scraped from cell culture wells in ice-cold PBS and sonicated to quantify total protein content. Total protein was measured using a bicinchoninic acid assay (BCA assay, Pierce) according to the manufacturer's instructions, and read using Sunrise™ microplate reader (Tecan, Switzerland) and absorbance was measured at 550 nm. Total protein concentration was obtained from a standard curve using Albumin Standard Ampoules, 2mg/mL.

3.4 Statistical Analysis

Experiments were performed in triplicate on at least three biological replicates. GraphPad software Prism®5 was used for statistical analysis. Results were reported as mean ± standard error (SEM). Student's unpaired t-test was used to compare all co-cultures to their appropriate HUVECs and C3As controls (statistical significance *$p<0.05$).

3.5 Results

3.5.1 Intracellular ATP levels as a measure of cell viability following 6hr and 24hr APAP exposure

APAP can be used as a hepatotoxic drug to test dose-dependent effects in hepatocytes *in vitro.* In this study, HUVECs and C3As were cultured for 3 days in both mono- and co-culture. Cells were exposed to APAP at low (5 mM), intermediate (10 mM) and high APAP (20 mM) doses for 6hr and 24hr after which intracellular ATP content was measured to determine cell viability following each time of APAP incubation.

In summary, percentages of ATP depletion following 6hr APAP at all concentrations were not significant between untreated and APAP treated HUVEC and C3A mono- and co-cultures (Figure 3-1A). When HUVECs mono-cultures were exposed to 5 mM APAP, ATP levels rose to 117.01 ± 11.74 % as compared to controls (untreated). At 10 mM and 20 mM APAP, the percentage of ATP was respectively 117.16 ± 11.20 % and 110.21 ± 12.03 % of HUVECs controls (untreated). In C3As mono-cultures, percentage of ATP levels went from 100% in controls (untreated) to 97.95 ± 5.28 % when C3As were exposed to 5 mM APAP. At 10 mM APAP, 93.93 ± 1.41 % of ATP values were observed and 82.52 ± 2.78 % at 20 mM APAP. In co-cultures, percentage of ATP values were 112.32 ± 3.4 % when co-cultures were exposed to 5 mM APAP, 104.07 ± 3.01 % at 10 mM and 97.81 ± 10.36 % at 20 mM APAP.

By contrast, significant changes in the percentage of ATP levels were detected in HUVECs and C3As in mono and co-cultures after 24hr of incubation with APAP. Results revealed that APAP incubation in HUVEC and C3A mono-cultures showed a relative decrease in ATP values at all doses, whereas in co-culture ATP levels were not significantly affected by intermediate (10 mM) doses of APAP.

After 5 mM APAP exposure, the percentage of ATP levels in HUVECs mono-culture declined to 50.46 ± 12.71 % of control ATP levels, which was also significantly different to the percentage of ATP levels observed in C3A mono-cultures (87.19 ± 4.92 % ;p=0.012) and also in HUVEC:C3A co-culture (103.71 ± 9.34 % ; p=0.009). Comparison of C3A mono- and co-cultures showed that there were no significant differences in ATP levels at 5 mM APAP (Figure 3-1B).

After 10 mM APAP exposure, ATP levels were reduced respectively to 44.73 ± 19.23 % and 62.41 ± 7.53 % in HUVEC and C3A mono-cultures. By comparison, after 10 mM APAP exposure ATP levels in co-cultures (106.49 ± 10.45 %) were maintained, and were significantly higher than HUVECs (p=0.007) and C3As (p=0.007) mono-cultures (Figure 3-1B).

After 20 mM APAP exposure, ATP levels were respectively 35.60 ± 20.72 % in HUVECs and 51.33 ± 12.16 % in C3As, whereas co-cultures showed the highest percentage with 81.29 ± 13.15 % of control ATP levels, though this value was not significantly different to ATP levels in HUVEC or C3A mono-cultures (Figure 3-2B).

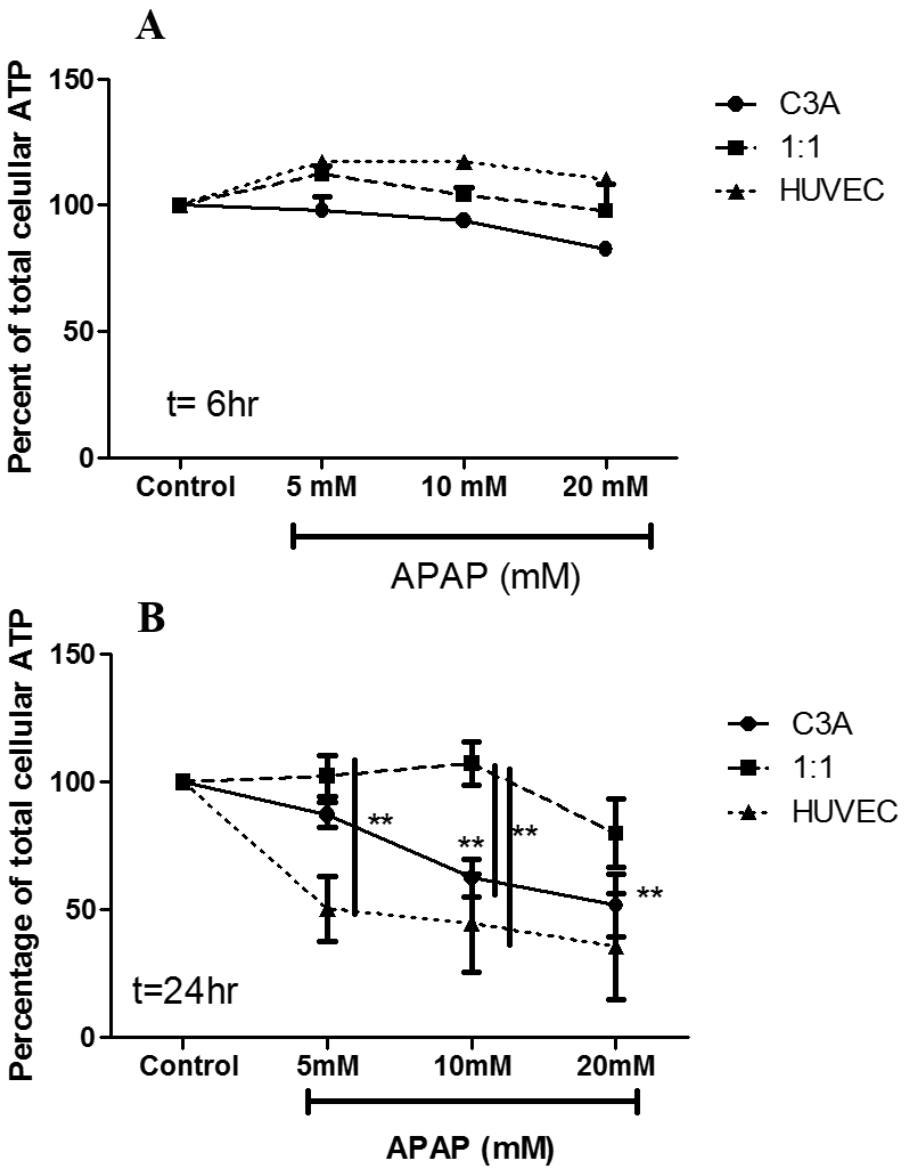

Figure 3-2 Effects of APAP treatment on intracellular ATP levels as a cell viability marker in C3As, HUVECs and co-cultures at time 6hr and 24hr

*Intracellular ATP levels were measured as a marker of cell viability using CellTiter-Glo Luminescent Cell Viability assay (Promega) in HUVECs and C3As mono- and co-cultures (at a ratio of 1:1) following exposure to serial concentrations of 0 mM, 5 mM, 10 mM and 20 mM APAP (0 mM APAP represents control) for either (A) 6hr and (B) 24hr. The Percentage of total intracellular ATP levels was obtained dividing relative luminescence units (RLU) in each group by their corresponding untreated RLU controls values and multiplying by 100. Data is expressed by the mean ± SEM of three different experiments with significant different at *P<0.05, **P<0.001. (n=3)*

3.5.2 Mitochondrial function and membrane integrity in APAP toxicity

Here, after 24hr exposure to low, intermediate and high doses (5 mM, 10 mM and 20 mM) of APAP, cells in mono- and co-cultures were incubated with galactose for 90 min to determine ATP generation, as described in Section 3.2.4, as a measure of the susceptibility of mitochondria to damage by APAP cytotoxicity. Injury caused by APAP affecting cell membrane and mitochondrial function was detected in both endothelial and hepatic cells. Data showed that although significant cytotoxic damage was observed to membrane integrity especially in HUVEC mono-cultures, cells were still able to take up galactose to produce ATP by oxidative phosphorylation (Figure 3-3).

When APAP-treated HUVEC and C3A mono- and co-cultures were incubated with D-galactose for 90 min, the evaluation of cytotoxicity in HUVEC mono-cultures revealed that exposure to 5 mM APAP can disrupt membrane integrity (Figure 3-3). 5 mM APAP caused cytotoxic effect in 38.16 ± 0.99 % on HUVECs, which is significantly greater than that on C3As (23.67 ± 4.18 %; p=0.03) and also significantly greater than that on co-cultures (14.11 ± 6.89 %; p = 0.03). Similarly, at 10 mM, while 27.71 ± 7.95% of C3As had damage to their membranes, 60.33 ± 7.68 % of HUVECs where affected, a significantly higher compared to C3As (p=0.04) and also co-cultures where only 27.94 ± 4.76 % of cells showed disruption (p=0.02) (Figure 3-3). No significant difference was observed between C3As alone and co-cultures.

At high dose (20 mM APAP), 89.59 ± 4.16 % of HUVECs showed damage, while only 53.68 ± 6.03% of C3As (significantly lower than HUVECs, p=0.0081), and 33.42 ± 15.56 % of co-cultures (significantly lower than HUVECs, p=0.025), showed damage due to APAP toxicity after 24hr) (Figure 3-3).

Taken together, the data shows that in all cell types, the capacity to generate mitochondrial ATP dropped proportionally as the dose of APAP increased (Figure 3-3). The percentage of ATP generated in C3As after APAP exposure compared to untreated was 88.32 ± 4.74 % of ATP produced after 5 mM APAP exposure, 61.42 ± 9.06 % of ATP produced after 10 mM APAP and 22.64 ± 11.32 % of ATP after 20 mM APAP. The percentage of ATP generated in HUVECs after 5 mM APAP exposure was 91.03 ± 21.89 %, 73.73 ± 20.62 % after 10 mM APAP exposure and 12.01 ± 6.05 % after 20 mM APAP exposure. In co-cultures exposed to APAP, HUVECs and C3As were still able to produce high levels of ATP, resulting in 96.72 ± 5.85 % of control after 5mM APAP exposure and 74.19 ± 19.14 % of control after 10 mM APAP exposure. A lower percentage of ATP was detected at doses of 20 mM APAP with only 40.95 ± 21.14 % of ATP being produced by HUVECs and C3As in co-cultures compared to that produced in untreated cells.

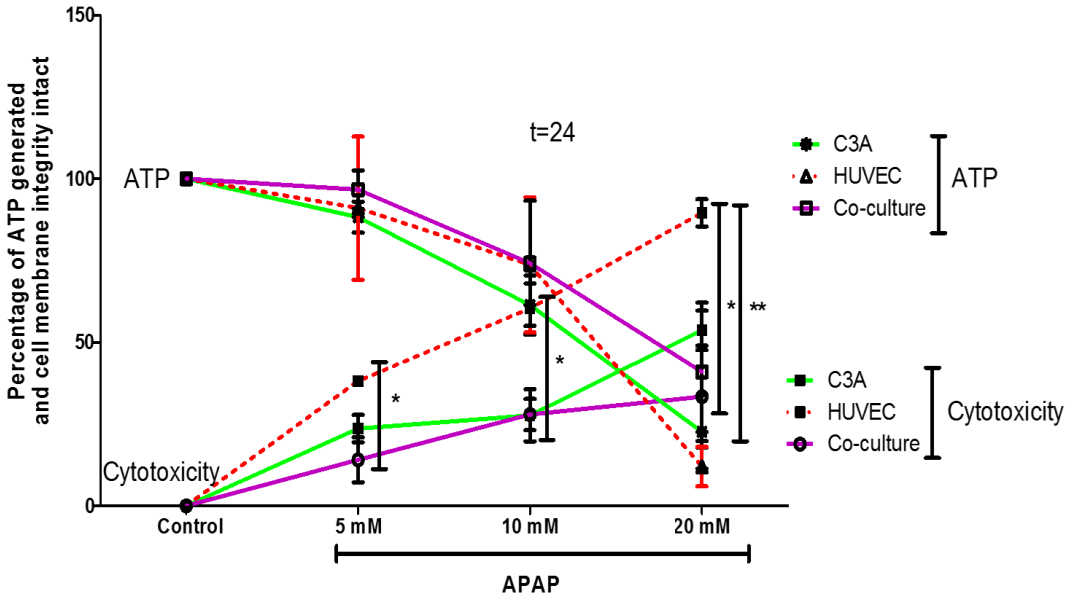

Figure 3-3 Mitochondrial ATP production and damage to the integrity of the membrane in HUVECs, C3As and co-cultures after APAP exposure

*HUVECs, C3As and co-cultures (at a ratio of 1:1) were incubated with low, intermediate and high doses (5 mM, 10 mM and 20 mM) of APAP for 24hr followed by an incubation with D-(+)-galactose for 90 min at 37ºC to evaluate mitochondria function using Mitochondria ToxGlo Assay (Promega). Percentages of total intracellular ATP levels and cytotoxicity were obtained by dividing relative luminescence units (RLU) in each group of controls by their corresponding untreated RLU values and multiplying by 100. Data is expressed by the mean ± SEM of three different experiments of three different replicates with significant different at *P<0.05 and **P<0.001 (n=3).*

3.5.3 Morphology in HUVECs and C3As after 24hr 10 mM APAP exposure

Previous results in Section 3.5.1 and 3.5.2 showed that co-cultures were significantly more resistant to an intermediate (10 mM) dose of APAP than in mono-cultures. Therefore mono and co-cultures were treated with 10 mM APAP for 24hr and analysed for signs of morphological changes as an indicator of APAP toxicity, by phase contrast microscopy using a cell viability fluorescent staining.

Cell viability and cell death were confirmed using phase contrast and immunofluorescence using live (bright green) and dead (bright red) staining following exposure to 10 mM APAP. Phase contrast images in Figure 3-4 show that HUVECs in mono-culture after 24hr treatment with APAP, compared to controls (Figure 3-4A) failed to maintain their characteristic endothelial cobblestone morphology (Figure 3-4B) and show poor viability (bright red) and increased cell death (bright red); while C3As or HUVEC:C3A co-cultures were relatively unaffected by APAP exposure (Figure 3-4C & D), suggesting that HUVECs are more sensitive than C3As to APAP toxicity.

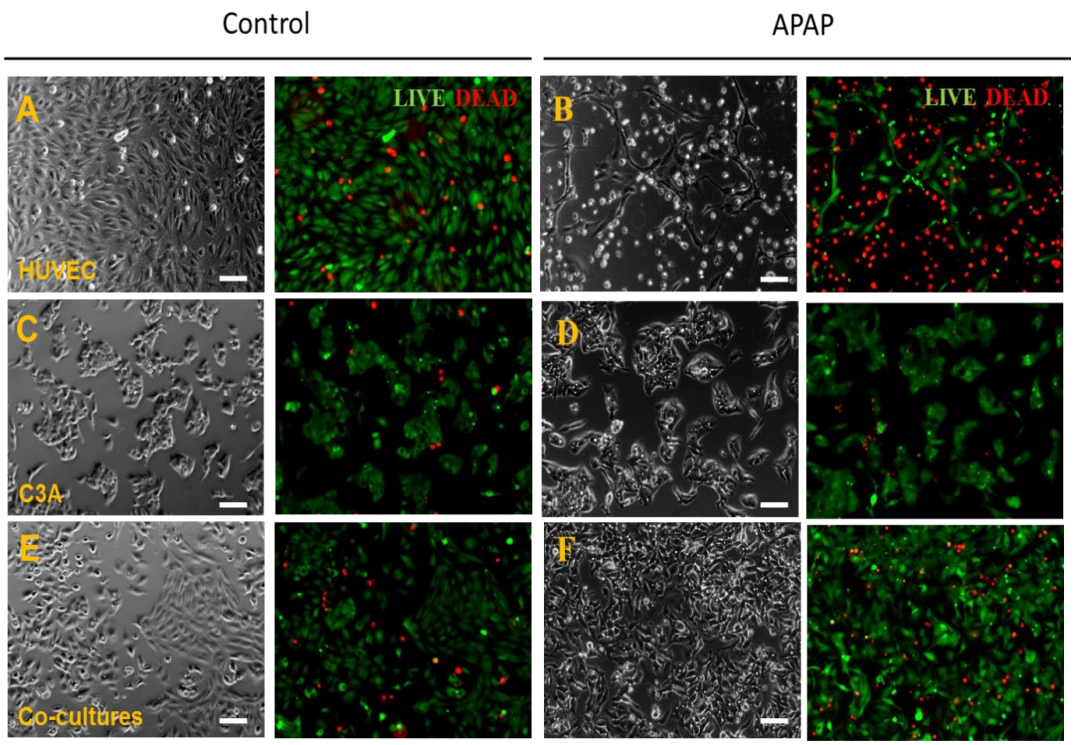

Figure 3-4 Cellular morphology and live and dead staining of HUVECs or C3A in mono and in co-cultures after 10 mM APAP exposure

HUVECs and C3As in mono- or co-culture (at a ratio of 1:1) were incubated with EGM-2 alone (controls) or containing 10 mM APAP for 24hr. Subsequently, live and dead staining reagents (LIVE/DEAD® Viability/Cytotoxicity Kit; Life technologies) was added to the culture wells and after 45 min of incubation at RT in the dark, phase contrast and fluorescence images of HUVECs (A), C3A (C) and co-culture (E) controls and HUVECs (B), C3A (D) and co-culture (F) APAP-treated cells were acquired to detect bright green fluorescence for live cells and bright red for death cells at magnification x10. Images were merged using ImageJ 1.46r. Scale bar 100µm.

3.5.4 Number of HUVEC and C3A in co-cultures following APAP for 24hr

Previously, Figure 3-4 showed that HUVECs in mono-culture showed considerably more cell death (bright red fluorescence) than C3As alone and in co-cultures exposed to APAP. Mitochondrial function (Figure 3-3) and cell morphology were maintained after APAP exposure in co-cultures (Figure 3-4). However, it is important to investigate whether the viability of HUVECs and/or C3As are maintained in co-culture. To demonstrate the presence of both cell lines together, cells were evaluated by flow cytometry to quantify the percentage of each cells affected in APAP toxicity by evaluating cell-specific markers.

As described previously, CD31 and EpCAM can be used respectively to identify HUVECs and C3As in co-cultures (Figure 2-7). Flow cytometry analysis confirmed that in HUVEC and C3A co-cultures, $CD31^+$ and $EpCAM^+$ expression were essentially maintained after 24hr APAP exposure. There was a slight reduction in $CD31^+$ of 0.87 ± 0.04 fold, whereas C3As showed a minor increase of 1.07 ± 0.04 fold increase observed, confirming that APAP had a modest effect on HUVEC and C3A numbers (Figure 3-5).

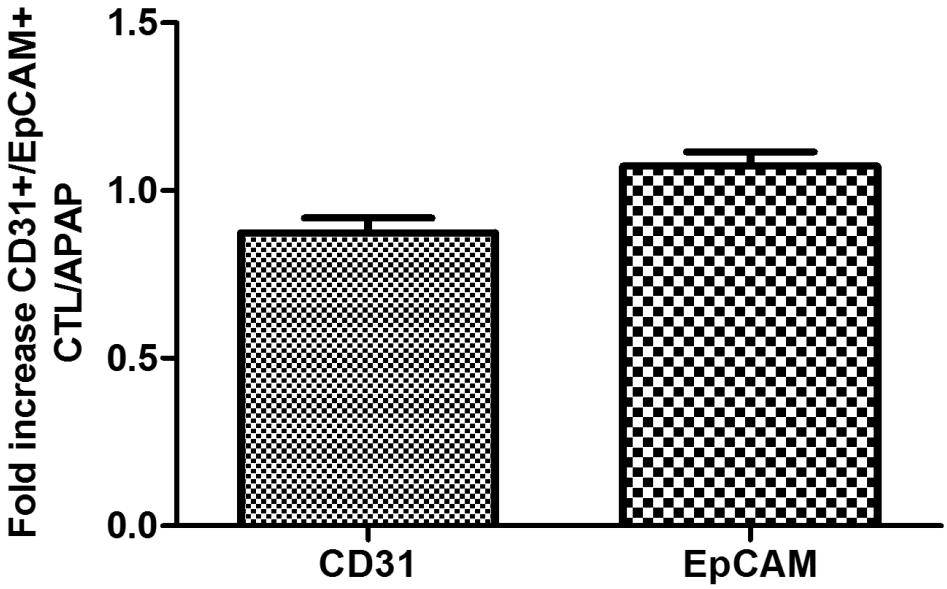

Figure 3-5 Fold increase of platelet endothelial cell adhesion molecule (CD31), and hepatic epithelial cell adhesion molecule (EpCAM) in co-cultures after 24hr of APAP exposure

HUVEC:C3A co-cultures at a ratio of 1:1, were exposed to 10 mM APAP for 24hr. Subsequently, cells were stained with CD31 and EpCAM and analysed by flow cytometry to obtain the percentage of $CD31^+$ and $EpCAM^+$ in co-cultures in untreated (controls) and APAP treated cells. Fold increase was obtained comparing to untreated $CD31^+/EpCAM^+$. Data is expressed as Mean ± SEM of three different experiments (n=3). Percentages of total intracellular ATP levels and cytotoxicity were obtained by dividing relative luminescence units (RLU) in each group of controls by their corresponding untreated RLU values and multiplying by 100.

3.5.5 Glycolysis and redox state in HUVECs and C3As after 24hr of APAP exposure followed by 24hr of NAC treatment

Pyruvate and lactate levels (end-products of glycolysis released into the supernatant) were measured in untreated (control) and treated (10 mM APAP) HUVEC and C3A mono- and co-cultures after 24hr. Furthermore, the addition of NAC for 24hr after APAP exposure was also evaluated.

Results showed several alterations in energy metabolism, especially in lactate concentrations. Pyruvate/lactate ratio of mono-cultures of HUVECs and C3As showed comparable changes when cells were exposed to 10 mM APAP; and when followed by 5 mM NAC treatment. The increase in P/L ratio of APAP-treated cells was not significantly different from untreated cells in mono-cultures; however, the P/L ratio rose significantly following NAC treatment of mono-cultures. In co-cultures no significant changes were observed (Figure 3-6A).

Pyruvate to lactate ratio (P/L) is proportional to the NAD/NADH ratio, i.e. the redox potential, itself depending on both the rate of NADH production (through glycolysis) and the function of mitochondria (Williamson et al., 1967).

Glycolysis metabolism

In C3A cells, treatment with 10mM APAP for 3 days had no effect the cytosolic redox potential (Figure 3-6A) or on glycolytic fluxes (Figure 3-6 B), as measured by the ratio of pyruvate to lactate. In the light of the previous results on ATP and cell integrity, this is quite surprising, as a decrease in ATP usually result in stimulation of glycolysis (Figure 3-2 B).

The addition of NAC for another 24hr significantly increased the pyruvate to lactate ratio, a sign that the cells were in a much more oxidised state. The lack of effect on glycolysis is

surprising here as there is usually a correlation between cell integrity, glycolytic fluxes and redox potential.

HUVECs in mono-cultures were much more sensitive to the addition of APAP, showing a strong and significant increase in glycolysis (mention the real values here 195.60 ± 59.09 vs 29.65 ± 5.13, $p<0.05$). The P/L ratio was not significantly different with our number of replicates, though it seemed to indicate a more oxidised state in HUVECs after APAP treatment (Figure 3-6B). Taken together with the ATP and cytotoxicity measurements, it seems like APAP resulted in oxidative stress in HUVECs resulting in mitochondrial damage and hence lower ATP production forcing the cells to increase glycolysis to compensate the lack of ATP.

The addition of NAC in HUVECs resulted in a much lower increase in the glycolytic flux, potentially a reflection of a lower damage to mitochondria. However, the P/L ratio indicated an even higher oxidation level in HUVECs, similar to the one found in C3As, a measurement of ATP and cell integrity in this case would have helped us determine the exact mechanism happening in these cells.

The fact that HUVECs were much more sensitive to APAP than C3As could be due to the higher levels of anti-oxidant constitutively present in hepatocytes.

Interestingly, the co-culture of HUVEC and C3A totally buffered the effects of APAP and the further addition of NAC, which is perfectly in line with the results found on ATP and cytotoxicity in the previous section (see Figure 3-2B).

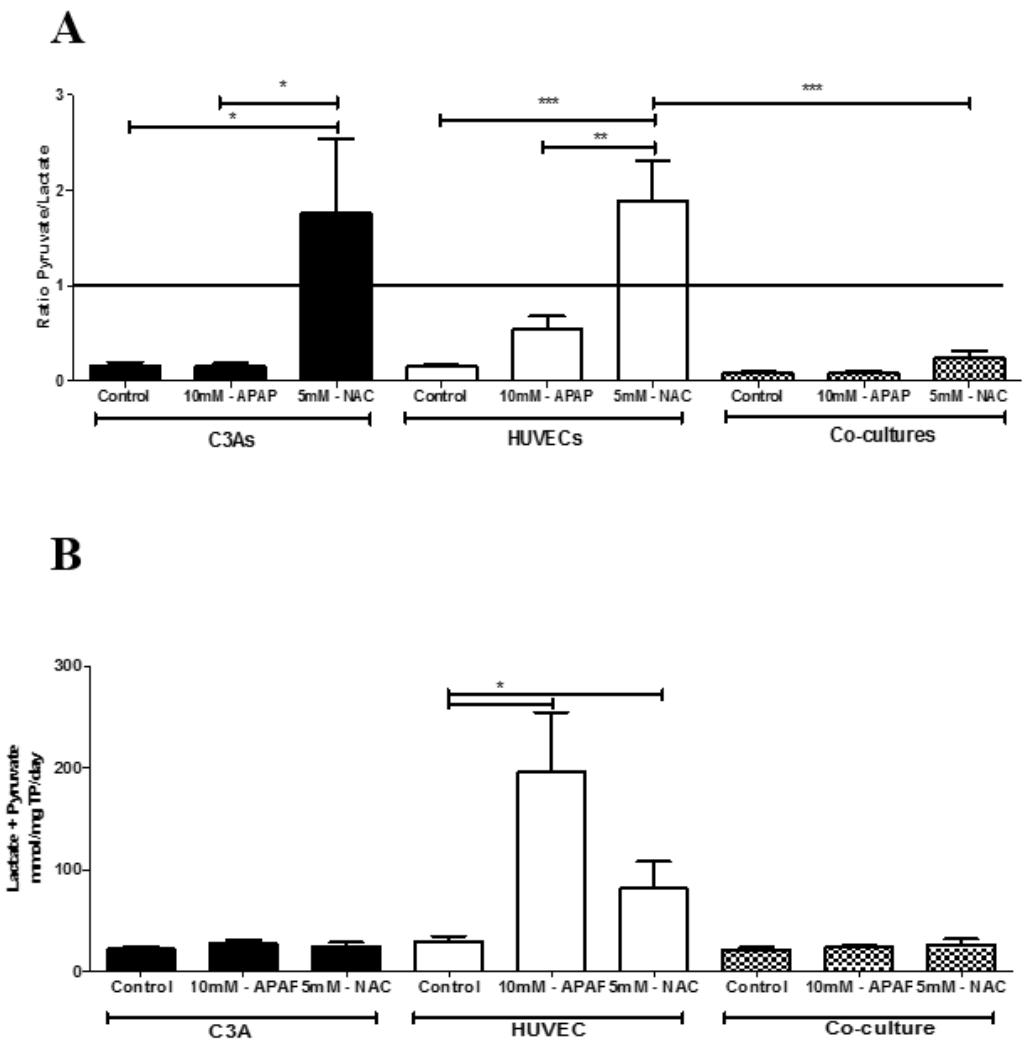

Figure 3-6 Lactate and pyruvate levels in C3A and HUVEC mono and co-cultures after 24hr of APAP exposure and 24hr of NAC treatment

*Cells were cultured with EGM-2 (control), or 10 mM APAP in EGM-2 and post-treatment with NAC for 24hr period. Supernatants were collected to measure the ratio of pyruvate/lactate (A) and glycolysis metabolism (B) C3A (black bars) and HUVEC (white bars) mono- and co-culture (patterned bars). Values were compared statistically between untreated cells (controls) and cells treated with 10 mM APAP on day 3, as well as after additional treatment with 5 mM NAC for another 24hr. Data is displayed as the mean ± SEM from at least three separate experiments in triplicate, * $p < 0.05$/ ** $p < 0.01$/ *** $p < 0.001$.*

3.5.6 Relative total protein in HUVECs and C3As after 24hr APAP exposure followed by 24hr NAC treatment

Here, the measurement of the percentages of total protein in untreated (control) HUVEC, and C3A mono- and co-cultures or treated with 10 mM APAP for 24hr and then NAC for another 24hr were measured to reveal the number of cells attached in the cultured plate after each treatment.

Data revealed that the percentage of total protein in HUVEC mono-cultures dropped from 100 % in controls to 26.96 ± 10.26 % after APAP treatment and to 13.22 ± 8.8 % after NAC treatment. C3A mono-cultures were slightly different in that the percentage of total protein measured was 70.09 ± 28.24 % after 24hr APAP exposure and 48.66 ± 26.66 % after NAC treatment. In co-culture, the respective percentages were 80.75 ± 23.04 % 24hr APAP exposure and 45.45 ± 21.64 % after NAC treatment (Figure 3-7).

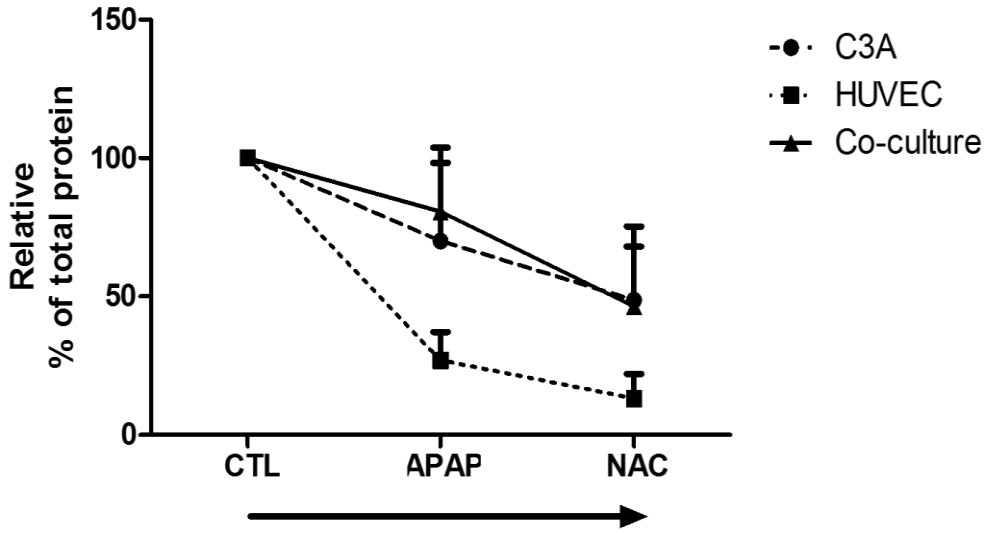

Figure 3-7 Relative total protein in HUVECs and C3As after 24hr APAP exposure followed by 24hr NAC treatment

Cells were cultured with EGM-2 (control), 10 mM APAP and post-treatment with NAC for 24hr period. Cells were collected to measure the total protein as indicated in Materials and Methods in Section 3.3. Percentage of total protein was obtained dividing the total protein concentration (mg/ml) in each group of controls by their corresponding untreated values and multiplying by 100. Data is expressed by the mean ± SEM of three different experiments (n=3).

3.6 Conclusions

Previously in Chapter 2, the *in vitro* human HUVEC:C3A co-culture model (at a ratio of 1:1) was shown to enhance hepatic functionality; albumin synthesis and CYP3A4 activity, while maintaining both endothelial and hepatic phenotypes on day 3 of co-culture. To demonstrate if the improved function seen in co-cultures might also extend to responses to hepatotoxic drugs, co-cultures were exposed to a well-known hepatotoxic drug, APAP (Han et al., 2013).

Data presented in this study has shown hepatotoxicity at doses of 10 mM APAP exposure for 24hr in HUVEC and C3A mono-cultures, whereas the human HUVEC:C3A co-cultures showed increased resistance to the induced hepatotoxicity caused by APAP, reflecting a potential cell-cell interaction between HUVECs and C3As.

The data obtained from the use of this heterotypic *in vitro* human hepatic model in hepatotoxicity studies revealed the following points:

(i) Hepatotoxicity was achieved in HUVEC and C3A mono-cultures with doses of 10 mM APAP 24hr. The effect of intermediate (10 mM) concentrations of APAP on intracellular ATP levels in HUVEC and C3A mono-cultures was only significant after 24hr, whereas no APAP toxicity was observed after 6hr of APAP incubation. The *in vitro* human HUVEC:C3A co-culture model maintained significantly greater intracellular ATP levels following 10 mM APAP exposure for 24hr, compared to mono-cultures.

(ii) APAP toxicity damaged the cell membranes and mitochondrial ATP generation in mono-cultures whereas the *in vitro* human HUVEC:C3A co-culture model was able to resist to APAP toxicity, showing ATP generation after incubation with galactose for 90 min.

(iii) APAP exposure altered morphology in HUVECs whereas morphology of C3A and co-cultures was not affected by APAP.

(iv) APAP did not affect the percentage of HUVECs or C3A in co-cultures, as relative $CD31^+$/$EpCAM^+$ proportions were maintained after APAP treatment.

(v) APAP toxicity strongly increase glycolytic metabolism in HUVECs mono-cultures whereas C3As and co-cultures maintained cellular metabolism at stable levels.

3.7 Discussion

Improved *in vitro* human hepatic models for hepatotoxicity studies that reproduce aspects of the liver *in vivo* could improve pre-clinical pharmaceutical drug testing strategies. Investigation into hepatotoxicity has shown altered drug metabolism and regulation in C3As in the presence of endothelial cells, and provided evidence of cellular cross-talk.

By confirming evidence that APAP can cause hepatotoxicity (Han et al., 2013), this study has shown that APAP cytotoxicity is time and dose-dependent. APAP can be highly toxic (>1 g per dose or 4 g total per day in adults (Schafer et al., 2013). In this, study, 10 mM and 20 mM APAP were respectively the equivalent of 1.5g and 3g of APAP, but both of these doses did not appear to have a detrimental effect on *in vitro* cell cultures after 6hr (Figure 3-2A). In contrast, 24hr exposure to 10 mM APAP demonstrated toxicity in mono-cultures, while 20 mM was required to demonstrate APAP toxicity in co-cultures (Figure 3-2B). Although ATP levels can be stimulated even before activation of cell death receptors during early cell death mechanisms (Zamaraeva et al., 2005, Klingenberg, 2008), this resistance to ATP-depletion may also be due the inhibition in apoptosis pathways or reactive oxygen species.

Representative *in vitro* hepatic models using mouse hepatocytes have demonstrated that doses of 10 mM APAP can inhibit mitochondrial ATP generation after 6hr, and that administration of fructose and glycine before APAP exposure, can protect the mitochondria (Kon et al., 2004). *In vivo,* mouse models seem to be more sensitive to APAP than rat models, where 5 mM APAP can result in mitochondrial dysfunction (Burcham and Harman, 1991). Recent studies have shown that HepG2 mono-cultures treated with high-dose 20 mM APAP for 24hr showed no evidence of mitochondrial dysfunction, or cell injury; suggesting very low levels of drug-metabolizing enzymes, which would radically reduce formation of the APAP intermediate NAPQI so preventing any toxicity in HepG2 cells (McGill et al.,

2011). Given that C3As are a clonal derivative of HepG2 cells, the data suggests that improved hepatocyte function in co-cultures results in greater suitability of the heterotypic HUVEC:C3A co-culture model for drug testing, as compared with standard hepatic cell line mono-cultures. By contrast, a recent study demonstrated increased sensitivity to APAP in co-cultures comprising mouse primary hepatocytes and HUVECs on Matrigel™ (Toyoda et al., 2012). Thus animal-based co-culture models do not necessarily result in consistency of outcome for *in vitro* drug toxicity studies. Whether this is due to the potential confounding variables introduced by rodent hepatocytes, and/or the composition and growth factor concentrations in Matrigel™ is not yet known. In this study, 10 mM APAP caused toxicity in C3As mono-cultures, which however showed higher resistance to toxicity at 24hr when in co-cultures. Intracellular ATP content in co-cultures was significantly higher than in either C3As or HUVECs in mono-cultures challenged with APAP and was maintained even after 24hr with 20 mM APAP (Figure 3-2B). Typically, ATP content is depleted following APAP challenge [≥ 10 mM], though cells have been shown to increase ATP content preceding apoptosis (Atlante et al., 2005). This could account for the effect of APAP on HUVECs intracellular ATP levels, having first increased by 6hr of APAP exposure and then being dramatically depleted at 24hr (Figure 3-2).

When indices of mitochondrial toxicity and necrosis following APAP challenge in HUVEC:C3A mono- and co-cultures were measured, they were associated with (short-exposure) changes in cellular ATP levels and cell membrane integrity, respectively, with the Mitochondrial ToxGlo™ Assay (Figure 3-3); and a cell viability assay as a measure of intracellular ATP content (ATP depletion) following 24hr exposure to different doses of APAP (Figure 3-2B). The latter clearly shows resistance to APAP toxicity in co-culture. The reduction in ATP with commensurate changes in membrane integrity (cytotoxicity) using the ToxGlo™ Assay, indicates that APAP is a mitochondrial toxin at an intermediate threshold dose of 10 mM APAP; with apparent (significant) primary necrosis also taking place (at the

lower dose of 5 mM APAP; Figure 3-2A). In co-cultures, the trend was greater resistance to mitochondrial toxicity and increased sensitivity to necrosis at all doses tested, compared with HUVEC and C3A mono-culture controls. Given this assay is designed to predict potential mitochondrial dysfunction as a result of xenobiotic exposure, initial cytotoxicity screening with organotypic co-cultures may inform subsequent screening strategies for complex adverse outcomes, and provide valuable information on whether to perform more stringent assays of mitochondrial dysfunction or mode of cell death, such as; Cytochrome c release (apoptosis marker), ROS production, mitochondrial APAP-protein-adduct formation; or the M65 necrosis marker.

The observed ATP depletion was supported with morphological observations on HUVECs and C3As using a LIVE/DEAD® Viability/Cytotoxicity Kit (Life technologies), which distinguished damaged cells from viable cells. Live/dead staining revealed than HUVECs suffered APAP toxicity causing death (bright red) when they were mono-cultured, but retained more viability in co-cultures (bright green). Figure 3-4, revealing that APAP exposure had an effect on the cellular integrity especially in HUVECs mono-cultures while having little effect in co-cultures.

It is important to highlight that HUVECs were more susceptible to damage, raising the question of whether this also occurs *in vivo* with the drug directly affecting the vascular system (Figure 3-4). This damage could activate receptors in hepatocytes and quiescent liver cells to contribute to endothelial cell recovery. This suggests the notion that hepatocytes effectively 'endure' the initial APAP toxicity event, and then accelerate metabolic function leading to initiation of cellular mechanisms involved in liver regeneration, provided that APAP levels are not so high as to deplete cellular glutathione levels and initiate a second round of hepatic cell death by oxidative stress.

It is also possible that increased levels of ATP in hepatic co-culture could reduce metabolic activation of APAP, resulting in increased resistance to toxicity compared to that seen in

mono-cultures. Hypoxia can also cause ATP-depletion in endothelial cells or hepatocytes (Linden, 2006, Amaral et al., 2013). This resistance to injury observed in co-cultures may also be related to reduction in lactate levels in co-culture supernatants, as compared with HUVEC mono-cultures (Figure 3-7), suggestive of reduced oxidative stress (Limonciel et al., 2011). Interestingly, lactate levels have previously been shown to increase in wound healing and high levels of lactate have been related to the capacity of HUVECs to up-regulate endothelial receptors such as VEGFR-2 (Ruan and Kazlauskas, 2013).

Investigation of the pyruvate and lactate ratio showed evidence of alterations in glycolysis metabolism, especially in HUVEC mono-cultures (Figure 3-7).

In vivo, lactate levels are related to liver dysfunction in early APAP overdose, indicative of damage in the endothelial sinusoid (Kim et al., 2001, Jaeschke et al., 2002, Ito et al., 2003, Badmann et al., 2012, Shah et al., 2011). In this study, lactate levels were lower in co-cultures suggesting that the mitochondria were not affected as significantly by APAP as they were in mono-cultures.

We observed an increase in P/L ratio most probably because an increase in oxidative stress in the presence of NAC following exposure to APAP in HUVECs mono-cultures. In C3As, there is no increase in glycolysis, though the cell viability seem to decrease. The consideration to measure mitochondrial function through cell respiration analysis would be an additional information to give an insight in the mechanism. Given 'normal' C3As metabolism is anaerobic (Patent No. WO 1991018087 A1; 1991), NAC may enhance the pool of cysteine which is then degraded and ends up as an energy substrate in the Krebs cycle to support oxidative phosphorylation resulting in enhanced mitochondrial energy (ATP) as well as pyruvate production (Figure 3-5).

DeLeve *et al*. investigated the APAP effect on LSECs in co-cultures with rat hepatocytes and they suggested that hepatocytes might kill endothelial cells when in co-cultures (DeLeve et

al., 1997). Here, $CD31^+$ expression was investigated in HUVECs co-cultured with C3As and the data showed that HUVECs were present in the co-cultures after APAP treatment and were able to maintain levels $CD31^+$ comparable with untreated cells (Figure 3-7). This suggests that C3As did not affect HUVECs in co-cultures, whereas the exposure of APAP to HUVECs mono-cultures caused mitochondria dysfunction (Figure 3-3), loss of morphology (Figure 3-4) and cell death (Figure 3-5).

We used APAP as a model hepatotoxin, which, as with other hepatotoxins, follows the 3-step model of drug-induced liver injury (Willett et al., 2014). The first step, as an example, might include direct cell stress (cytotoxicity) or direct mitochondrial inhibition (Figure 3-3); the second step may involve mitochondrial dysfunction, such as by disruption of the permeability transition pore (PTP), which determines the extent of ATP depletion (Figure 3-2); the third step essentially determines the type of cell death: necrosis (greater depletion of ATP) or apoptosis (a lesser depletion of ATP).

Evidence of activation of other cellular mechanisms via endothelial cells in hepatic co-culture in response to hepatotoxicity require further investigation, especially regulation of the endothelial phenotype and VEGFR-2 expression in co-cultures after APAP exposure *in vitro*. Understanding the role of endothelial cells in APAP toxicity compared with standard hepatocyte homotypic mono-cultures model may demonstrate the importance of using heterotypic hepatic models to more accurately represent liver-like function for pre-clinical *in vitro* testing of drug safety and efficacy studies. The complex interplay observed in heterotypic co-culture may better reflect the situation found *in vivo*, and provide an insight into the mechanisms of drug toxicity.

Although further studies are required to elucidate the cellular mechanism involved in hepatoprotection, it is tempting to speculate that the modulation of APAP toxicity in the HUVEC:C3A organotypic model may be in part due to the interaction between epithelial

hepatocytes and endothelial cells. As mentioned by Schafer *et al* pre-clinical studies have demonstrated that human and rodents can become resistant to APAP toxicity (Schafer et al., 2013) and *in vitro* co-culture models combining hepatocytes and fibroblasts can also show less toxicity and provide a protective effect probably due to the hepatic metabolism (Cole et al., 2014). One of these studies suggests that multidrug resistance-associated proteins (Mrp4) can be induced, resulting in potential resistance to a second dose of APAP (Aleksunes et al., 2008) but in this study, it seemed to be cell-cell communication between the cells which was crucial improvement in the *in vitro* human models suitable for drug testing in response to APAP toxicity (Donato et al., 2013).

4 Chapter 4: Characterization of hepatic phenotypic, antioxidant and oxidant parameters using a human hepatic co-culture model in acetaminophen toxicity

4.1 Introduction

Given the highly complex nature of APAP toxicity, more extensive investigations are required to fully understand the underlying mechanisms; including, for example, the effect of APAP on the endothelium and interaction with non-parenchymal cells (Badmann et al., 2012, Toyoda et al., 2012). To date, most studies of APAP hepatotoxicity have been performed in rodents (DeLeve et al., 1997, Ito et al., 2003, Jaeschke et al., 2012a). *In vitro* pharmacology studies using rat hepatocytes in mono-culture and more recently rodent co-culture models using endothelial cells, have shown the importance of the toxic effect of APAP on the endothelial cell mitochondrial apoptotic pathway during drug metabolism (Badmann et al., 2012, Toyoda et al., 2012). However, there is still a need to understand the role of human endothelial cells in a human hepatic model (Aritomi et al., 2014). In Chapter 3, we have seen that the outcome of APAP-induced liver injury in a human *in vitro* cell culture models was significantly improved in the presence of endothelial cells. We then focused on the generation of reactive nitrogen species (RNS) and reactive oxygen species (ROS) formation were not investigated.

At therapeutic doses, glucuronidation and sulfation (Phase II) reactions metabolise ~90% of APAP, and do not normally produce hepatotoxic effects. As discussed in detail in Section 1.4.1, published studies using rodents have shown that ~5-15% of APAP is catabolised in Phase I mainly by CYP450 (CYP2E1, CYP3A4, CYP1A2), which can result in production of reactive and hepatotoxic molecule such as N-acetyl-*p*-benzoquinone imine (NAPQI). NAPQI can be detoxified by glutathione S-transferase enzymes in the cytosol, microsomes, and mitochondria, using reduced glutathione (GSH) as substrate, but in APAP overdose, the

need to metabolise high concentrations of NAPQI can deplete intracellular GSH to the point where NAPQI begins to react with other cellular proteins, to form toxic nitric compounds – leading to an increase in ROS and RNS formation. The altered balance between antioxidant and oxidant levels leads eventually to mitochondrial dysfunction and cell death by necrosis (Agarwal et al., 2012, McGill and Jaeschke, 2013, Getachew et al., 2010).

The formation of peroxynitrite from the combination between superoxide and nitric oxide has also been associated in dropping antioxidants such as manganese superoxide dismutase, damaging the mitochondria permeability (Agarwal et al., 2012). Endothelial-derived nitric oxide (NO) regulates vascularization and also interacts with cysteine to form S-nitrosothiol which activates the erythroid 2-related factor 2 (Nrf-2) antioxidant pathway and is also associated with VEGFR-2 activation (Cox et al., 2014). Xenobiotic toxicity can therefore induce angiogenesis, ROS formation and regulation of inflammatory cytokines such as TNF-alpha or interleukins (Pires et al., 2014, Yang et al., 2013a, Xie et al., 2014a, Nagendra et al., 1997).

Previous studies in our laboratory have shown that β1-integrin receptor expression in hepatocytes can be altered following toxic APAP challenge affecting cell adhesion (Newsome et al., 2004). Vascular endothelial growth factor (VEGF) and receptors are also important in hepatic differentiation and are related to the capacity to enhance both angiogenesis and wound healing in liver macro-vascular injury. In APAP-induced hepatotoxicity, injury of LSECs, and collapse of the space of Disse, results in the accumulation of blood cells in the space leading to centrilobular necrosis (Donahower et al., 2010, Kato et al., 2011, Ito et al., 2003).

Drug toxicity can also cause the activation and regulation of vascular endothelial receptors (Badmann et al., 2012, Ito et al., 2003), suggesting that endothelial cells may be associated with the early events in hepatotoxicity. Other hepatotoxic drugs such as amidarone can also

regulate the expression of CD54 (Intercellular Adhesion Molecule 1 (ICAM-1)) receptor in association with metabolic activation by interleukin-1 or TNF-α (Endo et al., 2012).

In the present study, i) *in vitro* human mono and co-culture models were exposed to APAP to test the hypothesis that the presence of HUVECs could modulate APAP toxicity on C3A cells, for example, in conserving total intracellular glutathione levels (tGSH) and NO and ii) whether receptors whose expressions are known to be affected by drugs show any modification in HUVECs or C3As in response to hepatotoxic challenge. Oxidant and antioxidant levels and expression of cellular receptors by hepatocytes and HUVECs were evaluated, as outlined below:

(i) Cytochrome P450 enzyme activity mediation in APAP metabolism, through characterization of CYP2E1, CYP3A4, and CYP1A2 expression in mono and co-cultures;

(ii) Oxidative stress in APAP metabolism. Superoxide formation during mitochondrial respiration;

(iii) Endothelial and hepatic antioxidant and intracellular signalling in APAP toxicity; NO and tGSH levels as an antioxidant defence in APAP toxicity

(iv) CD54 (ICAM-1) regulation on HUVECs and C3As during APAP exposure.

4.2 Material and Methods

4.2.1 Experiment design

HUVECs and C3As were cultured at density of 21,000 cells/cm^2 in mono- or co-cultures, at ratio of 1:1 (HUVEC:C3A) in EGM-2 for a 3 day period. Subsequently, cells were incubated with: 0 mM, 5 mM, 10 mM and 20 mM APAP for 24 hr (0 mM APAP represents untreated control).

4.2.2 Real-time reverse-transcription polymerase chain reaction (RT-PCR)

CYP1A2 gene expression was measured in C3As and HUVECs after 3 days of culture and treatment with APAP for 24 hr. Cells were then washed twice with PBS and suspended in 0.5ml Trizol (Invitrogen) at -80ºC for later analysis.

Total RNA was isolated using Trizol (Life Technologies) from untreated and APAP-treated HUVEC and C3A mono- and co-cultures (1:1), and RNA concentration and purity measured using the Nanodrop ND100 spectrophotometer (Labtech International). 1µg of total RNA from each sample was reverse transcribed into cDNA using the High Capacity cDNA reverse transcription kit from Applied Biosystems.

Primers for human *CYP2E1* was obtained from Biopredic International and oligonucleotide primer was designed for human *GAPDH* genes using Primer 3 Output program for control (Table 4.1). *GADPH* was used as a housekeeping control. In Chapter 3, we showed that glycolysis was strongly affected by APAP treatment so selection of GAPDH as a housekeeping was probably a bad choice as GAPDH is an enzyme of the glycolysis and in this experiment, we might expect changes in glycolysis enzymes expression.

Standard and Real Time quantitative PCR (RT-PCR) amplification of control liver cDNA was performed to optimise *CYP2E1* and *GAPDH* primers. PCR products from standard PCR reactions were first tested on 2% gel electrophoresis to confirm the presence of a specific band corresponding to the anticipated length of the amplified product. Primer specificity in RT-PCR reactions was then tested by performing a melt curve analysis of RT-PCR data to confirm that only a single PCR product was amplified.

A SYBR green PCR assay using SYBR Green PCR master mix (Life Technologies) was employed for RT-PCR analysis (LightCycler® 96 System, Roche). Three biological replicates were used from each study group; and each biological replicate was tested three times i.e. three technical replicates/sample were run to test for any technical errors. The cDNA concentration was equal in all study groups (100ng/µl). The RT-PCR reactions were carried out using pre-incubation at 95ºC for 10 minutes, 3 step amplification for 35 cycles (95ºC for 20 seconds, 60 ºC for 15 seconds and 72 ºC for 15 seconds), cooling at 37 ºC for 30 second, melt curve analyses were carried out with cycling at 95 ºC for 10 seconds, 65 ºC for 1 minute and 97 ºC for 15 seconds.

Control cDNA was used to set up a standard curve for each of the studied genes and to test primers efficiency. The study conformed to the **MIQE** guidelines (***M***inimum ***I***nformation for Publication of ***Q***uantitative Real-Time PCR ***E***xperiments).

Data were reported as the fold change with GAPDH normalisation.

Table 4-1 Primers designed for gene expression analysis

Gene	Forward primer (5′…..3′)	Reverse primer (5′…..3′)	Product size (bp)
GAPDH	CTGACTTCAACAGCGACACC	GTGGTCCAGGGGTCTTACTC	172

CYP1A2 and CYP3A4 activity

CYP activity for CYP1A2 and CYP3A4 reactions were performed in HUVECs or C3As as mono-cultures, and in co-cultures at ratio of 1:1, using P450-Glo Luminometry Assays. CYP3A4 was measured directly in the cells using luminescence P450-Glo™ CYP3A4 Assay with Luciferin-IPA (Promega) (See Section 2.2.8.3) and CYP1A2 activity using a luminescence CYP1A2 Induction/Inhibition Assay, (Promega). For CYP1A2, Lucifering-1A2 was diluted in PBS containing 3 mM salicylamide in DMSO and added into the plate for 60 min incubation at 37ºC and 5% CO_2. Then, the same volume of supernatant was mixed with Luciferin detection reagent supplemented with D-cysteine. Samples were incubated at RT for 20 min before reading on a luminometer GloMax Multi+ plate reader (Promega). Wells with medium alone were also incubated with luciferin-IPA as a background control. Values were obtained in relative luminescence units (RLU) of activity.

4.2.3 Mitochondrial superoxide indicator

In oxidative phosphorylation electrons can react with molecular oxygen forming mitochondrial superoxide anion (O2·-) the main reactive oxygen species (ROS). Formation of O2·- was measured in untreated (control) and 10 mM APAP-treated HUVEC and C3A mono- and co-cultures using MitoSOX™ Red for live-cell Imaging (Molecular probes, Life Technologies, M36008) for 24hr, following manufacturer's instructions. O2·- formation causes oxidization of MitoSOX™ generating bright fluorescence at Ex/Em: 510/580 nm (red fluorescence).

For the experiment, HUVEC or C3A in mono- or co-cultures, were cultured for 2 days. Cells were then washed twice with PBS and control cells (untreated) were incubated with EGM-2 containing 4µM MitoSOX™; treated cells were incubated with EMG-2 containing 10mM APAP and 4µM MitoSOX™. After 24hr of incubation at 37˚C, phase contrast and

fluorescence images of controls and treated cells were acquired to detect the formation of mitochondrial superoxide under phase contrast microscopy inverted microscope (Zeiss Axio-Observer A1, Germany) and images were captured with a mounted camera (Zeiss AxioCam MRm). Then, images were processed and merged using ImageJ 1.46r (National Institute of Health, USA).

4.2.4 Total Nitric oxide and Nitrate/Nitrite assay

Total nitric oxide (NO) released by endothelial cells and hepatocytes into cell culture supernatant is synthesised from L-arginine. It is measured using an assay based on the Griess assay.

$$\text{L-arginine} \xrightarrow{\text{nNOS/eNOS}} \text{L-citrulline + NO (nitrite } (NO_2^-) \text{ + nitrate } (NO_3^-))$$

In this study, the same total number of HUVECs and C3As in mono- or co-cultures at ratio 1:1 (HUVEC:C3A) were cultured for two days before exposure to APAP (0 mM, 5 mM, 10 mM, and 20 mM) for 24hr. Supernatants were then collected and analysed to determinate total Nitric Oxide using the Total Nitric oxide and Nitrate/Nitrite Parameter assay kit (R&D systems) following the manufacturer's instructions. This assay measures concentration of nitrate/NO_3^- and nitrite/NO_2^- in two different procedures. The concentration of nitrite present is measured and then total NO is measured by converting nitrate to nitrite. Results were read in a 96 well plate using a Sunrise™ micro plate reader (Tecan, Switzerland).

4.2.5 Enzymatic method for quantitative determination of total intracellular glutathione levels (tGSH)

Total intracellular glutathione levels (tGSH) were measured in the cells following a modified protocol of Rahman *et al* (Rahman et al., 2006).

HUVECs and C3As in mono- and co-cultures at ratio 1:1 (HUVEC:C3A) were cultured for two days on 6 well plates. Cells were then washed twice with PBS-, and cell culture media was replaced with media-containing 10 mM APAP in EGM-2, or just EGM-2 for controls. After 24hr of APAP incubation, cells were washed twice with cold PBS- and collected from wells by scraping into 1 ml of ice-cold PBS. The cell suspensions were transferred into 1.5 ml safe lock tubes (Eppendorf, Germany) and centrifuged at 1000g for 5 minutes at 4ºC. Supernatants were discarded, and cell pellets re-suspended in 0.5 ml of ice-cold PBS-. Samples were centrifuged again and the cell pellets treated with 0.5 ml of ice-cold extraction KPE buffer (KPE buffer was made by mixing 8 ml of solution: A (6.8 g KH_2PO_4 to 500 ml) with 42 ml of solution: B (11.4 g $K_2HPO_4.3H_2O$ to 500 ml) and with 0.1.86 g EDTA.: 0.1% (v/v) Triton X-100 and 0.6% sulfosalicylic acid in 0.1M potassium phosphate buffer with 5 mM EDTA disodium salt; pH 7.5). The buffer was made up fresh each time. Cell pellets in 0.5ml of the extraction buffer were homogenised on ice using a PowerGen 125 Homogenizer (Fisher Scientific) for 30 s and then frozen at -80ºC for at least 24hr. The cell homogenates were then centrifuged at 3000g for 4 min at 4ºC, and two reagents added: 5,5′-dithio-bis (2-nitrobenzoic acid) (DTNB) (reagent 1; final concentration of 0.5 mM) and glutathione reductase (reagent 2; final concentration of 1µ/ml) for measurement of total intracellular glutathione levels (tGSH) (GSH + GSSG).

These measurements were performed on a Cobas Fara Centrifugal Analyser (Roche) with the collaboration of Dr Forbes Howie at The Queen's Medical Research Institute, The University of Edinburgh.

4.2.6 Flow cytometry

See Section 2.2.6

4.2.7 Determination of total protein

See Section 3.3

4.2.8 Statistical analysis

Experiments were performed in triplicate on at least three biological replicates. GraphPad Prism®5 software was used for statistical analysis. Results were reported as mean ± standard error (SEM). Student's unpaired t-test was used to compare all co-cultures to their appropriate C3A and HUVEC mono-culture controls (statistical significance *$p<0.05$).

4.3 Results

4.3.1 Cytochrome P450 (CYP2E1, CYP3A4 and CYP1A2) activity and expression analyses

Cytochrome P450 activity such as: CYP2E1, CYP3A4 and CYP1A2 were measured and compared in HUVEC:C3A mono- and co-cultures; either untreated for controls or following treatment for 24hr with a toxic dose of 10 mM APAP.

CYP2E1 was selected for RT-PCR expression analysis because of its involvement in the formation of the reactive metabolite NAPQI and ROS formation in response to APAP activation. CYP3A4 and CYP1A2 isoforms are associated with drug clearance and detoxification mechanisms and were evaluated by luminescence assays.

CYP2E1 gene expression

Untreated (EGM-2) C3As co-cultures compared to C3As alone had not significant 1.46 ± 0.28 fold increase in CYP2E1 gene expression ($p = 0.064$). When C3As mono- and co-cultures were treated with APAP, CYP2E1 levels were 0.76 ± 0.44 fold reduced in co-cultures compared to C3As mono-cultures (Figure 4-1). GADPH was used as a housekeeping control in this experiment where we might expect changes in glycolysis enzymes expression. Looking at the raw data, GADPH expression was 2,5 cycle difference between untreated and treated cells, so GAPDH was not an ideal housekeeping (Table 4-1).

CYP1A2 Activity

CYP1A2 activity showed a non-significant reduction in C3As treated with 10 mM APAP compared to untreated controls, levels dropping from 159.30 ± 39.58 RLU in untreated C3As to 101.50 ± 37.06 RLU in treated C3As. CYP1A2 activity in co-cultures also showed

a non-significant reduction from 142.60 ± 23.31 RLU in untreated co-cultures to 120.10 ± 16.24 RLU in APAP treated co-cultures (Figure 4-2 –A).

CYP3A4 Activity

As presented in Chapter 2 (Figure 2-12), untreated C3As showed significantly greater CYP3A4 activity when co-cultured with endothelial cells at 490.20 ± 62.95 RLU, compared with C3As in mono-cultures at 270.60 ± 38.73 RLU (p=0.0090).

APAP treatment of C3A mono-cultures resulted in a non-significant reduction in CYP3A4 activity compared with untreated mono-cultures at 160.60 ± 42.67 in 10mM APAP treated mono-culture vs 270.60 ± 38.73 RLU (untreated) *vs* (Figure 4-2-B).

However, CYP3A4 activity was significantly reduced from 490.2 ± 62.95 RLU in untreated HUVEC:C3A co-cultures to 288.40 ± 49.68 RLU in 10 mM APAP-treated co-cultures (p=0.02) (Figure 4-2-B).

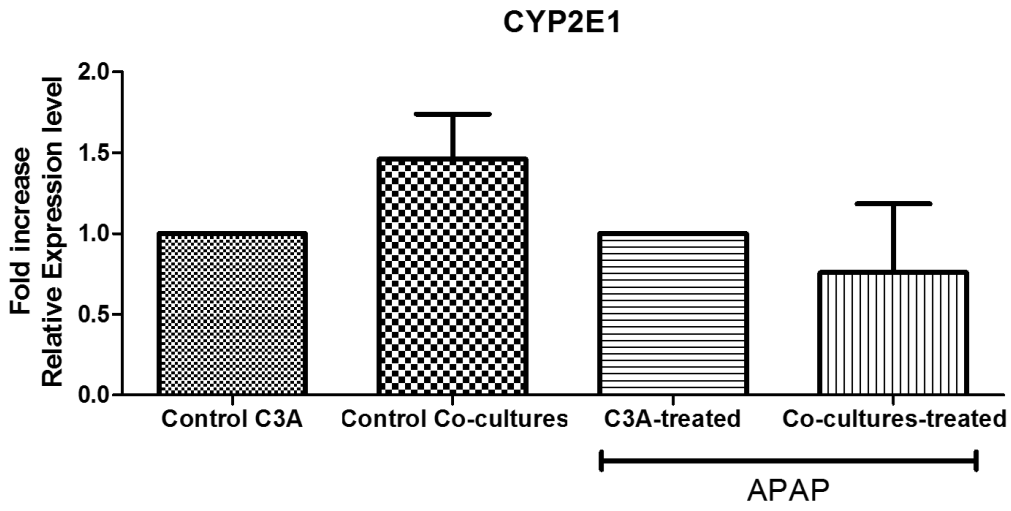

Figure 4-1 Cytochrome P450 CYP2E1 gene expression in C3As in mono- and co-cultures with HUVECs at ratio 1:1 (HUVEC:C3A) in EGM-2 and exposed to 10 mM APAP at time 24hr

C3As in mono- and co-cultures were cultured for 3 days. On the second day, cells were exposed to 10mM APAP and just EGM-2 for controls for 24hr. After 24hr, basal CYP2E1 gene expression was measured by RT-PCR as indicated in Material and Methods in Section 4.2.3. A) Fold increase of relative expression level of CYP2E1 detected by day 3 of culture in C3As in mono and HUVEC:C3A co-cultures at ratio 1:1 and APAP-treated cells compared to respectively controls. Values represent the mean ± SEM of three different experiment, (n=3).

Table 4-1 GAPDH and CYP2E1 Ct values

	C3A	1:1	C3A-APAP treated	1:1 APAP-treated
GAPDH Mean	18.44	18.89	20.78	19.15
SEM	0.12	0.05	0.68	0.1
CYP2E1 Mean	33.66	33.70	36.42	35.43
SEM	0.24	0.16	1.53	0.56
CYP2E1 Mean/GAPDH Mean	1.83	1.78	1.75	1.85

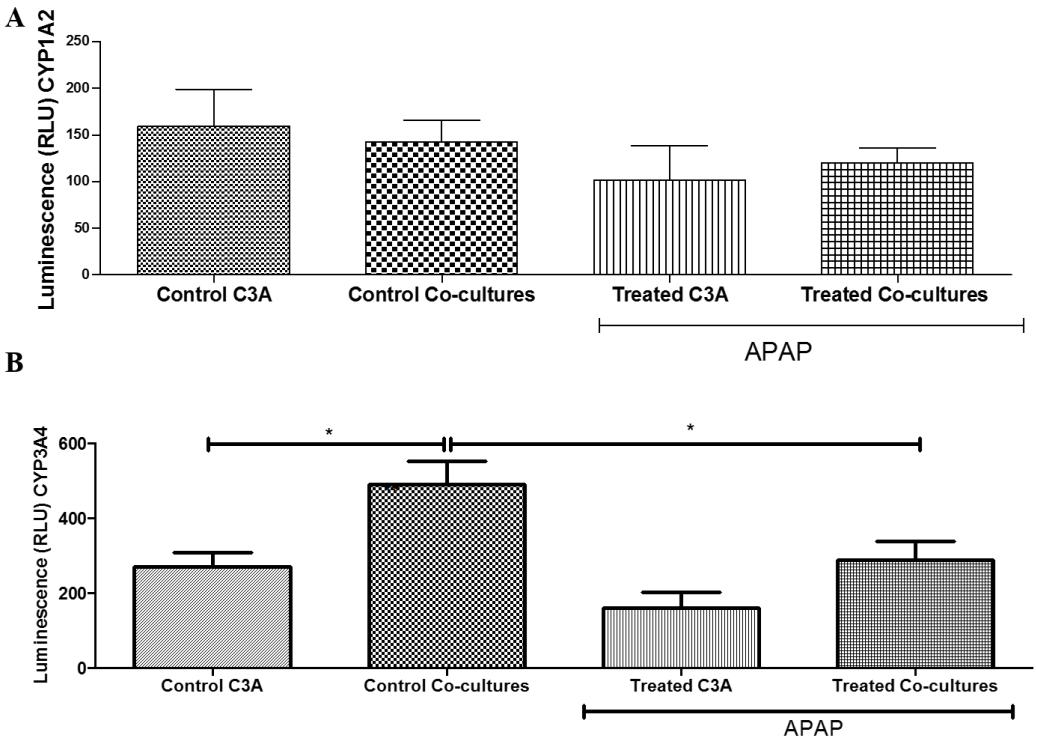

Figure 4-2 Cytochrome P450 CYP1A2 and CYP3A4 activity in C3As in mono and co-culture with HUVECs at ratio 1:1 (HUVEC:C3A) in EGM-2 and in 10 mM APAP at time 24hr

*HUVECs, C3As in mono- and HUVEC:C3A co-cultures were treated with 0 mM, 5 mM, 10 mM and 20 mM APAP (0 mM APAP untreated control) for 24 hr, after which CYP3A4 and CYP1A2 reactions performed directly on the cells using P450-Glo CYP3A4 and CYP1A2 Activity Assays with Luciferin-IPA (Promega), as described in Materials and Methods in Section 4.2.2. A) CYP3A4 and B) CYP1A2 activity in the cells is expressed in relative luminescence units (RLU) activity. Values represent the mean ± SEM of three different experiments in triplicate, (n=3), *p < 0.05.*

4.3.2 Superoxide formation in the mitochondria

Superoxide formation in HUVECs and C3As mono- and co-cultures were examined after 24hr of APAP incubation, by fluorescence imaging using the MitoSOX™ assay. Figure 4.3 shows representative phase contrast and fluorescence images of untreated control and 10 mM APAP-treated HUVEC:C3A mono- and co-cultures. The bright red fluorescence observed in these images demonstrated that peroxide formation occurred mainly in C3As in both mono- and co-cultures. These images revealed that HUVEC mono-cultures treated with APAP for 24hr significantly lost their cellular morphology whereas HUVECs in co-cultured appeared to maintain morphology (Figure 4-3) consistent with previously-reported observations (Figure 3-4).

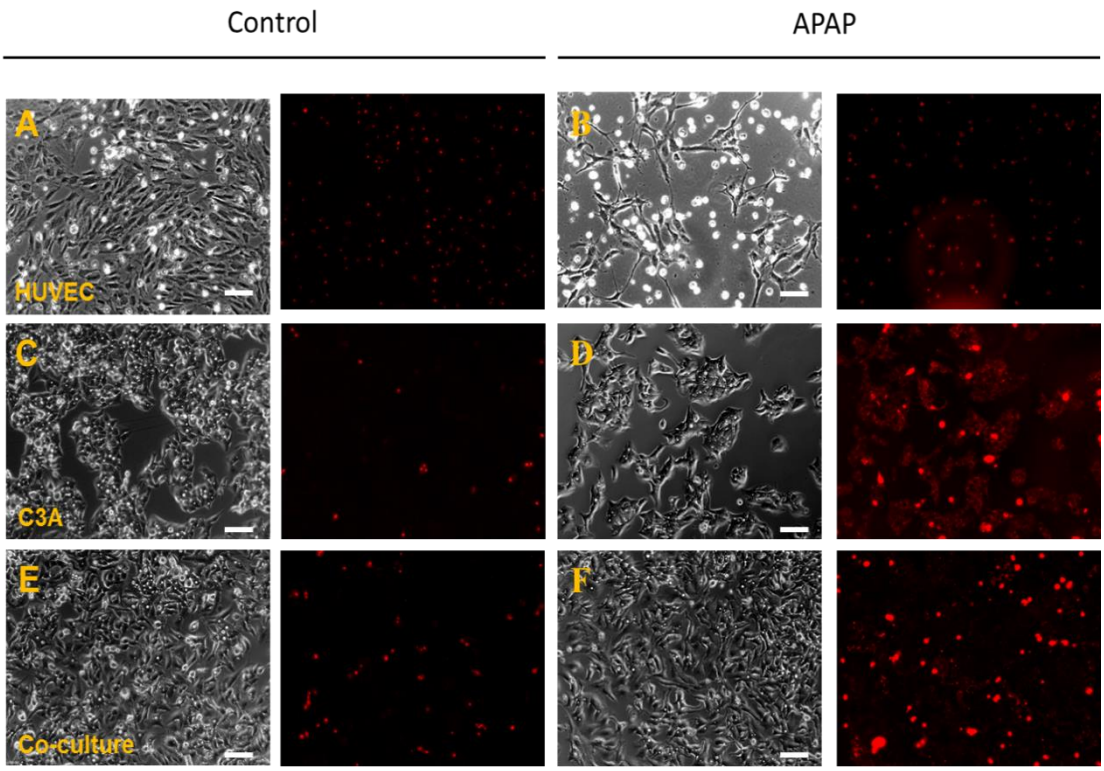

Figure 4-3 Phase contrast and fluorescence images of mitochondrial superoxide formation (bright red) measured by MitoSOX™ red staining in HUVECs and C3As in mono- and co-cultures treated with 10mM APAP

HUVEC:C3A mono- and co-cultures were incubated with EGM-2 containing MitoSOX™ for untreated controls in EGM-2 or treated with 10mM APAP containing MitoSOX™. After 24hr of incubation, cellular morphology and superoxide formation was evaluated by phase contrast and fluorescence imaging, respectively, in controls (A, C, E) and APAP treated cells (B, D, F) to detect the formation of mitochondrial superoxide formation (bright red); magnification x10. Images were merged using imageJ 1.46r. Scale bars 100µm.

4.3.3 Measurement of parameters of oxidative stress: Total nitric oxide (NO)

The effect of 10 mM APAP on the levels of total nitric oxide (NO) levels was investigated in HUVECs and C3As in mono- and co-cultures at 24hr.

Figure 4.4 shows that 24hr exposure to 10 mM APAP significantly dropped NO concentration in C3A mono-cultures from 6.08 ± 0.98 µmol/L to 3.56 ± 0.49 µmol/L ($p=0.04$) whereas, there was no significant difference in NO output between untreated and treated HUVEC mono-cultures at respectively 6.04 ± 1.14 µmol/L and 5.35 ± 1.11 µmol/L. NO concentrations in HUVEC:C3A co-cultures were from 6.57 ± 0.75 µmol/L in untreated cells to 16.77 ± 5.47 µmol/L after APAP treatment. However, NO levels in APAP-exposed HUVEC:C3A co-cultures were significantly higher than levels in APAP-exposed C3A mono-cultures ($p=0.03$). When total nitric oxide was broken down into nitrite and nitrate formation, there were no significant differences between control and treated C3A and HUVEC mono-cultures, though there was a non-significant trend ($p=0.21$) towards higher nitrite levels in APAP-treated co-cultures (Figure 4.4).

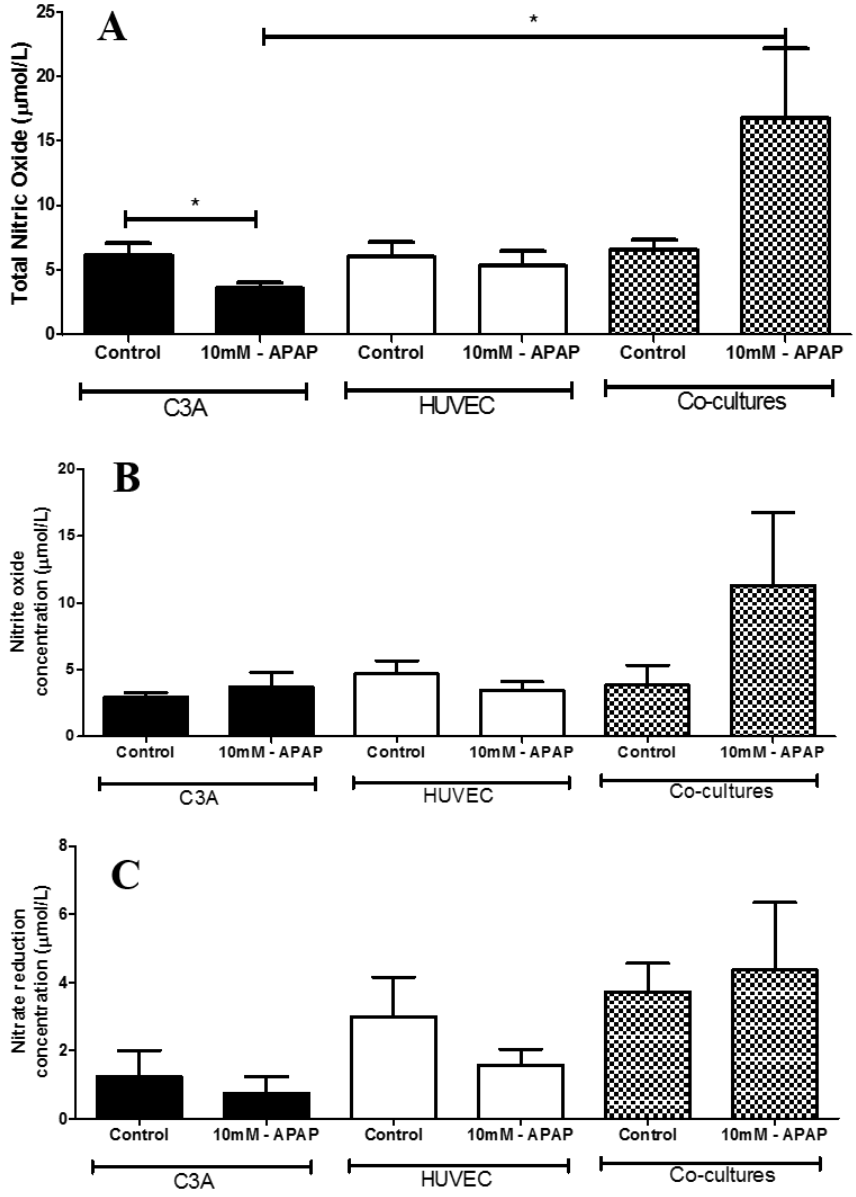

Figure 4-4 Effect of APAP on NO release into HUVEC and C3A cell supernatants in in untreated control mono and co-cultures or after treatment with 10 mM APAP

*Graphs A-C show the total levels of NO output in the cell supernatants of control (untreated) or HUVEC:C3A mono-or co-cultures treated with 10 mM APAP for 24 hr. C3As (black), HUVECs (white) mono- and co-cultures (stippled pattern). Total NO was measured as nitrate and nitrite in independent measurements based on Griess assay (Total Nitric oxide and Nitrate/Nitrite Parameter assay, R&D systems) as described in Material and Methods in Section 4.2.5: A) Total nitric oxide B) Nitrite; and C) Nitrate values represent the mean ± SEM of three independent experiments in triplicate; with significant difference at * $p < 0.05$. (n=3)*

4.3.4 Measurement of oxidative stress: Total intracellular glutathione levels (tGSH)

Total intracellular glutathione levels (tGSH) (GSH+GSSG) were assessed as a measure of oxidative stress. Effects of APAP on antioxidant defence were evaluated in endothelial and hepatocytes in untreated and 10mM APAP treated HUVEC:C3A mono- and co-cultures.

Figure 4-5 shows tGSH levels found in HUVEC, and C3A mono- and co-culture untreated controls and after treatment with 10 mM APAP for 24hr on day 2 of cell culture. C3A mono-cultures treated with APAP had significantly increased tGSH levels (47.4 ± 2.78 µmol/g, p=0.02) compared with controls (33.87 ± 4.39 µmol/g). tGSH levels decreased significantly in treated HUVECs from 32.73 ± 4.27 µmol/g to 9.26 ± 6.28 µmol/g (p=0.007). Treated-co-cultures showed a non-significant increase in GSH levels from 25.12 ± 6.53 µmol/g to 36.55 ± 7.57 µmol/g.

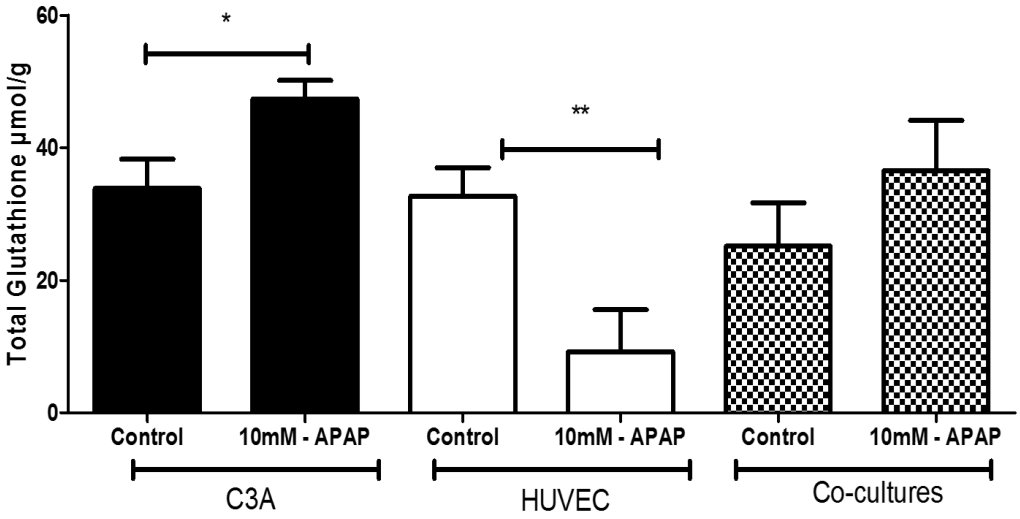

Figure 4-5 Total intracellular GSH levels in HUVECs and C3As mono- and co-cultures

*Total intracellular GSH levels in C3A (black bars), HUVEC (white), and co-cultures (stippled pattern) following 10 mM APAP incubation for 24hr, were measured using an enzymatic assay (as described in Materials and Methods in Section 4.2.6). Data is expressed as Mean ± SEM of three different experiments in triplicate with significant difference at * $p < 0.05$, ** $p < 0.005$ against controls (n=3).*

4.3.5 Cross-talk between HUVECs and C3As in co-culture: growth factor receptor-2 (VEGFR2)

To investigate possible changes in paracrine signalling in APAP toxicity, mean fluorescence intensity (MFI) obtained from flow cytometry histograms (Figure 4.6-A), were analysed as a measure of relative changes in expression of fluorescence markers, showed that endothelial expression of VEGFR-2 by HUVECs was altered by exposure to 10mM APAP .

VEGFR-2 was not difference in HUVEC mono-cultures (119.70 ± 17.56 RU), following 24hr treatment with APAP as compared with untreated controls (103.00 ± 9.40 RU). In HUVEC:C3A co-cultures however, the relative increase in VEGFR-2 expression was significantly greater in APAP-treated co-cultures (135.20 ± 24.18 RU; p=0.046) *versus* untreated controls (61.68 ± 8.97 RU) (Figure 4.6-B). Interestingly, basal VEGFR-2 levels in untreated HUVEC:C3A co-cultures (61.68 ± 8.97 RU) were significantly lower than in HUVEC mono-cultures (103.00 ± 9.40 RU, p=0.033), suggesting that from C3As might be exerting an inhibitory effect on VEGFR-2 expression in HUVECs and that APAP treatment eliminated much of this difference perhaps by disrupting paracrine signalling.

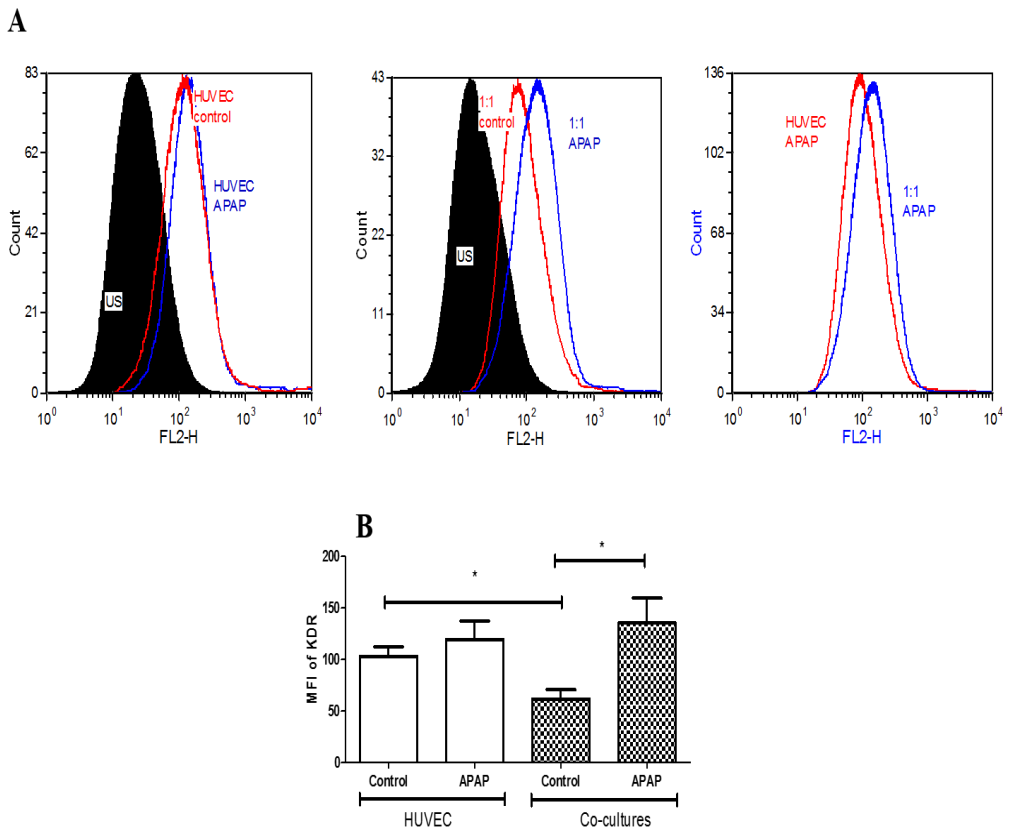

Figure 4-6 Endothelial expression of vascular endothelial growth factor receptor-2 (VEGFR2-KDR) in APAP toxicity

*HUVEC mono-cultures and HUVEC:C3A co-cultures in EGM-2 (untreated control) and treated with 10mM APAP in EGM-2 for 24hr were stained with VEGFR-2 and EpCAM and analysed by flow cytometry. Flow cytometry analysis of the Mean Fluorescence Intensity (MFI) of VEGFR-2 in HUVECs was performed with electronic gating of HUVECs, to exclude EpCAM+ for C3As as indicated in Figure 2-14: (A) Flow cytometry histograms of untreated control, and APAP-treated HUVEC mono-cultures and HUVEC:C3A co-cultures; B) MFI of untreated control and APAP-treated HUVEC mono- and HUVEC:C3A co-cultures. Data is expressed as Mean ± SEM of three independent experiments with significant difference at * $p < 0.05$, against controls (n=3).*

4.3.6 Cross-talk between HUVECs and C3As in co-culture: CD54 receptor

As shown in Figure 4-7 B, there was an increase in the expression of the inter-cellular adhesion molecule CD54 (ICAM-1) in HUVECs in both mono and co-culture when they were exposure to APAP. In HUVEC and C3A mono-cultures, there was an increase of 4.35 ± 2.54 fold and 1.62 ± 0.07 fold respectively. HUVECs and C3As in co-cultures also showed increased expression of CD54 after APAP exposure. HUVECs in co-culture had an increase of 6.17 ± 3.91 fold and C3As of 1.54 ± 0.18 fold (Figure 4.7 B).

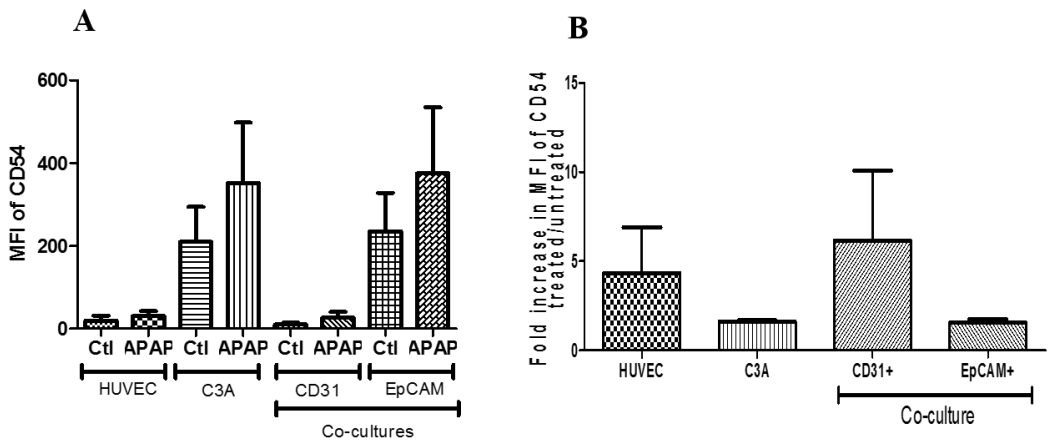

Figure 4-7 Fold increase in MFI of CD54 expression between treated with APAP and untreated HUVECs, C3As and co-cultures

HUVEC and C3As mono- and HUVEC:C3A co-culture untreated controls and treated with 10mM APAP for 24hr period were stained with CD54/CD31/EpCAM and analysed by flow cytometry. The mean fluorescence intensity (MFI) (A) and fold increase in MFI of CD54 (B) was measured in HUVECs and C3A using $CD31^+$ HUVECs to exclude $EpCAM^+$ for C3As and CD54 in C3As were analysed in $EpCAM^+$ C3As to exclude $CD31^+$ for HUVECs. Data is expressed as Mean ± SEM of three different experiments (n=3).

4.4 Conclusions

The aim was to investigate the effects on total intracellular glutathione levels (tGSH) and NO and associated receptors in HUVECs and C3As in mono- and co-cultures in response to 10 mM APAP hepatotoxicity and to evaluate whether the use of endothelial cells can modulate drug responses of hepatocytes. The use of an organotypic co-culture model compared with mono-cultures showed the reduced effects of acetaminophen toxicity in co-cultures. This work has demonstrated a relationship between endothelial and hepatic cells in APAP toxicity, as demonstrated by the positive modulation of CYP450 activity, oxidative stress and adhesion markers in co-cultures- leading to the following conclusions:

Specific effects in hepatotoxicity:

(i) APAP can significantly inhibited CYP3A4 activity in HUVEC:C3A co-cultures;

(ii) APAP seems not to increase superoxide formation in HUVECs.

(iii) APAP significantly dropped total nitric oxide in C3As and raised levels in co-cultures. APAP did not affect the release of NO from HUVECs;

(iv) APAP produced a significant tGSH depletion in HUVECs, whereas it induced GSH levels in C3As, while tGSH content remained constant in co-cultures;

(v) APAP up-regulates VEGFR-2 expression in HUVEC mono- and HUVEC:C3A co-cultures. In untreated cells, VEGFR-2 was down-regulated in co-cultures compared with mono-culture controls, whereas 10 mM APAP treatment significantly increased VEGFR-2 levels in co-cultures.

(vi) CD54 expression in HUVECs and C3As was up-regulated in response to APAP toxicity.

4.5 Discussion

Application of the current HUVEC:C3A *in vitro* human hepatic model to understanding responses to the hepatotoxic drug acetaminophen suggests that the heterotypic cell-cell interactions are crucial for better representation of drug toxicity *in vitro*.

Phase I CYP450 enzymes such as CYP1A2, CYP3A4 and CYP2E1 catalyse the activation of APAP, producing reactive molecules such as NAPQI which can result in ROS and RNS formation and damage to the mitochondria (Ribeiro et al., 2014, Jaeschke et al., 2012b). Current animal models of hepatotoxicity still do not fully represent the complex physiological mechanisms and processes of the liver *in vivo* (O'Brien et al., 2006, Gomez-Lechon et al., 2010). APAP can cause mitochondrial dysfunction, which is a late effect in cytotoxicity, while early mechanisms involved in APAP toxicity are still unknown. To date, CYP1A2 and CYP3A4 have not been investigated extensively in APAP metabolism, although both have been shown to enhance acetaminophen-induced toxicity (Cheng et al., 2009). In this study, CYP3A4 and CYP1A2 activity were investigated in HUVEC and C3A mono- and co-cultures demonstrating significantly higher CYP3A4 activity in control untreated co-cultures compared with untreated mono-cultures (Figure 4-1)

APAP toxicity can lead to oxidative stress and mitochondria dysfunction (Han et al., 2013). Superoxide formation in response to APAP treatment was observed in C3As and co-cultures, but not in HUVEC mono-cultures. Apparently, APAP-treated HUVECs in mono-cultures do not show lower NO concentration (Figure 4-4) or produce superoxide but HUVECs did lose cobblestone morphology (Figure 4-3) and tGSH content (Figure 4-5) after 10 mM APAP treatment, suggesting that APAP can be substantially toxic to HUVECs, via alternative toxicology pathways.

Therefore, it seems likely that superoxide formation in mitochondria of co-cultures exposed to 10 mM APAP was happening only in hepatocytes (Mukhopadhyay et al., 2007).

The absence of superoxide formation in HUVECs did not prevent injury, as HUVECs lost normal morphology and ATP levels were lower than C3As or co-cultures (Figure 4-3). Some studies have demonstrated that MitoSOX™ can detect superoxide formation in endothelial cells (Li et al., 2009), but here APAP did not significantly enhance superoxide formation in HUVECs at 24hr, possibly the HUVECs were no longer viable by this time. A recent hepatotoxicity study of superoxide formation used the bi-potential HepaRG hepatic cell line (hepatocytes and biliary epithelial-like cell co-culture) exposed to lethal doses of 20 mM APAP (McGill et al., 2011). In this study, it was demonstrated that superoxide formation occurred exclusively within hepatocytes, not in the biliary epithelial-like cells. HepaRG cells express sinusoidal and canalicular hepatic membrane transport proteins (Le Vee et al., 2006). The combination of those hepatic membrane transport proteins may boost drug clearance, by releasing drug metabolites into the biliary system and into the blood (Le Vee et al., 2006).

The formation of the reactive oxidant, peroxynitrite, is the result of the combination of superoxide and NO. The absence of superoxide formation in HUVECs, with maintenance of relatively high levels of NO, suggest than peroxynitrite may not be formed in HUVECs. These observations are very complex and may be in part due to the fact that the reactivity of nitric oxide may be greatly overestimated *in vitro*, due to an accumulation in cell cultures that would not occur normally *in vivo* in the intact liver. Peroxynitrite formation does however occur in APAP metabolism (superoxide + NO → peroxynitrite ($ONOO^-$), and is a highly reactive, potent oxidant and nitrating species, which causes mitochondrial damage and oxidative cellular stress. The main sources of peroxynitrite has been suggested to be from both Kupffer cells and neutrophils, although hepatocytes can also produce peroxynitrite in liver damage under stress conditions (Knight et al., 2002, Lawson et al., 2000).

A more in-depth investigation of oxidative stress mechanisms in response to APAP in our organotypic model showed that the NO level was unchanged in HUVECs, whereas C3As mono-cultures showed a significant decrease. However, given that increased NO levels were seen in co-cultures (Figure 4-4), we may also speculate that NO could induce an elevation of total intracellular glutathione levels thereby improving drug detoxification (Figure 4-4) (Alva et al., 2013). However, in this study, measurement of the independence values of GSH and GSSG may result in a better approach to understand total intracellular glutathione levels. GSH may be hepatotoprotective against APAP toxicity as a scavenger of ROS and peroxynitrite (Saito et al., 2010, Jaeschke et al., 2012a).

This has been observed in AML-12 hepatocytes where exposure to a NO donor was concomitant with activation of the antioxidant transcription factors Hypoxia-inducible factor 1α (HIF1α) and erythroid 2-related factor 2 (Nrf-2); leading to increased antioxidant defence (Aharoni-Simon et al., 2012). Moreover NO synthesis was dramatically increased in APAP toxicity in mice (Hinson et al., 2010), suggesting our organotypic model may mimic certain *in vivo* parameters of drug toxicity.

When endothelial cells are damaged, it has been shown that endothelial nitric oxide (eNO) production is reduced and the formation of peroxynitrites are increased (Li et al., 2013).

Nitric oxide can protect the liver vascular system, while lower concentration of NO can cause endothelial dysfunction (Alva et al., 2013, Forstermann and Munzel, 2006, Nagi et al., 2010, Nicotera and Melino, 2004). In mice, the administration of endothelial specific angiogenic growth factors protected hepatocytes from apoptosis in APAP overdose (Donahower et al., 2010).

Maintenance of hepatic phenotype and functional activity was observed in co-culture (Figures 3.5 and Figure 4.2), which exhibited resistance to APAP toxicity, likely through

enhanced production of total intracellular glutathione levels (tGSH) and cellular ATP, compared with mono-cultures of hepatocytes or endothelial cells alone (Figures 3.1).

The EGM-2 medium in providing biocompatible trophic support in HUVEC:C3A co-cultures contains defined supplements, including VEGF (EGM-2, CC-3162 Lonza). VEGFR-1 and VEGFR-2 are located in endothelial cells and play an important role in angiogenesis and permeability (LeCouter et al., 2003) and in orchestrating interactions with hepatocytes in organogenesis (Matsumoto et al., 2001). Treatment of mice with VEGF-A and activation of VEGFR-1 in co-cultures between hepatocytes and LSECs induce cell proliferation, and reduce by 86% carbon tetrachloride toxicity (LeCouter et al., 2003); whereas APAP treatment increased VEGF levels in mice, conferring hepatotoprotective effects, with concomitant increase in VEGFR2 expression (Hinson et al., 2010).

VEGF is induced *in vivo* in APAP toxicity (Donahower et al., 2010). Here, we demonstrated down-regulation of VEGF in co-cultures (Figure 4-6), which may mean that cross-talk between HUVECs and C3As confers the observed resistance to APAP toxicity at 10 mM APAP. Expression of the cell adhesion molecule CD54 (ICAM-1) was also investigated. CD54 has been associated with activation of the immune system, increasing the levels of cytokines such as IL-8 and TNF-α and causing mitochondrial dysfunction when exposued to a hepatotoxic amiodarone drug (Endo et al., 2012). In the current study, CD54 was moderately induced by APAP in HUVEC mono and co-cultures (Figure 5-8), suggesting that the cells were affected by APAP toxicity at 10 mM (Figure 4-8). TNF-α induced the activation of CD54 which facilitates trans-endothelial migration – inducing cellular damage and reducing angiogenesis (Kanzler et al., 2013, Kjaergaard et al., 2013, Knudsen and Kleinstreuer, 2011). Taken together, these data suggest improved functionality and drug detoxification as a result of cell-cell communication between endothelial and hepatic cells in response to APAP hepatotoxicity in heterotypic co-cultures.

5 Chapter 5: *In vitro* vascularised co-culture model using an extracellular matrix: migration and wound healing studies

5.1 Introduction

In Chapter 2, 3 and 4, HUVECs were co-cultured with C3As to develop a more physiological *in vitro* human hepatic model, where the main interest was to improve hepatic function in C3As for drug metabolism studies. However, the endothelial component of the liver also plays critical roles in drug clearance and nutrient transfer to the hepatocytes. In this Chapter, HUVECs and C3As were co-cultured in the presence of an extracellular matrix, with the aim of reconstructing an *in vitro* vascularised hepatic model to test the role of the vascular system in hepatocyte maintenance and in responding to drug toxicity. Endothelial cells form the thin inner lining of blood vessels throughout the vascular system, form a semi-selective barrier between the vessel lumen and surrounding tissue and can migrate and take part in blood vessel healing and new blood vessel formation in tissue regeneration (Takebe et al., 2013, Nahmias et al., 2006). To evaluate endothelial capacity to promote vascularisation and support normal hepatocyte function, including CYP450 activity, it is important to obtain insights into the mechanisms promoting angiogenesis and the morphology and migration of the individual cell types involved in these processes (Kavitha et al., 2011, Rivron et al., 2008, Soto-Gutierrez et al., 2010).

The use of extracellular matrix (ECM) as a support for endothelial cells can promote vascular network *in vitro* which promote albumin synthesis and CYP450 activity in hepatocytes to recapitulate drug metabolism *in vitro* (Nahmias et al., 2006). The most relevant ECM used to support formation of organised endothelial networks *in vitro*, is the animal-derived Matrigel™ which, despite not being fully-defined, is known to contain high concentrations of laminin, collagen, entactin and growth factors (Rohringer et al., 2014, Hadi

et al., 2013, Toyoda et al., 2012). Matrigel™ is an animal-derived scaffold. An experimental animal free ECM (xeno-free ECM), has also been developed to promote migration of growth in a 3D culture (Maas-Szabowski et al., 2005). However, formal comparison between xeno-free ECM and animal-derived ECM (Matrigel™) is still required.

Endothelial cells and hepatocytes, cultured in conventional tissue culture polystyrene, do not migrate to achieve self-organisation into defined vascular network (Nelson et al., 2010, Tourovskaia et al., 2014) in response to indirect stimulation by soluble trophic factors in endothelial-hepatic cross-talk. Cross-talk could generate a potential tool to maintain hepatocytes function *in vitro* (Hoehme et al., 2010, Rivron et al., 2008). Culturing rat primary hepatic cells using extracellular matrices has been shown, to some degree, overcome the loss of CYP3A3 activity and albumin synthesis seen when hepatocytes are cultured on polystyrene (Genove et al., 2009). Indeed, an *in vitro* angiogenesis model using rat hepatocytes and endothelial cells grown on Matrigel™ has demonstrated that the exchange of VEGF promotes endothelial cell migration and vascular tubes, and improved hepatic function (Nahmias et al., 2006), while the use of collagen-I as an ECM support, promotes cell-cell attachment between HUVECs and rat hepatocytes (Inamori et al., 2009).

Transmembrane adhesion glycoproteins expressed on parenchymal cells can be bound to components of the ECM, such as CD44, which binds hyaluronic acid. CD44 is associated with cell migration, cell adhesion (Deboux et al., 2013) and showed APAP susceptibility (Harrill et al., 2009). CD49f, which binds laminin, is associated with cell survival and migration (Yu et al., 2012).

The principal aim of this study was to evaluate endothelial function using HUVEC:C3A co-culture in the presence of ECM to promote vascular network, wound healing and facilitate growth factor transfer to facilitate the outgrowth of hepatocytes. The recapitulation of cell migration in an *in vitro* system would give insights in the endothelial capacity to adapt and

build a vascular system (e.g. liver sinusoid-like structures) which could be applied to drug discovery.

To develop an *in vitro* vascularised hepatic model using HUVECs and C3As, the following points were pursued:

i. Selection of a biocompatible ECM to promote vascular network by HUVECs in mono and co-culture with C3As, and to allow further investigation of cell migration.
ii. Investigation of the effect of using an ECM on hepatic function in C3As and on the endothelial function in HUVECs. The maintenance of albumin synthesis and CYP3A4 activity in a vascular network, is essential to recapitulate drug metabolism *in vitro*.
iii. Evaluation of the effect of APAP toxicity on hepatic function, on endothelial properties such as vascular formation, wound healing as well as investigation of regulation of cellular receptors in HUVEC:C3A mono- and co-cultures.

5.2 Methods

5.2.1 Matrigel™ coating of tissue culture plates

Matrigel™ Matrix Phenol Red-free (BD) or Matrigel™ Growth Factor Reduced (MG-GFR) (BD) was thawed overnight on ice in the cold room and handled with pre-cooled tips. Tissue culture plate wells were coated with cold liquid Matrigel™ and incubated at 37ºC and 5% CO_2 for 1hr to allow protein polymerisation and gel formation before addition of cell suspensions at density of 26.000 cells/cm^2.

5.2.2 MaxGel™-Human ECM coating of tissue culture plates

MaxGel™ (Sigma-Aldrich) is a human basement membrane extract containing extracellular matrix components which can be used to form a 3D environment for cell culture. This was selected to compare its effects with those of animal-derived hydrogels such as Matrigel™. To coat tissue culture plastic, MaxGel™ was thawed on ice in the cold room, handled with pre-cooled tips, diluted in 1:2 with cold cell culture media (EGM-2) and incubated at 37ºC and 5% CO_2 for 2 hours to allow to polymerisation before addition of cells at density of 26.000 cells/cm^2.

5.2.3 *In vitro* co-culture experiments

For *in vitro* co-culture experiments, HUVECs were seeded with C3A cells at ratio 1:1 (HUVEC:C3A) in pre-coated wells with ECM in EGM-2 for 3 days before the assessment of hepatic function, except where indicated. Starting cell density was based on surface area at 26.000 cells/cm^2.

5.2.4 Vybrant staining

HUVECs and C3As were labelled with two different lipophilic membrane stains Vybrant™ Cell-Labelling Solution (Molecular Probes). HUVECs and C3As at a density of $1x10^6$ cells per ml were labelled individually with DiI (red-fluorescent dye) or DiO (green-fluorescence dye), by incubation for 15 min at 37ºC and 5% CO_2 and washed 3 times with PBS before seeding the cells.

5.2.5 Hepatic activity

Albumin synthesis was measured in cell culture supernatants using Albumin Blue 580 Fluorescence Assay as indicated in Section 2.2.7.1, while CYP3A4 activity was measured as described in Section 2.2.7.3.

5.2.6 CYP3A4 and Filamentous action (F-actin) staining

HUVECs and C3As were cultured either separately or in co-culture at a density 21.000 cells/cm^2 on polystyrene well plate for 3 days. On day 3, cells were fixed and treated with 0.1% Triton X-100 in PBS for 1hr at RT and blocked with PBS containing 5% BSA for 30 min. Subsequently, they were stained for CYP3A4 and Filamentous actin (F-actin) as described in Section 2.2.4.2.

5.2.7 Time-lapse fluorescence microscopy

HUVECs and C3As were labelled with DiI (bright red-fluorescent dye) and DiO (bright green-fluorescent dye) respectively as described in Section 5.2.4 and seeded at the same time in 24 well plate pre-coated with Matrigel™.

Time-lapse fluorescence imaging was then performed for 20hr using an automated wide field observer inverted microscope (Zeiss Axio-Observer A1, Germany). The microscope was focused before the start point of time-lapse and was able to autofocus throughout the run. A total of 58 pictures were taken every 20 min for 20hr.

5.2.8 Vascular network formation assay

Standard experiments

HUVEC and C3A mono and co-cultures at ratio 1:1 were seeded in pre-coated with Matrigel™ with EGM-2 for one week and cell viability was determined using a LIVE/DEAD® Viability/Cytotoxicity Kit (Life technologies) at the end of the experiment as described in Section 3.2.2. Vascular structures were photographed at time 6hr, 72hr and one week using a confocal microscope and Nikon Digital camera DXM1200. Images were merged using ImageJ 1.46r (National Institute of Health, USA). The images were used to manually count the number of vascular tubes formed.

Drug toxicity studies

HUVEC and C3A mono and co-cultures at ratio 1:1 were seeded in pre-coated with Matrigel™ with EGM-2 (control) and with EGM-2 containing 10 mM APAP. Cultures were photographed at time 24hr using inverted microscope (Zeiss Axio-Observer A1, Germany) and images were captured with a mounted camera (Zeiss AxioCam MRm).

5.2.9 Trans-well cell migration assay

C3As migration to the interconnected vascular network made by HUVECs on Matrigel™ was investigated using an 8μm porous filter insert of a trans-well cell migration assay. 24 well tissue culture plates were pre-coated with Matrigel™ or with Matrigel-GFR as

described in Section 5.2.2. Then, unlabelled HUVECs were seeded on the Matrigel™ while C3As labelled with PE-DiI (red- fluorescent dye) (see Section 5.2.1.1) were placed in transwell inserts of 8µm pore diameter translucent ThinCert™ 24 Well Cell Culture Inserts (Greiner Bio-one) on the top of each 24 well plate (Figure 5-1). Then, wells were incubated at 37ºC and 5% CO_2 for 24hr with EGM-2 culture media.

After 24hr, EGM-2 and inserts were carefully removed and cells were washed with PBS and fixed in 4% (w/v) paraformaldehyde for 10 min at RT. The bottoms of the wells were photographed under fluorescence microscopy using a confocal microscope and Nikon Digital camera DXM1200 and images were merged using ImageJ 1.46r (National Institute of Health, USA).

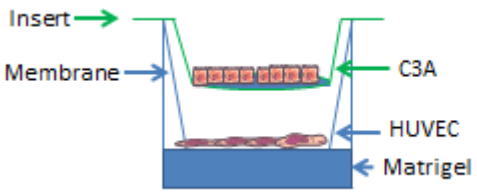

Figure 5-1 Representation of trans-well plate assay

HUVECs were seeded in wells of 24 well tissue culture plates were pre-coated with Matrigel™, Matrigel™ GFR or uncoated polystyrene for one hour in the incubator at 37ºC and 5% CO_2. C3As were labelled with DiI (red fluorescent dye) *and plated, at the same density as HUVECs, in transwell inserts of 8µm pore diameter translucent ThinCert™ 24 Well Cell Culture Inserts (Greiner Bio-one) on the top of each 24 well plate.*

5.2.9.1 Cell Imaging and Analysis Package

The percentage of area coverage by stained-DiI (red fluorescent dye) C3As was calculated using a Cell Imaging and Analysis Package designed by Dr. Scott Inglis (Department of Medical Physics, RIE, NHS Lothian) using the Matlab 7.1 (R14) Graphical User Interface (GUI) builder.

The Cell Imaging and Analysis Package functioned by loading the original image in JPEG or TIFF format with C3As tracker with DiI (red fluorescent dye) (see Section 5.2.1), and splitting the image into three different thresholding levels (red, green and blue). Red was used as the reference component and green and blue were subtracted from the reference. When channels from the image were subtracted, red staining was converted into a smoothed white mask image corresponding to stained C3As and the percentage of the mask image was calculated. The accuracy of the Cell Imaging and Analysis Package was validated by comparing actual values for objects of known area with experimentally determined values. To perform this comparison, calibration squares of predetermined area were designed using Microsoft PowerPoint and the real areas compared with areas obtained by converting the objects into JPEG or TIFF format and analysing them using the programme. The error observed between real and experimentally determined values was calculated, with the result that the Cell Imaging and Analysis Package can determine the area covered by an object with an error of 0.07% (Figure 5-2).

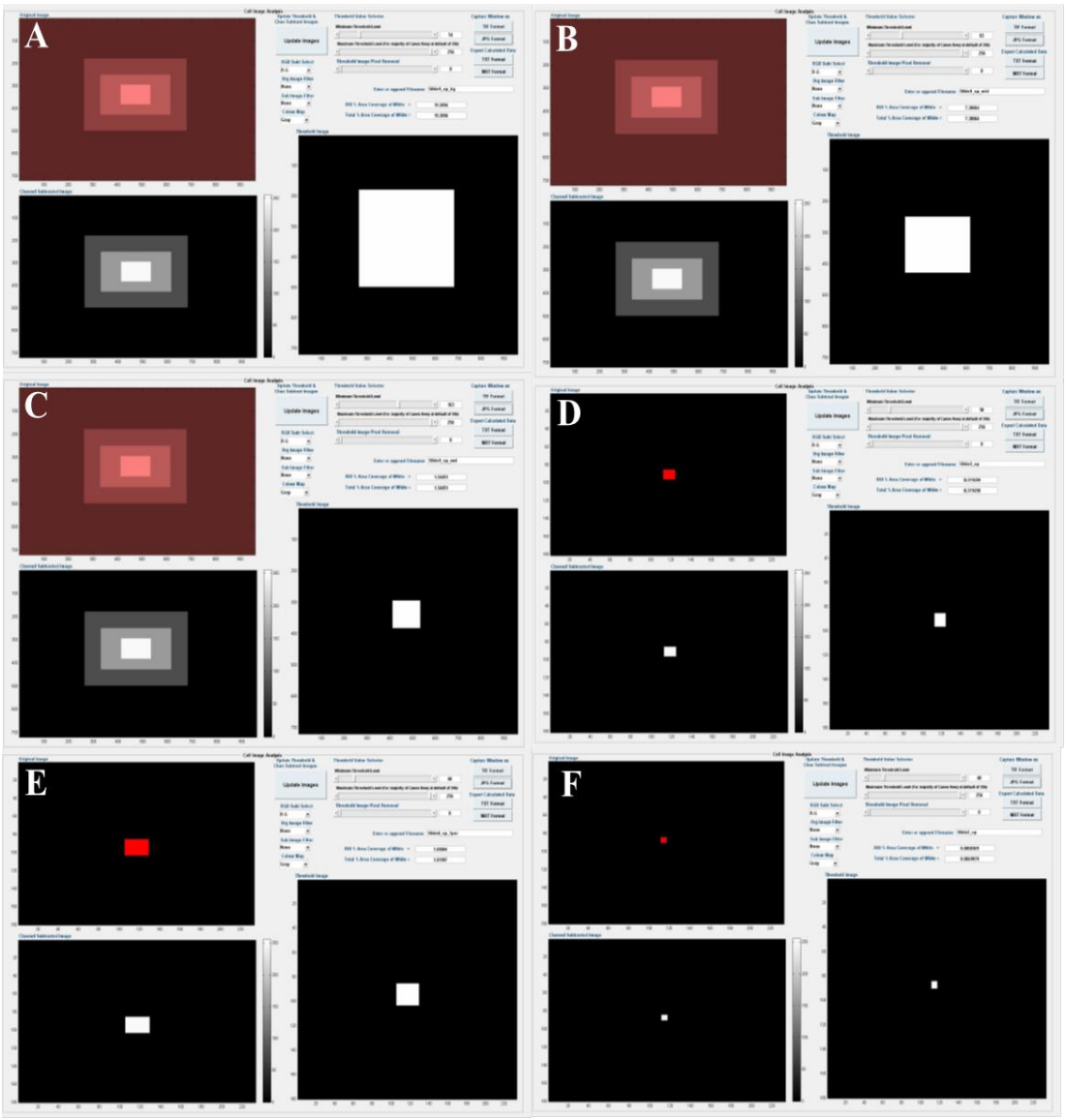

Figure 5-2 Cell Imaging and Analysis Package Calibration

*Cell Imaging and Analysis Package was designed using Matlab 7.1 (R14) Graphical User Interface (GUI) builder. To detect the systematic error of each measurement, different sizes of squares were measured and calculated in table 5-1 and compared to known values. To perform this comparison, squares were designed using power point and the area was calculated following the equation of the area of the rectangle: Area = length * width, giving real values. Then, the same squares were used to obtain the experimental values using the programme to detect the error.*

Table 5-1 Data calibration of real values compared to experimental values

Real values from known areas were compared to experimental values to calculate systematic error to validate the of Cell Imaging and Analysis Package programme. Different sizes of squares were measured and compared to real values. Data were compared between both groups and the error observed between real and experimental values was calculated and the result was that the programme can calculate the area covered with an error of 0.07%.

	Real values	**Real %**	**Experimental %**	**Systematic error**
Control	19.07*25.04=477.5	100		
A	8.46*11.03=93.3	19.54	19.31	0.23
B	4.73*7.54=35.7	7.48	7.38	0.1
C	2.34*3.22=7.53	1.58	1.54	0.04
Control	4.8*6.2=29.76	100		
D	0.48*0.62=0.30	1	1.03	0.03
E	0.28*0.31=0.09	0.34	0.31	0.03
F	0.14*0.15=0.021	0.07	0.085	0.015
Mean				**0.074**

5.2.10 Wound healing assay

Wound healing was evaluated by the ability of cells in confluent HUVEC and C3A mono- and co-cultures to migrate in response to an external 'scratch' wound.

HUVECs and C3As were propagated in mono and co-culture for 3 days. On day 2 of cell culture, culture medium was removed and cells were wounded by drawing a pipette tip at an angle of approximately 30 degrees across the cell monolayers which were then washed with PBS and supplemented with fresh EGM-2 (control) and with EGM-2 containing 10 mM APAP. Cultures were photographed using EVOS ® inverted microscope (Life Technologies) at time 0 of the initial scratch and at time 24hr.

Calculation of the percentage of HUVECs migration was evaluated as follow:

Percentage of HUVECs migration = (B*100%)/A

B = Distance of the width of the wound the final scratch at 24hr

A = Distance of the width of the wound at the initial scratch at 0hr

5.2.11 Flow cytometry

CD44 and CD49f expression was evaluated using flow cytometry as described previously in Material and Methods Section 2.2.6

5.3 Statistical Analysis

Experiments were performed in triplicate on at least three biological replicates. GraphPad software Prism®5 was used for statistical analysis. Results were reported as mean ± standard error (SEM). Student's unpaired t-test was used to compare all co-cultures to their appropriate HUVECs and C3As controls (statistical significance *$p<0.05$).

5.4 Results

5.4.1 Biocompatibility of an extracellular matrix (ECM) for HUVEC:C3A

The *in vitro* hepatic co-culture model established previously using HUVECs and C3As was evaluated after 24hr culture in the presence of ECM using two different commercial basement membranes, namely MaxGel™ and Matrigel™. MaxGel™ is isolated and purified from human epithelial fibroblasts to produce a basement membrane rich in laminin, and reduced growth factors (Maas-Szabowski et al., 2005), while Matrigel™ is an animal-derived hydrogel. Despite these differences, both of the hydrogels contain laminin and both were used here experimentally in assays to measure induction of angiogenesis using HUVECs. Because the MaxGel™ preparation contains only low levels of growth factors, VEGF was added to the gel to promote tube formation by HUVECs.

Co-culture of HUVEC:C3A on Matrigel™ for 24hr induced a vascular tube formation response as evidenced by the formation of hexagonal networks of endothelial cell tubes (Figure 5.3A, B green stain). Further analysis showed that the distribution of C3A cells in the co-culture were not random, but that majority of C3As seemed to have migrated towards the endothelial network, while C3As between the network were sparse or absent (Figure 5.3C red stain). Comparison of HUVEC:C3A co-cultures on Matrigel™-GFR with standard Matrigel™ preparations showed similar self-organisation of HUVECs and migration of C3As towards endothelial networks (data not shown). In contrast, co-culture of HUVEC:C3A on MaxGel™ failed to promote any such organisational response, with both HUVECS and C3As being randomly distributed, even with the addition of VEGF (Figure 5-3D-F). Together this suggests that HUVECs self-organisation and C3As migratory behaviours are due to a component of the Matrigel™, rather than growth factor content.

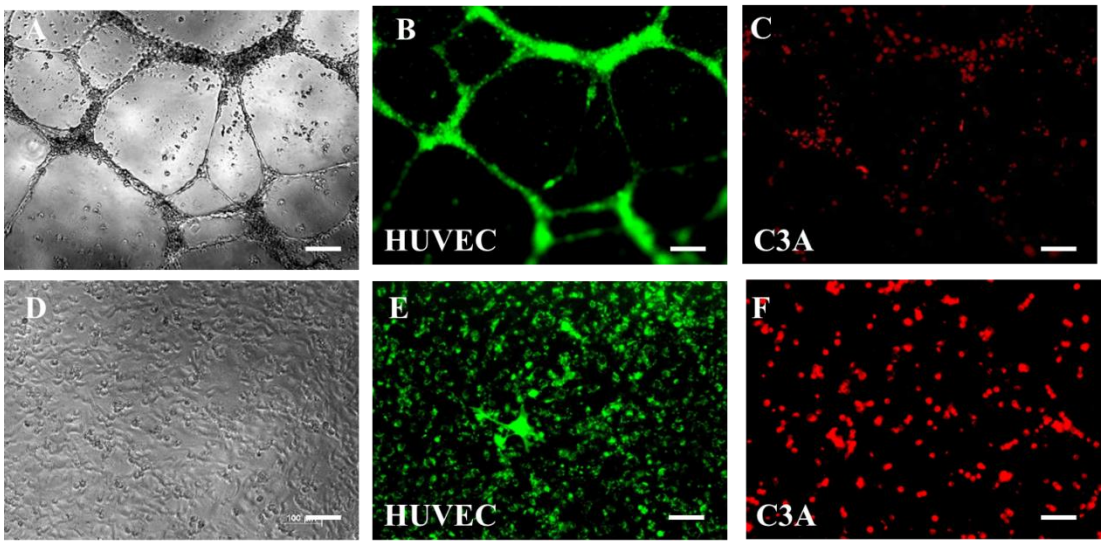

Figure 5-3 Biocompatibility of an ECM as a scaffold for HUVEC:C3A

HUVECs and C3As plated at a ratio of 1:1 were grown for up to 24hr in plates pre-coated with thick Matrigel™ and MaxGel™ as described in Sections 5.2.2 & 5.2.3 . MaxGel™ was preloaded with 1µg/ml of VEGF. Then, HUVECs and C3As were labellerd with Vybrant™ Cell-Labelling Solution (Molecular Probes) as described in section 5.2.1. DiO (green-fluorescence dye) was used for HUVECs and DiI (red-fluorescent dye) for C3As. Phase-contrast imaging for co-cultures in Matrigel™ (A-C) and MaxGel™ (D-F), and fluorescence images for HUVEC (bright green) in Matrigel™ (B) and MaxGel™ (E) C3As (bright red) in Matrigel™ (C) and MaxGel™ (F). Images were taken using inverted microscope (Zeiss Axio-Observer A1, Germany) and captured at magnification x10 and scale bar 100µm.

5.4.2 Effect of Matrigel™ on hepatic function

The effect of Matrigel™ on hepatic activity was evaluated by analysing both albumin synthesis and cytochrome P450 3A4 activity in C3A cells following 3 days of mono-culture or HUVEC:C3A co-culture at ratio 1:1 on Matrigel™ and compared to the data seen before when hepatocytes were cultured on polystyrene (Section 2.6.1 and 2.6.2).

Results revealed that culture on Matrigel™ significantly enhanced albumin synthesis in C3A mono-cultures to 30.64 ± 2.13 µg/10^6 initial cells compared to C3As grown on polystyrene 20.50 ± 3.46 µg/10^6 initial cells ($p=0.046$). In co-cultures, there was no significant difference in albumin synthesis between HUVEC:C3As co-cultures on polystyrene or Matrigel™, where synthesis was already enhanced at 34.17 ± 3.59 µg/10^6 initial cells and 31.89 ± 2.79 µg/10^6 initial cells respectively (Figure 5-4-A). This suggest that both culture of C3As on Matrigel™ and co-cultures with HUVECs is able to provide factors that increases hepatic albumin synthesis compared to simple culture on polystyrene.

Similarly, culture on Matrigel™ maintained CYP3A4 activity in C3As mono-cultures by day 3 compared to polystyrene, from 270.6 ± 38.73 RLU on polystyrene to 363.4 ± 32.36 RLU on Matrigel™. Again, co-culturing of HUVEC:C3A cells on Matrigel™ did not result in significantly increased CYP3A4 activity as compared to co-cultures on polystyrene, (360.6 ± 58.33 RLU in Matrigel™ vs 490.2 ± 62.95 RLU in polystyrene; Figure 5.4-B).

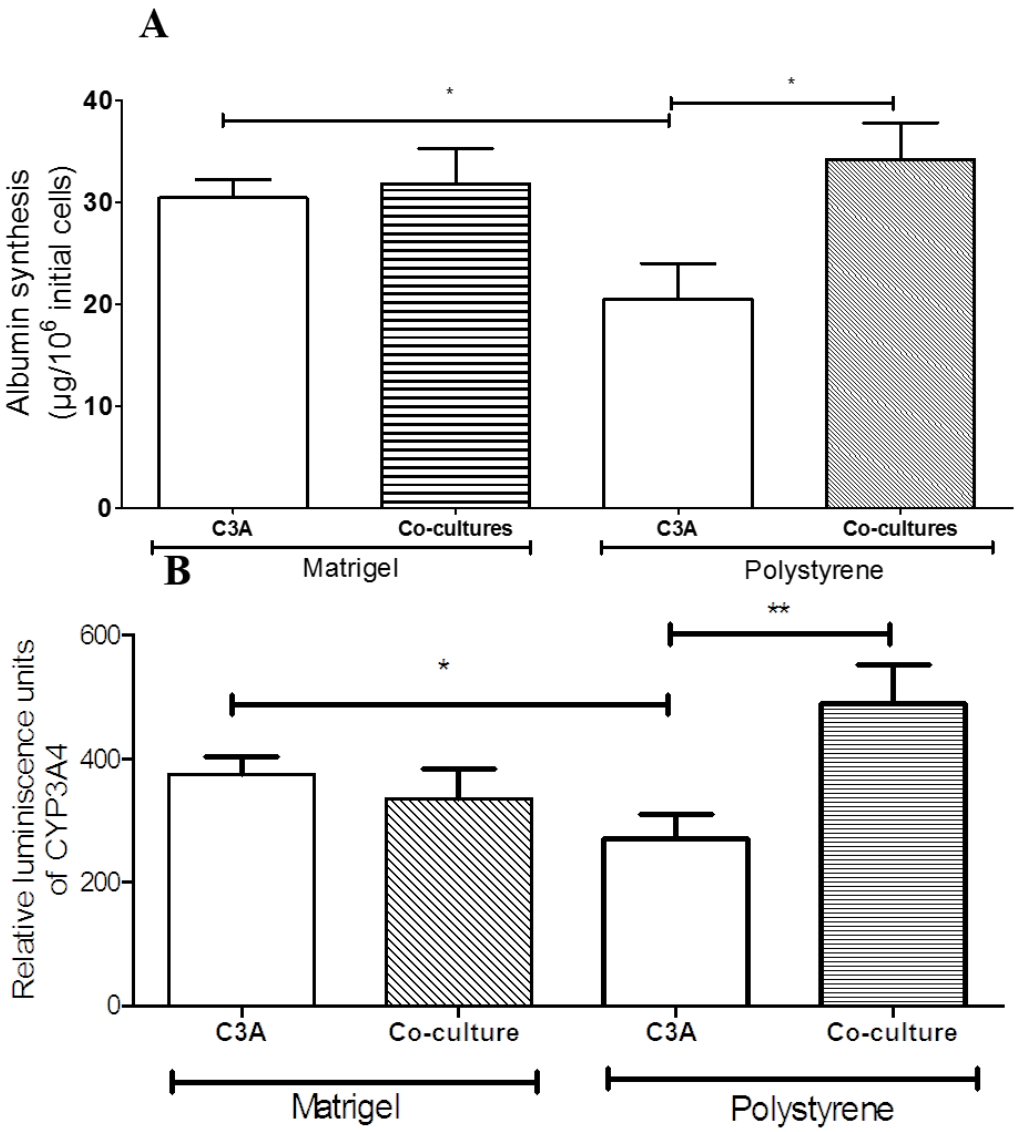

Figure 5-4 Hepatic-specific activity in C3A mono-cultures and HUVEC co-cultures on day 3 in EGM-2 medium

*C3As in mono-cultures and HUVEC:C3A co-cultures (ratio of 1:1) were cultured for 3 days on Matrigel™ or polystyrene. Albumin synthesis was measured in cell culture supernatants on day 3, and CYP3A4 activity was performed using P450-Glo CYP3A4 activity assays explained in Materials and Methods in Sections 2.2.7.1 and 2.2.7.3. Figure A) shows albumin synthesis; and B) CYP3A4 activity against Luciferin-IPA compared to previous data obtained from culturing cells in polystyrene. Data is expressed as the mean ± SEM of three different experiments in triplicate, * $p < 0.05$/ ** $p < 0.01$. (n=3).*

5.4.3 Effect of APAP on CYP3A4 activity in C3As and HUVEC:C3A cultured on Matrigel™

In the presence of Matrigel™, treatment with 10 mM APAP for 24hr significantly induced CYP3A4 activity between untreated and APAP treated cell in mono-cultures and co-culture with HUVECs. Both untreated C3A mono-cultures and HUVEC:C3A co-cultures showed similar low levels of CYP3A4 activity. Following APAP treatment, CYP3A4 activity in untreated C3A mono-cultures increased from 375.40 ± 27.43 RLU to 2119.00 ± 349.90 RLU following treatment ($p=0.0001$). A similar pattern was observed in HUVEC:C3A co-cultures when untreated co-cultures showed 334.20 ± 49.28 RLU CYP3A4 activity compared to 2467 ± 474.10 RLU ($p=0.0004$) following treatment. In total, APAP treatment induced CYP3A4 activity 7.4-fold in co-cultures and 5.6-fold activity in mono-cultures (Figure 5.5).

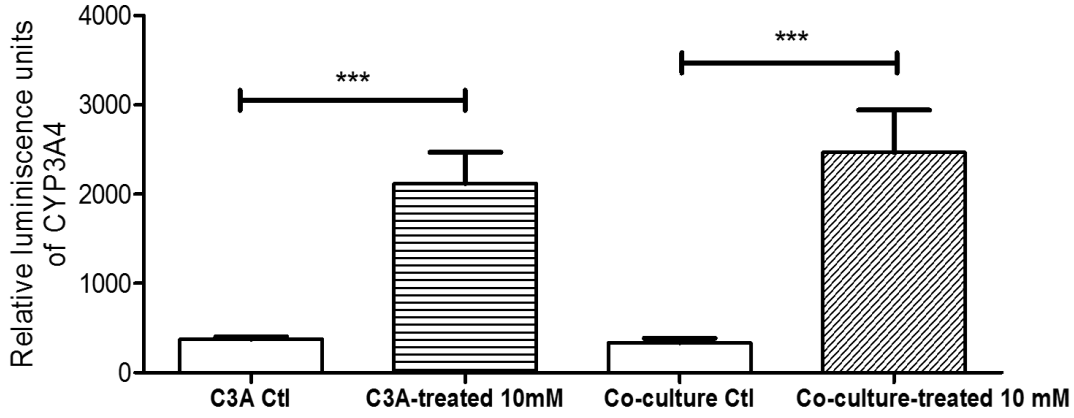

Figure 5-5 CYP3A4 activity APAP metabolism in C3A mono-cultures and HUVEC:C3A co-cultures on day 3 of culture on Matrigel™ in EGM-2 medium

*C3As in mono-cultures and HUVEC:C3A co-cultures (ratio of 1:1) were cultured on Matrigel™ for 3 days. On day 2, cells were treated for 24hr with 10 mM APAP or with just EGM-2 medium as a control. CYP3A4 activity assay was then measured using the P450-Glo CYP3A4 activity assay as described in Section 2.2.7.3. Data is expressed as the mean ± SEM of three different experiments, *** $p < 0.0001$. (n=3).*

5.4.4 Endothelial and hepatic cell migration on Matrigel™

At time 0hr, HUVECs and C3As were randomly distributed in a Matrigel™ coated well (Figure 5-6A). At time 10hr, HUVECs had formed an interconnected vascular network, with defined geometry and well organized endothelial vascular structures. Also HUVECs and C3As had moved toward each other and areas where HUVECs and C3As overlie one another can be seen as yellow points in Figure 5-6B. By time 20hr, more consolidated endothelial loops with closely associated C3As were apparent (Figure 5-6C). No differences were found between Matrigel™-GFR and standard Matrigel™ (data not shown). C3As seemed to surround the endothelial cells, suggesting that C3As migrate towards HUVECs.

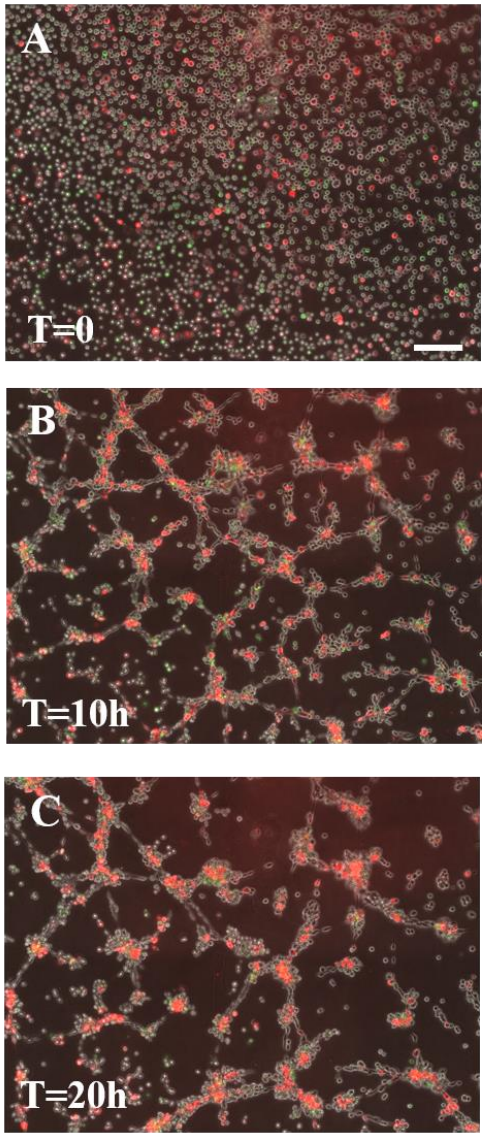

Figure 5-6 Time lapse fluorescence microscopy of HUVEC:C3A on Matrigel™ at time 0hr, 10hr and 20hr in EGM-2 media.

HUVECs and C3As at ratio 1:1 were suspended in EGM-2 medium and seeded on wells pre-coated with thick Matrigel™ to investigate interaction between the different cell types in more depth. To identify each cell line in co-cultures, HUVECs and C3As were labelled respectively with DiI (bright red) and DiO (bright green) fluorescent dyes (as described in Section 5.2.4). Then, cells were then observed using Time-lapse fluorescence imaging using automated wide field observer inverted microscope (Zeiss Axio-Observer A1, Germany). A total of 58 pictures were taken every 20 min for 20hr as described in Section 5.2.7. Sample pictures shown here at time 0hr (A), at time 10hr (B) and at time 20hr (C). Magnification of 10X and scale bar of 100µm.

5.4.5 Vascular network formation on Matrigel™

To determine the effect of toxic APAP challenge to vascular network formation, HUVECs and C3As in mono-culture or co-cultures seeded on Matrigel™ were exposed to 10 mM APAP in EGM-2 for 24hr or with EGM-2 as control, to determine APAP toxicity. As expected untreated HUVEC mono-cultures formed well-defined tube structures on Matrigel™, resulting in an organised network (Figure 5-7A). However APAP-treated HUVECs showed no organisation into vascular tubes, but instead formed cell clumps indicative of cell death after 24hr (Figure 5-7B). Meanwhile, C3A mono-cultures maintained their morphology after APAP treatment as compared to untreated controls (Figure 5-7C&D). In APAP treated HUVEC:C3A co-cultures, HUVECs were again able to form an interconnected vascular network with which C3As were closely associated. This was essentially comparable to that seen in untreated co-cultures though the tubes formed by APAP-treated HUVECs were shorter (Figure 5-7E&F), suggesting that C3A cells provide a 'survival' factor.

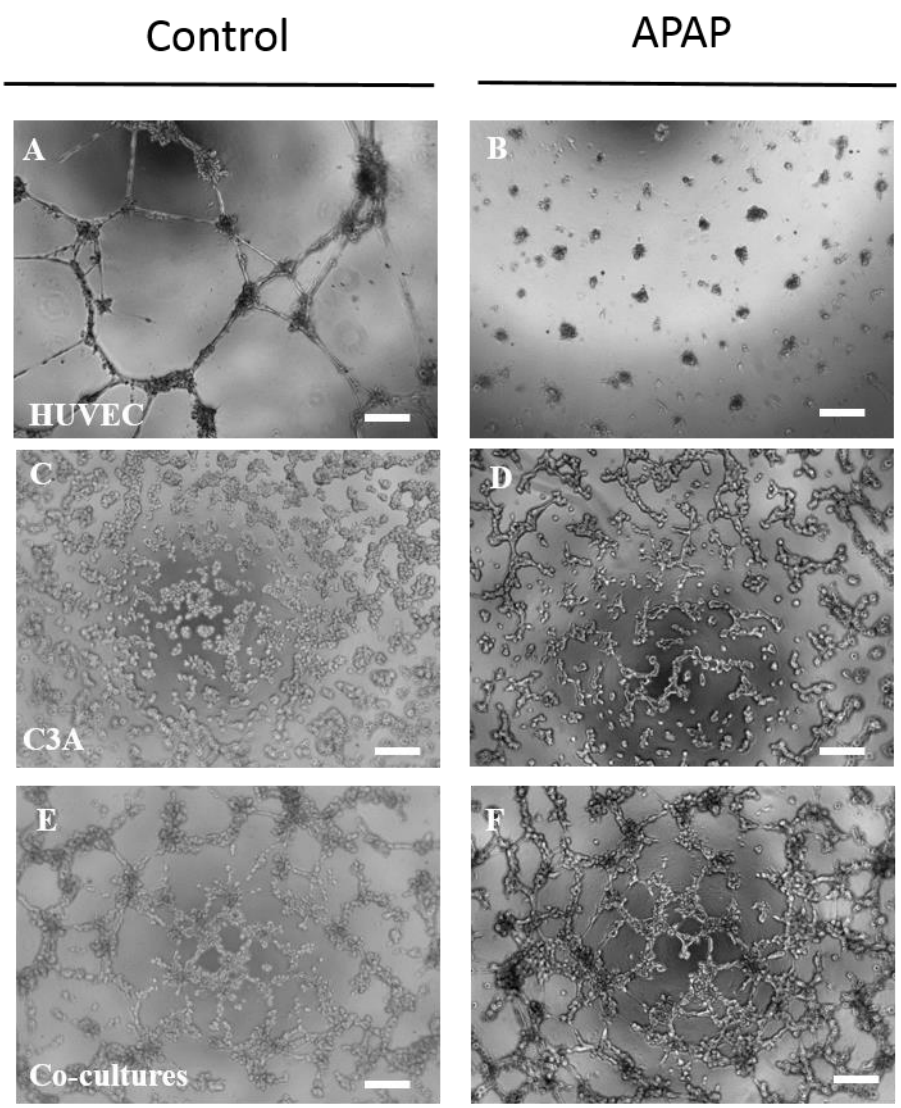

Figure 5-7 Light fluorescence microscopy of HUVECs, C3As and co-cultures at time 24hr in EGM-2 media (control) and 10 mM APAP (treated cells)

HUVECs and C3As seeded in mono-culture and in co-culture at ratio of 1:1 on pre-coated wells with Matrigel™, were photographed following 24hr of cell culture. Pictures here show (A) HUVECs untreated control, (B), HUVECs 10mM APAP-treated, (C) C3As untreated control, (D, C3As 10mM APAP-treated, (E) co-cultures untreated control, and (F) co-cultures 10mM APAP treated). Pictures were taken using an inverted microscope (Zeiss Axio-Observer A1, Germany) at magnification of 10X and scale bar of 100µm.

5.4.6 Endothelial functionality in the presence of C3As on Matrigel™

The effect of C3A cells on the vascular tube formation by HUVECs was assessed by monitoring the number of vascular tubes and loops formed in HUVECs mono-cultures and in the presence of C3As in co-cultures on Matrigel™ from 0hr to up to one week.

HUVECs formed 36 ± 5 vascular tubes following 6hr culture on Matrigel™ whereas 38 ± 5 vascular tubes were observed in HUVEC:C3A co-cultures after 6hr, the highest values observed over the period of study (Figure 5-8).

Following 72hr of culture, HUVEC mono-cultures showed a significant reduction in the number of vascular tubes to 19 ± 2 compared to HUVEC mono-cultures at 6hr ($p=0.0103$), where 25 ± 3 vascular tubes were observed at 72hr in HUVEC:C3A co-cultures ($p=0.1120$). The differences between HUVEC in mono-culture and co-cultures were only significant at one week. By this time, HUVEC mono-cultures displayed 14 ± 2 tube tubes compared to 25 ± 3 in HUVEC:C3A co-cultures ($p = 0.004$) (Figure 5.8-K). The same pattern was observed when counting the number of loops formed, resulting in significant difference at one week ($p= 0.006$) (Figure 5-8L).

Cell viability at the end of culture (one week) was confirmed using LIVE/DEAD® Viability/Cytotoxicity Kit (Life technologies) (Section 3.2.2). As can be seen from Figure 5-8 (D-E), HUVECs in mono-culture remained viable in endothelial vascular tubes (bright green) after one week on Matrigel™. Similar levels of cell viability are observed for HUVECs in HUVEC:C3A co-cultures (Figure 5-9 I-J), with the addition that qualitatively the integrity of the network formed by HUVECs appeared to better maintained and stronger in the presence of C3As compared to HUVECs in mono-cultures (Figure 5-8 D, I).

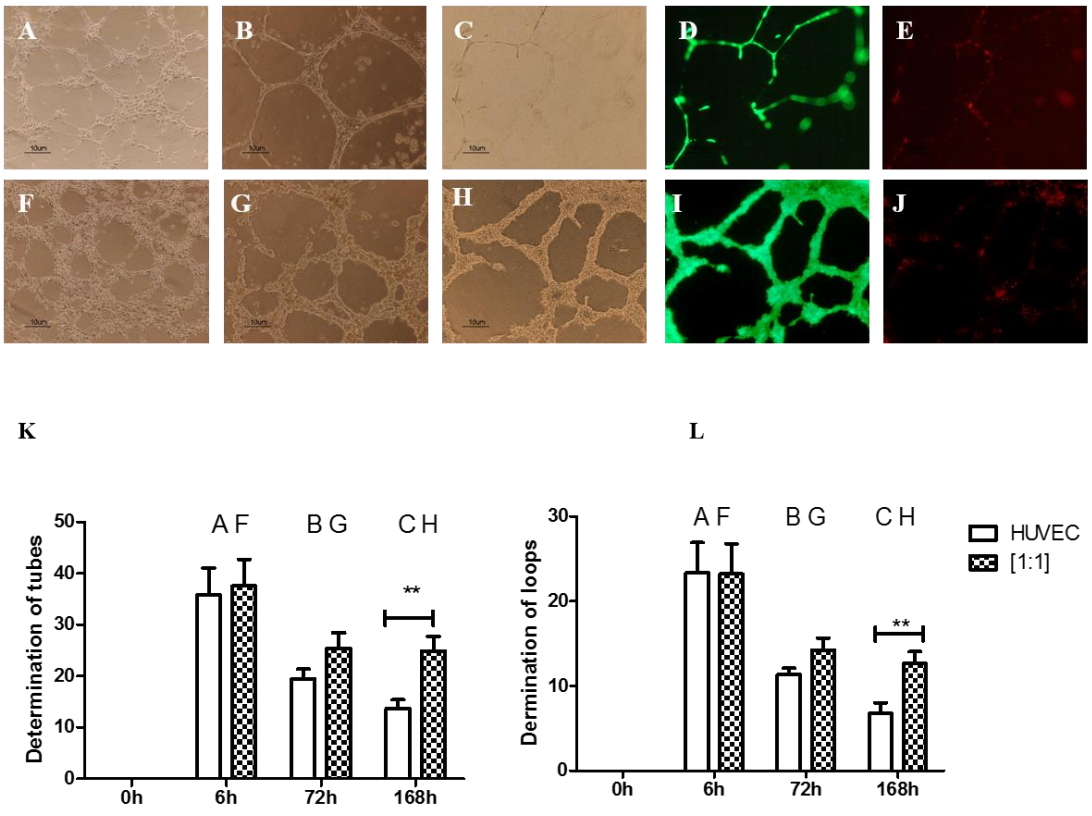

Figure 5-8 Endothelial vascular network in the presence of C3As on Matrigel™

HUVECs in mono-culture and HUVEC:C3A co-cultures in 24 well tissue culture plates pre-coated with Matrigel™. HUVECs (A-C) and HUVEC:C3A (D-F) were grown and photographed using a confocal microscope and Nikon Digital camera DXM1200 at time 6hr ***(A, D)****, 72hr* ***(B, E)*** *and one week* ***(C, F).*** *At time one week, cells were stained with live [bright green] and dead (bright red) (LIVE/DEAD® Viability/Cytotoxicity Kit (Life technologies)) as described in Section 3.2.2 for HUVECs* ***(D-E)*** *and HUVEC:C3A co-cultures* ***(I-J)****. Capillary tube and loop numbers were counted manually and results are presented as tubes and loop numbers present at specified time points. Images were merged using ImageJ 1.46r (National Institute of Health, USA). Data is expressed as the mean ± SEM of three different experiments, ** $p < 0.01$ (n=3).*

5.4.7 Filamentous actin and cell-junctions in HUVECs and C3As

The endothelial tube formation assays described above (Section 5.4.6) showed that vascular network formation in HUVEC:C3A co-cultures on Matrigel™ formed early on 6hr declined more slowly in co-culture as compared to HUVECs cultured on Matrigel™ alone. Previously, time lapse photography also demonstrated that C3As migrated to the vascular tube structures (Section 5.4.4). Actin microtubules are known to participate in cell migration and formation of cell-cell-junctions (Stroka et al., 2013). Here, the development of actin filaments was used as a measure of cell migration. HUVEC and C3A mono- and co-cultures were grown on polystyrene and stained on day 3 of cell culture with rhodamine phalloidin (bright red) which has a high-affinity probe for F-actin to detect the capacity of cells to migrate. Cultures were also co-stained for CYP3A4 expression to identify hepatic cell phenotype.

As shown in Figure 5-9-A, specific cells in C3A mono-cultures that demonstrated a hepatic phenotype, as evidenced by CYP3A4 staining, also stained prominently for F-actin at the cell junctions, reminiscent of bile canaliculi and the apical side of polarized epithelial cells (Goler-Baron and Assaraf, 2011). As shown in Figure 5-9-B, HUVECs cultured alone did not show F-actin bright staining at cell-cell junctions but did show F-actin staining cytoplasmic. As anticipated, CYP3A4 staining was not observed in HUVECs. In HUVEC:C3A co-cultures, F-actin filaments were probably increased in relation to chemotaxis or haptoxis migration. Meanwhile, C3As in co-cultures, stained more strongly for CYP3A4 activity (bright green) and more predominant foci of actin expression (bright red) were seen at junctions between HUVECs and C3As (Figure 5-9-C)

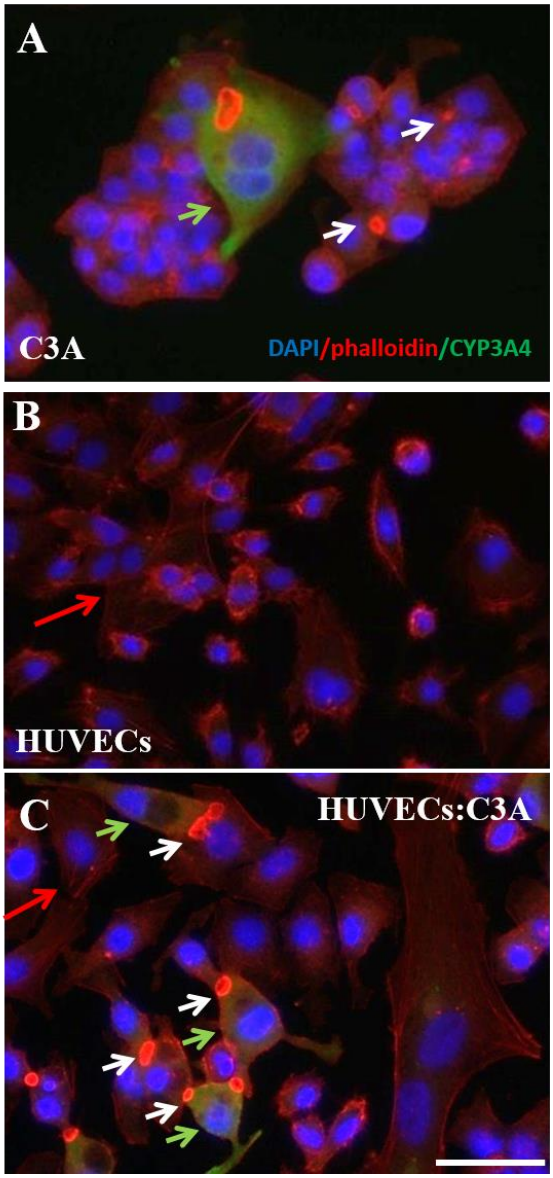

Figure 5-9 Actin filaments in C3As and HUVEC mono-cultures and HUVEC:C3A co-cultures at ratio 1:1 on polystyrene after 3 days culture in EGM-2.

HUVECs and C3A mono-cultures and HUVEC:C3A co-cultures grown for 3 days on polystyrene were fixed and stained with Rhodamine phalloidin (bright red) to detect F-actin, stained with CYP3A4 antibody (bright green) and DAPI nuclear stain (bright blue) as described in Section 2.2.5.2. Representative immunofluorescence images showing cell morphology and staining for F-actin, CYP3A4 and nuclei of (A) C3As, (B) HUVECs mono-cultures and (C) HUVEC:C3A co-cultures at ratio of 1:1. White arrows indicate cell-junctions, green arrows indicate C3As (CYP3A4 staining) and red arrows indicate HUVECs (cytoplasmic actin staining). These images were taken using an inverted microscope (Zeiss Axio-Observer A1, Germany) at magnification x10 and were merged using imageJ 1.46r. Scale bar 100µm.

5.4.8 Cell transmigration studies within HUVECs and C3As

To investigate further the apparent interaction between HUVECs and C3As in co-cultures, transwell cell migration assays were used. Transwell inserts containing red fluorescent labelled- C3As were added to 4 different condition wells: i) HUVECs seeded on the top of Matrigel™, ii) wells without HUVECs coated with Matrigel™, iii) wells without HUVECs coated with Matrigel™GFR and iiii) wells without HUVECs uncoated polystyrene. After 24hr, the transwell inserts were removed, wells were photographed and migration was quantified by calculating the area of the well covered by stained-C3As

As shown in Figure 5-10-A, C3A cells migrated from the transwell insert through the membrane to the vascular network formed by HUVECs in the base of the tissue culture wells and became associated with the vascular network rather than being randomly distributed. 3.30 ± 0.36 % of C3A cells migrated through the transwell membrane toward the vascular network formed by HUVECs plated on Matrigel™, as quantified by coverage of the well area and 1.67 ± 0.39 % of C3As migrated into wells containing Matrigel™ only ($p=0.0081$), while cells containing Matrigel™GFR or uncoated polystyrene attracted only 0.34 ± 0.066 % ($p<0.0001$) and 0.17 ± 0.04 % ($p<0.0001$) of C3As respectively (Figure 5.10). These findings are consistent with the previous data presented for C3A cells migration in HUVEC:C3A co-cultures obtained by time lapse photography (Section 5.4.4) and confirm that migration of C3As towards HUVECs is in part dependent on chemotactic factors produced by the HUVECs network.

A

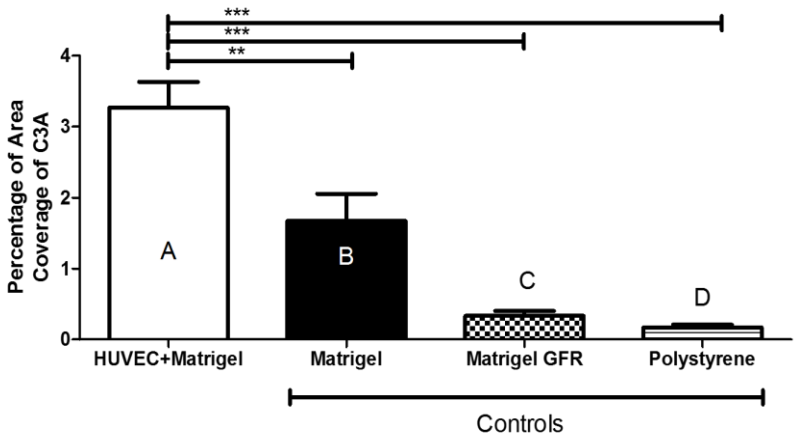

B

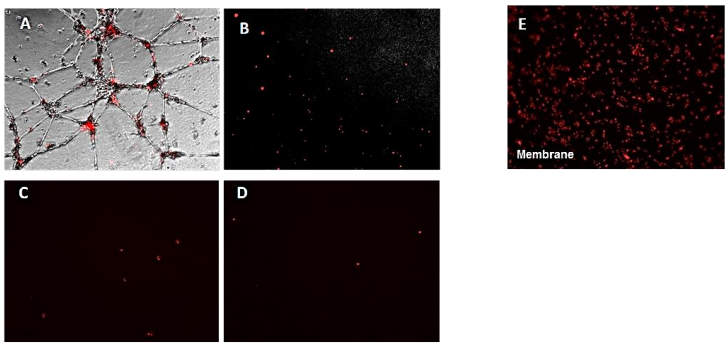

Figure 5-10 Percentage of area coverage by C3As (red dye) trans endothelial cell migration after 24hr.

*HUVECs were seeded in tissue culture wells pre-coated with Matrigel™. Uncoated wells (polystyrene) or wells pre-coated with Matrigel™, or growth factor reduced Matrigel™. C3As were labelled with DiI (red-fluorescent dye, Vybrant™ Cell-Labelling Solution (Molecular Probes) as described in Section 5.2.1 and placed in transwell inserts [8-µm pore size. After 24hr, bottoms of the well were photographed for graphical quantification of HUVECs on Matrigel™, Matrigel™, Matrigel™ GFR and polystyrene (A). Photographic images showing panel B: (A) C3As transmigration to HUVECs vascular network on Matrigel™, (B), C3As transmigration to Matrigel™ in the absence of HUVECs, (C) C3As transmigration to Matrigel™ GFR in the absence of HUVECs, (D) C3As transmigration to polystyrene in the absence of HUVECs and (E) an example transwell membrane showing retained C3A cells. Values are expressed as means ± SEM, **p<0.001 ***p<0.001. Images were takin using a confocal microscope and Nikon Digital camera DXM1200 and were merged using image J 1.46r. Magnification x10. (n=3).*

5.4.9 Endothelial capacity of repair in wound healing

HUVECs and C3As mono- and co-cultures were subjected to scratch injury on to assess wound healing capacity by measuring the percentage of cell migration across the scratch after 24hr. The effect of APAP on cell migration was also measured by scratch assay to evaluate the ability of HUVECs and C3As to metabolise drugs during injury. Data presented in Figure 5.11 shows that HUVECs migrated and achieved complete wound closure after 24hr, migrating to fill the damaged area and C3As did not appear to migrate (Figures 5.11). When HUVECs were cultured and scratched in the presence of 10mM APAP, their normal cobblestone morphology was altered and no cell migration was observed either in HUVECs or C3As (Figures 5.12 & 5-13).

In standard HUVEC:C3A co-cultures, HUVECs were able to migrate and achieve a significant level of wound closure after 24hr as expected (Figure 5-11), albeit apparently being impeded by having to move around non-migratory C3As. This migration is indicated by a white arrow in Figure 5-11. In HUVEC:C3A co-cultures, APAP did not affect morphology of either cell type, but the extent of endothelial healing was reduced in 10 mM-APAP as compared to untreated controls (35.42 ± 7.51 % vs 70.31 ± 4.69 % ($P = 0.007$), an approximate 50% reduction in cell migration (Figure 5.13). Since APAP-treated HUVEC mono-cultures showed no cell migration and wound healing, the C3As in co-cultures must have acted in some way to support HUVEC migration in a toxic environment.

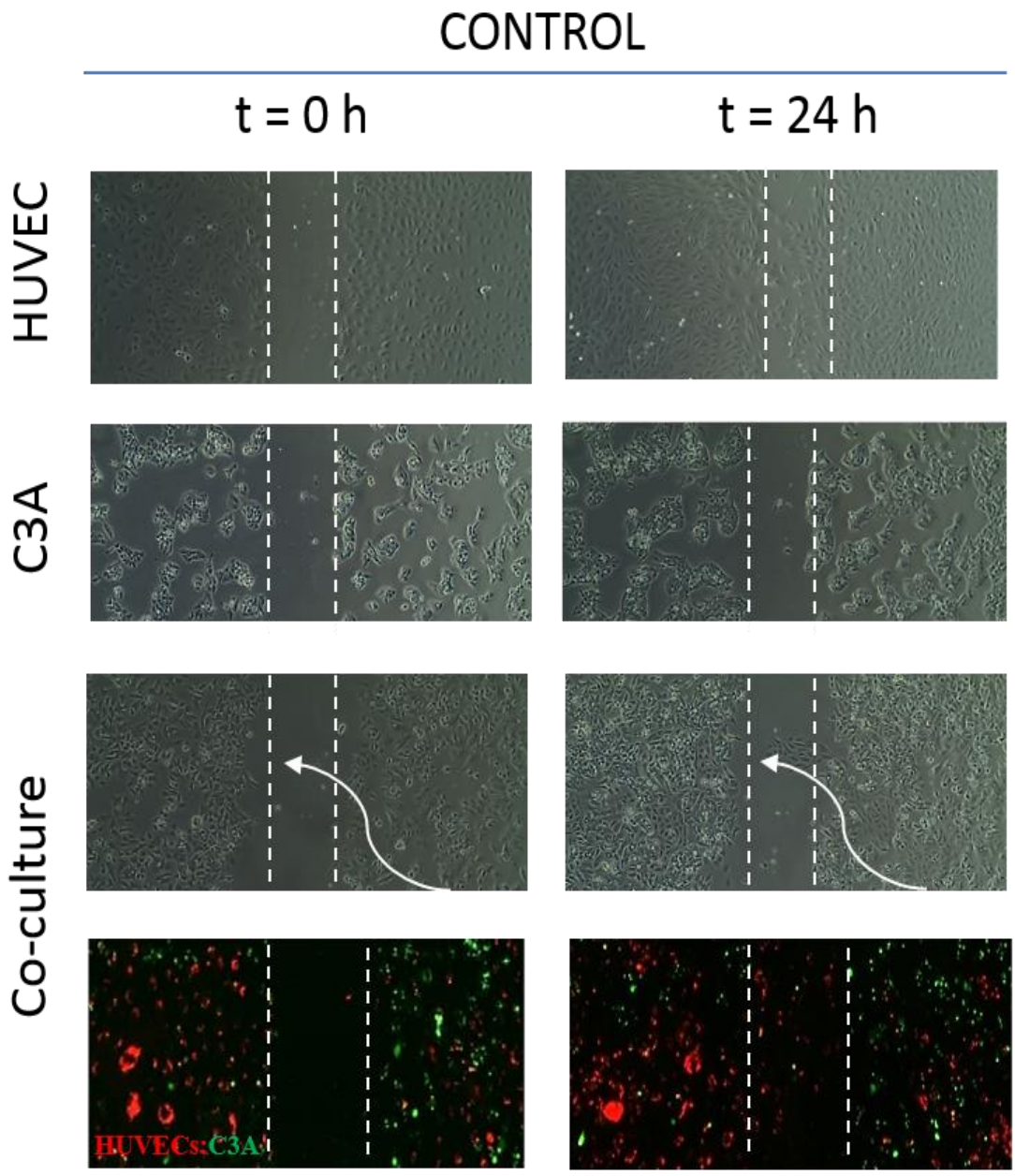

Figure 5-11 HUVECs and C3As in wound healing assay

HUVECs and C3As mono and co-cultured were wounded using a pipette tip under an angle of approximately of 30 degrees and washed with PBS. Then, cells were incubated with EGM-2 (control) for 24hr to evaluate HUVECs migration and wound healing. To identify HUVECs and C3As in co-cultures, HUVECs and C3As were stained respectively using DiI (bright red) and DiO (bright green) (Vybrant™ Cell-Labelling Solutions), as described in Section 5.2.1. Phase contrast images of HUVECs, C3As and co-cultures and labelled red-HUVEC and green-C3A of co-cultures at time 0hr and 24hr after scratching. Images were taken at 10x magnification Images were merged using imageJ 1.46r.

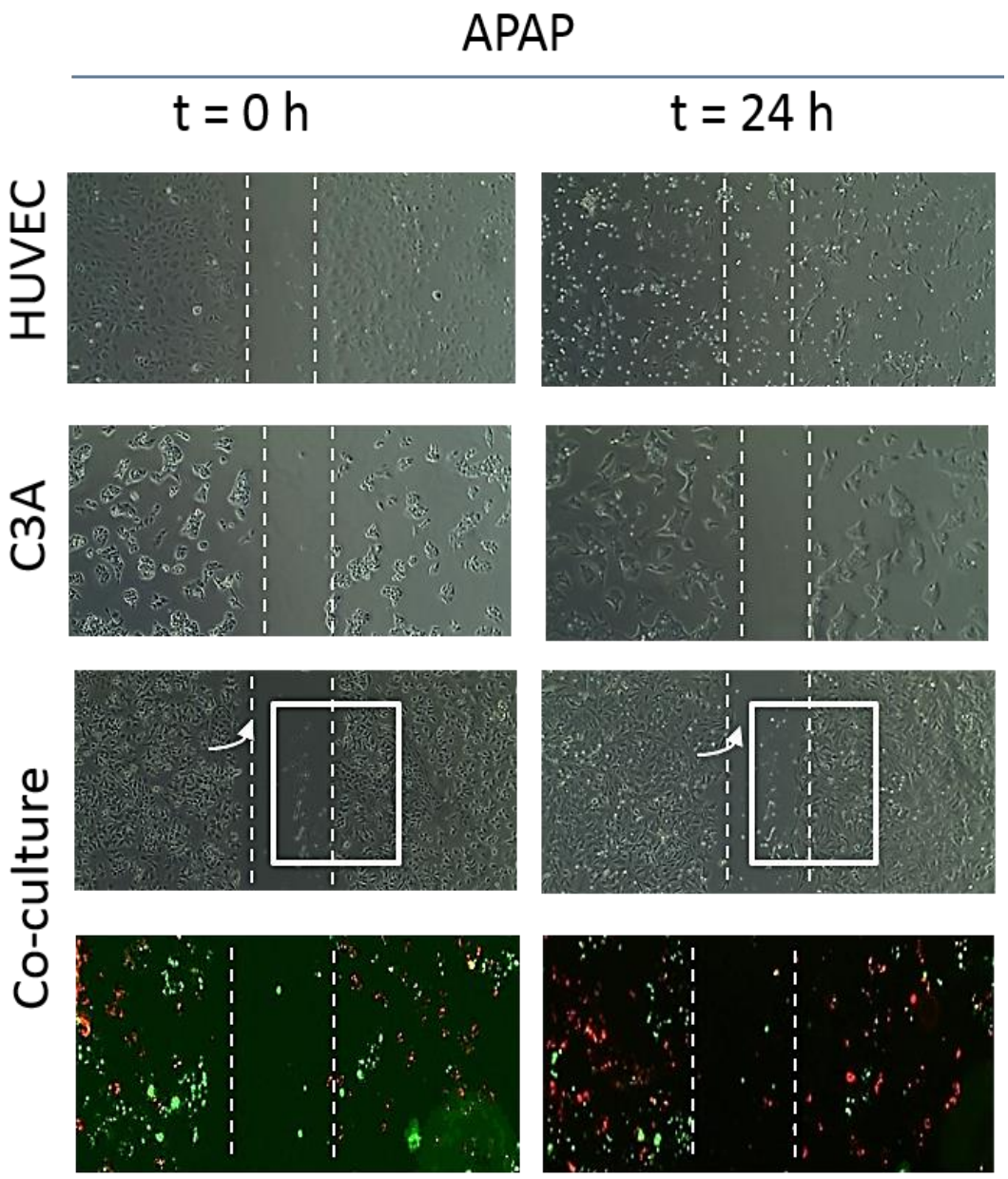

Figure 5-12 HUVECs and C3As in wound healing in the presence of APAP

HUVECs and C3As mono- and co-cultured were wounded using a pipette tip under an angle of approximately of 30 degrees and washed with PBS. Then, cells were incubated with 10 mM APAP for 24hr to evaluate HUVECs migration and wound healing in the presence of APAP. To identify HUVECs and C3As in co-cultures, HUVECs and C3As were stained respectively using DiI (bright red) and DiO (bright green) (Vybrant™ Cell-Labelling Solutions), as described in Section 5.2.1. Phase contrast images of HUVECs, C3As and co-cultures and labelled red-HUVEC and green-C3A of co-cultures at time 0hr and 24hr after scratching. Images were taken at 10x magnification Images were merged using imageJ 1.46r.

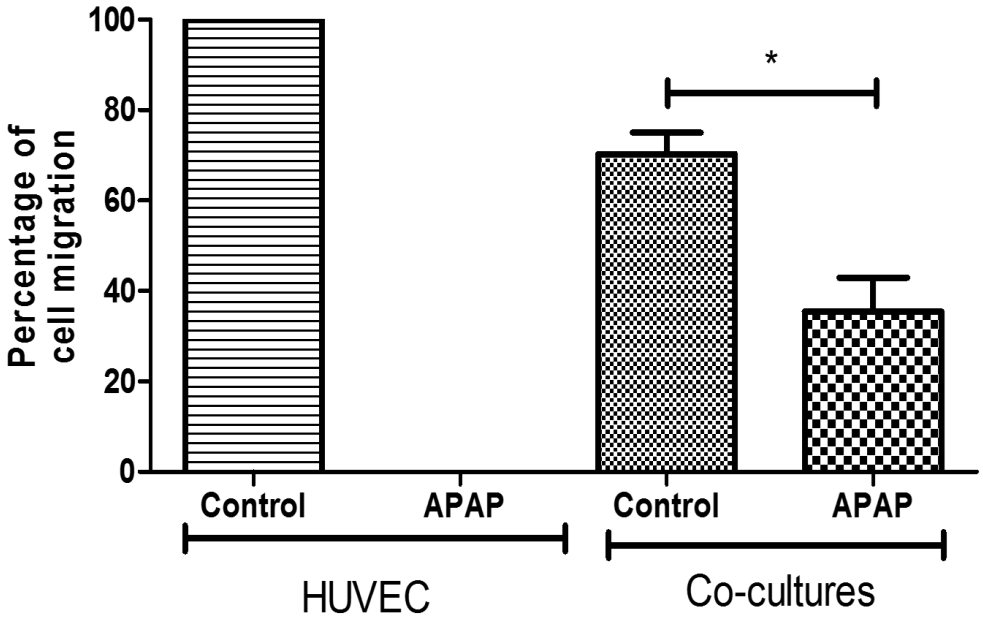

Figure 5-13 Percentage of HUVECs migration in wound healing assay

Percentage of HUVECs migration into the scratch wound after 24hr observed in untreated and APAP-treated HUVEC mono-cultures and HUVEC:C3A co-cultures. Data is expressed as the mean ± SEM of three different experiments. C3A vs Co-cultures, $p < 0.05$/ ** $p < 0.01$, (n=3).*

5.4.10 Regulation of CD49f and CD44 receptor expression in HUVECs and C3As by APAP-treatment

Endothelial and hepatic cells phenotype was analysed following APAP treatment using flow cytometry by comparing MFI data obtained from flow cytometry histograms between untreated and APAP treated cells. This revealed that APAP up-regulated the expression of receptors related to hyaluronic acid CD44 but had no effect on the laminin receptor CD49f expression (Figure 5.14).

CD49f receptor was expressed in HUVEC mono-cultures and in C3As controls and there was no significant difference between them, 164.70 ± 78.62 vs 90.26 ± 47.10 RU. After APAP exposure, CD49f receptor expression in HUVEC mono-cultures was slightly down-regulated (143.30 ± 64.76) while C3As showed increased expression at 111.50 ± 55.35 RU. In co-cultures, CD49f expression was maintain in HUVECs when they were exposed to APAP, from 157.20 ± 71.00 RU in untreated controls compared to 129.50 ± 63.78 RU in APAP-treated HUVECs, and CD49f was also maintained in C3As from 120.90 ± 62.38 RU in untreated controls compared to 154.30 ± 78.42 RU in APAP-treated C3As.

Similarly, in control (untreated) cells, the CD44 receptor was expressed in HUVEC mono-cultures with an MFI values of 389.30 ± 115.50 RU which was higher when HUVECs were exposed to APAP, rising to 957.10 ± 283.90 RU. CD44 was expressed at only low levels in untreated C3A mono-cultures at 28.83 ± 13.75 RU and was essentially unchanged in APAP-treated C3As, 39.23 ± 17.65 RU.

Comparison of CD44 expression in cell sorted populations of $CD31^+$ HUVECs and $EpCAM^+$ C3As, showed that there was no change in CD44 expression between mono- and co-cultures. CD44 MFI values in APAP treated HUVECs when in co-cultured did not showed any difference as compared to untreated HUVECs (respectively 466.60 ± 182.70 RU vs 297.30 ±

42.50 RU). Meanwhile, CD44 expression in C3As showed little change in co-cultures with APAP-treated values from 32.82 ± 34.37 RU in untreated controls to 44.52 ± 42.75 RU APAP-treated C3As.

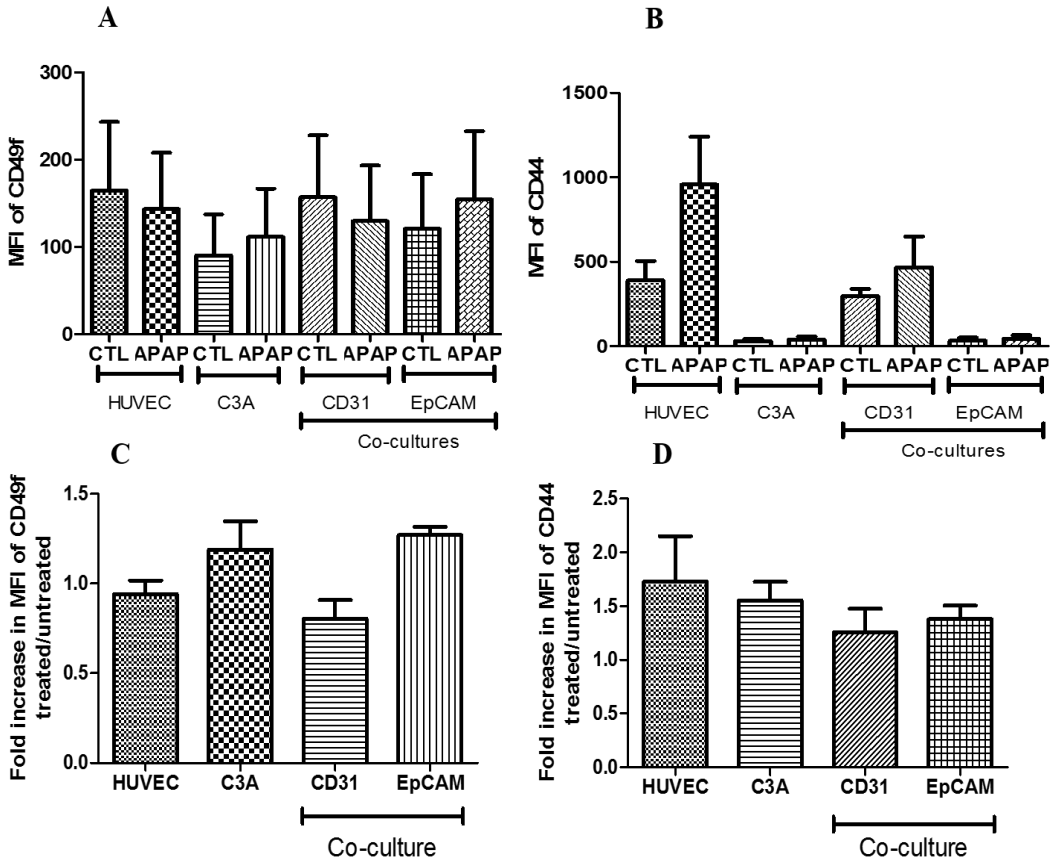

Figure 5-14 MFI of CD44 and CD49f expression in HUVECs and C3As following APAP treatment

HUVECs and C3As in mono and co-cultures were stained with CD49f or CD44 for flow cytometry analysis (See Section 2.2.6) after 24hr incubation with 10 mM APAP for treated cells (APAP) and EGM-2 for untreated controls (CTL). Flow cytometry analysis of the mean fluorescence intensity values (MFI) for (A) CD49f B) CD44 and fold increase in MFI of (C) CD49f and (D CD44 expression. Data is expressed as Mean ± SEM of three different experiments in triplicate (n=3). Fold increase was obtained from controls and APAP treated cells.

5.5 Conclusions

This evidence presented in this study demonstrates that HUVECs and C3As in co-cultures can together promote self-organization when plated on an appropriate ECM. This suggests that development of an *in vitro* vascularised hepatic model can be modulated *in vitro* by optimising conditions promoting self-organization and cell migration using ECM.

The success in developing an *in vitro* vascularised human hepatic model led to the following conclusions:

i. Matrigel™ was more biocompatible extracellular matrix (ECM) than MaxGel™ for promoting endothelial vascular network formation *in vitro*. Also, Matrigel™ ECM as a system on which to culture HUVECs and C3As, induced self-assembly of an interconnecting vascular network.

ii. HUVEC:C3A compared to C3As cultured alone maintained albumin synthesis on day 3 of culture in Matrigel™. However, albumin synthesis was not necessarily higher than when HUVEC:C3A co-cultures were cultured on polystyrene.

iii. Visualising cell mobility by microscopy, Matrigel™ revealed that HUVECs and C3As migrate and self-assemble into to an interconnected vascular network from time 10hr, demonstrating the importance of cell migration for vascular network formation.

iv. HUVECs function as assessed by endothelial vascular network formation, was inhibited by APAP toxicity when HUVECs were cultured alone but this effect was reduced in HUVEC:C3A co-cultures, which showed higher viability and resistance to APAP toxicity.

v. HUVECs in co-cultures maintained wound healing properties in EGM-2 and in APAP toxicity only in the presence of C3As in co-cultures. Wound healing in

HUVEC mono-cultures was inhibited by APAP but was partly restored in co-cultures in the presence of C3A cells.

vi. CD44 expression was up-regulated both in HUVEC and C3As mono- and co-cultures in response to APAP treatment.

Table 5-2 Tabular summary when comparing co-cultures of HUVECS and C3A cells with the corresponding mono-cultures in each condition

	Polystyrene	Matrigel
Phenotype	$CD31^{+}$Cobblestone and $EpCAM^{+}$Epithelial were maintained in co-cultures	Self-assembling of an interconnected vascular network in co-cultures
Albumin synthesis	Improved in co-cultures	Maintained in co-cultures
CYP3A4	Improved in co-cultures	Maintained in co-cultures
Migration	Observed effect in co-culture	Observed effect in co-cultures
APAP toxicity	More resistant in co-cultures	More resistant in co-cultures

5.6 Discussion

Pre-clinical studies using *in vitro* hepatic models for drug discovery would be improved by development of *in vitro* human hepatic models with physiological characteristics more comparable to those seen *in vivo*. Since *in vivo* hepatic physiology is not determined exclusively by hepatocytes, *in vitro* hepatocyte mono-culture models may not be fully representative of the *in vivo* situation and the development of heterotypic models that reproduce *in vivo* cell interactions would be a step towards this goal. The liver comprises about 15% vascular tissue through which materials are transported to the liver parenchyma for drug detoxification (Hammad et al., 2014). The development of vascular structures *in vitro* requires interaction between ECM and endothelial cells for their differentiation into vascular structures (Rohringer et al., 2014). The lack of heterotypic interactions between hepatocytes and endothelial cells in mono-cultures *in vitro* may limit structural and functional stability used to investigate drug metabolism (Nahmias et al., 2006).

The use of Matrigel™ in liver tissue engineering has demonstrated improvements in rat hepatic morphology, function (Germano et al., 2014) and also in drug metabolism activity in hepatocytes derived from mice (Toyoda et al., 2012).

The maturation of vascular network is induced when endothelial cells are co-cultured on Matrigel™ together with adipose stem cells (Rohringer et al., 2014), while culture on Matrigel™ can also prompt differentiation of human induced pluripotent stem cell into hepatocytes (Takebe et al., 2013), and endothelial cells to form endothelial vascular structures in combination with rat hepatocytes both *in vitro* and *in vivo* (Soto-Gutierrez et al., 2010, Nahmias et al., 2006).

It is clear from these reports that Matrigel™ has a significant capacity to promote endothelial properties but because of its undefined nature, the active components remain unknown.

Unfortunately, of the many new, synthetic ECM (e.g. puramatrix, hyaluronic acid, fibronectin or MaxGel) designed to provide defined animal- or blood-free replacement for Matrigel™, none have achieved the same formation of mature vessels by endothelial cells (Allen et al., 2011, Zeisberg et al., 2006). Matrigel™ has therefore become a standard component in advanced methods such as differentiation of stem cells into hepatocytes (Sullivan et al., 2010).

The aim of this Chapter was to define conditions to promote angiogenesis and cell migration to create an *in vitro* human vascularised co-culture model in which to evaluate drug toxicity. Exploration of the hypothesis that the use of an extracellular matrix would promote vascular network as measured by endothelial vascular tube formation in a HUVEC:C3A co-cultures resulted in a system in which Matrigel™ promoted the development of an interconnected vascular network between HUVECs and C3As in co-cultures.

In contrast to the results observed with Matrigel™, no angiogenesis was observed using MaxGel™ as ECM (Figure 5-3). Furthermore, the addition of VEGF did not enhance endothelial tube formation by HUVECs cultured on MaxGel, suggesting that vascular network formation *in vitro* is promoted by unknown components in Matrigel™ which are absent in MaxGel™.

It has been clear for some time that HUVECs can form vascular tubes following 2-24hr culture on Matrigel™ (Kubota et al., 1988). However, in addition to forming an interconnected vascular network on Matrigel™, in the present study HUVECs were shown to induce the migration of C3As into the vascular network in HUVEC:C3A co-cultures (Figure 5-3). Under these circumstances, C3As maintained hepatic activity, including albumin synthesis and CYP3A4 activity (Figure 5-4). In addition, CYP3A4 activity in C3As mono-cultures and in HUVEC:C3A co-cultures on Matrigel™ was significantly induced after APAP exposure, suggesting that Matrigel™ contains components that maintain

CYP450 activity and might therefore lead to an improved metabolism of APAP in C3As. In this context, primary human hepatocytes have been also reported to maintain CYP450 activity when grown on Matrigel™ (Skovseth et al., 2007, Kleinman and Martin, 2005, Silva et al., 1998). When these results are compared to those seen in Chapters 2, 3, 4, it can be seen that Matrigel™ did not provide higher hepatic activity but maintained the hepatic phenotype allowing the investigation of endothelial tube formation and C3As migration toward the vascular network. Time-lapse microscopy and the use of different fluorescent dyes with HUVECs (DiI bright red dye) and C3As (DiO bright green dye) showed the endothelial capacity to build an interconnected vascular network vascular structure and the close association of C3As with the vascular network in co-cultures, simulating sinusoid-like structures (Figure 5-6). This vascular network appeared to be viable for up to one week in the presence of C3As (Figure 5-8). Finally, staining with F-actin showed major foci of actin polymerization at hepatic and endothelial cell junctions in HUVEC:C3A co-cultures reminiscent of bile canaliculi and the apical side of polarized epithelial cells (Figure 5-9). Transwell cell migration assays were therefore used to further investigate cell-cell interactions between HUVEC and C3A in co-cultures. In this system, the migration of C3As into wells coated with growth factor reduced Matrigel™ or uncoated polystyrene was minimal, while some migration was observed using Matrigel™. However, the presence of HUVECs in cell culture wells provided the strongest attraction to C3As migration (Figure 5-10). This data provides preliminary evidence that cell migration between HUVECs and C3As, in a static environment, can be stimulated by a combination of direct contact and the effect of cross-talk.

The endothelial capacity to build a vascular system might be inhibited by the exposure to APAP, which affected HUVECs endothelial tube formation in mono-cultures in the absence of C3As (Figure 5-7A). This suggest that APAP can also affect the vascular formation without the formation of NAPQI, the metabolic product of CYP450 activity on APAP in

hepatocytes. However, inhibition of vascular network formation was not observed in HUVECs when in cultured with C3As in co-cultures (Figure 5-7C).

Further confirmation of these findings was achieved using another non-invasive migration assay, the wound healing assay. The wound healing assay, confirmed the maintenance of HUVECs viability and migration activity in the presence of APAP when in co-culture with C3As (Figure 5-12).

This data were consistent with the evidence presented in Chapter 3 (Section 3-3) and Chapter 4 (Section 4-3) where HUVECs mono-cultures lose their characteristic cobblestone morphology in response to APAP exposure, while HUVECs survive APAP treatment in the presence of C3As. The comparison of both studies suggests that APAP resistance in co-culture was not directly due to the use of an ECM, Matrigel™, but rather was promoted primarily by the combination of HUVECs and C3As in co-cultures.

Rodent hepatocytes migrate towards HUVECs plated on Matrigel™ (Nahmias et al., 2006, Soto-Gutierrez et al., 2010). However, to our knowledge, the establishment of a stable interconnected vascular network in HUVEC:C3A co-cultures (Figure 5-8) which shows resistance to hepatotoxicity has not been reported before. Interestingly, evidence of improved hepatocyte function has also been presented when hepatocytes are combined with fibroblasts (Cole et al., 2014).

Laminin is present surrounding blood vessels (Rauterberg et al., 1981, Stamati et al., 2014) and changes in laminin concentration and reduction in expression of integrin α6β1 in hepatocytes. Integrin α6β1 is a key regulator of cell surface receptor expression on hepatocytes and has been shown to be associated with fibrosis (Newsome et al., 2004), also to induce endothelial cells to form vascular structures *in vitro* (Kubota et al., 1988), cell migration, invasion and cell polarity in tissue organisation (Li et al., 2003, Ahmed et al., 2005)

When HUVECs and C3As were analysed for CD49f expression (integrin subunit α6 and ligand laminin), there was no significant regulation either in HUVEC mono-cultures or in C3As after APAP exposure (Figure 5-14). CD49f regulates cell survival, migration and apoptosis through the 3-kinase (PI3K)/AKT signalling pathway (Yu et al., 2012), resulting in significant roles in determining cell stability.

Expression of the CD44 receptor which binds hyaluronic acid, has also been reported on hepatocytes (Harrill et al., 2009, Kao et al., 2009). In previous published studies, CD44 receptor expression was affected by APAP treatment, probably due its role in TGF-β activation in hepatocytes (Harrill et al., 2009, Kao et al., 2009). In endothelial cells, CD44 has also been associated to caspase activation (Tsuneki and Madri, 2014).

In this study, the evaluation of CD44 expression showed that APAP toxicity did not affect CD44 expression in hepatocytes but it was up-regulated in APAP treated HUVECs (Figure 5-14), suggesting the activation of apoptosis mechanism.

In conclusion, recapitulation of the complex vascularization of the hepatic tissue *in vitro* requires understanding of the roles of cell migration and laminin receptors. In this context, HUVEC:C3A co cultured on Matrigel™ extracellular matrix components revealed events not seen in conventional polystyrene mono-cultures. The fact that the development of an *in vitro* human co-culture model has demonstrated migration activity between cells and the formation of vascular network, provides a rationale for why the co-culture of different cells lines may provide insights into establishing vascularised hepatic *in vitro* cell culture models for drug metabolism studies.

6 Chapter 6: General discussion

The liver is a soft organ, comprised of hepatocytes (70-80%), LSECs (20%), Kupffer cells and hepatic stellate cells (10%) (Godoy et al., 2013) and is the principal organ involved in drug detoxification. As explored in detail in the thesis introduction (Section 1.7), during the multiple phases of drug discovery (Figure 7-1), drug candidates are tested through successive stages of high throughput screening (HTS) using *in vitro* and *in vivo* animal hepatic models, before *in vivo* testing in human trials to demonstrate their therapeutic effect and efficacy, and safety for use in humans (Cecchelli et al., 2007, Kraljevic et al., 2004). However, even after significant spending on the clinical trial phases of drug discovery, drug-induced liver injury (DILI) is still a major issue as pre-clinical *in vitro* animal and human cell culture models remain poor in accurately predicting toxicity. Indeed, a high percentage of drugs that successfully pass *in vitro* and *in vivo* drug trials subsequently do not meet safety criteria and fail human clinical trials (Arrowsmith and Miller, 2013, Kola and Landis, 2004), thus proving a costly failure for the drug product. Furthermore, other drugs, having passed all clinical trial stages and having successfully gained regulatory drug approval for commercialization, subsequently have to be withdrawn from the market or require a warning to be displayed due to unforeseen rare adverse reactions (Kaplowitz, 2005, Gomez-Lechon et al., 2014).

Pharmaceutical companies are aware of the economic and safety benefits which would result from developing improved *in vitro* hepatic models and assays which could better mimic DILI *in vitro*, especially for high throughput screening (Kostadinova et al., 2013). The development of more physiological in *vitro* human hepatic model using human-derived cell lines would allow early detection of ineffective drugs, prediction of drug toxicity at low and high doses and would also reduce animal drug testing. Furthermore, the development of a

suitable *in vitro* hepatic model may provide greater insight into cellular mechanisms (e.g. crosstalk) involved in human hepatotoxicity (Tourovskaia et al., 2014, McGill et al., 2011).

In vitro human hepatic models, using only primary human hepatocytes or immortalised hepatocytes limit the interpretation of *in vivo* drug metabolism pathways and *in vivo* liver functions (Gomez-Lechon et al., 2010, Ramaiahgari et al., 2014).They also often fail to reproduce drug metabolism pathways seen *in vivo* due to the absence of homotypic and heterotypic cell-cell/cell-ECM interactions, occurring in human metabolism (Bhatia et al., 1999, Palakkan et al., 2013).

In the embryo and in adulthood, hepatic cellular communication and regulation is mediated by paracrine signalling. Signalling between hepatocytes and non-parenchymal cells enhances liver regeneration, restores the vascular system after hepatectomy (Stolz et al., 2007, Wang et al., 2012b) and improves hepatic function and vascular structures (Hwa et al., 2007, Nahmias et al., 2006).

In the liver, the hepatic sinusoid transports nutrients and oxygen and its porosity and permeability allow the filtration of drugs to the hepatocytes in the space of Disse (DeLeve, 2013) where specialised fenestrated, endocytic endothelial cells LSECs and hepatocytes are in contact. This in fact, suggests the possibility that LSECs could be the first target in drug toxicity (Ito et al., 2003) and also that the development of an *in vitro* hepatic model system based on culturing hepatocytes alone may be not relevant to correlate the data to *in vivo* responses.

LSECs mainly participate in clearance of waste molecules and their capacity for endocytosis differentiates them from other endothelial cells in the body (Elvevold et al., 2008) though characterization and optimization of phenotype *in vitro* is on-going (DeLeve et al., 2004, Salerno et al., 2011).

Thus it is reasonable to consider that *in vitro* hepatic models combining different cell types are necessary to represent cell-cell interaction in drug metabolism and achieve physiologically significant responses. Vascularisation and cell migration are important in the fabrication of organotypic structures to mimic aspects of the complex structure of the liver and overcome tissue engineering challenges.

Ideally this would include interaction of hepatocytes with non-parenchymal cells, which when affected by the drug toxicity would stimulate endothelial cells to release VEGF to boost early hepatic recovery and regeneration (Kato et al., 2011, Ito et al., 2003, Godoy et al., 2013).

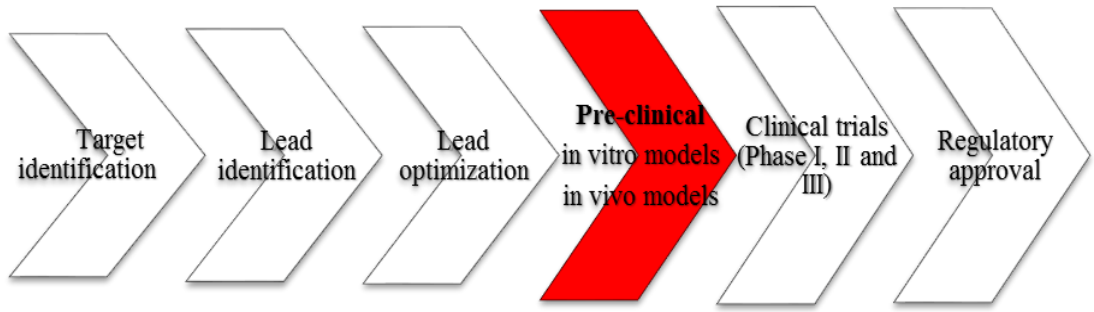

Figure 6-1 Phases of drug discovery

The early phase of drug discovery, High Throughput Screening (HTS) is used to identify and optimize compounds to be tested using in vitro and in vivo models. When new compounds pass toxicity assays and demonstrates their therapeutic effect, then the compound is tested in human clinical trials following the regulatory approval (Cecchelli et al., 2007, Kraljevic et al., 2004).

6.1 Thesis aims findings and outcomes

The main aim in this project was to explore the possibility that *in vitro* human hepatic models could be improved for drug testing, efficacy and safety by culturing hepatocytes and endothelial cells together. In this thesis, an improved *in vitro* human hepatic model using endothelial cells (HUVECs) and hepatocytes (C3As) was demonstrated to show better hepatic and endothelial function in drug metabolism. During the transitional development of a more physiological human hepatic organotypic model, four crucial aims were explored to verify the hypothesis:

1. Selection of human hepatocyte and endothelial cell lines to develop a biocompatible, functional *in vitro* human co-culture model with a stable specific-tissue phenotype. The *in vitro* human hepatic model developed using HUVECs and C3As at ratio 1:1 (HUVEC:C3A) cultured for 3 days in EGM-2 (endothelial media) resulted in a human hepatic model with higher hepatic function than using C3As alone. Crucially, both endothelial (CD31) and hepatic (EpCAM) cell phenotype were maintained on day 3.
2. The use of a model hepatotoxic dose-dependent drug (APAP) for the investigation of the principal cellular mechanisms involved in hepatotoxicity (e.g. ATP depletion and mitochondria dysfunction) using C3As in mono-culture and co-cultures with HUVECs. This revealed that endothelial co-culture conferred a significant hepatic mitochondrial protection and survival to APAP hepatotoxicity.
3. The investigation of the role of oxidative stress in the cellular mechanisms underpinning APAP drug toxicity on early events in the *in vitro* human co-culture model compared to mono-cultures, demonstrated that APAP can promote the regulation of vascular endothelial growth factor receptors.

4. Examination of the properties of endothelial cells in mono- and co-culture using cell migration assays showed that co-culture of HUVECs and C3As in Matrigel™ resulted in a long-term interconnected vascular network and enhanced survival in response to hepatotoxic challenge.

6.2 Discussion

The development of an improved *in vitro* human co-culture model for pre-clinical studies using HUVECs and C3As, provides a more physiological approach in investigating the role of the importance of endothelial-hepatic interactions in drug metabolism in order to improve the efficacy and safety of new drugs.

In this study, the combination of both cells lines required investigation initially into the selection of appropriate cell culture media. Endothelial cells are sensitive to changes in the media and they require growth factors to maintain phenotype *in vitro* (Bala et al., 2011), whereas C3As are a robust cell line. The comparison between hepatic (MEME) and endothelial media (EGM-2) revealed that the use of endothelial media allowed the co-culture of both cell lines together without losing the endothelial and hepatic phenotype (Figure 2.4). The assessment of interaction between endothelial and hepatic cells, using cell lines with different growth rates in long-term cultures, can result in varied and often challenging information. However, flow cytometry analysis after short term co-culture using specific antibodies allowed the identification of each cell line independently and the investigation of their endothelial phenotype ($CD31^{+}$) and hepatic phenotype ($EpCAM^{+}$) (Figure 2-6).

The characterization of different ratios, 3:1 (HUVEC:C3A), 1:1 (HUVEC:C3A) and 1:3 (HUVEC:C3A), revealed that using HUVECs and C3As, which have different growth rates, did not necessarily provide higher hepatic activity at the more physiological ratio of 1:3 (HUVEC:C3A) seen in the liver. The evaluation of these ratios showed that seeding at ratio 1:1 (HUVEC:C3A) overcame the difficulties caused by the difference in growth rate, achieving an *in vitro* controllable hepatic model, with improved hepatic function such as albumin synthesis and CYP3A4 activity as compared to C3A mono-cultures (Figure 2-10 &

Figure 2-12). Other *in vitro* hepatic co-culture models using endothelial:hepatocytes seeded at similar ratios (60%:40%) also showed improvement in hepatic function in short-term culture (Kim et al., 2012, Kostadinova et al., 2013).

The activity of the main drug metabolism enzymes in C3As such as CYP3A4 activity were improved in basal drug metabolism conditions in the presence of HUVECs when cultured on polystyrene (Figure 2-12). The selection of technique for measuring CYP450 activity and gene expression was controversial. I agreed with the view of Jaeschke *et al*, in his description that the best way to evaluate CYP450 activity is using P450 enzyme activity assays because it should reflect the metabolic activity of live cells under any given circumstance (Jaeschke et al., 2013). High-throughput, RT-PCR analysis of CYP450 gene expression offers the alternative of monitoring gene-expression changes to toxic drug challenge, but reports on upstream events that may not directly represent the metabolic status of the cell at that point, especially if the drug under examination directly inhibits CYP450 enzyme activity. Furthermore, CYP450 activity can be induced artificially using a cocktail of inducers (e.g. rifampicin for induction of CYP3A4 activity) but these compounds are not usually used for hepatotoxicity studies (Jaeschke et al., 2013). Here, endothelial cells improved CYP3A4 activity in C3As without the use of any inducer.

APAP is a well-characterised dose-dependent model hepatotoxic drug. In this study, APAP was used at both low and high does to determine which dose caused hepatotoxicity *in vitro*. Prediction of APAP toxicity *in vitro* required assessment of the main cellular properties known to be affected in APAP toxicity, namely cell viability, mitochondrial function and oxidative stress. Assessment of these criteria revealed that APAP toxicity can be achieved in mono-cultures at low doses (<10 mM) of APAP after 24hr of culture, showing reduced ATP content and causing damage in the mitochondria function, whereas higher doses (>20 mM) were required to achieve toxicity in HUVEC:C3A co-cultures with more complete detoxification of APAP under these circumstances.

At 5 mM APAP dose, APAP was observed only to affect the viability of HUVECs, whereas no effects were observed on C3A mono-cultures or HUVEC:C3A co-cultures. However, 10 mM APAP resulted in hepatic mitochondria dysfunction and reduction in ATP content in C3A mono-cultures, whereas a greater resistance was observed in HUVEC:C3A co-cultures (Figure 3-1 & Figure 3-2).

The exposure of HUVECs to >10 mM APAP for 24hr in the absence of C3As resulted in toxicity, affecting ATP production (Figure 3-1), and cell viability (Figure 3-3), suggesting that there is an alternative pathways (e.g. oxidative stress) in APAP toxicity as endothelial cells were affected without any toxic metabolism (formation of NAPQI) or detoxification of APAP by hepatocytes (DeLeve et al., 1997). HUVECs in combination with C3As, showed a different response to 10 mM APAP toxicity compared to when HUVECs were mono-cultured on their own, resulting in maintenance of mitochondria, ATP levels and cell viability (Figure 3-1 to 3-3). That observation suggests that there is protective effect and/or more complete APAP detoxification resulting from cross-talk between two different cells lines cultured together. Interestingly, this resistance to APAP toxicity is the opposite to that seen when rat hepatocytes and HUVECs were co-cultured in Matrigel™ (Toyoda et al., 2012).

Mitochondrial dysfunction is one of the main effects seen in APAP toxicity and it can result in alterations in lactate levels (Shah et al., 2011). Lactate is one of the parameters that healthcare professionals consider before liver transplantation in APAP overdose to evaluate the degree of liver damage and the necessity for transplant (Shah et al., 2011). In this study, APAP caused high levels of lactate in HUVECs in mono-cultures but did not affect lactate levels in co-cultures, where there was also an absence of response to NAC, suggesting that oxidant levels were unaffected (Figure 3.5). This suggests that in co-cultures, there might be a raised threshold of protection against lactate production in response to APAP at the doses

tested, as a result of cell-cell interactions, thus preserving HUVECs and also avoiding a reduction in cellular antioxidant levels (Reliene et al., 2004).

In APAP toxicity, the APAP metabolite NAPQI reacts with proteins to form APAP-protein adducts which cause oxidative stress in the mitochondria. Reduction in NO is a signal of endothelial dysfunction and its combination with superoxide formation can form peroxynitrite (Zhang et al., 2014, Agarwal et al., 2012).

In this study, mitochondria in both HUVECs and C3As were affected by APAP toxicity; however oxidative stress was not associated with mitochondrial dysfunction in HUVEC mono-cultures which did not form superoxide (Figure 4.3), and maintained NO and GSH levels, whereas C3A mono-cultures showed reduced NO levels and increased GSH after APAP exposure. By contrast, C3As in co-cultures did not show significant changes in NO and GSH levels (Figure 4-4 and Figure 4-5). This finding suggests that oxidative stress does not occur in HUVEC mono-cultures, possibly as there is no NAPQI formation in the absence of hepatocytes (DeLeve et al., 1997). APAP is associated with necrosis (Ito et al., 2003) and here APAP caused HUVEC death, without causing oxidative stress, although reducing ATP levels. This finding suggests that HUVECs may die via other mechanisms e.g. apoptosis due to unknown mechanisms in response to drug toxicity that is repressed in co-cultures.

The *in vitro* hepatic model described in this study improved drug metabolism activity using C3As co-cultured with HUVECs as compared to using C3As cultured alone. That finding suggested that the resistance to toxicity observed in co-cultures might be due to more complete APAP detoxification in C3As and for that reason, the co-culture system requires higher doses to mimic drug toxicity seen *in vivo*.

The optimisation of endothelial and hepatic co-culture protocols allowed the investigation of endothelial signalling and regulation of cellular mechanisms. Exposure of HUVECs to toxic challenge enabled the identification of the up-regulation of endothelial cellular receptors

such as VEGFR-2 in our co-culture system (Figure 4-6). VEGFR-2 has previously been reported to be up-regulated in drug hepatotoxicity and regeneration (Ito et al., 2003, Matsumoto et al., 2001, Ding et al., 2010).

Endothelial cell function is characterised by the capacity to migrate in response to scratch injury and promote angiogenesis as assessed by tube formation *in vitro*. The creation of a vascularized hepatic micro-environment in the *in vitro* co-cultured model albeit in 2D culture, maintained hepatic functionality and showed haptotactic interaction between HUVECs and C3As. Here, Matrigel™ induced CYP3A4 activity in C3As, while albumin synthesis was maintained (Figure 5-4). Tissue modelling of liver buds is very complex but the characterization of a vascular hepatic model shows that this requires appropriate hepatocyte and endothelial cell culture in an optimal extracellular matrix to simulate the human physiological environment (Takebe et al., 2013).

Use of time-lapse video and migration assay techniques, revealed evidence of migration between cells in co-cultures, as C3As migrated towards HUVECs cultured on Matrigel™ (Figure 5-6), resulting in a more numerous vascular network that was stable for at least one week (Figure 5-8).

These processes of micro-vascular formation and cell migration were apparently the result of the interaction of HUVECs and C3As both via paracrine signalling and direct contact between cells. The culture of HUVECs and C3As on Matrigel™ showed that using a more *in vitro*-liver like environment in the presence of growth factors and ECM elements such as laminin, can provide a technology which has the potential to develop an *in vitro* vascularised hepatic model. In particular, the use of ECM, as opposed to simple culture on plastic, revealed that endothelial cells are able to function and induce a vascular network connected with C3As.

The development of this *in vitro* co-culture model using hepatocytes with endothelial cells provides a clear justification for using endothelial cells in a hepatic co-culture models of hepatotoxicity studies.

It was also interesting to observe that in APAP-treated mono-cultures, HUVECs failed to make a network in Matrigel™, whereas in the presence of C3As, HUVECs formed and maintained the vascular network in the presence of 10 mM APAP (Figure 5-7). This suggests that C3As were able to detoxify APAP before it caused significant damage to HUVECs, which is reinforced by observed increase in C3A CYP3A4 activity.

The results of this study provide significant insights into the requirements for the creation of an *in vitro* human liver model which would be accurate and effective in mimicking drug metabolism and detoxification mechanisms in order to predict drug toxicity robustly. This would in turn greatly enhance the discovery of safer drugs. Crucially, it was discovered that APAP had a direct effect on HUVECs in mono-cultures, demonstrating that drugs can also have toxic effects on endothelial cells, and that improved *in vitro* hepatic models of hepatotoxicity should reproduce liver cell-cell interactions during drug metabolism. We determined that endothelial cells have an important role in response to injury caused by drug activation and liver failure. Furthermore, I suggest from the data presented in this thesis that the interaction of endothelial cells and hepatocytes could be a key factor in drug detoxification and in maintenance of hepatic function. The absence of endothelial cells in previous hepatic models results in difficulty with accurately simulating drug absorption, distribution, metabolism and detoxification and elimination as it occurs in the human liver.

This study has demonstrated a 2D *in vitro* hepatic culture system combining endothelial and hepatocytes in a more physiologically-relevant environment for hepatotoxicity studies,

which cover essential characteristics including preserving hepatic and endothelial functions, phenotype and improved responses to drug toxicity.

It is important to understand the role of cellular mechanisms involved in drug-induced liver injury such as hepatic and endothelial mitochondrial function and oxidative stress, as cell-cell communication is a crucial factor in permitting more efficient drug metabolism function and clearance to external agents.

The development of an *in vitro* hepatic model in a 3D environment could provide greater advantages in simulating human physiology than conventional 2D culture but this needs more consideration and research. As discussed previously, the characterization of a vascular hepatic model requires culture of functional hepatocytes and endothelial cells in an optimal extracellular matrix to simulate the human physiological environment (Takebe et al., 2013), with the advantage that in the 3D context, ECM could also be used to provide structure. 3D versus 2D culture systems need to be considered in relation to the proposed application. The 3D model would be advantageous for research purposes e.g. liver organogenesis for transplantation, whereas the 2D co-culture model, possibly incorporating ECM, would be more economic, reproducible and readily applicable in investigating the toxicity of compounds identified as drug candidates by HTS.

This study has demonstrated that 2D co-culture of a hepatocyte cell line with endothelial cells improves the function of hepatocytes even in the presence of a hepatotoxic compound. It also shows that hepatocytes have a protective effect on endothelial cells from toxic effects of drugs. The ideal approach to confirm these findings would be to demonstrate that improved drug modulation also occurs when using a combination of primary human hepatocytes and LSECs. The approach to improving prediction of drug toxicity described in this study also provides a platform that could be applied to HTS used in the pharmaceutical industry for drug discovery.

The use of co-cultures with hepatocytes and endothelial cells aimed to produce an accurate integrated model which could be used as a potential human hepatic model, for the purpose of predicting drug toxicity, reducing animal drug testing and improving the accuracy of identifying ineffective or hepatotoxic drugs (Bale et al., 2014b), before they reach human trial stages. The data presented in this study demonstrates the potential of 2D co-culture of hepatocyte cell lines with endothelial cells for improving drug testing, which could be incorporated into a HTS system, does not require extended periods of culture to generate results, and should be reproducible and relatively inexpensive.

6.3 Future work

Development of the hepatic/endothelial co-culture model presented in this study demonstrated that C3As co-cultured with HUVECs are more representative of functional hepatic metabolism than culture of C3As alone. Co-cultures showed the requirement for endothelial paracrine signalling in the development of a potentially more reproducible, functional and more stable *in vitro* human co-culture model.

This notion raises the question of whether this improvement in hepatic and endothelial function would also be seen using cells isolated from other lineages or differentiated from other sources. For example, embryonic and induced pluripotent stem cells have been shown to differentiate *in vitro* to hepatic and endothelial lineages and have been proposed as a reliable source of material for development of cell banks for use in cell-based therapies. Indeed, retinal tissue differentiated from human induced pluripotent stem cells (hiPSCs) derived originally from patient-specific skin cells is already being tested in early clinical trials and could pave the way for therapy of multiple tissue types in future (Reardon and Cyranoski, 2014). It is also possible that directed differentiation of induced pluripotent cells stem cells from individuals could be used to produce sustainable hepatocyte and endothelial cell lines as models for studies of drug toxicity and metabolism, liver infection, personalised medicine and cell therapeutics (Sullivan et al., 2010). However, problems still to be overcome include poor *in vitro* hepatic function and differentiation into the adult phenotype, while ES and hiPS-derived cell lines currently in use for drug testing are also limited by their derivation from a single individual which therefore does not take account of human polymorphism and its influence on patient-specific drug metabolism.

If it were possible to use human hiPSC -derived to hepatocytes (hiPSC-HE) co-cultured with endothelial cells, this would offer the possibility of selecting a defined panel of hiPSC lines for drug testing and the opportunity to investigate liver disease and treatment *in vitro*.

Generating multiple independent hiPSC-HE cell lines would offer the possibility of examining drug toxicity *in vitro* using a panel of individuals rather than a just a single individual as is the case today when using an established cell line. Therefore, using hiPSC-HE could reduce withdrawal rate, improve drug safety, reduce development of ineffective treatments and detect idiosyncratic side effects. However, achieving mature hepatocyte phenotype currently remains problematic, possibly due to a lack of paracrine signalling from non-parenchymal cells e.g. endothelial cells in hepatocytes differentiation (Matsumoto et al., 2001, Nahmias et al., 2006). The introduction of a proper vascularized microenvironment could improve hepatic function in hepatocyte cell lines currently used in drug testing and may overcome the limitations found in hiESC-HE, resulting in improved drug evaluation (Berger et al., 2014).

A short pilot study performed at the University of Oslo, during a short-stay sponsored by The Company of Biologists' journals – (Development, Journal of Cell Science, The Journal of Experimental Biology, and Disease Models & Mechanisms (DMM)), showed that human embryonic stem cell-derived hepatocytes could provide a physiologically relevant *in vitro* hepatic model. Considering the current requirement for expensive growth factors and the long differentiation protocol, this would currently be an unattractive option for application in pharmaceutical testing, but is likely to be amenable to further investigation and optimization.

The rationale for using scaffolds in the construction of a 3D environment for *in vitro* co-culture of hepatocytes with endothelial cells, is that it would allow for the formation of vascular structures, so that cell migration and cross-layer invasion, features of early steps of liver organogenesisis, could be reproduced and studied *in vitro*. 3D *in vitro* hepatic co-culture would also allow investigation of the role of hepatic membrane transport proteins (MTP) in the absorption of drugs, drug-drug interactions, and canalicular excretion of drugs into the biliary and sinusoidal system (Ulvestad et al., 2013, Aleksunes et al., 2008, Kunze et al., 2012, Shukla et al., 2014, Le Vee et al., 2013), especially using the HepaRG hepatocyte-

cholangiocyte bipotential cell line (Rebelo et al., 2014, Mueller et al., 2014). However, 3D *in vitro* hepatic co-culture, and employing approaches such as scaffolding and cell encapsulation, currently has disadvantages in cell viability, and the choice of hydrogel subtype supplemented with growth factors to mimic the stiffness and viability of the *in vivo* hepatic environment remains an ongoing challenge (Chan and Leong, 2008).

7 Reagents and materials

Table 7-1 Cell lines used in this study

Human cell lines	Growth Medium	Media Supplements	Cell Passage number	Supplier
C3As	Minimum Essential Medium Eagle (MEME)	10% fetal calf serum and antibiotics (100 IU/ml penicillin, 100mg/ml streptomycin)	4-20	American Type Culture Collection, Manassas, VA (CRL-10741). Sigma
HUVECs	EGM™-2 BulletKit™, EBM™-2 plus SingleQuots™ of Growth Supplements	· No BBE (Bovine Brain Extract) · hEGF · Hydrocortisone · GA-1000 (Gentamicin, Amphotericin-B) · FBS (Fetal Bovine Serum) 10 ml · VEGF · hFGF-B · R3-IGF-1 · Ascorbic Acid · Heparin	1-7	Lonza, UK (C2519A) (CC-3162)

Table 7-2 Chemical and reagents

Chemical and reagents	**Company**
Acetaminophen	Sigma-Aldrich
Ammonium Chloride	Sigma-Aldrich
Bovine serum albumin (BSA)	Sigma-Aldrich
4′,6-diamidino-2-phenylindole dihydrochloride (DAPI)	Sigma-Aldrich
VECTASHIELD® Mounting with DAPI	Vector Labs
Dipotassium hydrogen orthophosphate 3-hydrate (K2HPO4.3H2O)	BDH
D-(+) Galactose	Sigma-Aldrich
DMSO	
DTNB	Sigma-Aldrich
Dye albumin Blue 580 fluorescence assay	Molecular Probes (Eugene, OR)
Dulbecco's Phosphate Buffered Saline With $MgCl_2$ and $CaCl_2$	Sigma-Aldrich
Dulbecco's PBS—Ca_2+/Mg_2+ free	Sigma-Aldrich
Ethylenediaminetetraacetic acid (EDTA)	Sigma-Aldrich
Ethanol absolute, prolabo	VWR Chemicals
Flow cytometry Permeabilization/Wash Buffer I	R&D Systems

(1X)	
Flow cytometry Fixation Buffer (1X)	R&D Systems
Fetal bovine serum	Sigma-Aldrich
Formalin solution, neutral buffered, 10%	Sigma-Aldrich
β-Galactose Dehydrogenase S.	Roche Diagnostics
Glutathione reductase (250 units ml–1)	Sigma-Aldrich
Glutathione (reduced form), GSH,	Sigma-Aldrich
Glutathione (disulfide form), GSSG,	Sigma-Aldrich
Hank's balanced salt solution (HBSS)	Sigma
Hexokinase, 1500U 11426362001	Roche
Matrigel - Basement Membrane Matrix, Phenol Red-free, 10 ml – 356237	BD eBioscience
MitoSOX™	Molecular Probes (Life Technogies)
MOPS free acid	Sigma-Aldrich
MOPS sodium salt	Sigma-Aldrich
L-Lactate Dehydrogenase L-LDH 10254754103	Roche
NADH, appprox.98 1012802300	Roche
Salicylamide 99%	Sigma-Aldrich
Tetramethylrhodamine Isothiocyanate Rhodamine phalloidin	Molecular Probes (Life Technologies)
Testosterone soluble	Sigma-Aldrich
Triton X-100	Sigma-Aldrich
Triazol	Invitrogen
Trypan Blue	Invitrogen
Pig gamma globulin	Sigma-Aldrich
Potassium phosphate monobasic (KH_2PO_4)	Sigma-Aldrich
Potassium phosphate dibasic (K_2HPO_4)	Sigma-Aldrich
2-Vinylpyridine	Sigma-Aldrich

Table 7-3 Buffers

	Composition
MOPS Buffer	0.6g MOPS free acid 1.8g MOPS sodium salt 2.4g NaCl 0.2g EDTA disodium 20ml isopropanol H2O qsp 200 ml pH=7.4 with NaOH
Phosphate buffer of 100 ml	0.54g KH_2PO_4 0.18g K_2HPO_4 0.9g NaCl 0.1g EDTA disodium 10mg pig gamma globulin

Table 7-4 Materials for cell culture

Materials	Company
6,12,24 and 96 well cell culture cluster	Corning
96 well plate, polystyrene, non-treated, white flat bottom wells, non-sterile, white	Corning
24 well Thincert, 8µm pore diameter translucent	Greiner Bio-one
Polystyrene tube specifically designed for flow cytometry (5ml)	Bioscience Technology
Cryogenic tube	Thermo Scientific-Nunc
Cell scrapers	Fisher Scientific
Chamber slides	Nunc Lab Tek
Cuvettes Semi micro ps 100/pk	Fisherbrand, UK
Safe-lock tubes (1.5ml)	AG, Germany
Improved Neubauer	Hawksley, UK
Microscope Cover glass 22 x 22 mm	Menzel-Glaser, Braunschweig

Table 7-5 Equipment

Equipment	Company
Camera	Carl Zeiss, Germany
Cobas Fara Centrifugal Analyser	Roche
Countess® Automated Cell Counter	Life technologies
CytoFluor® series 4000 Fluorescence Multi-Well Plate Reader	Applied Biosystems
Heraeus Biofuge Fresco	DJB labcare
Galaxy S+ CO_2Incubator	RS Biotech
GLS Aqua Plus Series Linear Shaking Water Bath	Grant
EVOS ® inverted microscope	Life Technologies
FACS Calibur flow cytometer	Becton Dickinson, UK
GloMax®-Multi-Microplate Multimode Reader	Promega
LabTech-Nanodrop ND100 spectrophotometer	Labtech International
LightCycler® 96 System	Roche Life Science
Microscope	Zeiss Axio Observe A.1, Germany
PowerGen 125 Homogenize	Fisher Scientific
Refrigerated laboratory centrifuge, 4K15	Sigma
Soniprep 150	MSE
Veriti® Thermal Cycler	Life Technologies
Z™ Series coulter counter® Cell and Particle Counter	Beckman coulter

Table 7-6 Flow cytometry antibodies

Antibody	Isotype	Company
PE/Cy7 anti-mouse/human CD44 Antibody (103029)	Mouse	BioLegend
Alexa Fluor® 488 anti-human/mouse CD49f Antibody (313607)	Mouse	BioLegend
FITC anti-human CD54 Antibody (353107)	Mouse	BioLegend
Alexa Fluor® 647 anti-human CD326 (EpCAM) Antibody (324212)	Mouse	BioLegend
CD31/PECAM-1 (PerCP)	Mouse	BD Bioscience
VEGF-R2/KDR (PE)	Mouse	R&D Systems
VEGF-R2/KDR (FITC)	Mouse	R&D Systems

Table 7-7 Primary antibodies

Antibody	Source	Company
Human/Mouse Phospho-HRF R/c-met (Y1234/Y1235)	Rabbit	R&D Systems
CD31 (PECAM-1) Human/mouse	Rabbit	BD BioScience
Cytochrome P450 enzyme CYP3A4 polyclonal	Rabbit	Millipore

Table 7-8 Secondary antibodies

Antibody	Source	Company
Alexa Fluor 488 Anti-rabbit	Goat	Life Technologies
Alexa Fluor 488 Anti Mouse	Rabbit	Life Technologies
Alexa Fluor 555 Anti-mouse	Goat	Life Technologies

8 Publication and poster presentations

1. GRACIA-SANCHO, J., MAESO-DIAZ, R., FERNANDEZ-IGLESIAS, A., NAVARRO-ZORNOZA, M. & BOSCH, J. 2015. New cellular and molecular targets for the treatment of portal hypertension. *Hepatol Int*.

8.1 Selected conference presentations and published abstracts

1. **M. NAVARRO**, L. NELSON, K. BURGESS, O. TURA, K. SAMUEL, J. PLEVRIS. Hepatic/ endothelial cell co-culture; establishing optimal conditions for liver tissue engineering. British Association for the Study of the Liver, poster – (Liverpool, 2012)
2. **M. NAVARRO**, L. NELSON, O. TURA, K. SAMUEL, P.HAYES, J. PLEVRIS. Defining in vitro co-culture systems for human liver tissue engineering – Tissue and Cell Engineering Society, poster – (Liverpool 2012)
3. **M. NAVARRO**, O.TURA, K.SAMUEL, L.NELSON, J.PLEVRIS. Liver tissue engineering: hepatocytes and endothelial co-culture cross-talk in a liver model – European Society for Artificial Organs 2013, Oral communication – (Glasgow 2013)
4. **M. NAVARRO**, L. J. NELSON, P. TRESKES, P.C.HAYES, K. SAMUEL, J. N.PLEVRIS. Hepatoprotective effect of HUVECs in an *in vitro* hepatic co- culture model of APAP toxicity", European International Liver Congress (London, 2014)
5. **M. NAVARRO**, L. J. NELSON, P. TRESKES, P.C.HAYES, K. SAMUEL, J. N.PLEVRIS. Hepatocytes improve their drug metabolic activity with the presence of endothelial cells in an in vitro hepatic co-culture model of APAP toxicity", European International Liver Congress (London, 2014)

9 Bibliography

Abdel-Misih, S. R. & Bloomston, M. 2010. Liver anatomy. *Surg Clin North Am,* 90**,** 643-53.

Adeva, M., Gonzalez-Lucan, M., Seco, M. & Donapetry, C. 2013. Enzymes involved in l-lactate metabolism in humans. *Mitochondrion,* 13**,** 615-29.

Agarwal, R., Hennings, L., Rafferty, T. M., Letzig, L. G., McCullough, S., James, L. P., MacMillan-Crow, L. A. & Hinson, J. A. 2012. Acetaminophen-induced hepatotoxicity and protein nitration in neuronal nitric-oxide synthase knockout mice. *J Pharmacol Exp Ther,* 340**,** 134-42.

Aguer, C., Gambarotta, D., Mailloux, R. J., Moffat, C., Dent, R., McPherson, R. & Harper, M. E. 2011. Galactose enhances oxidative metabolism and reveals mitochondrial dysfunction in human primary muscle cells. *PLoS One,* 6**,** e28536.

Aharoni-Simon, M., Anavi, S., Beifuss, U., Madar, Z. & Tirosh, O. 2012. Nitric oxide, can it be only good? Increasing the antioxidant properties of nitric oxide in hepatocytes by YC-1 compound. *Nitric Oxide,* 27**,** 248-56.

Ahmed, N., Riley, C., Rice, G. & Quinn, M. 2005. Role of integrin receptors for fibronectin, collagen and laminin in the regulation of ovarian carcinoma functions in response to a matrix microenvironment. *Clin Exp Metastasis,* 22**,** 391-402.

Aleksunes, L. M., Campion, S. N., Goedken, M. J. & Manautou, J. E. 2008. Acquired resistance to acetaminophen hepatotoxicity is associated with induction of multidrug resistance-associated protein 4 (Mrp4) in proliferating hepatocytes. *Toxicol Sci,* 104**,** 261-73.

Allen, J. W., Khetani, S. R. & Bhatia, S. N. 2005. In vitro zonation and toxicity in a hepatocyte bioreactor. *Toxicol Sci,* 84**,** 110-9.

Allen, P., Melero-Martin, J. & Bischoff, J. 2011. Type I collagen, fibrin and PuraMatrix matrices provide permissive environments for human endothelial and mesenchymal progenitor cells to form neovascular networks. *J Tissue Eng Regen Med,* 5**,** e74-86.

Alva, N., Cruz, D., Sanchez, S., Valentin, J. M., Bermudez, J. & Carbonell, T. 2013. Nitric oxide as a mediator of fructose 1,6-bisphosphate protection in galactosamine-induced hepatotoxicity in rats. *Nitric Oxide,* 28**,** 17-23.

Amaral, S. S., Oliveira, A. G., Marques, P. E., Quintao, J. L., Pires, D. A., Resende, R. R., Sousa, B. R., Melgaco, J. G., Pinto, M. A., Russo, R. C., Gomes, A. K., Andrade, L. M., Zanin, R. F., Pereira, R. V., Bonorino, C., Soriani, F. M., Lima, C. X., Cara, D. C., Teixeira, M. M., Leite, M. F. & Menezes, G. B. 2013. Altered responsiveness to extracellular ATP enhances acetaminophen hepatotoxicity. *Cell Commun Signal,* 11**,** 10.

Aninat, C., Piton, A., Glaise, D., Le Charpentier, T., Langouet, S., Morel, F., Guguen-Guillouzo, C. & Guillouzo, A. 2006. Expression of cytochromes P450, conjugating enzymes and nuclear receptors in human hepatoma HepaRG cells. *Drug Metab Dispos,* 34**,** 75-83.

Aritomi, K., Ishitsuka, Y., Tomishima, Y., Shimizu, D., Abe, N., Shuto, T., Irikura, M., Kai, H. & Irie, T. 2014. Evaluation of three-dimensional cultured HepG2

cells in a nano culture plate system: an in vitro human model of acetaminophen hepatotoxicity. *J Pharmacol Sci,* 124**,** 218-29.
Arrowsmith, J. & Miller, P. 2013. Trial watch: phase II and phase III attrition rates 2011-2012. *Nat Rev Drug Discov.* England.
Atlante, A., Giannattasio, S., Bobba, A., Gagliardi, S., Petragallo, V., Calissano, P., Marra, E. & Passarella, S. 2005. An increase in the ATP levels occurs in cerebellar granule cells en route to apoptosis in which ATP derives from both oxidative phosphorylation and anaerobic glycolysis. *Biochim Biophys Acta,* 1708**,** 50-62.
Badmann, A., Langsch, S., Keogh, A., Brunner, T., Kaufmann, T. & Corazza, N. 2012. TRAIL enhances paracetamol-induced liver sinusoidal endothelial cell death in a Bim- and Bid-dependent manner. *Cell Death Dis,* 3**,** e447.
Bala, K., Ambwani, K. & Gohil, N. K. 2011. Effect of different mitogens and serum concentration on HUVEC morphology and characteristics: implication on use of higher passage cells. *Tissue Cell,* 43**,** 216-22.
Bale, S. S., Golberg, I., Jindal, R., McCarty, W. J., Luitje, M., Hegde, M., Bhushan, A., Usta, O. B. & Yarmush, M. 2014a. Long Term Co-culture Strategies for Primary Hepatocytes and Liver Sinusoidal Endothelial Cells. *Tissue Eng Part C Methods*.
Bale, S. S., Vernetti, L., Senutovitch, N., Jindal, R., Hegde, M., Gough, A., McCarty, W. J., Bakan, A., Bhushan, A., Shun, T. Y., Golberg, I., Debiasio, R., Usta, B. O., Taylor, D. L. & Yarmush, M. L. 2014b. In vitro platforms for evaluating liver toxicity. *Exp Biol Med (Maywood)*.
Berger, D. R., Ware, B. R., Davidson, M. D., Allsup, S. R. & Khetani, S. R. 2014. Enhancing the functional maturity of iPSC-derived human hepatocytes via controlled presentation of cell-cell interactions in vitro. *Hepatology*.
Bhatia, S. N., Balis, U. J., Yarmush, M. L. & Toner, M. 1999. Effect of cell-cell interactions in preservation of cellular phenotype: cocultivation of hepatocytes and nonparenchymal cells. *Faseb j,* 13**,** 1883-900.
Bhatia, S. N. & Ingber, D. E. 2014. Microfluidic organs-on-chips. *Nat Biotechnol,* 32**,** 760-72.
Bhogal, R. H., Hodson, J., Bartlett, D. C., Weston, C. J., Curbishley, S. M., Haughton, E., Williams, K. T., Reynolds, G. M., Newsome, P. N., Adams, D. H. & Afford, S. C. 2011. Isolation of primary human hepatocytes from normal and diseased liver tissue: a one hundred liver experience. *PLoS One,* 6**,** e18222.
Bhushan, A., Senutovitch, N., Bale, S. S., McCarty, W. J., Hegde, M., Jindal, R., Golberg, I., Berk Usta, O., Yarmush, M. L., Vernetti, L., Gough, A., Bakan, A., Shun, T. Y., DeBiasio, R. & Lansing Taylor, D. 2013. Towards a three-dimensional microfluidic liver platform for predicting drug efficacy and toxicity in humans. *Stem Cell Res Ther,* 4 Suppl 1**,** S16.
Biron-Andreani, C., Raulet, E., Pichard-Garcia, L. & Maurel, P. 2010. Use of human hepatocytes to investigate blood coagulation factor. *Methods Mol Biol,* 640**,** 431-45.
Blachier, M., Leleu, H., Peck-Radosavljevic, M., Valla, D. C. & Roudot-Thoraval, F. 2013. The burden of liver disease in Europe: a review of available epidemiological data. *J Hepatol,* 58**,** 593-608.

Blouin, A., Bolender, R. P. & Weibel, E. R. 1977. Distribution of organelles and membranes between hepatocytes and nonhepatocytes in the rat liver parenchyma. A stereological study. *J Cell Biol,* 72**,** 441-55.

Burcham, P. C. & Harman, A. W. 1991. Acetaminophen toxicity results in site-specific mitochondrial damage in isolated mouse hepatocytes. *J Biol Chem,* 266**,** 5049-54.

Carmeliet, P. 2000. Mechanisms of angiogenesis and arteriogenesis. *Nat Med,* 6**,** 389-95.

Cecchelli, R., Berezowski, V., Lundquist, S., Culot, M., Renftel, M., Dehouck, M. P. & Fenart, L. 2007. Modelling of the blood-brain barrier in drug discovery and development. *Nat Rev Drug Discov,* 6**,** 650-61.

Chalasani, N. & Bjornsson, E. 2010. Risk factors for idiosyncratic drug-induced liver injury. *Gastroenterology,* 138**,** 2246-59.

Chan, B. P. & Leong, K. W. 2008. Scaffolding in tissue engineering: general approaches and tissue-specific considerations. *Eur Spine J,* 17 Suppl 4**,** 467-79.

Cheng, J., Ma, X., Krausz, K. W., Idle, J. R. & Gonzalez, F. J. 2009. Rifampicin-activated human pregnane X receptor and CYP3A4 induction enhance acetaminophen-induced toxicity. *Drug Metab Dispos,* 37**,** 1611-21.

Chou, M. J., Hsieh, C. H., Yeh, P. L., Chen, P. C., Wang, C. H. & Huang, Y. Y. 2013. Application of open porous poly(D,L-lactide-co-glycolide) microspheres and the strategy of hydrophobic seeding in hepatic tissue cultivation. *J Biomed Mater Res A,* 101**,** 2862-9.

Choucha Snouber, L., Bunescu, A., Naudot, M., Legallais, C., Brochot, C., Dumas, M. E., Elena-Herrmann, B. & Leclerc, E. 2013. Metabolomics-on-a-chip of hepatotoxicity induced by anticancer drug flutamide and Its active metabolite hydroxyflutamide using HepG2/C3a microfluidic biochips. *Toxicol Sci,* 132**,** 8-20.

Ciociola, A. A., Cohen, L. B. & Kulkarni, P. 2014. How Drugs are Developed and Approved by the FDA: Current Process and Future Directions. *Am J Gastroenterol,* 109**,** 620-3.

Cole, S. D., Madren-Whalley, J. S., Li, A. P., Dorsey, R. & Salem, H. 2014. High Content Analysis of an In Vitro Model for Metabolic Toxicity: Results with the Model Toxicants 4-Aminophenol and Cyclophosphamide. *J Biomol Screen*.

Cox, A. G., Saunders, D. C., Kelsey, P. B., Jr., Conway, A. A., Tesmenitsky, Y., Marchini, J. F., Brown, K. K., Stamler, J. S., Colagiovanni, D. B., Rosenthal, G. J., Croce, K. J., North, T. E. & Goessling, W. 2014. S-nitrosothiol signaling regulates liver development and improves outcome following toxic liver injury. *Cell Rep,* 6**,** 56-69.

De Kock, J., Ceelen, L., De Spiegelaere, W., Casteleyn, C., Claes, P., Vanhaecke, T. & Rogiers, V. 2011. Simple and quick method for whole-liver decellularization: a novel in vitro three-dimensional bioengineering tool? *Arch Toxicol,* 85**,** 607-12.

Deavall, D. G., Martin, E. A., Horner, J. M. & Roberts, R. 2012. Drug-induced oxidative stress and toxicity. *J Toxicol,* 2012**,** 645460.

Deboux, C., Ladraa, S., Cazaubon, S., Ghribi-Mallah, S., Weiss, N., Chaverot, N., Couraud, P. O. & Baron-Van Evercooren, A. 2013. Overexpression of CD44

in neural precursor cells improves trans-endothelial migration and facilitates their invasion of perivascular tissues in vivo. *PLoS One,* 8**,** e57430.
Deenen, M. J., Cats, A., Beijnen, J. H. & Schellens, J. H. 2011. Part 2: pharmacogenetic variability in drug transport and phase I anticancer drug metabolism. *Oncologist,* 16**,** 820-34.
Deleve, L. D. 1994. Dacarbazine toxicity in murine liver cells: a model of hepatic endothelial injury and glutathione defense. *J Pharmacol Exp Ther,* 268**,** 1261-70.
DeLeve, L. D. 2013. Liver sinusoidal endothelial cells and liver regeneration. *J Clin Invest,* 123**,** 1861-6.
DeLeve, L. D. 2014. Liver sinusoidal endothelial cells in hepatic fibrosis. *Hepatology*.
DeLeve, L. D., Wang, X., Hu, L., McCuskey, M. K. & McCuskey, R. S. 2004. Rat liver sinusoidal endothelial cell phenotype is maintained by paracrine and autocrine regulation. *Am J Physiol Gastrointest Liver Physiol,* 287**,** G757-63.
DeLeve, L. D., Wang, X., Kaplowitz, N., Shulman, H. M., Bart, J. A. & van der Hoek, A. 1997. Sinusoidal endothelial cells as a target for acetaminophen toxicity. Direct action versus requirement for hepatocyte activation in different mouse strains. *Biochem Pharmacol,* 53**,** 1339-45.
Diehl, A. M. & Rai, R. M. 1996. Liver regeneration 3: Regulation of signal transduction during liver regeneration. *Faseb j,* 10**,** 215-27.
Ding, B. S., Nolan, D. J., Butler, J. M., James, D., Babazadeh, A. O., Rosenwaks, Z., Mittal, V., Kobayashi, H., Shido, K., Lyden, D., Sato, T. N., Rabbany, S. Y. & Rafii, S. 2010. Inductive angiocrine signals from sinusoidal endothelium are required for liver regeneration. *Nature,* 468**,** 310-5.
Donahower, B. C., McCullough, S. S., Hennings, L., Simpson, P. M., Stowe, C. D., Saad, A. G., Kurten, R. C., Hinson, J. A. & James, L. P. 2010. Human recombinant vascular endothelial growth factor reduces necrosis and enhances hepatocyte regeneration in a mouse model of acetaminophen toxicity. *J Pharmacol Exp Ther,* 334**,** 33-43.
Donato, M. T., Jover, R. & Gomez-Lechon, M. J. 2013. Hepatic cell lines for drug hepatotoxicity testing: limitations and strategies to upgrade their metabolic competence by gene engineering. *Curr Drug Metab,* 14**,** 946-68.
Dott, W., Mistry, P., Wright, J., Cain, K. & Herbert, K. E. 2014. Modulation of mitochondrial bioenergetics in a skeletal muscle cell line model of mitochondrial toxicity. *Redox Biol,* 2**,** 224-33.
Du, K., Williams, C. D., McGill, M. R., Xie, Y., Farhood, A., Vinken, M. & Jaeschke, H. 2013. The gap junction inhibitor 2-aminoethoxy-diphenyl-borate protects against acetaminophen hepatotoxicity by inhibiting cytochrome P450 enzymes and c-jun N-terminal kinase activation. *Toxicol Appl Pharmacol,* 273**,** 484-91.
Elvevold, K., Smedsrod, B. & Martinez, I. 2008. The liver sinusoidal endothelial cell: a cell type of controversial and confusing identity. *Am J Physiol Gastrointest Liver Physiol,* 294**,** G391-400.
Endo, S., Toyoda, Y., Fukami, T., Nakajima, M. & Yokoi, T. 2012. Stimulation of human monocytic THP-1 cells by metabolic activation of hepatotoxic drugs. *Drug Metab Pharmacokinet,* 27**,** 621-30.

Feichtinger, R. G., Sperl, W., Bauer, J. W. & Kofler, B. 2014. Mitochondrial dysfunction: a neglected component of skin diseases. *Exp Dermatol*.

Feldstein, A. E., Canbay, A., Angulo, P., Taniai, M., Burgart, L. J., Lindor, K. D. & Gores, G. J.

Ferreira, A., Rodrigues, M., Silvestre, S., Falcao, A. & Alves, G. 2014. HepaRG cell line as an in vitro model for screening drug-drug interactions mediated by metabolic induction: Amiodarone used as a model substance. *Toxicol In Vitro*.

Filippi, C., Keatch, S. A., Rangar, D., Nelson, L. J., Hayes, P. C. & Plevris, J. N. 2004. Improvement of C3A cell metabolism for usage in bioartificial liver support systems. *J Hepatol,* 41**,** 599-605.

Flecknell, P. 2002. Replacement, reduction and refinement. *Altex,* 19**,** 73-8.

Fomin, M. E., Zhou, Y., Beyer, A. I., Publicover, J., Baron, J. L. & Muench, M. O. 2013. Production of factor VIII by human liver sinusoidal endothelial cells transplanted in immunodeficient uPA mice. *PLoS One,* 8**,** e77255.

Forstermann, U. & Munzel, T. 2006. Endothelial nitric oxide synthase in vascular disease: from marvel to menace. *Circulation,* 113**,** 1708-14.

Fransen, M., Nordgren, M., Wang, B. & Apanasets, O. 2012. Role of peroxisomes in ROS/RNS-metabolism: implications for human disease. *Biochim Biophys Acta,* 1822**,** 1363-73.

Genove, E., Schmitmeier, S., Sala, A., Borros, S., Bader, A., Griffith, L. G. & Semino, C. E. 2009. Functionalized self-assembling peptide hydrogel enhance maintenance of hepatocyte activity in vitro. *J Cell Mol Med,* 13**,** 3387-97.

Gerets, H. H., Tilmant, K., Gerin, B., Chanteux, H., Depelchin, B. O., Dhalluin, S. & Atienzar, F. A. 2012. Characterization of primary human hepatocytes, HepG2 cells, and HepaRG cells at the mRNA level and CYP activity in response to inducers and their predictivity for the detection of human hepatotoxins. *Cell Biol Toxicol,* 28**,** 69-87.

Germano, D., Uteng, M., Pognan, F., Chibout, S. D. & Wolf, A. 2014. Determination of Liver Specific Toxicities in Rat Hepatocytes by High Content Imaging during 2-Week Multiple Treatment. *Toxicol In Vitro*.

Getachew, Y., James, L., Lee, W. M., Thiele, D. L. & Miller, B. C. 2010. Susceptibility to acetaminophen (APAP) toxicity unexpectedly is decreased during acute viral hepatitis in mice. *Biochem Pharmacol,* 79**,** 1363-71.

Giri, S., Braumann, U. D., Giri, P., Acikgoz, A., Scheibe, P., Nieber, K. & Bader, A. 2013. Nanostructured self-assembling peptides as a defined extracellular matrix for long-term functional maintenance of primary hepatocytes in a bioartificial liver modular device. *Int J Nanomedicine,* 8**,** 1525-39.

Godoy, P., Hewitt, N. J., Albrecht, U., Andersen, M. E., Ansari, N., Bhattacharya, S., Bode, J. G., Bolleyn, J., Borner, C., Bottger, J., Braeuning, A., Budinsky, R. A., Burkhardt, B., Cameron, N. R., Camussi, G., Cho, C. S., Choi, Y. J., Craig Rowlands, J., Dahmen, U., Damm, G., Dirsch, O., Donato, M. T., Dong, J., Dooley, S., Drasdo, D., Eakins, R., Ferreira, K. S., Fonsato, V., Fraczek, J., Gebhardt, R., Gibson, A., Glanemann, M., Goldring, C. E., Gomez-Lechon, M. J., Groothuis, G. M., Gustavsson, L., Guyot, C., Hallifax, D., Hammad, S., Hayward, A., Haussinger, D., Hellerbrand, C., Hewitt, P., Hoehme, S., Holzhutter, H. G., Houston, J. B., Hrach, J., Ito, K., Jaeschke,

H., Keitel, V., Kelm, J. M., Kevin Park, B., Kordes, C., Kullak-Ublick, G. A., LeCluyse, E. L., Lu, P., Luebke-Wheeler, J., Lutz, A., Maltman, D. J., Matz-Soja, M., McMullen, P., Merfort, I., Messner, S., Meyer, C., Mwinyi, J., Naisbitt, D. J., Nussler, A. K., Olinga, P., Pampaloni, F., Pi, J., Pluta, L., Przyborski, S. A., Ramachandran, A., Rogiers, V., Rowe, C., Schelcher, C., Schmich, K., Schwarz, M., Singh, B., Stelzer, E. H., Stieger, B., Stober, R., Sugiyama, Y., Tetta, C., Thasler, W. E., Vanhaecke, T., Vinken, M., Weiss, T. S., Widera, A., Woods, C. G., Xu, J. J., Yarborough, K. M. & Hengstler, J. G. 2013. Recent advances in 2D and 3D in vitro systems using primary hepatocytes, alternative hepatocyte sources and non-parenchymal liver cells and their use in investigating mechanisms of hepatotoxicity, cell signaling and ADME. *Arch Toxicol,* 87**,** 1315-530.

Godoy, P., Reif, R. & Bolt, H. M. 2012. Alcohol hepatotoxicity: Kupffer cells surface to the top. *Arch Toxicol,* 86**,** 1331-2.

Goler-Baron, V. & Assaraf, Y. G. 2011. Structure and function of ABCG2-rich extracellular vesicles mediating multidrug resistance. *PLoS One,* 6**,** e16007.

Gomez-Lechon, M. J., Castell, J. V. & Donato, M. T. 2010. The use of hepatocytes to investigate drug toxicity. *Methods Mol Biol,* 640**,** 389-415.

Gomez-Lechon, M. J., Donato, M. T., Castell, J. V. & Jover, R. 2004. Human hepatocytes in primary culture: the choice to investigate drug metabolism in man. *Curr Drug Metab,* 5**,** 443-62.

Gomez-Lechon, M. J., Tolosa, L., Conde, I. & Donato, M. T. 2014. Competency of different cell models to predict human hepatotoxic drugs. *Expert Opin Drug Metab Toxicol,* 10**,** 1553-68.

Gripon, P., Rumin, S., Urban, S., Le Seyec, J., Glaise, D., Cannie, I., Guyomard, C., Lucas, J., Trepo, C. & Guguen-Guillouzo, C. 2002. Infection of a human hepatoma cell line by hepatitis B virus. *Proc Natl Acad Sci U S A,* 99**,** 15655-60.

Gulmez, S. E., Larrey, D., Pageaux, G. P., Lignot, S., Lassalle, R., Jove, J., Gatta, A., McCormick, P. A., Metselaar, H. J., Monteiro, E., Thorburn, D., Bernal, W., Zouboulis-Vafiadis, I., de Vries, C., Perez-Gutthann, S., Sturkenboom, M., Benichou, J., Montastruc, J. L., Horsmans, Y., Salvo, F., Hamoud, F., Micon, S., Droz-Perroteau, C., Blin, P. & Moore, N. 2013. Transplantation for acute liver failure in patients exposed to NSAIDs or paracetamol (acetaminophen): the multinational case-population SALT study. *Drug Saf,* 36**,** 135-44.

Guo, L., Dial, S., Shi, L., Branham, W., Liu, J., Fang, J. L., Green, B., Deng, H., Kaput, J. & Ning, B. 2011. Similarities and differences in the expression of drug-metabolizing enzymes between human hepatic cell lines and primary human hepatocytes. *Drug Metab Dispos,* 39**,** 528-38.

Hadi, M., Westra, I. M., Starokozhko, V., Dragovic, S., Merema, M. T. & Groothuis, G. M. 2013. Human precision-cut liver slices as an ex vivo model to study idiosyncratic drug-induced liver injury. *Chem Res Toxicol,* 26**,** 710-20.

Hammad, S., Hoehme, S., Friebel, A., von Recklinghausen, I., Othman, A., Begher-Tibbe, B., Reif, R., Godoy, P., Johann, T., Vartak, A., Golka, K., Bucur, P. O., Vibert, E., Marchan, R., Christ, B., Dooley, S., Meyer, C., Ilkavets, I., Dahmen, U., Dirsch, O., Bottger, J., Gebhardt, R., Drasdo, D. & Hengstler, J. G. 2014. Protocols for staining of bile canalicular and sinusoidal networks of human, mouse and pig livers, three-dimensional reconstruction and

quantification of tissue microarchitecture by image processing and analysis. *Arch Toxicol,* 88**,** 1161-83.

Han, D., Dara, L., Win, S., Than, T. A., Yuan, L., Abbasi, S. Q., Liu, Z. X. & Kaplowitz, N. 2013. Regulation of drug-induced liver injury by signal transduction pathways: critical role of mitochondria. *Trends Pharmacol Sci,* 34**,** 243-53.

Harimoto, M., Yamato, M., Hirose, M., Takahashi, C., Isoi, Y., Kikuchi, A. & Okano, T. 2002. Novel approach for achieving double-layered cell sheets co-culture: overlaying endothelial cell sheets onto monolayer hepatocytes utilizing temperature-responsive culture dishes. *J Biomed Mater Res,* 62**,** 464-70.

Harrill, A. H., Watkins, P. B., Su, S., Ross, P. K., Harbourt, D. E., Stylianou, I. M., Boorman, G. A., Russo, M. W., Sackler, R. S., Harris, S. C., Smith, P. C., Tennant, R., Bogue, M., Paigen, K., Harris, C., Contractor, T., Wiltshire, T., Rusyn, I. & Threadgill, D. W. 2009. Mouse population-guided resequencing reveals that variants in CD44 contribute to acetaminophen-induced liver injury in humans. *Genome Res,* 19**,** 1507-15.

Hart, S. N., Li, Y., Nakamoto, K., Subileau, E. A., Steen, D. & Zhong, X. B. 2010. A comparison of whole genome gene expression profiles of HepaRG cells and HepG2 cells to primary human hepatocytes and human liver tissues. *Drug Metab Dispos,* 38**,** 988-94.

Hastings, R., Qureshi, M., Verma, R., Lacy, P. S. & Williams, B. 2004. Telomere attrition and accumulation of senescent cells in cultured human endothelial cells. *Cell Prolif,* 37**,** 317-24.

Hinson, J. A., Roberts, D. W. & James, L. P. 2010. Mechanisms of acetaminophen-induced liver necrosis. *Handb Exp Pharmacol***,** 369-405.

Ho, C. T., Lin, R. Z., Chen, R. J., Chin, C. K., Gong, S. E., Chang, H. Y., Peng, H. L., Hsu, L., Yew, T. R., Chang, S. F. & Liu, C. H. 2013. Liver-cell patterning lab chip: mimicking the morphology of liver lobule tissue. *Lab Chip,* 13**,** 3578-87.

Hoehme, S., Brulport, M., Bauer, A., Bedawy, E., Schormann, W., Hermes, M., Puppe, V., Gebhardt, R., Zellmer, S., Schwarz, M., Bockamp, E., Timmel, T., Hengstler, J. G. & Drasdo, D. 2010. Prediction and validation of cell alignment along microvessels as order principle to restore tissue architecture in liver regeneration. *Proc Natl Acad Sci U S A,* 107**,** 10371-6.

Hoekstra, R., Nibourg, G. A., van der Hoeven, T. V., Plomer, G., Seppen, J., Ackermans, M. T., Camus, S., Kulik, W., van Gulik, T. M., Elferink, R. P. & Chamuleau, R. A. 2013. Phase 1 and phase 2 drug metabolism and bile acid production of HepaRG cells in a bioartificial liver in absence of dimethyl sulfoxide. *Drug Metab Dispos,* 41**,** 562-7.

Hsieh, S. C., Wu, C. H., Wu, C. C., Yen, J. H., Liu, M. C., Hsueh, C. M. & Hsu, S. L. 2014. Gallic acid selectively induces the necrosis of activated hepatic stellate cells via a calcium-dependent calpain I activation pathway. *Life Sci,* 102**,** 55-64.

Hwa, A. J., Fry, R. C., Sivaraman, A., So, P. T., Samson, L. D., Stolz, D. B. & Griffith, L. G. 2007. Rat liver sinusoidal endothelial cells survive without exogenous VEGF in 3D perfused co-cultures with hepatocytes. *Faseb j,* 21**,** 2564-79.

Hynes, R. O. 2007. Cell-matrix adhesion in vascular development. *J Thromb Haemost,* 5 Suppl 1**,** 32-40.
Inamori, M., Mizumoto, H. & Kajiwara, T. 2009. An approach for formation of vascularized liver tissue by endothelial cell-covered hepatocyte spheroid integration. *Tissue Eng Part A,* 15**,** 2029-37.
Ito, Y., Bethea, N. W., Abril, E. R. & McCuskey, R. S. 2003. Early hepatic microvascular injury in response to acetaminophen toxicity. *Microcirculation,* 10**,** 391-400.
Jaeschke, H., Gores, G. J., Cederbaum, A. I., Hinson, J. A., Pessayre, D. & Lemasters, J. J. 2002. Mechanisms of hepatotoxicity. *Toxicol Sci,* 65**,** 166-76.
Jaeschke, H., Knight, T. R. & Bajt, M. L. 2003. The role of oxidant stress and reactive nitrogen species in acetaminophen hepatotoxicity. *Toxicol Lett,* 144**,** 279-88.
Jaeschke, H., McGill, M. R. & Ramachandran, A. 2012a. Oxidant stress, mitochondria, and cell death mechanisms in drug-induced liver injury: Lessons learned from acetaminophen hepatotoxicity. *Drug Metabolism Reviews,* 44**,** 88-106.
Jaeschke, H., McGill, M. R. & Ramachandran, A. 2012b. Oxidant stress, mitochondria, and cell death mechanisms in drug-induced liver injury: lessons learned from acetaminophen hepatotoxicity. *Drug Metab Rev,* 44**,** 88-106.
Jaeschke, H., Williams, C. D., McGill, M. R., Xie, Y. & Ramachandran, A. 2013. Models of drug-induced liver injury for evaluation of phytotherapeutics and other natural products. *Food Chem Toxicol,* 55**,** 279-89.
Jancova, P., Anzenbacher, P. & Anzenbacherova, E. 2010. Phase II drug metabolizing enzymes. *Biomed Pap Med Fac Univ Palacky Olomouc Czech Repub,* 154**,** 103-16.
Jetten, M. J., Kleinjans, J. C., Claessen, S. M., Chesne, C. & van Delft, J. H. 2013. Baseline and genotoxic compound induced gene expression profiles in HepG2 and HepaRG compared to primary human hepatocytes. *Toxicol In Vitro,* 27**,** 2031-40.
Jungermann, K. & Kietzmann, T. 1996. Zonation of parenchymal and nonparenchymal metabolism in liver. *Annu Rev Nutr,* 16**,** 179-203.
Kamel, A. & Harriman, S. 2013. Inhibition of cytochrome P450 enzymes and biochemical aspects of mechanism-based inactivation (MBI). *Drug Discov Today Technol,* 10**,** e177-89.
Kanzler, I., Seitz-Merwald, I., Schleger, S., Kaczmarek, I., Kur, F. & Beiras-Fernandez, A. 2013. In vitro effects of ATG-Fresenius on immune cell adhesion. *Transplant Proc,* 45**,** 1846-9.
Kao, Y. H., Jawan, B., Goto, S., Pan, M. C., Lin, Y. C., Sun, C. K., Hsu, L. W., Tai, M. H., Cheng, Y. F., Nakano, T., Wang, C. S., Huang, C. J. & Chen, C. L. 2009. Serum factors potentiate hypoxia-induced hepatotoxicity in vitro through increasing transforming growth factor-beta1 activation and release. *Cytokine,* 47**,** 11-22.
Kaplowitz, N. 2005. Idiosyncratic drug hepatotoxicity. *Nat Rev Drug Discov,* 4**,** 489-99.
Kato, T., Ito, Y., Hosono, K., Suzuki, T., Tamaki, H., Minamino, T., Kato, S., Sakagami, H., Shibuya, M. & Majima, M. 2011. Vascular endothelial growth

factor receptor-1 signaling promotes liver repair through restoration of liver microvasculature after acetaminophen hepatotoxicity. *Toxicol Sci,* 120**,** 218-29.

Kavitha, C. V., Agarwal, C., Agarwal, R. & Deep, G. 2011. Asiatic acid inhibits pro-angiogenic effects of VEGF and human gliomas in endothelial cell culture models. *PLoS One,* 6**,** e22745.

Khodarev, N. N., Yu, J., Labay, E., Darga, T., Brown, C. K., Mauceri, H. J., Yassari, R., Gupta, N. & Weichselbaum, R. R. 2003. Tumour-endothelium interactions in co-culture: coordinated changes of gene expression profiles and phenotypic properties of endothelial cells. *J Cell Sci,* 116**,** 1013-22.

Kim, K., Ohashi, K., Utoh, R., Kano, K. & Okano, T. 2012. Preserved liver-specific functions of hepatocytes in 3D co-culture with endothelial cell sheets. *Biomaterials,* 33**,** 1406-13.

Kim, P. K., Zamora, R., Petrosko, P. & Billiar, T. R. 2001. The regulatory role of nitric oxide in apoptosis. *Int Immunopharmacol,* 1**,** 1421-41.

Kjaergaard, A. G., Dige, A., Krog, J., Tonnesen, E. & Wogensen, L. 2013. Soluble adhesion molecules correlate with surface expression in an in vitro model of endothelial activation. *Basic Clin Pharmacol Toxicol,* 113**,** 273-9.

Kleinman, H. K. & Martin, G. R. 2005. Matrigel: basement membrane matrix with biological activity. *Semin Cancer Biol,* 15**,** 378-86.

Klingenberg, M. 2008. The ADP and ATP transport in mitochondria and its carrier. *Biochim Biophys Acta,* 1778**,** 1978-2021.

Knight, T. R., Ho, Y. S., Farhood, A. & Jaeschke, H. 2002. Peroxynitrite is a critical mediator of acetaminophen hepatotoxicity in murine livers: protection by glutathione. *J Pharmacol Exp Ther,* 303**,** 468-75.

Knudsen, T. B. & Kleinstreuer, N. C. 2011. Disruption of embryonic vascular development in predictive toxicology. *Birth Defects Res C Embryo Today,* 93**,** 312-23.

Kojima, S., Negishi, Y., Tsukimoto, M., Takenouchi, T., Kitani, H. & Takeda, K. 2014. Purinergic signaling via P2X7 receptor mediates IL-1beta production in Kupffer cells exposed to silica nanoparticle. *Toxicology,* 321**,** 13-20.

Kola, I. & Landis, J. 2004. Can the pharmaceutical industry reduce attrition rates? *Nat Rev Drug Discov,* 3**,** 711-5.

Kon, K., Kim, J. S., Jaeschke, H. & Lemasters, J. J. 2004. Mitochondrial permeability transition in acetaminophen-induced necrosis and apoptosis of cultured mouse hepatocytes. *Hepatology,* 40**,** 1170-9.

Kostadinova, R., Boess, F., Applegate, D., Suter, L., Weiser, T., Singer, T., Naughton, B. & Roth, A. 2013. A long-term three dimensional liver co-culture system for improved prediction of clinically relevant drug-induced hepatotoxicity. *Toxicol Appl Pharmacol,* 268**,** 1-16.

Kraljevic, S., Stambrook, P. J. & Pavelic, K. 2004. Accelerating drug discovery. *EMBO Rep,* 5**,** 837-42.

Kubota, Y., Kleinman, H. K., Martin, G. R. & Lawley, T. J. 1988. Role of laminin and basement membrane in the morphological differentiation of human endothelial cells into capillary-like structures. *J Cell Biol,* 107**,** 1589-98.

Kunze, A., Huwyler, J., Camenisch, G. & Gutmann, H. 2012. Interaction of the antiviral drug telaprevir with renal and hepatic drug transporters. *Biochem Pharmacol,* 84**,** 1096-102.

Lawson, J. A., Farhood, A., Hopper, R. D., Bajt, M. L. & Jaeschke, H. 2000. The hepatic inflammatory response after acetaminophen overdose: role of neutrophils. *Toxicol Sci,* 54**,** 509-16.

Le Vee, M., Jigorel, E., Glaise, D., Gripon, P., Guguen-Guillouzo, C. & Fardel, O. 2006. Functional expression of sinusoidal and canalicular hepatic drug transporters in the differentiated human hepatoma HepaRG cell line. *Eur J Pharm Sci,* 28**,** 109-17.

Le Vee, M., Noel, G., Jouan, E., Stieger, B. & Fardel, O. 2013. Polarized expression of drug transporters in differentiated human hepatoma HepaRG cells. *Toxicol In Vitro,* 27**,** 1979-86.

LeCluyse, E. L., Witek, R. P., Andersen, M. E. & Powers, M. J. 2012. Organotypic liver culture models: meeting current challenges in toxicity testing. *Crit Rev Toxicol,* 42**,** 501-48.

LeCouter, J., Moritz, D. R., Li, B., Phillips, G. L., Liang, X. H., Gerber, H. P., Hillan, K. J. & Ferrara, N. 2003. Angiogenesis-independent endothelial protection of liver: role of VEGFR-1. *Science,* 299**,** 890-3.

Lee, E. J. & Niklason, L. E. 2010. A novel flow bioreactor for in vitro microvascularization. *Tissue Eng Part C Methods,* 16**,** 1191-200.

Leong, M. F., Toh, J. K., Du, C., Narayanan, K., Lu, H. F., Lim, T. C., Wan, A. C. & Ying, J. Y. 2013. Patterned prevascularised tissue constructs by assembly of polyelectrolyte hydrogel fibres. *Nat Commun,* 4**,** 2353.

Li, H., Horke, S. & Forstermann, U. 2013. Oxidative stress in vascular disease and its pharmacological prevention. *Trends Pharmacol Sci,* 34**,** 313-9.

Li, L., Zhang, B., Tao, Y., Wang, Y., Wei, H., Zhao, J., Huang, R. & Pei, Z. 2009. DL-3-n-butylphthalide protects endothelial cells against oxidative/nitrosative stress, mitochondrial damage and subsequent cell death after oxygen glucose deprivation in vitro. *Brain Res,* 1290**,** 91-101.

Li, M., Zhou, X., Mei, J., Geng, X., Zhou, Y., Zhang, W. & Xu, C. 2014. Study on the activity of the signaling pathways regulating hepatocytes from G0 phase into G1 phase during rat liver regeneration. *Cell Mol Biol Lett,* 19**,** 181-200.

Li, R., Oteiza, A., Sorensen, K. K., McCourt, P., Olsen, R., Smedsrod, B. & Svistounov, D. 2011. Role of liver sinusoidal endothelial cells and stabilins in elimination of oxidized low-density lipoproteins. *Am J Physiol Gastrointest Liver Physiol,* 300**,** G71-81.

Li, S., Edgar, D., Fassler, R., Wadsworth, W. & Yurchenco, P. D. 2003. The role of laminin in embryonic cell polarization and tissue organization. *Dev Cell,* 4**,** 613-24.

Limonciel, A., Aschauer, L., Wilmes, A., Prajczer, S., Leonard, M. O., Pfaller, W. & Jennings, P. 2011. Lactate is an ideal non-invasive marker for evaluating temporal alterations in cell stress and toxicity in repeat dose testing regimes. *Toxicol In Vitro,* 25**,** 1855-62.

Linden, J. 2006. New insights into the regulation of inflammation by adenosine. *J Clin Invest,* 116**,** 1835-7.

Liu, Y., Bubolz, A. H., Shi, Y., Newman, P. J., Newman, D. K. & Gutterman, D. D. 2006. Peroxynitrite reduces the endothelium-derived hyperpolarizing factor component of coronary flow-mediated dilation in PECAM-1-knockout mice. *Am J Physiol Regul Integr Comp Physiol,* 290**,** R57-65.

Lockman, K. A., Baren, J. P., Pemberton, C. J., Baghdadi, H., Burgess, K. E., Plevris-Papaioannou, N., Lee, P., Howie, F., Beckett, G., Pryde, A., Jaap, A. J., Hayes, P. C., Filippi, C. & Plevris, J. N. 2012. Oxidative stress rather than triglyceride accumulation is a determinant of mitochondrial dysfunction in in vitro models of hepatic cellular steatosis. *Liver Int,* 32**,** 1079-92.

Lübberstedt, M., Müller-Vieira, U., Mayer, M., Biemel, K. M., Knöspel, F., Knobeloch, D., Nüssler, A. K., Gerlach, J. C. & Zeilinger, K. 2011. HepaRG human hepatic cell line utility as a surrogate for primary human hepatocytes in drug metabolism assessment in vitro. *J Pharmacol Toxicol Methods,* 63**,** 59-68.

Maas-Szabowski, N., Fusenig, N. E. & Stark, H. J. 2005. Experimental models to analyze differentiation functions of cultured keratinocytes in vitro and in vivo. *Methods Mol Biol,* 289**,** 47-60.

Maharjan, S., Oku, M., Tsuda, M., Hoseki, J. & Sakai, Y. 2014. Mitochondrial impairment triggers cytosolic oxidative stress and cell death following proteasome inhibition. *Sci Rep,* 4**,** 5896.

Maher, S. P., Crouse, R. B., Conway, A. J., Bannister, E. C., Achyuta, A. K., Clark, A. Y., Sinatra, F. L., Cuiffi, J. D., Adams, J. H., Kyle, D. E. & Saadi, W. M. 2014. Microphysical space of a liver sinusoid device enables simplified long-term maintenance of chimeric mouse-expanded human hepatocytes. *Biomed Microdevices,* 16**,** 727-36.

Manov, I., Hirsh, M. & Iancu, T. C. 2004. N-acetylcysteine does not protect HepG2 cells against acetaminophen-induced apoptosis. *Basic Clin Pharmacol Toxicol,* 94**,** 213-25.

March, S., Hui, E. E., Underhill, G. H., Khetani, S. & Bhatia, S. N. 2009. Microenvironmental regulation of the sinusoidal endothelial cell phenotype in vitro. *Hepatology,* 50**,** 920-8.

Marin-Juez, R., Rovira, M., Crespo, D., van der Vaart, M., Spaink, H. P. & Planas, J. V. 2014. GLUT2-mediated glucose uptake and availability are required for embryonic brain development in zebrafish. *J Cereb Blood Flow Metab*.

Marrone, G., Maeso-Diaz, R., Garcia-Cardena, G., Abraldes, J. G., Garcia-Pagan, J. C., Bosch, J. & Gracia-Sancho, J. 2014. KLF2 exerts antifibrotic and vasoprotective effects in cirrhotic rat livers: behind the molecular mechanisms of statins. *Gut*.

Marroquin, L. D., Hynes, J., Dykens, J. A., Jamieson, J. D. & Will, Y. 2007. Circumventing the Crabtree effect: replacing media glucose with galactose increases susceptibility of HepG2 cells to mitochondrial toxicants. *Toxicol Sci.* United States.

Martin, E. J., Racz, W. J. & Forkert, P. G. 2003. Mitochondrial dysfunction is an early manifestation of 1,1-dichloroethylene-induced hepatotoxicity in mice. *J Pharmacol Exp Ther,* 304**,** 121-9.

Matsumoto, K., Yoshitomi, H., Rossant, J. & Zaret, K. S. 2001. Liver organogenesis promoted by endothelial cells prior to vascular function. *Science,* 294**,** 559-63.

Mavri-Damelin, D., Damelin, L. H., Eaton, S., Rees, M., Selden, C. & Hodgson, H. J. 2008. Cells for bioartificial liver devices: the human hepatoma-derived cell line C3A produces urea but does not detoxify ammonia. *Biotechnol Bioeng,* 99**,** 644-51.

McCuskey, R. S. 2008. The hepatic microvascular system in health and its response to toxicants. *Anat Rec (Hoboken),* 291**,** 661-71.
McGill, M. R. & Jaeschke, H. 2013. Metabolism and disposition of acetaminophen: recent advances in relation to hepatotoxicity and diagnosis. *Pharm Res,* 30**,** 2174-87.
McGill, M. R., Staggs, V. S., Sharpe, M. R., Lee, W. M. & Jaeschke, H. 2014. Serum mitochondrial biomarkers and damage-associated molecular patterns are higher in acetaminophen overdose patients with poor outcome. *Hepatology*.
McGill, M. R., Yan, H. M., Ramachandran, A., Murray, G. J., Rollins, D. E. & Jaeschke, H. 2011. HepaRG cells: a human model to study mechanisms of acetaminophen hepatotoxicity. *Hepatology,* 53**,** 974-82.
Mitra, M., Kandalam, M., Harilal, A., Verma, R. S., Krishnan, U. M., Swaminathan, S. & Krishnakumar, S. 2012. EpCAM is a putative stem marker in retinoblastoma and an effective target for T-cell-mediated immunotherapy. *Mol Vis,* 18**,** 290-308.
Moir, L. M., Black, J. L. & Krymskaya, V. P. 2012. TSC2 modulates cell adhesion and migration via integrin-alpha1beta1. *Am J Physiol Lung Cell Mol Physiol,* 303**,** L703-10.
Mottino, A. D. & Catania, V. A. 2008. Hepatic drug transporters and nuclear receptors: regulation by therapeutic agents. *World J Gastroenterol,* 14**,** 7068-74.
Moyer, A. M., Fridley, B. L., Jenkins, G. D., Batzler, A. J., Pelleymounter, L. L., Kalari, K. R., Ji, Y., Chai, Y., Nordgren, K. K. & Weinshilboum, R. M. 2011. Acetaminophen-NAPQI hepatotoxicity: a cell line model system genome-wide association study. *Toxicol Sci,* 120**,** 33-41.
Mueller, D., Kramer, L., Hoffmann, E., Klein, S. & Noor, F. 2014. 3D organotypic HepaRG cultures as in vitro model for acute and repeated dose toxicity studies. *Toxicol In Vitro,* 28**,** 104-12.
Mukhopadhyay, P., Rajesh, M., Hasko, G., Hawkins, B. J., Madesh, M. & Pacher, P. 2007. Simultaneous detection of apoptosis and mitochondrial superoxide production in live cells by flow cytometry and confocal microscopy. *Nat Protoc,* 2**,** 2295-301.
Nagendra, A. R., Mickelson, J. K. & Smith, C. W. 1997. CD18 integrin and CD54-dependent neutrophil adhesion to cytokine-stimulated human hepatocytes. *Am J Physiol,* 272**,** G408-16.
Nagi, M. N., Almakki, H. A., Sayed-Ahmed, M. M. & Al-Bekairi, A. M. 2010. Thymoquinone supplementation reverses acetaminophen-induced oxidative stress, nitric oxide production and energy decline in mice liver. *Food Chem Toxicol,* 48**,** 2361-5.
Nahmias, Y., Schwartz, R. E., Hu, W. S., Verfaillie, C. M. & Odde, D. J. 2006. Endothelium-mediated hepatocyte recruitment in the establishment of liver-like tissue in vitro. *Tissue Eng,* 12**,** 1627-38.
Nel, A., Xia, T., Madler, L. & Li, N. 2006. Toxic potential of materials at the nanolevel. *Science,* 311**,** 622-7.
Nelson, L. J., Walker, S. W., Hayes, P. C. & Plevris, J. N. 2010. Low-shear modelled microgravity environment maintains morphology and differentiated functionality of primary porcine hepatocyte cultures. *Cells Tissues Organs,* 192**,** 125-40.

Newsome, P. N., Tsiaoussis, J., Masson, S., Buttery, R., Livingston, C., Ansell, I., Ross, J. A., Sethi, T., Hayes, P. C. & Plevris, J. N. 2004. Serum from patients with fulminant hepatic failure causes hepatocyte detachment and apoptosis by a beta(1)-integrin pathway. *Hepatology,* 40**,** 636-45.

Nicotera, P. & Melino, G. 2004. Regulation of the apoptosis-necrosis switch. *Oncogene,* 23**,** 2757-65.

O'Brien, P. J., Irwin, W., Diaz, D., Howard-Cofield, E., Krejsa, C. M., Slaughter, M. R., Gao, B., Kaludercic, N., Angeline, A., Bernardi, P., Brain, P. & Hougham, C. 2006. High concordance of drug-induced human hepatotoxicity with in vitro cytotoxicity measured in a novel cell-based model using high content screening. *Arch Toxicol,* 80**,** 580-604.

Ohno, M., Motojima, K., Okano, T. & Taniguchi, A. 2009. Induction of drug-metabolizing enzymes by phenobarbital in layered co-culture of a human liver cell line and endothelial cells. *Biol Pharm Bull,* 32**,** 813-7.

Ostergaard, S., Olsson, L., Johnston, M. & Nielsen, J. 2000. Increasing galactose consumption by Saccharomyces cerevisiae through metabolic engineering of the GAL gene regulatory network. *Nat Biotechnol,* 18**,** 1283-6.

Paine, M. F., Hart, H. L., Ludington, S. S., Haining, R. L., Rettie, A. E. & Zeldin, D. C. 2006. The human intestinal cytochrome P450 "pie". *Drug Metab Dispos,* 34**,** 880-6.

Palakkan, A. A., Hay, D. C., Anil Kumar, P. R., Kumary, T. V. & Ross, J. A. 2013. Liver tissue engineering and cell sources: issues and challenges. *Liver Int,* 33**,** 666-76.

Panatto, J. P., Jeremias, I. C., Ferreira, G. K., Ramos, A. C., Rochi, N., Goncalves, C. L., Daufenbach, J. F., Jeremias, G. C., Carvalho-Silva, M., Rezin, G. T., Scaini, G. & Streck, E. L. 2011. Inhibition of mitochondrial respiratory chain in the brain of rats after hepatic failure induced by acetaminophen. *Mol Cell Biochem,* 350**,** 149-54.

Parent, R., Marion, M. J., Furio, L., Trepo, C. & Petit, M. A. 2004. Origin and characterization of a human bipotent liver progenitor cell line. *Gastroenterology,* 126**,** 1147-56.

Pernelle, K., Le Guevel, R., Glaise, D., Stasio, C. G., Le Charpentier, T., Bouaita, B., Corlu, A. & Guguen-Guillouzo, C. 2011. Automated detection of hepatotoxic compounds in human hepatocytes using HepaRG cells and image-based analysis of mitochondrial dysfunction with JC-1 dye. *Toxicol Appl Pharmacol,* 254**,** 256-66.

Pessayre, D., Mansouri, A., Berson, A. & Fromenty, B. 2010. Mitochondrial involvement in drug-induced liver injury. *Handb Exp Pharmacol***,** 311-65.

Pires, D. A., Marques, P. E., Pereira, R. V., David, B. A., Gomides, L. F., Dias, A. C., Nunes-Silva, A., Pinho, V., Cara, D. C., Vieira, L. Q., Teixeira, M. M. & Menezes, G. B. 2014. Interleukin-4 deficiency protects mice from acetaminophen-induced liver injury and inflammation by prevention of glutathione depletion. *Inflamm Res,* 63**,** 61-9.

Pivovarova, N. B. & Andrews, S. B. 2010. Calcium-dependent mitochondrial function and dysfunction in neurons. *Febs j,* 277**,** 3622-36.

Pullikotil, P., Chen, H., Muniyappa, R., Greenberg, C. C., Yang, S., Reiter, C. E., Lee, J. W., Chung, J. H. & Quon, M. J. 2012. Epigallocatechin gallate induces expression of heme oxygenase-1 in endothelial cells via p38 MAPK

and Nrf-2 that suppresses proinflammatory actions of TNF-alpha. *J Nutr Biochem,* 23**,** 1134-45.

Rahman, I., Kode, A. & Biswas, S. K. 2006. Assay for quantitative determination of glutathione and glutathione disulfide levels using enzymatic recycling method. *Nat Protoc,* 1**,** 3159-65.

Ramaiahgari, S. C., den Braver, M. W., Herpers, B., Terpstra, V., Commandeur, J. N., van de Water, B. & Price, L. S. 2014. A 3D in vitro model of differentiated HepG2 cell spheroids with improved liver-like properties for repeated dose high-throughput toxicity studies. *Arch Toxicol,* 88**,** 1083-95.

Rashid, K., Sinha, K. & Sil, P. C. 2013. An update on oxidative stress-mediated organ pathophysiology. *Food Chem Toxicol,* 62**,** 584-600.

Rauterberg, J., Voss, B., Pott, G. & Gerlach, U. 1981. Connective tissue components of the normal and fibrotic liver. I. Structure, local distribution and metabolism of connective tissue components in the normal liver and changes in chronic liver diseases. *Klin Wochenschr,* 59**,** 767-79.

Ray, S. D. & Jena, N. 2000. A hepatotoxic dose of acetaminophen modulates expression of BCL-2, BCL-X(L), and BCL-X(S) during apoptotic and necrotic death of mouse liver cells in vivo. *Arch Toxicol,* 73**,** 594-606.

Raynaud, P., Carpentier, R., Antoniou, A. & Lemaigre, F. P. 2011. Biliary differentiation and bile duct morphogenesis in development and disease. *Int J Biochem Cell Biol.* Netherlands: 2009 Elsevier Ltd.

Reardon, S. & Cyranoski, D. 2014. Japan stem-cell trial stirs envy. *Nature.* England.

Rebelo, S. P., Costa, R., Estrada, M., Shevchenko, V., Brito, C. & Alves, P. M. 2014. HepaRG microencapsulated spheroids in DMSO-free culture: novel culturing approaches for enhanced xenobiotic and biosynthetic metabolism. *Arch Toxicol.*

Reichen, J. 1999. The Role of the Sinusoidal Endothelium in Liver Function. *News Physiol Sci,* 14**,** 117-121.

Reliene, R., Fischer, E. & Schiestl, R. H. 2004. Effect of N-acetyl cysteine on oxidative DNA damage and the frequency of DNA deletions in atm-deficient mice. *Cancer Res,* 64**,** 5148-53.

Ribeiro, M. P., Santos, A. E. & Custodio, J. B. 2014. Mitochondria: The gateway for tamoxifen-induced liver injury. *Toxicology,* 323c**,** 10-18.

Rivron, N. C., Liu, J. J., Rouwkema, J., de Boer, J. & van Blitterswijk, C. A. 2008. Engineering vascularised tissues in vitro. *Eur Cell Mater,* 15**,** 27-40.

Rohringer, S., Hofbauer, P., Schneider, K. H., Husa, A. M., Feichtinger, G., Peterbauer-Scherb, A., Redl, H. & Holnthoner, W. 2014. Mechanisms of vasculogenesis in 3D fibrin matrices mediated by the interaction of adipose-derived stem cells and endothelial cells. *Angiogenesis*.

Rotroff, D. M., Beam, A. L., Dix, D. J., Farmer, A., Freeman, K. M., Houck, K. A., Judson, R. S., LeCluyse, E. L., Martin, M. T., Reif, D. M. & Ferguson, S. S. 2010. Xenobiotic-metabolizing enzyme and transporter gene expression in primary cultures of human hepatocytes modulated by ToxCast chemicals. *J Toxicol Environ Health B Crit Rev,* 13**,** 329-46.

Rowland, T. J., Blaschke, A. J., Buchholz, D. E., Hikita, S. T., Johnson, L. V. & Clegg, D. O. 2013. Differentiation of human pluripotent stem cells to retinal pigmented epithelium in defined conditions using purified extracellular matrix proteins. *J Tissue Eng Regen Med,* 7**,** 642-53.

Ruan, G. X. & Kazlauskas, A. 2013. Lactate engages receptor tyrosine kinases Axl, Tie2, and vascular endothelial growth factor receptor 2 to activate phosphoinositide 3-kinase/Akt and promote angiogenesis. *J Biol Chem,* 288**,** 21161-72.

Sahi, J., Shord, S. S., Lindley, C., Ferguson, S. & LeCluyse, E. L. 2009. Regulation of cytochrome P450 2C9 expression in primary cultures of human hepatocytes. *J Biochem Mol Toxicol,* 23**,** 43-58.

Saito, C., Zwingmann, C. & Jaeschke, H. 2010. Novel mechanisms of protection against acetaminophen hepatotoxicity in mice by glutathione and N-acetylcysteine. *Hepatology,* 51**,** 246-54.

Salerno, S., Campana, C., Morelli, S., Drioli, E. & De Bartolo, L. 2011. Human hepatocytes and endothelial cells in organotypic membrane systems. *Biomaterials,* 32**,** 8848-59.

Saragih, H., Zilian, E., Jaimes, Y., Paine, A., Figueiredo, C., Eiz-Vesper, B., Blasczyk, R., Larmann, J., Theilmeier, G., Burg-Roderfeld, M., Andrei-Selmer, L. C., Becker, J. U., Santoso, S. & Immenschuh, S. 2014. PECAM-1-dependent heme oxygenase-1 regulation via an Nrf2-mediated pathway in endothelial cells. *Thromb Haemost,* 111**,** 1077-88.

Saraswati, S., Agrawal, S. S. & Alhaider, A. A. 2013. Ursolic acid inhibits tumor angiogenesis and induces apoptosis through mitochondrial-dependent pathway in Ehrlich ascites carcinoma tumor. *Chem Biol Interact,* 206**,** 153-65.

Sassi, N., Mattarei, A., Azzolini, M., Szabo, I., Paradisi, C., Zoratti, M. & Biasutto, L. 2014. Cytotoxicity of mitochondria-targeted resveratrol derivatives: interactions with respiratory chain complexes and ATP synthase. *Biochim Biophys Acta,* 1837**,** 1781-9.

Schafer, C., Schroder, K. R., Hoglinger, O., Tollabimazraehno, S. & Lornejad-Schafer, M. R. 2013. Acetaminophen changes intestinal epithelial cell membrane properties, subsequently affecting absorption processes. *Cell Physiol Biochem,* 32**,** 431-47.

Schmelzer, E., Mutig, K., Schrade, P., Bachmann, S., Gerlach, J. C. & Zeilinger, K. 2009. Effect of human patient plasma ex vivo treatment on gene expression and progenitor cell activation of primary human liver cells in multi-compartment 3D perfusion bioreactors for extra-corporeal liver support. *Biotechnol Bioeng,* 103**,** 817-27.

Schmidt, A., Brixius, K. & Bloch, W. 2007. Endothelial precursor cell migration during vasculogenesis. *Circ Res,* 101**,** 125-36.

Schneider, F., Poidevin, A., Riehm, S., Herbrecht, J. E. & Guillot, M. 2014. Liver transplantation in case of acetaminophen poisoning: importance of assessment of the colon if arterial lactate increases despite appropriate care. *Transplantation.* United States.

Schuppan, D., Ruehl, M., Somasundaram, R. & Hahn, E. G. 2001. Matrix as a modulator of hepatic fibrogenesis. *Semin Liver Dis,* 21**,** 351-72.

Seeland, S., Torok, M., Kettiger, H., Treiber, A., Hafner, M. & Huwyler, J. 2013. A cell-based, multiparametric sensor approach characterises drug-induced cytotoxicity in human liver HepG2 cells. *Toxicol In Vitro,* 27**,** 1109-20.

Sekine, S., Kimura, T., Motoyama, M., Shitara, Y., Wakazono, H., Oida, H. & Horie, T. 2013. The role of cyclophilin D in interspecies differences in susceptibility

to hepatotoxic drug-induced mitochondrial injury. *Biochem Pharmacol,* 86**,** 1507-14.
Shah, A. D., Wood, D. M. & Dargan, P. I. 2011. Understanding lactic acidosis in paracetamol (acetaminophen) poisoning. *Br J Clin Pharmacol,* 71**,** 20-8.
Shah, R. R., Morganroth, J. & Shah, D. R. 2013. Hepatotoxicity of tyrosine kinase inhibitors: clinical and regulatory perspectives. *Drug Saf,* 36**,** 491-503.
Shahidi, M., Barati, M., Hayat, P., Tavasoli, B. & Bakhshayesh, M. 2014. The in vitro effects of sodium salicylate on von Willebrand factor and C-reactive protein production by endothelial cells. *Inflammopharmacology*.
Shuey, D. & Kim, J. H. 2011. Overview: developmental toxicology: new directions. *Birth Defects Res B Dev Reprod Toxicol,* 92**,** 381-3.
Shukla, S., Kouanda, A., Silverton, L., Talele, T. T. & Ambudkar, S. V. 2014. Pharmacophore Modeling of Nilotinib as an Inhibitor of ATP-Binding Cassette Drug Transporters and BCR-ABL Kinase Using a Three-Dimensional Quantitative Structure-Activity Relationship Approach. *Mol Pharm,* 11**,** 2313-22.
Silva, J. M., Morin, P. E., Day, S. H., Kennedy, B. P., Payette, P., Rushmore, T., Yergey, J. A. & Nicoll-Griffith, D. A. 1998. Refinement of an in vitro cell model for cytochrome P450 induction. *Drug Metab Dispos,* 26**,** 490-6.
Simon-Santamaria, J., Malovic, I., Warren, A., Oteiza, A., Le Couteur, D., Smedsrod, B., McCourt, P. & Sorensen, K. K. 2010. Age-related changes in scavenger receptor-mediated endocytosis in rat liver sinusoidal endothelial cells. *J Gerontol A Biol Sci Med Sci,* 65**,** 951-60.
Sjogren, A. K., Liljevald, M., Glinghammar, B., Sagemark, J., Li, X. Q., Jonebring, A., Cotgreave, I., Brolen, G. & Andersson, T. B. 2014. Critical differences in toxicity mechanisms in induced pluripotent stem cell-derived hepatocytes, hepatic cell lines and primary hepatocytes. *Arch Toxicol,* 88**,** 1427-37.
Skovseth, D. K., Kuchler, A. M. & Haraldsen, G. 2007. The HUVEC/Matrigel assay: an in vivo assay of human angiogenesis suitable for drug validation. *Methods Mol Biol,* 360**,** 253-68.
Smedsrod, B., Melkko, J., Risteli, L. & Risteli, J. 1990. Circulating C-terminal propeptide of type I procollagen is cleared mainly via the mannose receptor in liver endothelial cells. *Biochem J,* 271**,** 345-50.
Soldatow, V. Y., Lecluyse, E. L., Griffith, L. G. & Rusyn, I. 2013. models for liver toxicity testing. *Toxicol Res (Camb),* 2**,** 23-39.
Soto-Gutierrez, A., Navarro-Alvarez, N., Yagi, H., Nahmias, Y., Yarmush, M. L. & Kobayashi, N. 2010. Engineering of an hepatic organoid to develop liver assist devices. *Cell Transplant,* 19**,** 815-22.
Stamati, K., Priestley, J. V., Mudera, V. & Cheema, U. 2014. Laminin promotes vascular network formation in 3D in vitro collagen scaffolds by regulating VEGF uptake. *Exp Cell Res*.
Stolz, D. B., Ross, M. A., Ikeda, A., Tomiyama, K., Kaizu, T., Geller, D. A. & Murase, N. 2007. Sinusoidal endothelial cell repopulation following ischemia/reperfusion injury in rat liver transplantation. *Hepatology,* 46**,** 1464-75.
Stroka, K. M., Hayenga, H. N. & Aranda-Espinoza, H. 2013. Human neutrophil cytoskeletal dynamics and contractility actively contribute to trans-endothelial migration. *PLoS One,* 8**,** e61377.

Sullivan, G. J., Hay, D. C., Park, I. H., Fletcher, J., Hannoun, Z., Payne, C. M., Dalgetty, D., Black, J. R., Ross, J. A., Samuel, K., Wang, G., Daley, G. Q., Lee, J. H., Church, G. M., Forbes, S. J., Iredale, J. P. & Wilmut, I. 2010. Generation of functional human hepatic endoderm from human induced pluripotent stem cells. *Hepatology,* 51**,** 329-35.

Swartz, M. A. & Fleury, M. E. 2007. Interstitial flow and its effects in soft tissues. *Annu Rev Biomed Eng,* 9**,** 229-56.

Takebe, T., Sekine, K., Enomura, M., Koike, H., Kimura, M., Ogaeri, T., Zhang, R. R., Ueno, Y., Zheng, Y. W., Koike, N., Aoyama, S., Adachi, Y. & Taniguchi, H. 2013. Vascularized and functional human liver from an iPSC-derived organ bud transplant. *Nature,* 499**,** 481-4.

Tang, N. H., Wang, X. Q., Li, X. J. & Chen, Y. L. 2008. Ammonia metabolism capacity of HepG2 cells with high expression of human glutamine synthetase. *Hepatobiliary Pancreat Dis Int,* 7**,** 621-7.

Temple, R. J. & Himmel, M. H. 2002. Safety of newly approved drugs: implications for prescribing. *Jama.* United States.

Tomizawa, M., Shinozaki, F., Motoyoshi, Y., Sugiyama, T., Yamamoto, S. & Ishige, N. 2014. Co-culture of hepatocellular carcinoma cells and human umbilical endothelial cells damaged by SU11274. *Biomed Rep,* 2**,** 799-803.

Tourovskaia, A., Fauver, M., Kramer, G., Simonson, S. & Neumann, T. 2014. Tissue-engineered microenvironment systems for modeling human vasculature. *Exp Biol Med (Maywood).*

Toyoda, Y., Tamai, M., Kashikura, K., Kobayashi, S., Fujiyama, Y., Soga, T. & Tagawa, Y. 2012. Acetaminophen-induced hepatotoxicity in a liver tissue model consisting of primary hepatocytes assembling around an endothelial cell network. *Drug Metab Dispos,* 40**,** 169-77.

Tsiaoussis, J., Newsome, P. N., Nelson, L. J., Hayes, P. C. & Plevris, J. N. 2001. Which hepatocyte will it be? Hepatocyte choice for bioartificial liver support systems. *Liver Transpl,* 7**,** 2-10.

Tsuneki, M. & Madri, J. A. 2014. CD44 regulation of endothelial cell proliferation and apoptosis via modulation of CD31 and VE-cadherin expression. *J Biol Chem,* 289**,** 5357-70.

Ukairo, O., McVay, M., Krzyzewski, S., Aoyama, S., Rose, K., Andersen, M. E., Khetani, S. R. & Lecluyse, E. L. 2013. Bioactivation and toxicity of acetaminophen in a rat hepatocyte micropatterned coculture system. *J Biochem Mol Toxicol,* 27**,** 471-8.

Ulvestad, M., Nordell, P., Asplund, A., Rehnstrom, M., Jacobsson, S., Holmgren, G., Davidson, L., Brolen, G., Edsbagge, J., Bjorquist, P., Kuppers-Munther, B. & Andersson, T. B. 2013. Drug metabolizing enzyme and transporter protein profiles of hepatocytes derived from human embryonic and induced pluripotent stem cells. *Biochem Pharmacol,* 86**,** 691-702.

Vinken, M. 2013. The adverse outcome pathway concept: a pragmatic tool in toxicology. *Toxicology,* 312**,** 158-65.

Vrochides, D., Papanikolaou, V., Pertoft, H., Antoniades, A. A. & Heldin, P. 1996. Biosynthesis and degradation of hyaluronan by nonparenchymal liver cells during liver regeneration. *Hepatology,* 23**,** 1650-5.

Wang, A. G., Xia, T., Yuan, J., Yu, R. A., Yang, K. D., Chen, X. M., Qu, W. & Waalkes, M. P. 2004. Effects of phenobarbital on metabolism and toxicity of

diclofenac sodium in rat hepatocytes in vitro. *Food Chem Toxicol,* 42**,** 1647-53.

Wang, L., Wang, X., Chiu, J. D., van de Ven, G., Gaarde, W. A. & Deleve, L. D. 2012a. Hepatic vascular endothelial growth factor regulates recruitment of rat liver sinusoidal endothelial cell progenitor cells. *Gastroenterology,* 143**,** 1555-1563.e2.

Wang, L., Wang, X., Xie, G., Hill, C. K. & DeLeve, L. D. 2012b. Liver sinusoidal endothelial cell progenitor cells promote liver regeneration in rats. *J Clin Invest,* 122**,** 1567-73.

Willett, C., Rae, J. C., Goyak, K. O., Minsavage, G., Westmoreland, C., Andersen, M., Avigan, M., Duche, D., Hartung, T., Jaeschke, H., Kleensang, A., Landesmann, B., Toole, C., Rowan, A., Schultz, T., Seed, J., Senior, J., Shah, I., Subramanian, K., Vinken, M. & Watkins, P. 2014. Building Shared Experience to Advance Practical Application of Pathway-Based Toxicology: Liver Toxicity Mode-of-Action. *Altex.*

Williamson, D. H., Lund, P. & Krebs, H. A. 1967. The redox state of free nicotinamide-adenine dinucleotide in the cytoplasm and mitochondria of rat liver. *Biochem J,* 103**,** 514-27.

Wisse, E., Braet, F., Luo, D., De Zanger, R., Jans, D., Crabbe, E. & Vermoesen, A. 1996. Structure and function of sinusoidal lining cells in the liver. *Toxicol Pathol,* 24**,** 100-11.

Xie, W., Sun, J., Zhang, X. & Melzig, M. F. 2014a. Necrosis factor-alpha (TNF-alpha) response in human hepatoma HepG2 cells treated with hepatotoxic agents. *Pharmazie,* 69**,** 379-84.

Xie, Y., McGill, M. R., Dorko, K., Kumer, S. C., Schmitt, T. M., Forster, J. & Jaeschke, H. 2014b. Mechanisms of acetaminophen-induced cell death in primary human hepatocytes. *Toxicol Appl Pharmacol,* 279**,** 266-274.

Xin, X., Yang, S., Ingle, G., Zlot, C., Rangell, L., Kowalski, J., Schwall, R., Ferrara, N. & Gerritsen, M. E. 2001. Hepatocyte growth factor enhances vascular endothelial growth factor-induced angiogenesis in vitro and in vivo. *Am J Pathol,* 158**,** 1111-20.

Xiong, S., Mu, T., Wang, G. & Jiang, X. 2014. Mitochondria-mediated apoptosis in mammals. *Protein Cell*.

Yang, L., Yue, S., Liu, X., Han, Z., Zhang, Y. & Li, L. 2013a. Sphingosine kinase/sphingosine 1-phosphate (S1P)/S1P receptor axis is involved in liver fibrosis-associated angiogenesis. *J Hepatol,* 59**,** 114-23.

Yang, Y., Li, J., Pan, X., Zhou, P., Yu, X., Cao, H., Wang, Y. & Li, L. 2013b. Co-culture with mesenchymal stem cells enhances metabolic functions of liver cells in bioartificial liver system. *Biotechnol Bioeng,* 110**,** 958-68.

Yehuda-Shnaidman, E., Nimri, L., Tarnovscki, T., Kirshtein, B., Rudich, A. & Schwartz, B. 2013. Secreted human adipose leptin decreases mitochondrial respiration in HCT116 colon cancer cells. *PLoS One,* 8**,** e74843.

Yoon, M., Kedderis, G. L., Yan, G. Z. & Clewell, H. J., 3rd 2014. Use of in vitro data in developing a physiologically based pharmacokinetic model: Carbaryl as a case study. *Toxicology*.

Yoshida, K., Maeda, K. & Sugiyama, Y. 2012. Transporter-mediated drug--drug interactions involving OATP substrates: predictions based on in vitro inhibition studies. *Clin Pharmacol Ther,* 91**,** 1053-64.

Yovchev, M. I., Dabeva, M. D. & Oertel, M. 2013. Isolation, characterization, and transplantation of adult liver progenitor cells. *Methods Mol Biol,* 976**,** 37-51.

Yu, K. R., Yang, S. R., Jung, J. W., Kim, H., Ko, K., Han, D. W., Park, S. B., Choi, S. W., Kang, S. K., Scholer, H. & Kang, K. S. 2012. CD49f enhances multipotency and maintains stemness through the direct regulation of OCT4 and SOX2. *Stem Cells,* 30**,** 876-87.

Zachary, I. & Gliki, G. 2001. Signaling transduction mechanisms mediating biological actions of the vascular endothelial growth factor family. *Cardiovasc Res,* 49**,** 568-81.

Zamaraeva, M. V., Sabirov, R. Z., Maeno, E., Ando-Akatsuka, Y., Bessonova, S. V. & Okada, Y. 2005. Cells die with increased cytosolic ATP during apoptosis: a bioluminescence study with intracellular luciferase. *Cell Death Differ,* 12**,** 1390-7.

Zanger, U. M. & Schwab, M. 2013. Cytochrome P450 enzymes in drug metabolism: regulation of gene expression, enzyme activities, and impact of genetic variation. *Pharmacol Ther,* 138**,** 103-41.

Zeisberg, M., Kramer, K., Sindhi, N., Sarkar, P., Upton, M. & Kalluri, R. 2006. De-differentiation of primary human hepatocytes depends on the composition of specialized liver basement membrane. *Mol Cell Biochem,* 283**,** 181-9.

Zhang, Q., Liu, J., Huang, W., Tian, L., Quan, J., Wang, Y. & Niu, R. 2014. oxLDL induces injury and defenestration of human liver sinusoidal endothelial cells via LOX1. *J Mol Endocrinol,* 53**,** 281-93.

Zhou, S. F., Liu, J. P. & Chowbay, B. 2009. Polymorphism of human cytochrome P450 enzymes and its clinical impact. *Drug Metab Rev,* 41**,** 89-295.

Zhu, B. T. 2010. On the general mechanism of selective induction of cytochrome P450 enzymes by chemicals: some theoretical considerations. *Expert Opin Drug Metab Toxicol,* 6**,** 483-94.